

# Development and Characterisation of an Osteoclastic *in vitro* Model of Multiple Myeloma

Division of Cancer and Genetics, School of Medicine, Cardiff  
University

Supervisors: Professor Chris Pepper, Dr Stephen Man and  
Professor Chris Fegan

Thomas Lewis

December 2019

This thesis is submitted to Cardiff University to fulfil the requirements for  
a degree of Doctor of Philosophy

## Declaration and Statements

### **STATEMENT 1**

This thesis is being submitted in partial fulfilment of the requirements for the degree of PhD.

Signed \_\_\_\_\_

Date \_\_\_\_\_

### **STATEMENT 2**

This work has not been submitted in substance for any other degree or award at this or any other university or place of learning, nor is it being submitted concurrently for any other degree or award (outside of any formal collaboration agreement between the University and a partner organisation)

Signed \_\_\_\_\_

Date \_\_\_\_\_

### **STATEMENT 3**

I hereby give consent for my thesis, if accepted, to be available in the University's Open Access repository (or, where approved, to be available in the University's library and for inter-library loan), and for the title and summary to be made available to outside organisations, subject to the expiry of a University-approved bar on access if applicable.

Signed \_\_\_\_\_

Date \_\_\_\_\_

### **DECLARATION**

This thesis is the result of my own independent work, except where otherwise stated, and the views expressed are my own. Other sources are acknowledged by explicit references. The thesis has not been edited by a third party beyond what is permitted by Cardiff University's Use of Third Party Editors by Research Degree Students Procedure.

Signed \_\_\_\_\_

Date \_\_\_\_\_

### **WORD COUNT** \_\_\_\_\_

(Excluding summary, acknowledgements, declarations, contents pages, appendices, tables, diagrams and figures, references, bibliography, footnotes and endnotes)

## Publications, Conferences and Achievements

### Publications

Corcoran DB, Lewis T, Nahar KS, Jamshidi S, Fegan C, Pepper C, Thurston DE, Rahman KM. Effects of Systematic Shortening of Noncovalent C8 Side Chain on the Cytotoxicity and NF- $\kappa$ B Inhibitory Capacity of Pyrrolbenzodiazepines (PBDs). *JMed Chem*. 2019 Feb 28;62(4):2127-2139. doi: 10.1021/acs.jmedchem.8b01849. Epub2019 Feb 13. PubMed PMID: 30688457.

Lewis T, Walsby EJ, Man S, Fegan C and Pepper C. Development and Characterisation of an *in vitro* Model of Multiple Myeloma Blood 2018 132:4505; doi: <https://doi.org/10.1182/blood-2018-99-111842>

### Presentations and Conferences

Cardiff University Division of Cancer and Genetics Research Symposium, October 2017

Cardiff University Division of Cancer and Genetics Seminar Series, February 2018

Brighton and Sussex Medical School, Haematology Seminar Series, May 2018

Cardiff University School of Medicine Haematology Seminar, November 2018

American Society of Haematology Annual Meeting, December 2018

School of Medicine Post-graduate Research Symposium, January 2019

British Lymphoma Pathology Group Spring Meeting, May 2019

### Achievements

Associate Fellowship of the Higher Education Academy

Chair of the Student-Staff Panel for the School of Medicine and a Student Academic Representative for the Academic Year of 2017-18

## Acknowledgements

There are a number of people worthy of thanks who have supported me throughout this PhD, none more so than my supervisors Prof Chris Pepper, Dr Steve Man and Prof Chris Fegan. You've all been an incredible help throughout my studies, and I couldn't have wished for a better team of supervisors. It really has been a privilege to work with you all.

I would like to give a special thanks to Dr Beth Walsby. You were a huge help during the first two years of this PhD, and it was a pleasure to have you as a supervisor throughout that time. Whilst it was sad to see you leave Cardiff, I'm very glad you've settled comfortably in Ireland and I wish you and your family all the very best in the future.

To Dr Ann Kift-Morgan, Dr Catherine Naseriyan, Dr Bronwen Evans, Dr Chris von Ruhland, Prof Rachel Errington and Dr Anna Evans, I would like to extend my thanks for your help and advice with my experiments and data analysis, relating to your associated specialties.

I'm a firm believer in the principle that in many scenarios in life, it's not where you are that necessarily matters, it's who you're with. I consider myself incredibly lucky to have worked with so many hard-working, caring, hilarious and supportive people, all of whom grew to be fantastic friends. I want to say a big thank you to Alys, Helene, Jim, Jo, Julia, Kate, Liam, Pete, Rhi, Stefan, Trish and Vicky. It's been a wonderful couple of years working with you all, you made it a joy to come into work.

To my grandparents Gwen and Tom who have always been a fantastic support through my life and this PhD. You've always been on hand for a chat after work, provided me with plenty of tea and biscuits when I've come to visit and never fail to put a smile on my face. Thank you, I love you both.

Finally, to my parents Annette and Mark. This work would not have been possible without you. Your support throughout everything I've ever done has been unwavering and this process has been no different. You're the most selfless, kind and caring people I know, and I am immensely proud to call you my mam and dad. You both inspire me more than you realise, and I love you very much. Thank you for everything.

This work was generously funded by the Leukaemia Research Appeal for Wales.

*For Mam and Dad*

## Abstract

Multiple myeloma is an incurable malignancy of terminally differentiated B-cells – also known as plasma cells. These malignant cells are extremely reliant on the bone marrow microenvironment for their growth and survival, as well as their acquired ability to resist therapeutic intervention. Consequently, maintaining primary myeloma cells *in vitro* remains a challenge. Patients suffering from this incurable disease often develop osteolytic lesions, due to an imbalance between osteoblasts and osteoclasts, which cause bone pain and a high frequency of fractures. This project aimed to create a physiologically relevant *in vitro* model of myeloma, incorporating an osteoclast microenvironment. Osteoclasts normally work in concert with osteoblasts during bone remodelling. In myeloma their activity predominates and is intrinsic to disease progression. It is now clear that osteoclasts also contribute to the survival of myeloma cells but the precise mechanism(s) for this remain unresolved. The first aim of this research was to develop and characterise an *in vitro* osteoclastic model using the myelo-monocytic U937 cell line. Treatment with 100nM PMA and 10nM 1,25(OH)<sub>2</sub>D<sub>3</sub> caused these cells to merge and form multi-nucleated, TRAP positive and RANK positive cells with bone resorbing capabilities. Culturing two different myeloma cell lines, H929 and JJN3, in co-culture with these osteoclast-like cells for a period of 48 hours resulted in the preferential expansion of a small subpopulation of myeloma cells that were CD138<sup>dim</sup>. RNA-sequencing was performed on cell sorted CD138<sup>bright</sup> and CD138<sup>dim</sup>, which revealed substantial differences in the transcriptomes of CD138<sup>dim</sup> and CD138<sup>bright</sup> cells. Comparative analysis inferred an activation of signalling pathways relating to adhesion, migration and survival in CD138<sup>dim</sup> cells. Phenotypic analysis showed that CD138<sup>dim</sup> cells had significantly higher expression of adhesion markers CXCR4, CD40, CD45 and CD49e, the angiogenesis inducer CXCL8 and the activation marker CD69 ( $p \leq 0.05$ ) in both cell lines as a result of co-culture with differentiated U937 osteoclast-like cells. Functionally, CD138<sup>dim</sup> had greater migratory capacity and increased chemoresistance to bortezomib in comparison with CD138<sup>bright</sup> cells. These data could imply a role for CD138<sup>dim</sup> myeloma cells in disease propagation in both the pre and post-treatment settings. As a result, this model could provide a good foundation for future studies on the influence of the bone marrow microenvironment on resistance mechanisms in myeloma.

# Table of Contents

<b>CHAPTER 1: INTRODUCTION</b>	<b>1</b>
<b>1.1. Multiple Myeloma</b>	<b>1</b>
1.1.1. Epidemiology of myeloma	2
1.1.2. Aetiology of myeloma	2
1.1.3. Plasma cell biology	3
1.1.4. Surface phenotype of myeloma cells	4
1.1.5. Development and progression of myeloma	6
1.1.5.1. Monoclonal Gammopathy of Undetermined Significance (MGUS)	7
1.1.5.2. Smouldering Multiple Myeloma (SMM)	8
1.1.5.3. Symptomatic myeloma	9
1.1.5.4. Extramedullary disease	11
1.1.6. Genetic aberrations	12
1.1.7. Myeloma staging and prognostic factors	15
1.1.8. Treatment of myeloma	16
1.1.8.1. Current treatments	18
1.1.8.2. Future treatments	21
<b>1.2. The Bone Marrow Microenvironment in Multiple Myeloma</b>	<b>24</b>
1.2.1. Bone marrow stromal cells	26
1.2.2. Bone marrow endothelial cells	26
1.2.3. Osteoblasts	27
1.2.4. Osteoclasts	28
1.2.4.1. RANK/RANKL/OPG signalling	29
1.2.4.2. Interleukin-6	31
1.2.4.3. Vitamin D	32
<b>1.3. Myeloma Research Models</b>	<b>34</b>
1.3.1. <i>In vivo</i> models	34
1.3.2. <i>In vitro</i> models	35
1.3.2.1. Myeloma models	35
1.3.2.2. Osteoclast models	36
1.3.2.3. Co-culture models	37
<b>1.4. Project Aims</b>	<b>39</b>
<b>CHAPTER 2: MATERIALS AND METHODS</b>	<b>40</b>
<b>2.1. Tissue Culture</b>	<b>40</b>
2.1.1. Media, buffer and cell staining solutions	40
2.1.1.1. RPMI 1640 media	40
2.1.1.2. DMEM media	40
2.1.1.3. M199 media	40
2.1.1.4. Cryopreservation media solution	40
2.1.1.5. Paraformaldehyde fixation solution	40
2.1.1.6. Tolidine blue solution	41
2.1.2. Tissue culture plastics	41
2.1.3. Assessing cell density and viability	41
2.1.4. Mycoplasma testing	41
2.1.5. Cell line culture	43
2.1.5.1. Suspension cell lines	43
2.1.5.2. Adherent cell lines	43
2.1.6. Differentiation of U937 cells	43
2.1.7. U937 cell culture on ivory disks	44

2.1.8. Myeloma cell co-culture with differentiated U937 cells	45
2.1.9. Myeloma cell co-culture with adherent cell lines	45
2.1.10. Assessment of myeloma cell migration	45
2.1.11. Treatment of myeloma cells with bortezomib	46
2.1.12. Cryopreservation of cell lines	46
2.1.13. Thawing of cryopreserved cells	46
<b>2.2. Flow Cytometry</b>	<b>47</b>
2.2.1. Compensation of multicolour antibody panels	47
2.2.2. Myeloma cell staining	47
2.2.2.1. Determination of surface marker expression	48
2.2.2.2. CFSE assay	48
2.2.2.3. Cell sorting	49
2.2.3. U937 cell staining	49
2.2.3.1. Determination of RANK expression on U937 cells.	49
2.2.3.2. DNA content analysis	50
2.2.4. Annexin V staining	50
<b>2.3. Microscopy</b>	<b>51</b>
2.3.1. Tartrate resistant acid phosphatase (TRAP) Staining	51
2.3.2. SEM imaging	51
2.3.3. Fluorescence microscopy	52
<b>2.4. Gene expression analysis</b>	<b>53</b>
2.4.1. RNA sequencing	53
2.4.1.1. RNA Isolation	53
2.4.1.2. RNA Sample Preparation and Sequencing	54
2.4.1.3. RNA sequencing data analysis	54
2.4.1.4. Ingenuity Pathway Analysis (IPA)	55
2.4.2. Validation of protein expression	57
2.4.2.1. Reverse transcription reaction	57
2.4.2.2. Primer selection and design	58
2.4.2.3. Real-Time Polymerase Chain Reaction (qPCR)	59
2.4.2.4. Analysis of qPCR data	61
<b>2.5. Statistical analysis</b>	<b>62</b>
<b>CHAPTER 3: RESULTS</b>	<b>63</b>
<b>DEVELOPMENT AND CHARACTERISATION OF AN OSTEOCLAST-LIKE <i>IN VITRO</i> NICHE</b>	<b>63</b>
<b>3.1. Introduction</b>	<b>63</b>
3.1.1. Aims	65
<b>3.2. Differentiation of U937 cells into osteoclast-like cells</b>	<b>66</b>
3.2.1. Treatment with 1,25(OH) <sub>2</sub> D <sub>3</sub> induces morphological changes in U937 cells	66
3.2.2. Treatment with PMA and 1,25(OH) <sub>2</sub> D <sub>3</sub> causes U937 cells to increase in size	69
3.2.3. Treatment with PMA and 1,25(OH) <sub>2</sub> D <sub>3</sub> increases in DNA content in U937 cells	71
3.2.4. Treatment with PMA and 1,25(OH) <sub>2</sub> D <sub>3</sub> induces U937 cell multinucleation	74
3.2.5. Tartrate resistant acid phosphatase (TRAP) expression in U937 cells	76
3.2.6. U937 cell expression of Receptor Activator of Nuclear Factor-kappa B (RANK)	78
3.2.7. Resorption of bone material by differentiated U937 cells	80
<b>3.3. CD138 expression in myeloma cells</b>	<b>83</b>
3.3.1. Identification of a CD138 <sup>dim</sup> population of myeloma cells	85
3.3.2. CD138 <sup>dim</sup> myeloma cells represent a live population	86
3.3.3. CD138 <sup>dim</sup> cells represent a true subset of myeloma cells	90

<b>3.4. Discussion</b>	<b>92</b>
3.4.1. Development of an <i>in vitro</i> osteoclast-like model	92
3.4.2. Characterisation of myeloma cells cultured with differentiated U937 cells	96
3.4.3. The role of CD138 <sup>dim</sup> cells in myeloma	98
3.4.4. Final conclusions	99
<b>CHAPTER 4: RESULTS</b>	<b>101</b>
<b>ASSESSMENT OF THE GLOBAL CHANGES OF THE MYELOMA TRANSCRIPTOME IN AN OSTEOCLAST-LIKE MICROENVIRONMENT</b>	<b>101</b>
<b>4.1. Introduction</b>	<b>101</b>
4.1.1. Aims	104
<b>4.2. Assessing changes in the global transcriptome of CD138<sup>bright</sup> and CD138<sup>dim</sup> myeloma cells</b>	<b>105</b>
4.2.1. Experimental design and rationale	105
4.2.2. RNA-seq data processing and quality control	108
4.2.3. Assessment of sample correlation and hierarchical clustering	111
4.2.4. Principal component analysis of RNA-seq data	114
<b>4.3. Establishment of differentially expressed (DE) genes between CD138<sup>bright</sup> and CD138<sup>dim</sup> myeloma cells</b>	<b>116</b>
4.3.1. Comparison strategy to determine DE genes	116
4.3.2. Visualisation of DE genes in each dataset	117
4.3.2.1. MvA plots	117
4.3.2.2. Heatmaps	118
4.3.2.3. Venn Diagrams	122
<b>4.4. Over-representation of differentially expressed genes</b>	<b>125</b>
4.4.1. Overrepresentation of cellular functions	125
4.4.2. Quantification of overrepresented pathways	128
4.4.3. Evaluation of overrepresented pathways	130
<b>4.5. Validation of DE genes using qPCR</b>	<b>134</b>
4.5.1. Selection of targets to be used for validation	134
4.5.2. Expression of genes selected for validation	135
4.5.3. Validation of candidate genes using qPCR	138
<b>4.6. Discussion</b>	<b>142</b>
4.6.1. Assessment of differentially expressed genes through RNA-seq	142
4.6.2. Evaluation of overrepresented pathways	143
4.6.2.1. CD138 <sup>bright</sup> overrepresented pathways	144
4.6.2.2. CD138 <sup>dim</sup> overrepresented pathways	145
4.6.3. Validation of gene expression through qPCR	150
4.6.4. Limitations to the study	151
4.6.5. Final conclusions	152
<b>CHAPTER 5: RESULTS</b>	<b>154</b>
<b>ASSESSMENT OF CD138<sup>BRIGHT</sup> AND CD138<sup>DIM</sup> MYELOMA CELL FUNCTIONALITY IN RESPONSE TO CO-CULTURE WITH OSTEOCLAST-LIKE CELLS.</b>	<b>154</b>
<b>5.1. Introduction</b>	<b>154</b>
5.1.1. Aims	156
<b>5.2. Evaluation of transcriptional activity of myeloma markers</b>	<b>157</b>

5.2.1.	Loss of CD138 is a transcriptionally regulated event	157
5.2.2.	Transcriptional overview of myeloma phenotypic identifiers	160
5.2.3.	Assessment of immunoglobulin gene expression	165
5.2.4.	Assessment of CD138 <sup>dim</sup> cell activation through expression of CD69	167
<b>5.3.</b>	<b>Evaluation of the adhesive, angiogenic and migratory capacity of myeloma cells</b>	<b>169</b>
5.3.1.	Assessment of adhesion markers in CD138 <sup>dim</sup> myeloma cells	169
5.3.2.	Determination of angiogenic potential of myeloma cells	174
5.3.3.	Functional assessment of migratory potential of myeloma cells	178
<b>5.4.</b>	<b>Assessment of myeloma cell activation and chemoresistance</b>	<b>182</b>
5.4.1.	Assessment of chemoresistance in CD138 <sup>dim</sup> myeloma cells	182
5.4.1.1.	Differentiated U937 cells provide a protective effect against bortezomib	183
5.4.1.2.	CD138 <sup>dim</sup> myeloma cells are more chemo-resistant than CD138 <sup>bright</sup> cells	183
<b>5.5.</b>	<b>Discussion</b>	<b>188</b>
5.5.1.	Identification of CD138 <sup>dim</sup> cells	189
5.5.2.	CD138 <sup>dim</sup> cells are representative of a more migratory subpopulation of myeloma cells	191
5.5.3.	CD138 <sup>dim</sup> cells are a more chemo-resistant subset of myeloma cells	193
5.5.4.	Final conclusions	194
<b>CHAPTER 6: GENERAL DISCUSSION</b>		<b>196</b>
<b>6.1.</b>	<b>Summary of key findings</b>	<b>196</b>
<b>6.2.</b>	<b>Final discussion</b>	<b>197</b>
6.2.1.	Limitations to this study	202
6.2.2.	Future work and clinical impact	205
<b>SUPPLEMENTARY DATA</b>		<b>210</b>
<b>BIBLIOGRAPHY</b>		<b>221</b>

## List of Figures

Figure 1.1: Stages of multiple myeloma development .....	7
Figure 1.2: Genetic abnormalities associated with the initiation and progression of multiple myeloma	14
Figure 1.3: Treatment options for patients diagnosed with multiple myeloma .....	19
Figure 1.4: Overview of myeloma cell influence within the bone marrow microenvironment .....	25
Figure 1.5: X-ray images of focal osteolytic lesions from a myeloma patient .....	30
Figure 2.1. A flowchart illustrating the processes involved in the analysis of RNA sequencing data .....	56
Figure 3.1. Timeline of U937 cell treatment with PMA and 1,25(OH) <sub>2</sub> D <sub>3</sub> .....	67
Figure 3.2. The effect of PMA and 1,25(OH) <sub>2</sub> D <sub>3</sub> on U937 cell morphology, number and viability .....	68
Figure 3.3. The effect of PMA and 1,25(OH) <sub>2</sub> D <sub>3</sub> on U937 cell size .....	70
Figure 3.4A. The effect of PMA and 1,25(OH) <sub>2</sub> D <sub>3</sub> on the DNA content of U937 cells .....	72
Figure 3.4B. The effect of PMA and 1,25(OH) <sub>2</sub> D <sub>3</sub> on the DNA content of U937 cells .....	73
Figure 3.5. The effect of PMA and 1,25(OH) <sub>2</sub> D <sub>3</sub> on U937 cell multinucleation .....	75
Figure 3.6. The effect of PMA and 1,25(OH) <sub>2</sub> D <sub>3</sub> on U937 TRAP expression.....	77
Figure 3.7. The effect of PMA and 1,25(OH) <sub>2</sub> D <sub>3</sub> on RANK expression in U937 cells .....	79
Figure 3.8. Scanning electron microscopy (SEM) imaging of ivory disks after culture with treated U937 cells .....	81
Figure 3.9. Gating strategy to assess the expression of CD138 and CD38 in myeloma cells lines .....	84
Figure 3.10. Identification and quantification of a subpopulation of CD138 <sup>dim</sup> myeloma cells .....	87
Figure 3.11: Identification of CD138 <sup>dim</sup> myeloma cells after Transwell® co-culture with differentiated U937 cells .....	88
Figure 3.12. Viability of CD138 <sup>dim</sup> myeloma cells after co-culture with differentiated U937 cells.....	89
Figure 3.13. CFSE labelling of CD138 <sup>dim</sup> myeloma cells .....	91
Figure 4.1. A schematic flowchart illustrating the experimental design and workflow of an RNA-seq experiment.....	107
Figure 4.2. Quality control of raw and transformed data .....	110
Figure 4.3. Pearson's correlation and unsupervised hierarchical clustering .....	113
Figure 4.4. Principal component analysis of variance stabilising transformed counts .....	115
Figure 4.5. A diagram illustrating the comparisons made between each sample to investigate differential gene expression .....	116
Figure 4.6. MvA plots facilitating the visualisation of differentially expressed genes.....	119
Figure 4.7A. Heatmap illustrating the top 200 differentially expressed genes in H929 cells .....	120
Figure 4.7B. Heatmap illustrating the top 200 differentially expressed genes in JN3 cells.....	121
Figure 4.8. Venn diagrams highlighting the number of significant differentially expressed genes (q<0.05) that have log <sub>2</sub> fold changes >1 and <-1 .....	124
Figure 4.9. Summary of overrepresented cellular functions determined by IPA analysis.....	127
Figure 4.10. Distribution of overrepresented pathways in each dataset .....	129
Figure 4.11A. Summary of significantly overrepresented pathways in CD138 <sup>bright</sup> comparisons.....	132
Figure 4.11B. Summary of significantly overrepresented pathways in CD138 <sup>dim</sup> comparisons .....	133
Figure 4.12. Expression of differentially expressed genes selected for qPCR validation in H929 and JN3 cells .....	137

Figure 4.13. Validation of differentially expressed genes in H929 and JLN3 cells using qPCR.....	140
Figure 4.14. Correlation between gene expression and fold change in each condition assessed using qPCR or each gene selected for validation .....	141
Figure 5.1. Expression of CD138 in H929 and JLN3 cells determined by RNA-seq and flow cytometry .	159
Figure 5.2A. Heatmap illustrating the expression of genes involved in the phenotypic identification of myeloma cells .....	163
Figure 5.2B. Heatmap illustrating the expression of genes involved in the phenotypic identification of myeloma cells .....	164
Figure 5.3. Expression changes of immunoglobulin genes in CD138 <sup>bright</sup> and CD138 <sup>dim</sup> myeloma cells .	166
Figure 5.4. Expression of CD69 in CD138 <sup>bright</sup> and CD138 <sup>dim</sup> myeloma subsets .....	168
Figure 5.5. Expression of genes associated with cell adhesion in H929 and JLN3 cells as determined by RNA-seq.....	172
Figure 5.6. Validation of differentially expressed adhesion markers using flow cytometry .....	173
Figure 5.7A. A schematic of CXCL8 signalling and associated DE genes from CD138 <sup>dim</sup> H929 cells. ....	176
Figure 5.7B. A schematic of CXCL8 signalling and associated DE genes from CD138 <sup>dim</sup> JLN3 cells.....	177
Figure 5.8. Migration of myeloma cell lines following co-culture with differentiated U937 cells.....	180
Figure 5.9. Gating strategy to assess myeloma cell viability following treatment with bortezomib.....	185
Figure 5.10. The toxicity of bortezomib in myeloma cells cultured with differentiated U937 cells.....	186
Figure 5.11. The toxicity of bortezomib in CD138 <sup>bright</sup> and CD138 <sup>dim</sup> myeloma cells .....	187
Supplementary Figure Ia. Gating strategy used to sort CD138 <sup>bright</sup> and CD138 <sup>dim</sup> H929 cells.....	210
Supplementary Figure Ib. Gating strategy used to sort CD138 <sup>bright</sup> and CD138 <sup>dim</sup> JLN3 cells.....	211
Supplementary Figure II. RIN plots produced from each RNA sample used in RNA-seq and qPCR experiments. ....	212
Supplementary Figure III. Melt curves produced from a qPCR experiment for each gene and sample analysed for validation of gene expression .....	217
Supplementary Figure IV. A Venn diagram illustrating the commonly expressed genes between CD138 <sup>dim</sup> cells from H929 and JLN3 cells and U937 cells treated with PMA .....	218
Supplementary Figure V. CXCL8 related genes significantly differentially expressed after co-culture with differentiated U937 cells .....	219
Supplementary Figure VI: Von kossa staining of calcified secretions produced by SAOS-2 cells .....	220

## List of Tables

Table 1.1: Proportions of heavy and light-chain immunoglobulin distributions in myeloma patients. ....	4
Table 1.2: Prognostic criteria and overall survival of patients defined in the International Staging System for patients diagnosed with multiple myeloma.....	15
Table 1.3: Prognostic criteria and overall survival of patients defined in the Revised International Staging System for patients diagnosed with multiple myeloma. ....	16
Table 2.1. Components of a PCR master mix to assess for presence of mycoplasma .....	42
Table 2.2. PCR cycling times and temperatures to facilitate PCR reaction .....	42
Table 2.3. Fluorescently conjugated monoclonal antibodies selected to assess surface marker expression of myeloma cells.....	48
Table 2.4. Fluorescently conjugated monoclonal antibody used to assess surface expression of RANK on U937 cells.....	50
Table 2.5. Components of Acid phosphatase staining kit used to assess expression of TRAP in U937 cells. ....	51
Table 2.6. Summary of conditions and samples used to produce RNA extracts and their corresponding identifiers .....	53
Table 2.7. A summary of the comparisons made to assess differential gene expression between each sample.....	56
Table 2.8. Components of a High Capacity cDNA Reverse Transcription Kit used to generate cDNA from RNA extracts.....	57
Table 2.9. Optimal temperature and time settings input into a Veriti DX thermocycler .....	57
Table 2.10. A list of target genes and corresponding forward and reverse primer pairs to be used in qPCR analysis .....	59
Table 2.11. Components of a qPCR master mix containing SYBR® Green to make a single 15µL reaction .....	60
Table 2.12. Stages of thermocycling throughout a qPCR reaction to facilitate cDNA denaturation, primer annealing and production of cDNA amplicons .....	60
Figure 3.8 (continued). Image of ivory disks stained with toluidine blue following culture with treated U937 cells.....	82
Table 2.6. Summary of conditions and samples used to produce RNA extracts and their corresponding identifiers .....	109
Table 4.1. A summary and description of genes selected for validation using qPCR .....	136
Table 4.2a. Overrepresented pathways produced from CD138 <sup>dim</sup> H929 and JN3 myeloma cells that are directly related to cytokine and chemokine signalling .....	146
Table 4.2b. Functional descriptions of overrepresented pathways produced from CD138 <sup>dim</sup> H929 and JN3 myeloma cells that are directly related to cytokine and chemokine signalling. ....	147
Table 4.3. Overrepresented pathways produced from CD138 <sup>dim</sup> H929 and JN3 myeloma cells that are directly related to growth and proliferation signalling.....	148
Table 4.4. Overrepresented pathways produced from CD138 <sup>dim</sup> H929 and JN3 myeloma cells that are directly related to adhesion, angiogenesis, motility and metastasis signalling .....	149
Table 5.1. Summary of the identity and function of surface markers used in immunophenotyping of myeloma cells .....	162
Table 5.2. A functional summary of adhesion-related antigens. ....	171
Supplementary Table I. A table containing a list of the commonly overrepresented pathways in both H929 and JN3 CD138 <sup>dim</sup> cells when compared with respective CD138 <sup>bright</sup> monoculture controls .....	215

## Abbreviations

<b>Abbreviation</b>	<b>Description</b>
<i>1,25(OH)<sub>2</sub>D<sub>3</sub></i>	1,25-dihydroxyvitamin D <sub>3</sub> /Calcitriol
<i>ASCT</i>	Autologous stem cell transplant
<i>ATP</i>	Adenosine triphosphate
<i>BCMA</i>	B-cell maturation antigen
<i>bFGF</i>	Basic fibroblast growth factor
<i>BMSC</i>	Bone marrow stromal cell
<i>C</i>	Cyclophosphamide
<i>CAM-DR</i>	Cell adhesion mediated drug resistance
<i>CAR</i>	Chimeric antigen receptor
<i>CD</i>	Cluster of differentiation
<i>cDNA</i>	Complementary RNA
<i>cIAP</i>	Cellular inhibitor of apoptosis protein
<i>CRAB</i>	Calcium, renal failure, anaemia, bone lesions
<i>CXCL</i>	C-X-C motif chemokine ligand
<i>CXCR</i>	C-X-C motif chemokine receptor
<i>D</i>	Dexamethasone
<i>d</i>	Daratumumab
<i>DE</i>	Differentially expressed
<i>DKK-1</i>	Dickkopf WNT signalling pathway inhibitor 1
<i>DNA</i>	Deoxyribonucleic acid
<i>EC</i>	Endothelial cell
<i>ECM</i>	Extracellular matrix
<i>EFS</i>	Event-free survival
<i>EMD</i>	Extramedullary disease
<i>FGFR3</i>	Fibroblast growth factor receptor
<i>FISH</i>	Fluorescence in situ hybridisation
<i>FITC</i>	Fluorescein isothiocyanate
<i>FLC</i>	Free light-chain
<i>FSC</i>	Forward scatter
<i>HMCB</i>	H929 CD138 <sup>bright</sup> mono-culture
<i>HUCB</i>	H929 CD138 <sup>bright</sup> U937 co-culture
<i>HUCD</i>	H929 CD138 <sup>dim</sup> U937 co-culture
<i>ICAM</i>	Intracellular adhesion molecule
<i>Ig</i>	Immunoglobulin
<i>IGF</i>	Insulin-like growth factor
<i>IgH</i>	Immunoglobulin heavy chain
<i>IL6</i>	Interleukin-6
<i>IL8/CXCL8</i>	Interleukin-8
<i>iMID</i>	Immunomodulatory drug
<i>IMWG</i>	International Myeloma Working Group
<i>ISS</i>	International Staging System
<i>JMCB</i>	JJN3 CD138 <sup>bright</sup> mono-culture
<i>JUCB</i>	JJN3 CD138 <sup>bright</sup> U937 co-culture
<i>JUCD</i>	JJN3 CD138 <sup>dim</sup> U937 co-culture
<i>M</i>	Melphalan
<i>M-CSF</i>	Macrophage colony stimulating factor
<i>mAB</i>	Monoclonal antibody
<i>MGUS</i>	Monoclonal gammopathy of undetermined significance
<i>MM</i>	Multiple myeloma
<i>MMP</i>	Matrix Metalloproteinase
<i>MMSET</i>	Multiple myeloma SET domain containing protein
<i>MRI</i>	Magnetic resonance imaging

<i>mRNA</i>	Messenger RNA
<i>N</i>	Ixazomib (Ninlaro)
<i>NF-κB</i>	Nuclear factor kappa-light-chain-enhancer of activated B cells
<i>NICE</i>	National Institute for Health and Care Excellence
<i>NIK</i>	NF-κB inducing kinase
<i>OPG</i>	Osteoprotegerin
<i>OS</i>	Overall survival
<i>P</i>	Pomalidomide
<i>PBMC</i>	Peripheral blood mononuclear cell
<i>PBS</i>	Phosphate buffered saline
<i>PCA</i>	Principal component analysis
<i>PCL</i>	Plasma cell leukaemia
<i>PE</i>	Phycoerythrin
<i>PerCP</i>	Peridinin Chlorophyll Protein
<i>PFS</i>	Progression-free survival
<i>PI</i>	Propidium Iodide
<i>PMA</i>	Phorbol 12-myristate 13-acetate
<i>qPCR</i>	Quantitative real-time polymerase chain reaction
<i>R</i>	Lenalidomide (Revlamid)
<i>R-ISS</i>	Revised International Staging System
<i>RANK</i>	Receptor activator of NF-κB
<i>RANKL</i>	Receptor activator of NF-κB ligand
<i>Rb</i>	Retinoblastoma protein
<i>RNA</i>	Ribonucleic acid
<i>RNA-seq</i>	RNA sequencing
<i>RPMI 1640</i>	Roswell Park Memorial Institute 1640 media
<i>RUNX</i>	Runt-related transcription factor
<i>SCID</i>	Severe combined immunodeficiency
<i>SD</i>	Standard deviation
<i>SEM</i>	Scanning electron microscopy
<i>SMM</i>	Smouldering multiple myeloma
<i>SSC</i>	Side scatter
<i>T</i>	Thalidomide
<i>TRAF</i>	TNF-receptor associated factor
<i>V</i>	Bortezomib (Velcade)
<i>VCAM</i>	Vascular cell adhesion molecule
<i>VEFG</i>	Vascular endothelial growth factor
<i>WM</i>	Waldenström's macroglobulinemia

## CHAPTER 1: Introduction

### 1.1. Multiple Myeloma

The first clinical account of multiple myeloma was reported by Dr Samuel Solly in 1844<sup>1</sup>. Myeloma is now recognised as the second most common haematological malignancy diagnosed in the Western World<sup>2</sup>. It is defined by the accumulation and clonal expansion of terminally differentiated CD138<sup>+</sup>CD38<sup>+</sup> B-lymphocytes – known as plasma cells – in the bone marrow microenvironment<sup>3</sup>. Myeloma is characterised by the excessive secretion of dysfunctional monoclonal immunoglobulin, commonly known as paraprotein. In turn, this characteristic can be utilised in the detection, diagnosis and post-treatment monitoring of multiple myeloma and its associated non-malignant precursor condition, monoclonal gammopathy of undetermined significance (MGUS). Myeloma clinically manifests in end-organ damage that leads to renal impairment, hypercalcaemia, anaemia, recurrent infections and the formation of bone lesions, which are caused by the catastrophic manipulation of the homeostatic process of bone remodelling<sup>4</sup>.

Although the introduction of new targeted therapies has led to an improvement in patient response rates, this malignancy remains incurable with approximately half of all patients surviving for less than 5 years post-diagnosis<sup>5</sup>. It is clear that myeloma cells rely heavily on the bone marrow microenvironment, which contributes to enhanced proliferation, survival and resistance against therapeutic intervention<sup>6</sup>. It is within this microenvironment that drug resistant cells often accrue, ultimately leading to patient relapse, with the duration of remission usually being found to decrease with every treatment course a patient receives<sup>7,8</sup>. Understanding the interactions and mechanisms of the reliance that malignant plasma cells have on the bone marrow is of great interest and importance to counteract these protective effects. This could lead to the identification of new therapeutic targets and provide a rationale to develop more effective treatment strategies for myeloma patients.

### 1.1.1. Epidemiology of myeloma

Multiple myeloma, whilst considered a relatively rare neoplasm, accounts for 13% of all blood cancer diagnoses with an average age-adjusted incidence rate of approximately 5.6 cases per 100,000 persons per year<sup>2</sup>. Worldwide, 0.8% of all cancer diagnoses and 1% of all cancer deaths are attributed to myeloma. The incidence of myeloma is hugely variable according to ethnicity, with black populations experiencing greater incidences of diagnoses than white populations, at a ratio of 2:1<sup>2</sup>. The global regions of highest myeloma incidence occur in Australasia, Europe and North America<sup>9</sup>. Asian populations experience the lowest incidence rates of myeloma, however studies have recently reported significant increases of incidence in Asian countries<sup>10</sup>. Myeloma diagnoses are also more common in males than females (58% vs 42%)<sup>2</sup>. Whilst the exact causes of this discrepancy are widely unknown, there is evidence to suggest that there are gender-dependent differences in primary genetic aberrations observed in myeloma; one study showed that males experienced a greater frequency of hyperdiploidy (62% vs 50%), whilst females had a higher incidence of immunoglobulin heavy chain gene (IgH) translocations (32% vs 50%)<sup>11</sup>.

The average age of myeloma patients at diagnosis is 66, with 38% of diagnoses occurring in patients over the age of 70. Myeloma is considerably rarer in younger patients, with just 2% of diagnoses occurring in patients under the age of 40 years old<sup>12,13</sup>. The current overall 5-year survival rate of patients is 51.6% for symptomatic patients. Myeloma survival steadily decreases with increasing age and patients who are younger than 50 years at diagnosis present with more favourable prognostic features and have significantly higher 5-year survival rates than patients older than 50 years<sup>14</sup>.

### 1.1.2. Aetiology of myeloma

The exact origin and cause of multiple myeloma has been disputed since its discovery. It is now well-established that symptomatic myeloma is a product of clinical progression from the asymptomatic condition monoclonal gammopathy of undetermined significance (MGUS)<sup>15</sup>. However, to date there has been no definitive identification of an individual aetiological event attributed to the origin of myeloma or its asymptomatic precursors. There are environmental, lifestyle and occupational risk

factors associated with an increased risk of myeloma development including obesity and poor diet<sup>16</sup>. There has also been some evidence to suggest that farmers experience an elevated risk of developing myeloma, which could be attributed to high levels of exposure to agricultural chemicals<sup>17,18</sup>. To date, little is known about hereditary associations in myeloma aetiology. Overall it is not considered to be an explicitly inherited malignancy, however some studies have reported familial links that lead to a significant increase in risk of myeloma development in family members with first degree relatives who have myeloma<sup>19,20</sup>.

### 1.1.3. Plasma cell biology

Plasma cells are terminally differentiated, post-germinal cells of B-lymphocyte lineage that home to and mature within the bone marrow microenvironment – which plays a crucial role in ensuring their prolonged survival<sup>21</sup>. Despite existing in very small proportions – representing just 1-3% of cells within the bone marrow – plasma cells are responsible for all antigen-specific antibody secreted in circulation<sup>22</sup>. B-lymphocytes are generally categorised as either follicular B-cells or marginal-zone B-cells that are activated in T-cell dependent or independent fashion, respectively. Upon activation, these B-cells proliferate within germinal centres in the lymph nodes and spleen, with a small number of these cells actively dividing to become short-lived antibody-secreting plasmablasts that ultimately differentiate into long-lived plasma cells in the bone marrow<sup>23</sup>. These cells are primarily responsible for the secretion of monoclonal antibody into peripheral circulation which are defined by the following isotypes: IgG, IgA, IgM, IgE and IgD. These isotypes are inferred by the immunoglobulin heavy chain (IgH) sequence after the process of class switch recombination and can also be further categorised by light-chain classification as either kappa ( $\kappa$ ) or lambda ( $\lambda$ )<sup>24</sup>.

The majority of myeloma patients present with either IgG (52%) or IgA (21%) paraprotein<sup>12</sup>. IgM-myeloma is a very rare form of this plasma cell neoplasm and is associated with poor survival outcomes. It shares numerous diagnostic characteristics with Waldenström's macroglobulinemia (WM) making it difficult to differentiate between these two disorders. However, the presence of end organ damage observed in myeloma, such as the formation of bone lesions, is exclusive to myeloma and not

WM<sup>25</sup>. There has also been a cytogenetic association made between the presence of the t(11;14) translocation and IgM myeloma, which again could distinguish it from WM<sup>26</sup>.

The presentation of IgD and IgE-myeloma are also considerably rarer than IgG, IgA and light-chain secretory myeloma. IgD-myeloma accounts for approximately 2% of all diagnoses and is associated with diagnosis at younger age, more aggressive disease and poorer prognosis compared with more common IgH subtypes<sup>27,28</sup>. The incidence of IgE-myeloma is incredibly uncommon, with only around 50 cases being reported in the literature<sup>29</sup>. It has been reported that up to 7% of myeloma patients are classed as non-secretors, although since the introduction of the serum free light-chain assay, it has been demonstrated that the majority of these cases were in fact oligo-secretors. This has now led to approximately 1-2% of newly diagnosed multiple myeloma patients being classified as true non-secretors<sup>30,31</sup>.

<i>IgH classification</i>	<i>Light-chain classification</i>	<i>Proportion of myeloma patients (%)</i>
<i>IgG</i>	κ	34
	λ	18
<i>IgA</i>	κ	13
	λ	8
<i>IgD</i>	κ	1
	λ	1
<i>IgM</i>	κ	0.3
	λ	0.2
<i>Free light chain (Bence Jones protein)</i>	κ	9
	λ	7
<i>Non-secretory</i>	-	7

**Table 1.1: Proportions of heavy and light-chain immunoglobulin distributions in myeloma patients.**  
Data obtained from Kyle. RA *et al*, 2003<sup>12</sup>.

#### 1.1.4. Surface phenotype of myeloma cells

The expression of surface markers is key to determining the identity of cells that are not able to be distinguished solely through the assessment of morphological features.

This means that cells can be correctly identified through the analysis of their unique surface expression profile, which in the case of myeloma is critical for confirming the relative number of malignant plasma cells within the bone marrow to establish a diagnosis. Myeloma is a malignancy that demonstrates significant heterogeneity, however there are common features of plasma cells that can be utilised to determine disease progression and response to therapy<sup>32</sup>. This is particularly useful in the detection of residual myeloma cells that remain present within the bone marrow following treatment, known as minimal residual disease (MRD).

Syndecan-1, also known as CD138, is a membrane-bound receptor of the heparin sulphate proteoglycan family<sup>33</sup>. It acts as an extracellular matrix receptor and has important functions primarily relating to plasma cell adhesion to the extracellular matrix of the bone marrow<sup>34,35</sup>. Amongst cells of haematopoietic origin, CD138 is exclusively expressed on plasmablasts and mature plasma cells, following differentiation from B-lymphocytes<sup>36</sup>. This characteristic is also true of malignant plasma cells, making CD138 an excellent marker for the identification of myeloma cells in the bone marrow and peripheral blood<sup>37</sup>. Loss of CD138 through membrane shedding, leading to an increased level of soluble CD138, has also been linked with poor prognosis in patients<sup>38</sup>. The presence of CD138<sup>neg</sup> myeloma cells has also been reported in a number of myeloma-related studies in both primary malignant plasma cells derived from patients and myeloma cell lines<sup>39,40</sup>. These studies have demonstrated that CD138<sup>neg</sup> myeloma cells have greater clonogenic capacity and infer increased resistance against established treatments<sup>41-43</sup>. These cells have also been speculated to possess stem cell-like properties and considering the inevitable relapse of myeloma patients after treatment, it has been hypothesised that CD138<sup>neg</sup> cells are responsible for the regrowth of myeloma tumour sites within the bone marrow<sup>44</sup>.

The expression of CD38 is another key phenotypic characteristic of myeloma cells, to such an extent that it has been recently highlighted for therapeutic targeting using the monoclonal antibody treatment, daratumumab<sup>45</sup>. Whilst the expression of this marker is also found on a number of other cells of haematopoietic origin, it is much more highly expressed on the surface of myeloma cells. Its combination of expression with CD138 is highly specific to the myeloma surface phenotype. These two markers are

often recommended to be used in the primary gating strategy during flow cytometric analysis of myeloma cells<sup>46</sup>.

Despite these well-established markers that can be detected using flow cytometry to identify malignant plasma cells in patients, the heterogenic nature of this malignancy inherently means that the phenotype of these cells can differ between patients and alter throughout the course of treatment. Other markers also recommended for neoplastic plasma cell identification include CD45, a pan-leucocyte marker which is known to be expressed at varying levels in neoplastic plasma cells, CD19 which is lost from the surface of myeloma cells following terminal differentiation from mature B-cells<sup>47</sup>, and CD56, an adhesion marker which is found to be expressed on malignant plasma cells in up to 80% of patients. Lack of CD56 expression is indicative of late stage disease and poor prognosis<sup>48</sup>. Additional markers that can also be included in MRD analysis include CD27, CD81, CD200 and CD117, all of which have been previously identified as markers that most frequently deviate from the phenotype of normal plasma cells<sup>49</sup>.

#### **1.1.5. Development and progression of myeloma**

Multiple myeloma is a bone marrow residing plasma cell neoplasm that evolves from a pre-malignant state (MGUS) and in some cases eventually develops into symptomatic disease (Figure 1.1). Infrequently, patients may also clinically progress to extramedullary disease and plasma cell leukaemia where plasma cells escape the bone marrow microenvironment and infiltrate peripheral circulation and home to other tissues and organs such as the liver and kidneys, which often occurs in relapsed/refractory patients and infers very poor prognosis<sup>50</sup>.

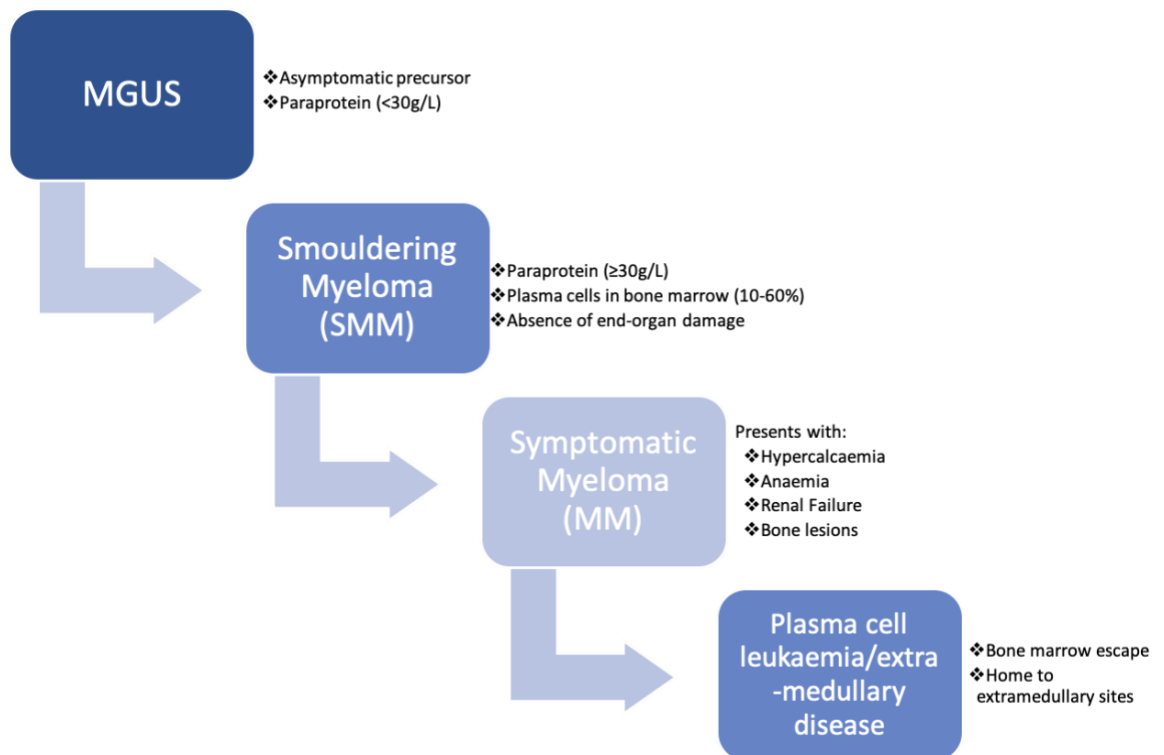


**Figure 1.1: Stages of multiple myeloma development.** The plasma cell gammopathies that are involved in progression from MGUS to symptomatic myeloma and end-stage disease, coupled with associated symptoms and physiological and diagnostic characteristics.

#### 1.1.5.1. Monoclonal Gammopathy of Undetermined Significance (MGUS)

Monoclonal gammopathy of undetermined significance (MGUS) is an asymptomatic condition that represents an accumulative life-long risk of progression to symptomatic myeloma. Whilst not all cases of MGUS progress to symptomatic myeloma, it is well established that myeloma is consistently preceded by MGUS<sup>15</sup>. Progression from MGUS to symptomatic myeloma occurs at a consistent rate of 1.5% per year<sup>51</sup>. MGUS is considerably more common in the general population than myeloma and affects approximately 3.2% of people over 50 years of age<sup>52</sup>. It is often detected accidentally when patients present with other unrelated co-morbidities. As a result, it is reasonable to assume that current epidemiological data relating to MGUS might be biased to an extent that could suggest that a much greater proportion of patients across the country could be clinically classified as having MGUS.

MGUS is clinically diagnosed in patients demonstrating elevated levels of serum paraprotein <30g/L, a bone marrow plasma cell proportion of <10% and an absence of

end organ damage that is commonly associated with symptomatic myeloma<sup>53</sup>. Patients with MGUS are not recommended for treatment and are only required to be monitored for disease progression to smouldering or symptomatic myeloma. However, due to MGUS commonly being diagnosed as a coincidental finding in association with other co-morbidities, it is difficult to ascertain the extent to which MGUS might be a contributing factor towards such clinical manifestations. Although there is evidence to suggest that patients diagnosed with MGUS do demonstrate a clinical relationship with increased infections, osteoporosis, thrombosis and other associated malignancies including myelodysplastic syndrome (MDS)<sup>54</sup>. This is arguably to be expected given that the categorisation of MGUS constitutes a clinically significant clonal expansion of plasma cells, which whilst not manifesting in end-organ damage such as renal failure or anaemia, can certainly contribute to increased bone fragility and thrombotic risk.

Whilst the exact cause(s) of transition from MGUS to myeloma is currently unknown, there are factors that have been taken into consideration that account for relative risk of progression. Abnormal kappa/lambda serum free light-chain ratios (normal reference: 0.26-1.65mg/L) have been shown to elude to an increased risk of progression to myeloma from MGUS<sup>55,56</sup>. Paraprotein type and quantity in the blood has also been considered a risk factor, with a non-IgG subtype coupled with a paraprotein count >15g/L being linked with greater risk of progression from MGUS to myeloma<sup>56</sup>. The International Myeloma Working Group (IMWG) general consensus is for low-risk patients (paraprotein <15g/L, IgG subtype, normal FLC ratio (0.26-1.65)) to be monitored every 2-3 years and intermediate to high-risk patients (paraprotein >15g/L, non-IgG subtype, abnormal FLC ratio (0.26-1.65)) being recommended for monitoring 6 months after diagnosis followed by annual follow-up<sup>57</sup>.

#### *1.1.5.2. Smouldering Multiple Myeloma (SMM)*

Smouldering multiple myeloma is an intermediate and commonly asymptomatic condition that succeeds MGUS and precedes symptomatic myeloma. It is defined by detection of serum paraprotein ( $\geq 30\text{g/L}$ ) and an elevated bone marrow plasma cell count ( $\geq 10\%$ ), but in the same manner as MGUS, SMM does not manifest in end-organ damage<sup>53</sup>. The rate of progression from SMM to myeloma is time-dependent, unlike the rate of progression from MGUS which remains constant<sup>51</sup>. The risk of progression

from SMM to myeloma is approximately 10% in the first 5 years following diagnosis, 3% for the next 5 years and 1% per following year<sup>58</sup>. Approximately 3.2% of patients diagnosed with SMM possess a clonal plasma cell count  $\geq 60\%$ . Of this subgroup of patients, reports have highlighted between 80-95% have been found to progress to symptomatic myeloma within 2 years and were found to have a significantly poorer prognosis when compared with patients with a clonal plasma cell count  $< 60\%$ <sup>59,60</sup>. There is also evidence that an abnormal serum free light-chain ratio ( $> 100$ ) signifies an independent prognostic factor that increases risk of progression to symptomatic myeloma<sup>61,62</sup>. These patients have also been shown to present with two or more focal bone lesions as identified through MRI scanning. As a result, the criteria for the diagnosis of symptomatic myeloma were updated to include these biomarkers of increased risk of progression from smouldering to symptomatic myeloma and are collectively known as the SLiM-CRAB criteria<sup>63</sup>. Therefore, patients with SMM who are at very high-risk of developing symptomatic myeloma are now recommended to undergo appropriate treatment<sup>63</sup>.

#### 1.1.5.3. Symptomatic myeloma

Diagnosis of myeloma is defined by the presence of paraprotein in the serum or urine of patients ( $\geq 30\text{g/L}$ ) and an elevated bone marrow clonal plasma cell count ( $\geq 10\%$  or  $\geq 60\%$ ). Myeloma is a clinicopathological disorder and requires evidence of end organ damage in order to fulfil a diagnosis. End organ damage presents in the form of hypercalcaemia, renal impairment, anaemia and osteolytic bone lesion formation commonly referred to as CRAB<sup>63</sup>. The most recent update to the diagnostic criteria for myeloma was defined by the International Myeloma Working Group (IMWG) and included the involved:uninvolved serum-free light chain ratio  $\geq 100$  as a diagnostic factor<sup>63</sup>. Fluorescence *in situ* hybridisation (FISH) on CD138-selected bone marrow plasma cells is also recommended to identify genetic aberrations that are linked to disease prognosis.

Clinical presentation of myeloma often begins with bone pain which occurs in 80% of patients<sup>12</sup>. This is primarily caused by myeloma-induced upregulation of bone-resorbing activity from cells known as osteoclasts, coupled with downregulation of bone-producing activity from cells known as osteoblasts. Consequently, this leads to a

net increase of bone resorption resulting in the formation of painful bone lesions in patients which frequently leads to spontaneous fractures that often occur at sites of red bone marrow such as the ribs, spine, skull and pelvis<sup>64</sup>. The presence of these osteolytic bone lesions are monitored by MRI scans that are able to quantify their number and distribution throughout the skeleton<sup>63</sup>. Hypercalcaemia – elevated concentration of calcium in the blood – is a symptom that develops as a direct consequence of osteoclast-mediated bone resorption which results in the excessive efflux of calcium into the serum. Whilst reducing tumour burden is known to directly influence bone lesion formation and hypercalcaemia, these myeloma-associated morbidities are additionally treated with bisphosphonates such as zoledronic acid and pamidronate to alleviate these symptoms through inhibition of osteoclast activity through the induction apoptosis in these cells<sup>65,66</sup>.

It is estimated that approximately 20% of myeloma patients present with renal failure at diagnosis, with up to 50% of patients experiencing impaired renal function over the course of their disease<sup>67</sup>. This is measured by an increase in the levels of serum creatinine (>20mg/L). Cast nephropathy is the leading cause of renal damage in myeloma patients and is attributed to 90% of these cases. The cause of this is a result of excessive secretion of free light chains into the blood, which in turn puts immense physiological pressure on the kidney's filtration mechanisms that leads to nephrotic damage. Free light chains are normally filtered through the glomerulus and reabsorbed in the proximal tubules of the nephron, however in myeloma the resorptive capacity of this mechanism is vastly exceeded leading to the formation of protein casts in the distal tubules<sup>68</sup>. This characteristic can also be utilised as a diagnostic criterion of myeloma through the detection of free light chains in the urine, also known as Bence Jones protein. Patients who present with more advanced instances of renal failure can be recommended for dialysis to replace aberrant kidney function. Reduction of tumour burden with established therapies has been attributed to reducing these symptoms<sup>69</sup>.

Patients also commonly develop recurrent bacterial and viral infections, which is the leading cause of death in myeloma. Approximately 22% of myeloma-related deaths occurring as a result of infection after 1 year, post-diagnosis<sup>70</sup>. These infections are a result of immunodeficiency caused by a decrease in the abundance of CD19<sup>+</sup> B-cells

and CD4<sup>+</sup> and CD8<sup>+</sup> T-cells, coupled with defects in dendritic and natural killer cell function<sup>71</sup>. Despite significant advances in myeloma treatment, these more intense regimens incorporating newer novel agents have also been found to impair immune function whilst also inducing positive responses in reducing tumour burden<sup>72</sup>.

#### *1.1.5.4. Extramedullary disease*

Extramedullary disease (EMD) is a diagnosis used to describe myeloma cells that have escaped the bone marrow and infiltrated the peripheral circulation that presents as plasma cell leukaemia. These circulating myeloma cells are also capable of invading foreign tissue to form soft-tissue plasmacytomas<sup>73</sup>. Plasma cell leukaemia (PCL) is a highly aggressive dyscrasia that is classed either as primary, when it is detected at the point of diagnosis, or secondary, when it arises as part of end-stage leukemic transformation from multiple myeloma following relapse from treatment. Both primary and secondary classifications arise as a result of malignant progression from multiple myeloma that occurs in very high-risk patients, with the proportions of plasma cell leukaemia patients who develop either primary or secondary disease being approximately 1:1. Plasma cell leukaemia occurs in approximately 4% of myeloma patients, confers very poor prognosis as a result of a high-risk genetic signature and is associated with short remissions, with median survival reported as being as low as 1.3 months<sup>74</sup>. It is characterised by malignant plasma cell escape from the bone marrow microenvironment into peripheral circulation with a percentage proportion of  $\geq 20\%$  and an absolute count of  $\geq 2 \times 10^9$  circulating plasma cells<sup>75</sup>. Secondary plasma cell leukaemia occurs at the end-stage of myeloma disease and occurs in patients who have been heavily pre-treated thus becoming refractory to treatment. Therefore, given the extremely short survival times of these patients, emphasis is generally placed on appropriate supportive care and palliative treatment<sup>76</sup>.

Following escape from the bone marrow microenvironment, myeloma cells can also invade other tissues to form plasmacytomas on bone material local to the site of the primary tumour or in distant soft tissue organs. The location of these soft-tissue secondary tumour sites can vary between patients with the most common appearing in the skin, liver and lymph nodes<sup>77</sup>. The overall survival of patients with soft tissue plasmacytomas is significantly shorter than patients with local bone plasmacytomas

and patients who have not progressed to EMD, with studies reporting an overall survival of just 5 months in these patients<sup>78</sup>.

#### 1.1.6. Genetic aberrations

Genetic abnormalities have been attributed to the pathogenesis and progression of all known cancers. In myeloma, these genetic alterations are commonly divided into two broad subgroups: primary events – which are considered as factors in disease initiation and subsequent progression from MGUS – and secondary events – which are considered to accumulate throughout myeloma disease progression and contribute to relapse and resistance to therapy (Figure 1.2)<sup>79</sup>. Both of these subgroups have impacts on patient prognosis with over 90% of patients possessing at least 1 chromosomal abnormality that can be identified by FISH analysis<sup>80,81</sup>.

Primary genetic initiating events involve either hyperdiploidy, defined by trisomies of 2 or more odd-numbered chromosomes, or chromosomal translocations involving the immunoglobulin heavy chain gene locus. Although an overlapping proportion of 10% of patients with both of these aberrations have been reported<sup>79,80</sup>. The most common primary translocation events associated with myeloma relate to upregulation of cyclin D proteins that enable myeloma cells to acquire indefinite replicative capacity. Translocations that contribute to this include t(11;14) and t(6;14) which affect the activity of cyclin D1 and D3, respectively. These are early initiating events in myeloma pathogenesis and occur in approximately 20% of all myeloma cases<sup>82</sup>. Other primary translocations include t(4;14), which causes increased expression of FGFR3 and MMSET and t(14;16) which upregulates c-MAF activity. Both of these translocations have been found to influence cyclin D2 activity and occur in approximately 15% and 5% of patients, respectively<sup>82-84</sup>.

The deletion of chromosome 13 is the most common genetic abnormality in myeloma and has been identified in approximately 50% of myeloma patients<sup>85</sup>. There is also evidence showing that up to 40% of MGUS patients also possess this chromosomal loss<sup>86,87</sup>. This implies that this genetic event could be an early event in myeloma pathogenesis, or it could be accumulated at a later stage of disease progression. It can manifest either as a deletion – del(13q) – or through monosomy of chromosome 13<sup>88</sup>.

It is also closely associated with a primary t(4;14) translocation with 90% of patients possessing this translocation having also been identified with a chromosome 13 abnormality<sup>89,90</sup>.

Arguably, the most unfavourable secondary genetic aberration associated with myeloma is del(17p) which results in the loss of p53 expression and is present in approximately 11% of patients and infers very poor prognosis in patients<sup>81</sup>. Other secondary genetic aberrations include activating mutations in RAS oncogenes, which have been found to be present in 7% MGUS patients, 25% symptomatic myeloma patients and 45% of relapsed patients and is associated with greater tumour burden and poorer prognosis<sup>91</sup>. The activity of c-myc has also been shown to increase throughout myeloma progression with rearrangements in the c-myc oncogene occurring in up to 15% of patients with myeloma<sup>92</sup>. These re-arrangements were also found to correlate with high  $\beta_2$ -microglobulin, which infers more aggressive disease and a poorer prognosis<sup>93</sup>.

Mutations in genes that encode for components of the NF- $\kappa$ B pathway are also present in myeloma, with 17% of patients being reported to possess such mutations that lead to constitutive activation of both canonical and non-canonical branches of this pathway<sup>94</sup>. Mutations that cause an activation in NF- $\kappa$ B signalling occur in genes that encode NIK, CD40, TACI, p50 and p52. Whilst other mutations occur in genes that encode regulators of NF- $\kappa$ B that leads to their inactivation such as TRAF2/3, CYLD and cIAP1/2. Overall however, these mutations favour non-canonical pathway propagation<sup>94,95</sup>.

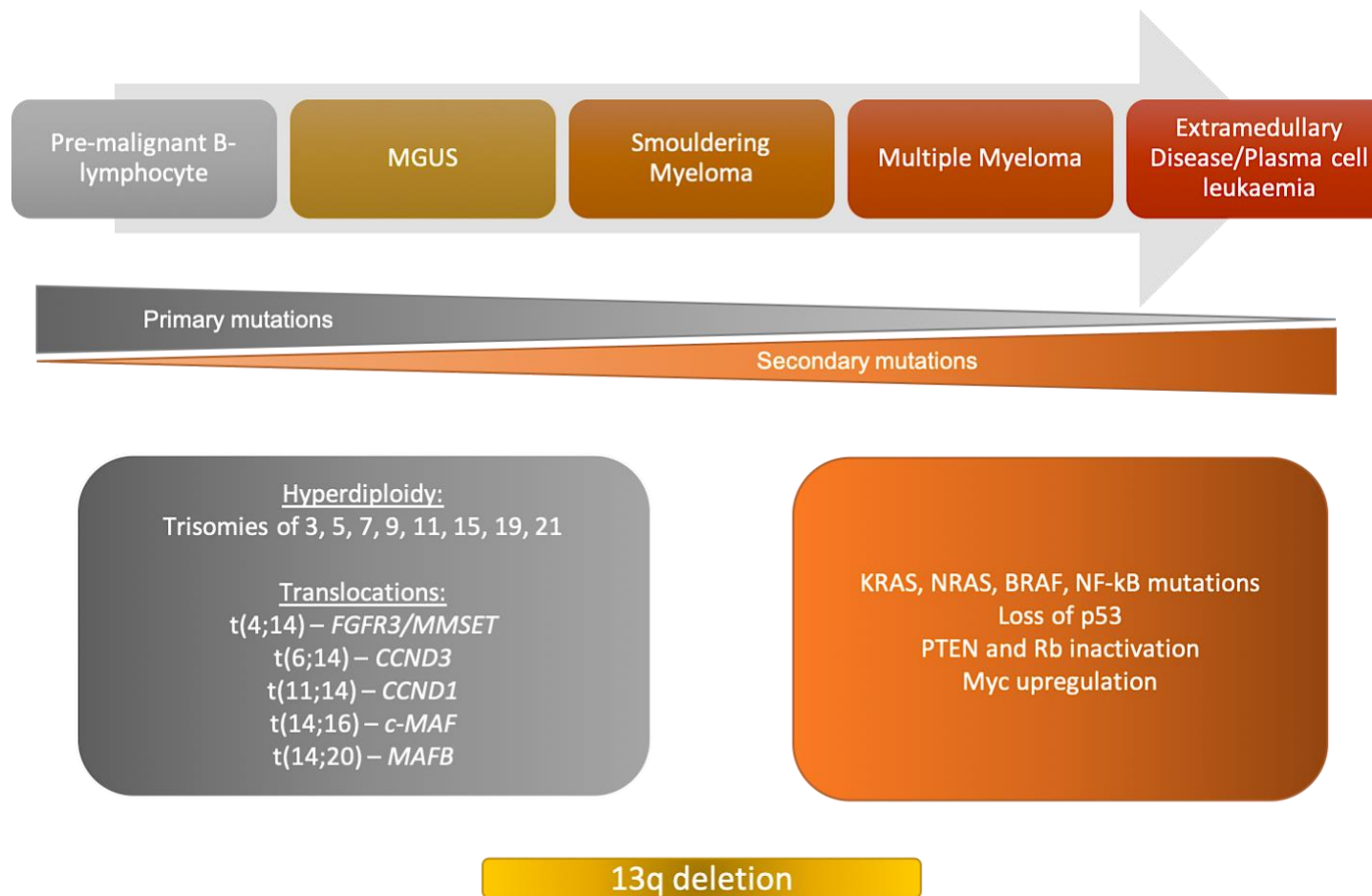


**Figure 1.2: Genetic abnormalities associated with the initiation and progression of multiple myeloma.** A flow chart illustrating the primary genetic initiation events and accumulation of secondary genetic abnormalities that are key to disease progression and have a critical relationship with risk and prognosis. Adapted from ‘Monoclonal gammopathy of undetermined significance and Smouldering Multiple Myeloma: A review of the current understanding of epidemiology, biology, risk stratification and management of myeloma precursor disease’. Agarwal and Ghobrial, 2013 <sup>96</sup>.

### 1.1.7. Myeloma staging and prognostic factors

Whilst the median survival for patients diagnosed with myeloma is approximately 4.9 years, myeloma is a cytogenetically heterogeneous malignancy which accounts for a range of survival times post-diagnosis. This highlights the requirement for an internationally recognised staging system that encapsulates a variety of physiological and genetic characteristics to help predict patient outcomes. The first such system was reported in 1975 by Durie and Salmon who linked tumour burden with the presence of clinical symptoms<sup>97</sup>. However, in 2005, there was a simplification of myeloma staging through the measurement of serum albumin and  $\beta_2$ -microglobulin. These were identified as two independent prognostic markers that defined 3 sub-groups of patient outcomes, which formed the basis of the International Staging System (ISS) for myeloma prognosis (Table 1.2)<sup>98</sup>. Whilst globally respected and commonly utilised, this staging system was criticised for not considering the prognostic significance of myeloma-specific genetic abnormalities. Therefore, this staging system was revised in 2015 (R-ISS) to include LDH serum quantification and fluorescence *in situ* hybridisation (FISH) analysis where high-risk myeloma was defined by del(17p) and/or translocation t(4;14) and/or t(14;16) (Table 1.3). It was found that 28% of patients were staged at R-ISS I, 62% of patients at R-ISS II and 10% of patients at R-ISS III<sup>99</sup>.

ISS Stage	Prognostic Criteria (ISS)	Median OS (months)
I	Serum albumin $\geq$ 35g/L $\beta_2$ -microglobulin <3.5g/dL	62
II	Neither ISS Stage I or III	44
III	$\beta_2$ -microglobulin >5.5mg/L	29

**Table 1.2: Prognostic criteria and overall survival of patients defined in the International Staging System for patients diagnosed with multiple myeloma.** Table adapted from data published in International Staging System for Multiple Myeloma<sup>98</sup>.

(R-)ISS Stage	Prognostic Criteria (Revised-ISS)	PFS (months)	Median OS (months)
I	ISS Stage 1 Standard risk FISH Normal serum LDH	66	Not reached
II	Neither R-ISS Stage I or III	42	83
III	ISS Stage III High-risk FISH and/or high serum LDH	29	43

**Table 1.3: Prognostic criteria and overall survival of patients defined in the Revised International Staging System for patients diagnosed with multiple myeloma.** Table adapted from data published in Revised International Staging System for Multiple Myeloma<sup>99</sup>.

### 1.1.8. Treatment of myeloma

As standard practice, myeloma patients are recommended for treatment immediately after a diagnosis has been made. Patients with MGUS and SMM are monitored for disease progression but are not recommended for treatment until the diagnostic CRAB criteria indicating the presence of symptomatic multiple myeloma are fulfilled, with the exception of high-risk SMM patients with a clonal bone marrow plasma cell count  $\geq 60\%$ , a high FLC ratio  $>100$  (providing tumour FLC  $>100$ ) or 2 or more asymptomatic lytic lesions on cross sectional imaging<sup>63</sup>.

From the late 1960's myeloma was often treated with a combination regimen of the alkylating agent melphalan and the glucocorticoid prednisone, with very few advances in clinical management in subsequent years<sup>100</sup>. However, in the last two decades the number of novel treatments available to patients has increased dramatically, which has led to a significant improvement in clinical outcomes<sup>101</sup>. These new therapies include immunomodulatory drugs (iMIDs), proteasome inhibitors and corticosteroids. Briefly the primary mechanisms of action of each of these classes of drug are described as follows:

- Immunomodulatory drugs such as lenalidomide (a less toxic and more potent analogue of thalidomide) are complex in their action but are known to act through multiple mechanisms that include immune cell modulation through T-cell activation, inhibition of pro-inflammatory cytokine secretion and inhibition of angiogenesis. These drugs not only target myeloma cells themselves but also

contribute to halting the progression of the malignancy through deregulation of the surrounding supportive microenvironment<sup>102</sup>.

- Proteasomes are complex protein structures responsible for the degradation of ubiquitinated proteins within cells<sup>103</sup>. It is known that malignant cells are more reliant on these structures to clear aberrant proteins which are present in much greater abundance when compared with normal cells. This has been demonstrated by the capacity of proteasome inhibitors to induce tumour-specific toxic effects, with bortezomib being the first clinically approved proteasome inhibitor for the treatment of myeloma<sup>104</sup>.
- Corticosteroids such as dexamethasone are long standing treatments used in myeloma therapy and have shown great success in the clinic. Whilst it has been established that these drugs inhibit their receptor, the glucocorticoid receptor, the resulting downstream actions of this inhibition that lead to apoptosis are still disputed. However, there have been a number of studies that have implicated corticosteroids such as dexamethasone in the inhibition of transcription factors such as NF- $\kappa$ B and AP-1<sup>105</sup>.

This advance in the myeloma treatment arsenal means that patients can be treated on a more personalised basis to accommodate the heterogeneity of this malignancy. Decisions made about a patient's treatment are stratified depending on tumour burden, disease stage, cytogenetics, age and treatment history – all of which can be used as indicators of a patient's ability to tolerate and respond to treatment<sup>106</sup>. The most crucial stages of myeloma treatment are induction therapy, autologous stem cell transplant (if eligible), maintenance therapy and treatment of relapsed/refractory disease (Figure 1.3)<sup>5</sup>.

Myeloma is generally a disease of the elderly with approximately two thirds of patients being diagnosed at an age greater than 65<sup>2</sup>. Age is considered an independent prognostic marker in myeloma, with younger patients experiencing better survival outcomes and generally being more capable of tolerating a greater range of treatments at higher doses, as well as autologous stem cell transplant (ASCT)<sup>14,107</sup>.

However, whilst younger, fitter patients are most commonly considered for stem cell transplant, there is evidence of older patients also being able to tolerate high dose therapy and ASCT who are capable of achieving clinical responses similar to those of younger patients<sup>108</sup>. This highlights the importance of using performance factors in addition to age to assess patients' general health when considering treatment options. These include the presence of co-morbidities that affect renal, hepatic and cardiac function as well as considering a patients' frailty relating to fatigue and low levels of physical activity. Such considerations aid clinicians in identifying patients who are at the lowest risk of transplant-related complications and can therefore sufficiently tolerate the procedure<sup>109</sup>.

#### *1.1.8.1. Current treatments*

Treatment is recommended to commence as soon as possible after a myeloma diagnosis has been made. In newly diagnosed patients who are eligible to undergo ASCT, NICE recommends an induction treatment regimen to be administered with the purpose of reducing tumour burden whilst also maintaining a recoverable population of CD34<sup>+</sup> haematopoietic stem cells from peripheral circulation for subsequent transplantation. The recommended course of induction treatment incorporates a combination of bortezomib, thalidomide and dexamethasone<sup>110</sup>. This is collectively known as VTD. It has been shown that the VTD triplet regimen is clinically superior to a VD doublet regimen<sup>111,112</sup>. There is also evidence to suggest that where treatment with thalidomide is not possible, the inclusion of cyclophosphamide (VCD) or lenalidomide (VRD) – a 2<sup>nd</sup> generation thalidomide analogue – is again clinically superior to VD alone<sup>113,114</sup>. The latter of which has been linked to greater progression-free survival in high-risk patients based on t(4;14) and del(17p) cytogenetic abnormalities<sup>115</sup>.

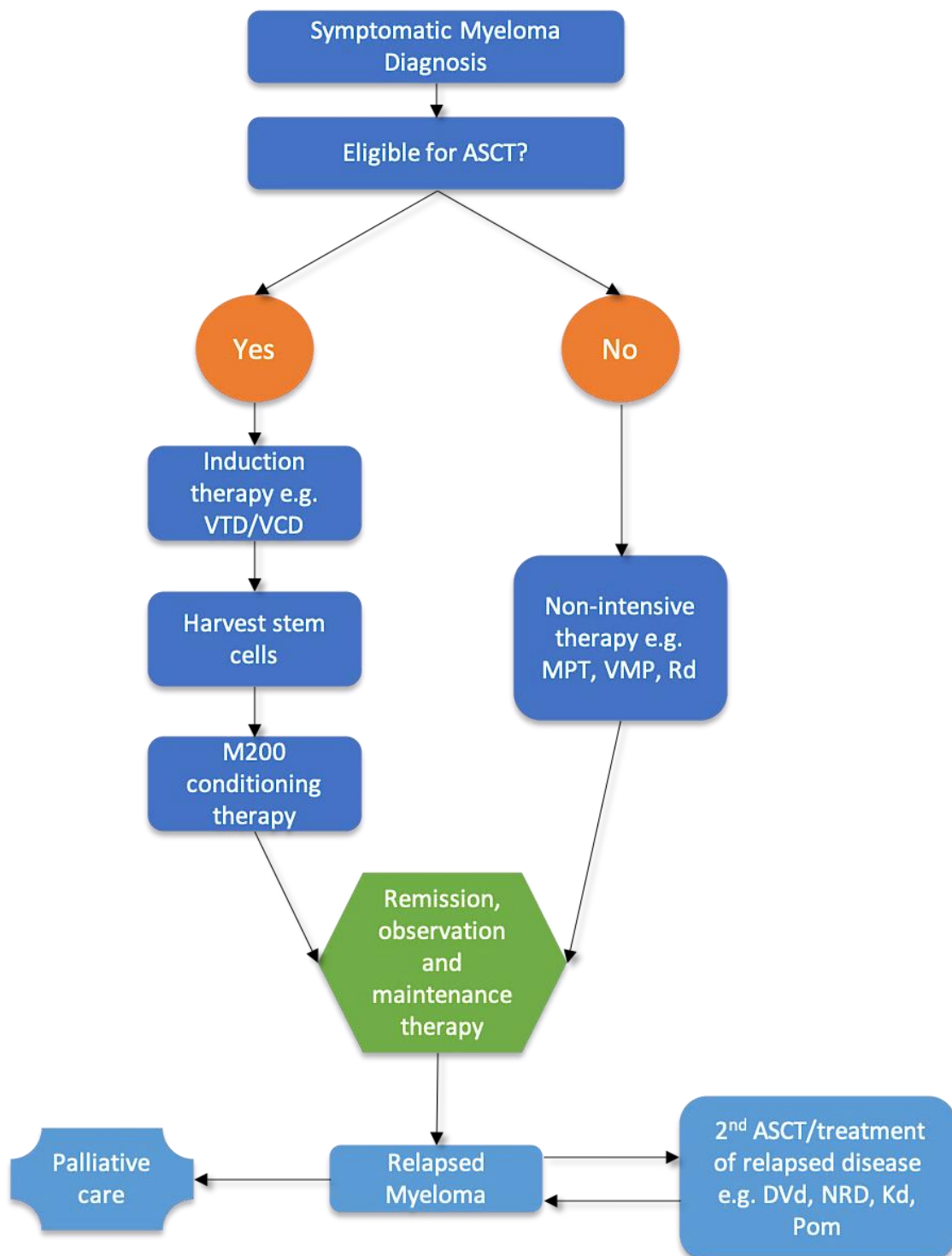


**Figure 1.3: Treatment options for patients diagnosed with multiple myeloma.** A flow chart illustrating the main stages of treatment experienced by myeloma patients who are either eligible or ineligible for ASCT, with examples of the treatment regimens available to them at each stage of disease progression.

The vast majority of patients who are eligible for a stem cell transplant undergo the procedure in an autologous fashion. High dose chemotherapy followed by ASCT has been shown to result in a significant increase in median survival when compared with patients who were only treated with conventional chemotherapy, by up to 12 months<sup>116,117</sup>. Prior to the administration of high dose therapy, stem cells are collected from the patient and cryogenically frozen to be transplanted at a later timepoint. Immediately prior to transplant, patients undergo a conditioning regimen which aims to achieve the best response rate following transplantation. The current standard practice for this is treatment with 200mg/m<sup>2</sup> melphalan<sup>118</sup>. Transplantation can then take place soon after conditioning therapy<sup>119</sup>.

Allogeneic stem cell transplantation has the advantage of eliminating any possible tumour cell contamination from the infused stem cells compared to an autologous stem cell transplant but is far less commonly administered than its autologous counterpart. This is because it is more commonly associated with higher levels of treatment-related mortality due to graft vs host disease and an increased infection risk<sup>120</sup>. There are some conflicting reports over the successful response of allogeneic transplantation compared with autologous transplantation. Two studies compared the difference in outcome in patients who were treated with an auto-auto SCT with patients treated with an auto-allo SCT. One study showed no significant difference between the two tandem transplants<sup>121</sup>, whilst the other demonstrated a superior response in the auto-allo patient cohort<sup>122</sup>. Overall, the general consensus amongst clinicians is that allogeneic stem cell transplantation should not be administered as a standard therapy and should only be considered as a treatment option for younger patients with high-risk disease following a first or second relapse<sup>120</sup>.

Given that approximately two thirds of patients are over the age of 65, the majority of these patients are ineligible for ASCT. The standard therapy for these transplant-ineligible patients is lenalidomide/dexamethasone or melphalan and prednisone combined with bortezomib (VMP), with the latter showing promising outcomes in high-risk patients, similar to the responses observed in standard-risk patients<sup>123,124</sup>.

It is known that the duration of remission has an impact on overall survival, with longer remission periods after initial treatment being linked with greater survival rates<sup>125</sup>. However, an overwhelming majority of myeloma patients experience post-treatment relapse due to the emergence of drug-resistant sub-clones<sup>126,127</sup>. Therefore, efforts to prolong the length of remission forms the rationale of providing patients with maintenance therapy following induction treatment. Lenalidomide treatment represents a promising maintenance strategy post-ASCT, with some studies confirming a significant increase in PFS in lenalidomide-treated patients and one study also demonstrating a significantly enhanced OS<sup>128-130</sup>. Data from the recent Myeloma XI trial has also expanded on these observations and has shown lenalidomide monotherapy maintenance to improve PFS in both transplant eligible and ineligible patients and has been implicated in improving responses in high-risk patients – particularly in patients with del(17p) cytogenetics<sup>131</sup>. However, these studies also reported a considerable number of haematological adverse events and an increase in risk of secondary malignancy development<sup>132</sup>. Whilst the benefits and risks of lenalidomide maintenance must be carefully considered before patient administration, it is accepted that the favourable response to treatment in patients outweighs the fairly minimal risk of secondary malignancy development.

Bortezomib is another option for post-ASCT maintenance therapy and has been shown to improve PFS and OS, particularly in high-risk patients<sup>133</sup>. There has also been data demonstrating bortezomib and lenalidomide being administered as part of a triplet regimen incorporating dexamethasone (RVD), which has shown promising responses regarding PFS and OS in high-risk patients<sup>134</sup>. The use of bortezomib in maintenance therapy can also prolong progression-free survival in transplant ineligible patients. An induction quadruplet regimen of bortezomib, melphalan, prednisone and thalidomide (VMPT) followed by a maintenance regimen of bortezomib and thalidomide (VT) produced superior progression-free survival to just VMP alone<sup>135</sup>.

#### *1.1.8.2. Future treatments*

Progressive or relapsed disease is defined by an increase in serum paraprotein greater than 25% and an increase in bone marrow plasma cell count to >10%. It can also be identified by the identification of new bone lesions or development of further end-

organ damage<sup>136</sup>. The eventual relapse of myeloma patients presents a number of complications regarding treatment options, with the malignancy often becoming refractory to treatments that have previously been administered to the patient. The introduction of new therapies is often initially approved at the point of relapse in myeloma, meaning patients have an increased number of treatment options available to them at this point in the progression of their disease.

There are also a wide array of common side effects that myeloma patients develop in direct response to treatment that most commonly include peripheral neuropathy, nausea, vomiting, severe diarrhoea and skin irritation<sup>137</sup>. It is therefore of importance to develop new treatments that show increased potency and specificity against malignant plasma cells, whilst reducing toxicity in non-malignant cells in order to make these treatments more tolerable for patients.

The introduction of the next generation of proteasome inhibitors – carfilzomib and ixazomib – and the 3<sup>rd</sup> generation immunomodulatory drug pomalidomide are now approved for use in relapsed disease<sup>138-140</sup>. Pomalidomide has been shown to produce favourable clinical responses in patients who have been previously treated with lenalidomide and low-dose dexamethasone<sup>141,142</sup>. Proteasome inhibitors carfilzomib and ixazomib have also shown promising activity as both single agents and in combination regimens with lenalidomide and dexamethasone in relapsed/refractory myeloma<sup>143-145</sup>.

Immunotherapy in myeloma has also produced promising results and has the aim of enhancing the host immune response against malignant cells. Two monoclonal antibodies have recently been approved for treatment of relapsed myeloma. Elotuzumab targets SLAMF7 and has shown clinical efficacy in a triplet regimen with lenalidomide and dexamethasone after failing to produce favourable single agent activity<sup>146</sup>. It has also recently improved clinical responses in combination with pomalidomide and dexamethasone in relapsed myeloma<sup>147</sup>. Daratumumab is an anti-CD38 monoclonal antibody that has shown very promising single agent activity in relapsed patients<sup>148,149</sup>. It has also shown favourable effects in combination with lenalidomide and dexamethasone and has recently been approved by NICE for use in

combination with bortezomib and dexamethasone in relapsed patients<sup>150-152</sup>. NICE currently has not yet approved daratumumab for induction therapy, however it is regularly administered in standard practice and will undoubtedly be approved for this by NICE in the near future.

Chimeric antigen receptor (CAR) T-cell therapy is another immunotherapeutic option that has produced remarkable clinical responses in patients with relapsed ALL and CLL leading to a surge of interest in its application to the treatment of myeloma<sup>153,154</sup>. Briefly, CARs are synthetic receptors that redirect T-cell specificity and function towards a cell surface tumour target in an HLA-independent manner. This is an extremely powerful principle that has been utilised in cancer treatment to elicit a highly specific immune response to tumour-specific targets<sup>155</sup>. The selection of appropriate target antigens is of utmost importance to ensure that bioengineered CAR T-cells produce a response specific to the tumour. Currently there are a number of targets being investigated in myeloma, with clinical trials currently assessing surface antigens such as B-cell maturation antigen (BCMA), CD19, CD38, CD138 and SLAMF7<sup>156</sup>. Data released from a recent phase 1 trial revealed good overall response rates of 83% in heavily treated relapsed patients following infusion with CAR-BCMA T-cells. The patients experienced a partial anti-myeloma response or greater achieved minimal residual disease-negative status<sup>157</sup>.

## 1.2. The Bone Marrow Microenvironment in Multiple Myeloma

Bone marrow tissue can be found within the majority of bones of the human skeleton. This microenvironment is composed of cellular and non-cellular compartments that form a complex myriad of tissue that collectively facilitate the bone marrow's primary functions of haematopoiesis and the formation and subsequent maintenance of bones<sup>158</sup>. The cellular compartment of the bone marrow microenvironment is composed of multiple types of cells that include haematopoietic stem cells, stromal cells (BMSC), endothelial cells (EC), osteoblasts and osteoclasts. Myeloma cells are reliant on the cells of the bone marrow to facilitate homing to and adhesion within this microenvironment. This subsequently supports myeloma cell survival, proliferation, propagation of angiogenesis and resistance to chemotherapeutic intervention which is mediated both through cell-cell contact and soluble factor signalling (Figure 1.4)<sup>6</sup>.

The non-cellular compartment of the bone marrow is composed of extracellular matrix (ECM) proteins and a liquid milieu that is rich in factors such as cytokines, chemokines and growth factors, all of which contribute to myeloma cell homing and adherence to the bone marrow and subsequent survival within that microenvironment. The role of the growth factor IL-6 is of particular importance in myeloma. It is produced by myeloma cells which also induce its expression and secretion from neighbouring cells within the bone marrow in a paracrine fashion and is critical to the differentiation, sustenance and proliferation of malignant plasma cells<sup>159</sup>. Proteins within the ECM include collagen type 1 and fibronectin which bind to CD138 and CD49d, that are expressed on the surface of myeloma cells, respectively<sup>160</sup>. In turn, this effect has been linked to propagating the effect of cell adhesion-mediated drug resistance (CAM-DR) that is commonly associated with myeloma<sup>161</sup>. The reliance of myeloma cells on the bone marrow microenvironment has therefore provided a therapeutic targeting strategy to more comprehensively treat patients with myeloma<sup>162</sup>.

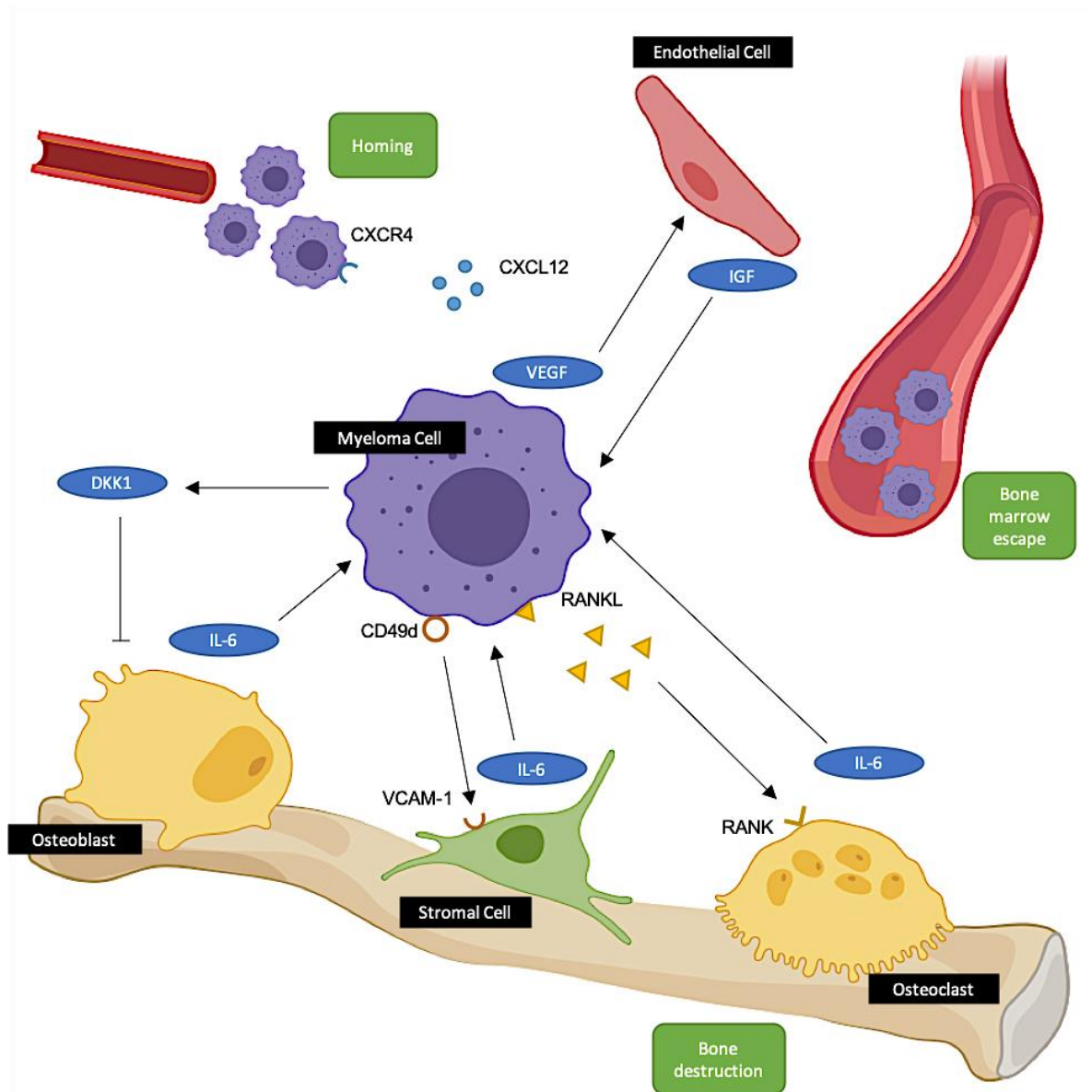


**Figure 1.4: Overview of myeloma cell influence within the bone marrow microenvironment.** A schematic illustration of the signalling interactions involved in myeloma cell homing, adherence and escape from the bone marrow microenvironment, including the primary mechanisms involved in manipulation of normal bone remodelling. Figure developed using BioRender online software.

### 1.2.1. Bone marrow stromal cells

Myeloma cells home and adhere to the bone marrow microenvironment, a process that is mediated through soluble factor signalling and subsequent cell-cell or cell-ECM interactions<sup>163,164</sup>. These interactions result in dysregulation of processes that mediate the cell cycle and apoptosis, thus favouring myeloma cell proliferation and survival<sup>165</sup>. BMSCs have been implicated in the terminal differentiation of post-germinal centre B-cells to plasma cells<sup>160</sup>.

Homing to the bone marrow is critically mediated by CXCR4/CXCL12 signalling. Myeloma cells express CXCR4 on their surface and migrate in response to CXCL12 interaction, which is secreted by BMSCs and ECs to produce a chemokine gradient<sup>166</sup>. Myeloma cells that reside in the bone marrow have also been found to significantly reduce levels of CXCR4 expression when compared with myeloma cells located in peripheral circulation, highlighting the requirement of this signalling cascade to facilitate the process of homing<sup>166</sup>. This also highlights the role of the CXCR4/CXCL12 signalling axis on egress from the bone marrow in late stage disease.

Adhesion of myeloma cells to the bone marrow is primarily mediated by integrins such as CD49d binding to VCAM-1 – which is expressed on BMSCs<sup>167</sup>. In turn, this results in activation of the NF- $\kappa$ B pathway and secretion of IL-6 from both myeloma cells and BMSCs to facilitate autocrine and paracrine signalling cascades that promote myeloma cell proliferation, survival and drug resistance<sup>168-170</sup>. Adhesion to BMSCs also results in the upregulation of VEGF and IGF from BMSCs which again confers increased secretion of IL-6<sup>171-173</sup>.

### 1.2.2. Bone marrow endothelial cells

Endothelial cells are constituent cellular components of human vasculature and the sole cellular components of human microvasculature<sup>174</sup>. Myeloma cells are able to manipulate the process of angiogenesis to disseminate from the site of tumour origin to occupy multiple sites across the human skeleton<sup>175</sup>. This has been shown to become increasingly prevalent throughout disease progression from MGUS to symptomatic myeloma<sup>176</sup>. The mechanisms behind this increased level of angiogenesis in patients with myeloma have yet to be completely understood, but have so far been attributed

to increased levels of VEGF and bFGF secreted by myeloma cells in response to the IL-6 paracrine signalling loop following interactions with BMSCs and ECs<sup>171,177</sup>. It has also been shown that bFGF is additionally secreted by BMSCs in response to myeloma cell stimulation, which further supports the hypothesis that myeloma cells induce a pro-angiogenic environment within the bone marrow<sup>178</sup>. Endothelial cells in myeloma patients have also been found to behave differently to ECs found in a non-malignant environment with regard to phenotype, morphology and chemokine secretion profile, all of which enhance the capabilities of myeloma cells to induce a pro-angiogenic environment within the bone marrow<sup>179,180</sup>. Targeting angiogenesis has also been part of a therapeutic strategy in myeloma treatment, with thalidomide (and subsequent analogues lenalidomide and pomalidomide) being a mainstay of myeloma treatment for a number of years. Whilst the exact mechanisms of action of these therapies are still disputed, it is clear that they possess anti-angiogenic capabilities, which have shown clinical benefits in patients<sup>181,182</sup>.

### 1.2.3. Osteoblasts

Osteoblasts are bone-producing cells that normally exist in a homeostatic relationship with bone-resorbing osteoclasts<sup>183</sup>. These cells have important roles in bone formation and the overall maintenance of the human skeleton. In myeloma however, this homeostatic balance is unfavourably disrupted through upregulation of osteoclast activity and simultaneous inhibition of osteoblast activity, which consequently results the formation of bone lesions in patients, coupled with related co-morbidities such as the excess release of calcium into the blood, known as hypercalcaemia<sup>184</sup>. Myeloma cell interaction via direct cell-cell contact with osteoblasts again confers an upregulation of IL-6 secretion that supports myeloma cell growth and proliferation<sup>185,186</sup>. The Wnt signalling pathway plays a key role in osteoblast differentiation and activation and has been found to be inhibited in myeloma<sup>187</sup>. Osteoblasts are known to regulate the activity of osteoclasts through secretion of osteoprotegerin (OPG) – an antagonist of RANK/RANKL signalling<sup>188</sup>. Inhibition of Wnt signalling has been shown to down-regulate secretion of OPG which directly enhances the activity of osteoclasts, thus highlighting the effect that myeloma cells have on influencing osteoclast activity<sup>189</sup>. The natural antagonist for Wnt signalling is dickkopf1 (DKK1), which functions through an autocrine signalling loop to regulate the

differentiation of osteoblasts and subsequent formation of bone material. In myeloma, it has been found that levels of DKK-1 are significantly upregulated, thus leading to overall inhibition of Wnt signalling and suppression of osteoblast activity<sup>190</sup>. DKK-1 has been implicated in upregulating IL-6 secretion from undifferentiated BMSCs, thus contributing to myeloma cell growth and survival<sup>191</sup>. The RUNX-2 transcription factor is also involved in osteoblast differentiation from precursor cells. Direct myeloma cell contact with osteoblast precursors has been shown to result in an inhibition of RUNX-2 activity and thus result in a reduction in osteoblast formation and activity. This observation was also emulated in patient data, where patients with bone lesions inferred a significant reduction in RUNX-2 activity compared with patients who carried no evidence of osteolytic lesion presentation<sup>192</sup>. Together these observations have provided a suitable rationale for therapeutic intervention in patients with bone disease where targeting DKK1 has shown favourable effects in both reducing the presence of bone disease and also reducing tumour burden<sup>193,194</sup>.

#### 1.2.4. Osteoclasts

Osteoclasts are differentiated from haematopoietic monocytic precursor cells in response to M-CSF stimulation and activation of the RANK/RANKL signalling pathway<sup>195</sup>. This induces the expression of various genes such as tartrate resistant acid phosphatase (TRAP), cathepsin K and the calcitonin receptor, that promote osteoclast development and function<sup>196</sup>. In addition to contributing to the generation of osteoclasts, signalling from RANKL also results in the propagation of bone resorptive activity in mature osteoclasts<sup>197</sup>. Once differentiated, osteoclasts acquire a polarised morphology and adhere to the bone surface forming a tight sealing zone between its ruffled border membrane and the calcified matrix of the bone<sup>198</sup>. Within this space occupied by the adhered osteoclast, an acidic environment is created through secretion of H<sup>+</sup> ions through ATP-controlled proton pumps<sup>199</sup>. Collagenolytic enzymes such cathepsin K and matrix metalloproteases are secreted, which leads to bone degradation and mineral dissolution which causes the release of calcium as a byproduct of this osteolytic process<sup>200,201</sup>. In normal bone remodelling, osteoblasts are able to replace this dissolved bone with a freshly secreted calcified matrix. In myeloma however, osteoblast inhibition coupled with an increase in osteoclast differentiation, quantity and activity in the bone marrow leads to a change in the homeostatic balance

of bone maintenance in favour of bone resorption. As a result of this catastrophic mechanistic alteration in the process of bone remodelling, painful bone lesions are found in approximately 80-90% of myeloma patients (Figure 1.5), with approximately 60% of these patients also experiencing spontaneous fractures<sup>64</sup>.

Myeloma cells are always found in close proximity to sites of bone degradation and are known to bind to osteoclasts which fundamentally highlights their ability to directly influence the process of bone remodelling<sup>202</sup>. Osteoclast behaviour is influenced by myeloma cells directly through cell-cell contact and secretion of soluble factors such as membrane bound, or secreted RANKL<sup>203</sup>. Myeloma cells can also influence osteoclast activity indirectly through inhibition of osteoblast function, consequently leading to a reduction in levels of the RANKL antagonist, osteoprotegerin<sup>184</sup>. Osteoclasts have also been implicated in myeloma cell survival, proliferation and drug resistance through direct cell-cell contact<sup>204</sup>.

#### *1.2.4.1. RANK/RANKL/OPG signalling*

The RANK receptor and its corresponding ligands RANKL and OPG are members of the TNF superfamily of proteins. Activation of this pathway results in the generation of osteoclasts and subsequent resorption of bone<sup>205</sup>. RANK is a receptor that is expressed on the surface of monocytic osteoclast precursors and mature osteoclasts, whilst RANKL is normally expressed or secreted by osteoblasts and BMSCs<sup>206,207</sup>. The natural antagonist of this signalling pathway is OPG which is also secreted by osteoblasts and BMSCs<sup>207</sup>. Binding of OPG to RANKL prevents the interaction of RANKL with its receptor and thus inhibits activation of downstream signalling that contributes to osteoclast function.

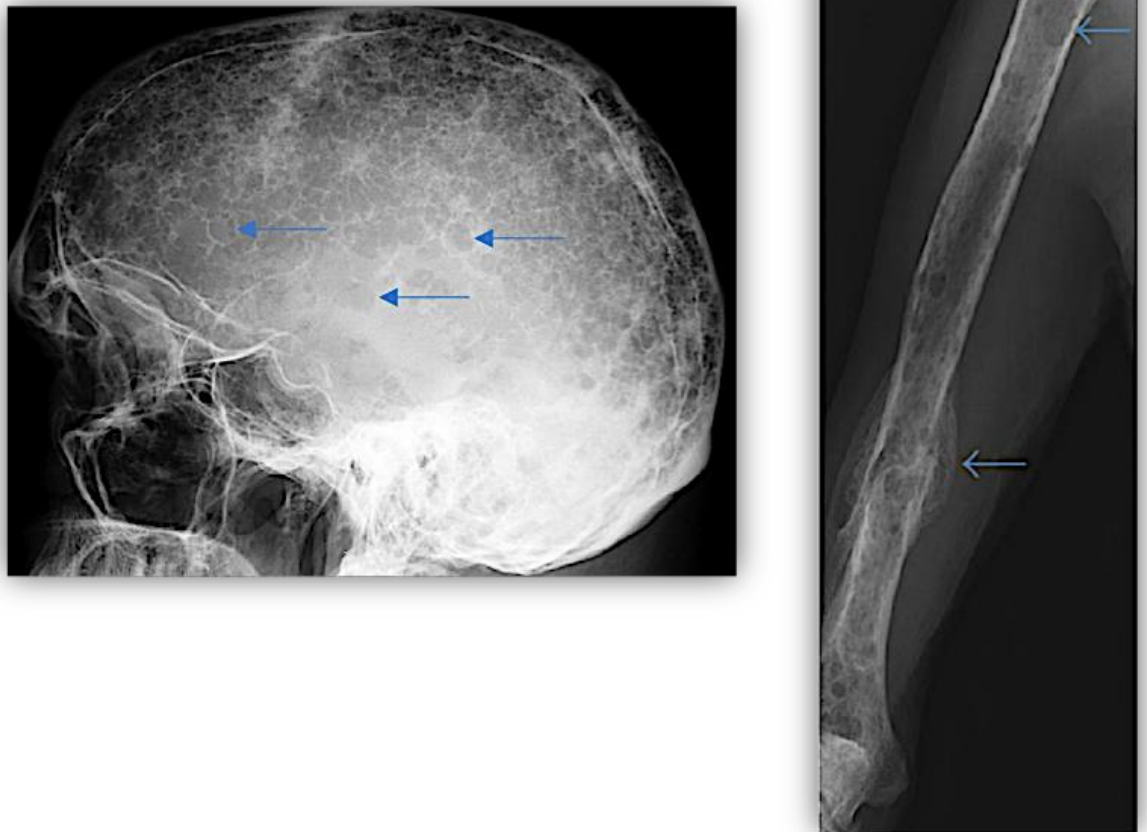


**Figure 1.5: X-ray images of focal osteolytic lesions from a myeloma patient.** The skull of this patient is liberally scattered with bone lesions that is often referred to as a ‘pepperpot skull’ (A). These lesions are also present on the humeral bone of this patient (B). Typical lesions are highlighted by blue arrows. Adapted from Healy *et al*<sup>208</sup>.

Myeloma cells are capable of influencing this pathway two-fold, firstly by stimulating the production, surface expression and secretion of RANKL, which directly correlates to prevalence of bone lesions in patients<sup>209</sup>. There have also been studies that have shown that myeloma cells indirectly influence RANK/RANKL signalling by inducing the upregulation of RANKL on the surface of osteoblasts and BMSCs<sup>210,211</sup>. More recently it has also been established that levels of total RANKL in the serum are also upregulated in myeloma<sup>212</sup>. The second mode of action that influences RANK/RANKL signalling is the acquired capability of myeloma cells to activate RANK/RANKL signalling through inhibition of OPG function<sup>213</sup>. Malignant plasma cells are able to downregulate the transcription of OPG mRNA and subsequent translation of OPG protein from BMSC's which enables the sustained activation of RANK/RANKL signalling, thus directly contributing to increased levels of bone resorption observed in myeloma patients<sup>214</sup>.

The lifespan of an osteoclast is variable and depends on the extent of bone remodelling through bone degradation. This process is primarily mediated through RANK/RANKL signalling, with continued propagation of this pathway promoting osteoclast survival and function. It has been found that the removal of RANKL from this environment leads to osteoclast apoptosis<sup>215</sup>. In myeloma however, RANKL signalling is continuously propagated through surface membrane expression and secretion of RANKL by myeloma cells, thus promoting osteoclast differentiation, survival and function that leads to bone erosion and eventual formation of osteolytic lesions in patients<sup>216</sup>.

#### *1.2.4.2. Interleukin-6*

IL-6 is a well-established growth and survival factor that is significantly upregulated in myeloma patients and has been previously highlighted as a prognostic factor, with increased levels of IL-6 inferring poorer prognosis in patients<sup>217</sup>. IL-6 secretion is significantly increased in myeloma cells when compared with non-malignant plasma cells, with myeloma cells also possessing the capabilities to induce IL-6 secretion from BMSCs<sup>168,218</sup>. The activity of IL-6 has also been implicated in osteoclastogenesis, both directly through a mechanism that is independent of RANK/RANKL signalling and indirectly through stimulation of RANKL expression by myeloma cells and BMSCs<sup>219,220</sup>. However, despite the significant role that IL-6 plays in myeloma pathophysiology and

osteoclastogenesis, treatment with anti-IL6 antibodies has shown to have no anti-myeloma effect<sup>221</sup>.

#### 1.2.4.3. Vitamin D

Vitamin D is obtained from diet and exposure to sunlight and is a crucial metabolite that contributes to the regulation of calcium homeostasis<sup>222</sup>. Vitamin D deficiency has been strongly linked to negatively affecting the process of bone mineralisation by decreasing the capacity of intestinal calcium absorption. This leads to increased resorption of skeletal material in order to maintain a normal serum calcium concentration, which correlates with conditions associated with bone lysis such as osteoporosis<sup>223</sup>. Vitamin D deficiency has also been noted in patients with multiple myeloma, the incidence of which has been shown to increase with more advanced stages of disease<sup>224,225</sup>. Vitamin D is a nutrient that is commonly found to be deficient or insufficient in citizens of the UK, so it does not appear that myeloma patients are any more susceptible to being vitamin D deficient, but given the complications of myeloma pathology it is expected to certainly have a greater impact on their disease maintenance and overall wellbeing.

Vitamin D is initially metabolised in the liver to form 25-hydroxyvitamin D which is further metabolised in the kidneys to produce  $1,25(\text{OH})_2\text{D}_3$ . This is the active metabolite of vitamin D and has long been implicated in bone remodelling<sup>226</sup>. Despite vitamin D deficiency being linked to conditions associated with bone degradation, it has also been established that  $1,25(\text{OH})_2\text{D}_3$  plays an active role in osteoclast differentiation and has the capability to stimulate bone resorption<sup>227,228</sup>. This demonstrates that vitamin D signalling is carefully regulated in normal human bone physiology to facilitate the appropriate balance between bone resorption and formation. The active vitamin D metabolite,  $1,25(\text{OH})_2\text{D}_3$ , functions through binding to the vitamin D receptor (VDR), which in the context of normal homeostatic bone remodelling, is expressed on osteoblasts and bone marrow stromal cells. Activation of this pathway downstream of VDR and  $1,25(\text{OH})_2\text{D}_3$  interaction results in significantly enhanced expression and secretion of soluble factors, such as RANKL and M-CSF, that initiate osteoclastogenesis and subsequent resorptive activity<sup>229</sup>. Early studies demonstrated a significant increase in  $^{45}\text{Ca}$  from pre-labelled rat bones in response to

treatment with  $1,25(\text{OH})_2\text{D}_3$ , thus implicating  $1,25(\text{OH})_2\text{D}_3$  in increasing and prolonging osteolytic activity that leads to bone resorption and subsequent release of calcium into the serum<sup>230</sup>.

### 1.3. Myeloma Research Models

Multiple myeloma is a malignancy that is highly dependent on the bone marrow microenvironment for survival, proliferation and differentiation<sup>6</sup>. This environment is extremely complex and is composed of a number of different cell types, a liquid milieu containing cytokines and chemokines and non-cellular material, all of which have roles in facilitating myeloma cell sustenance and disease progression. This presents many difficulties in replicating this complex environment in a research setting and also creates a challenge for culturing primary myeloma cells in an *ex vivo* setting due to their reliance on the bone marrow microenvironment.

#### 1.3.1. *In vivo* models

The use of *in vivo* models in a preclinical setting in myeloma provides a useful tool to assess therapeutic efficacy and strategy prior to human administration and can also reveal information about disease biology and progression. Murine models are the most commonly used *in vivo* models in myeloma research and are either immunocompetent as with the 5T murine model, or immunodeficient as with xenograft severe combined immunodeficient (SCID) models<sup>231</sup>. The 5T murine model was originally discovered after a small subset of C57BL/KaLwRij mice developed a series of B-cell malignancies including multiple myeloma<sup>232</sup>. This is a frequently used immunocompetent model of myeloma that is representative of a number of key myeloma features relating to excessive secretion of paraprotein, tumour growth within the bone marrow and development of osteolytic bone disease. A number of cell lines have also been developed from these 5T murine models including 5T2, 5T33 and 5TGM1. However, human cells cannot be engrafted in immunocompetent mice due to graft vs host immune incompatibility, meaning these murine models and the cell lines that have been produced from them are not entirely representative of human disease biology.

An example of a murine model that has been developed to more specifically address issues involving the clinical efficacy of myeloma therapies is the Vk\*MYC murine model. It is important to not only show that potential myeloma therapies are safe for administration in patients, but also that they have a good chance of being clinically

effective. The Vk\* MYC model is representative of indolent bone marrow localised myeloma and can reproduce a number of features of myeloma that include high IgG paraprotein secretion and CRAB-related symptoms. As a result, it has been shown to be reasonably predictive of the clinical efficacy of drugs in untreated and relapsed myeloma<sup>233</sup>.

Xenograft SCID murine models are immunodeficient and lack functional B and T-cell mediated immune responses which enables the engraftment of human tumour cells in these models. This characteristic has led to the demonstrable ability of several myeloma cell lines being successfully engrafted in these models, as well as primary myeloma cells obtained from patients<sup>234</sup>. Whilst these models are useful for the testing of therapeutics in a preclinical setting, there is also a capability to assess myeloma cell homing to the bone marrow microenvironment following administration of myeloma cells to these mice. However, the murine bone marrow is not entirely physiologically comparable to the human bone marrow, which does provide some limitation to the use of these models in the assessment of disease pathophysiology.

### 1.3.2. *In vitro* models

The use of *in vitro* models in cell-based research over the last six decades has shown incredible value since the establishment of the first cell line – HeLa cells<sup>235</sup>. Cell lines are often derived from cancer cells and are immortalised so that they can be indefinitely grown under appropriate culture conditions. In myeloma, the use of cell lines in research has proved to be highly valuable in the assessment and development of therapeutics and the characterisation of the biological mechanisms that underpin disease pathophysiology and progression.

#### 1.3.2.1. *Myeloma models*

Primary myeloma cells are notoriously difficult to isolate and maintain in an *ex vivo* setting, due to the lack of suitable *in vitro* models that can replicate the complexity of the bone marrow microenvironment to support these cells<sup>236</sup>. It would of course be highly beneficial to use an *in vitro* microenvironment to sustain myeloma cell survival, however there are currently no well-established models that can facilitate this. There

are also limitations to using primary myeloma cells, given that it is a heterogeneous disease and of course there is considerable heterogeneity between patients<sup>32</sup>.

Consequently, the use of human cell lines in myeloma research is widespread, with a number of advantages to this research strategy being noted. These include ease of accessibility and maintenance, the potential to culture unlimited numbers of cells and relative phenotypic stability within appropriate culture periods<sup>237</sup>. There are a large number of human myeloma cell lines (HMCL) currently used in research practice including the two cell lines utilised in this research, H929 and JJN3<sup>238-240</sup>. Despite these cell lines not being fully representative of primary tissue, as is the case with cell line research in general, they do still possess a number of useful characteristics that make them valid research models for myeloma, such as Ig gene rearrangement, expression of key phenotypic markers such as CD138 and CD38 and production and response to fundamental disease regulators including cytokines such as IL-6<sup>241</sup>. These characteristics have enabled myeloma cell lines to be used to study the physiological and genetic behaviour within the biology of the disease. These cell lines have also been successfully utilised to develop and optimise therapeutic regimens that can be used in patient treatment<sup>237</sup>.

#### 1.3.2.2. Osteoclast models

Fully differentiated, multinucleated osteoclasts are found in very small numbers in human physiology, making them very difficult to isolate and use in *in vitro* research. They are also terminally differentiated and non-proliferative meaning they cannot be cultured long-term in a laboratory setting. This is because they are generally not long-lived cells, surviving on average for approximately two weeks in human bone, and are only differentiated when required from mononuclear precursor cells in response to RANK/RANKL/OPG signalling during the process of homeostatic bone remodelling<sup>201</sup>. The development and use of *in vitro* models that are representative of osteoclasts is of great interest both to investigate osteoclast-specific biology and also their disease-propagating effects in a number of bone-related diseases such as myeloma. To date, there have been methods established to differentiate and culture osteoclasts in an *in vitro* setting from CD14<sup>+</sup> peripheral blood mononuclear cells (PBMC) and macrophages obtained from human bone marrow<sup>242,243</sup>. However, both of these methods present

challenges relating to reproducibility, variability between different sample donors and availability of suitable samples in the case of using bone marrow macrophages, due to the invasive nature of extracting these samples. Therefore, the requirement for using a more reproducible and readily available alternative would be highly valuable in osteoclast research.

The use of cell lines in osteoclast research is currently limited, however there is evidence to suggest that multinucleated, bone resorbing cells that possess the morphological, phenotypic and genetic characteristics of differentiated osteoclasts can be developed from myelo-monocytic cell lines. The RAW264.7 murine cell line is arguably the most established cell line used in osteoclast research. These cells are capable of forming osteoclasts in response to both RANKL and M-CSF treatment<sup>244-247</sup>. However, due to their murine origin, they are fundamentally not representative of human physiology, meaning there is still considerable interest to generate osteoclasts using a reproducible human model.

The U937 human cell line is representative of monocytic cells of myeloid lineage<sup>248</sup>. These cells have been shown to be capable of differentiating into osteoclast-like cells in response to treatment with  $1,25(\text{OH})_2\text{D}_3$  following initial induction with phorbol esters such as phorbol 12-myristate 13-acetate<sup>249,250</sup>. They are also capable of resorbing bone material and expressing genes related to osteoclast function such as TRAP, RANK and cathepsin K<sup>250</sup>. This highlights the potential for these cells to be used in osteoclast research and to also investigate the role of osteoclasts in osteolytic diseases, including myeloma.

### 1.3.2.3. Co-culture models

The use of co-culture models in myeloma research is common to investigate the role of various cells that are found within the bone marrow microenvironment on myeloma biology. Such models have been previously used to investigate chemoresistance, proliferative capacity, alterations to surface phenotype, roles of signalling mediators and determination of transcriptomic alterations. The complexity of the bone marrow in human physiology often means *in vitro* research is carried out in a reductionist fashion. There are a number of *in vitro* models that have been used in myeloma

research that have utilised stromal cells, osteoblasts and endothelial cells<sup>251-253</sup>. There are very few legitimate models being reported that can effectively imitate the osteoclastic environment of the myeloma bone marrow in humans<sup>254</sup>. This presents an opportunity to investigate the development of a reproducible *in vitro* research model that can effectively replicate osteoclast function that can be used in myeloma research. Such a model could provide a good foundation for future studies of the influence of the microenvironment on resistance mechanisms in myeloma, provide another platform for therapeutic testing and also potentially sustain primary myeloma tissue *ex vivo*.

## 1.4. Project Aims

This research project aims to develop a reproducible *in vitro* osteoclast microenvironment from the myelo-monocytic U937 cell line, which can then be used in a co-culture model with H929 and JJN3 myeloma cell lines to investigate phenotypic, functional and transcriptional changes that occur in these myeloma cells as a result of co-culture.

The primary aims of this project are therefore to:

1. Characterise the differentiation of U937 cells into osteoclast-like cells following treatment with phorbol 12-myristate 13-acetate (PMA) and  $1,25(\text{OH})_2\text{D}_3$ . Treated U937 cells will be assessed for multinucleation, expression of osteoclast markers such as TRAP and RANK and their capability of resorbing bone material.
2. Investigate the influence of differentiated U937 cells on H929 and JJN3 CD138 expression, activation, survival and resistance to treatment with clinically approved therapy.
3. Determine transcriptional differences between two CD138 subpopulations in each myeloma cell line using RNA sequencing and investigate differences in expression of genes that regulate proliferation, cell cycle regulation and survival.

## CHAPTER 2: Materials and Methods

### 2.1. Tissue Culture

#### 2.1.1. Media, buffer and cell staining solutions

##### 2.1.1.1. RPMI 1640 media

Roswell Park Memorial Institute (RPMI) 1640 media (Gibco) was supplemented with 2mM L-Glutamine (Invitrogen), 100U/mL penicillin and 100µg/mL streptomycin (Invitrogen) and 10% foetal bovine serum (Gibco).

##### 2.1.1.2. DMEM media

Dulbecco's Modified Eagle's Media (DMEM) (Gibco) was supplemented with 2mM sodium pyruvate (Invitrogen), 100U/mL penicillin and 100µg/mL streptomycin (Invitrogen) and 10% foetal bovine serum (Gibco).

##### 2.1.1.3. M199 media

Medium 199 (M199) media (Sigma) was supplemented with 100U/mL penicillin and 100µg/mL streptomycin (Invitrogen) and 20% foetal bovine serum (Gibco).

##### 2.1.1.4. Cryopreservation media solution

Cryopreservation media was made using either RPMI 1640, DMEM or M199 media at a proportion of 60% and supplemented with 30% foetal bovine serum and 10% Dimethyl Sulfoxide (DMSO) (Sigma).

##### 2.1.1.5. Paraformaldehyde fixation solution

40g of paraformaldehyde powder (Sigma) was dissolved in sterile PBS that had been warmed to 60°C. The solution was cooled and made up to a final volume of 1 litre to make a 4% solution. This was stored between 2-8°C and diluted to a 1% working solution in PBS to fix cells.

#### 2.1.1.6. Toluidine blue solution

0.5g of toluidine blue powder (Sigma) and 0.5 of boric acid (Sigma) were dissolved in 75mL of distilled water with the pH of the solution adjusted to 7.3 using 1M sodium hydroxide with a final volume being made up to 100mL. The solution was filtered through coarse filter paper and stored at room temperature.

#### 2.1.2. Tissue culture plastics

All cells were cultured in either 25cm<sup>2</sup>, 75cm<sup>2</sup> or 175cm<sup>2</sup> single tier flasks or 175cm<sup>2</sup> 3-tier flasks (Greiner). Cells were also cultured in 6, 12, 24, 48 and 96 well tissue culture plates (Nunc) and were transferred using 10, 20, 200 and 1000µL pipette tips (Fisher) as well as 5, 10 and 25mL Stripettes® (Sigma). For flow cytometry experiments cells were placed in FACS tubes (Greiner). Falcon tubes (15mL and 50mL) (Fisher) were also used for centrifugation of cells.

#### 2.1.3. Assessing cell density and viability

Cell density and viability in each culture was assessed by diluting aliquots of cell culture 1:1 in sterile PBS (300µL cell culture in 300µL PBS), and being placed in a ViCell XR cell counter (Beckman Coulter). As part of the ViCell XR's viability assessment, cells were stained with trypan blue - a live cell exclusion azo dye that stains dead cells, producing a distinction in colour between live and dead cells, which can be quantified to provide cell density and viability values<sup>255</sup>. Fifty representative images were taken which were then automatically assessed for viability and cell density (x10<sup>6</sup>/mL) by ViCell XR integrated software.

#### 2.1.4. Mycoplasma testing

Mycoplasma tests were routinely carried out every 3 months on samples of cells being used in culture, using a Venor® Gem Classic mycoplasma detection kit (Minerva Biolabs). Supernatants from each cell line in culture were collected and heated to 95°C for 10 minutes and briefly centrifuged at 10,000xg to remove excess cellular debris. A master mix of reagents provided in this detection kit was produced as shown in Table 2.1.

<b>Component</b>	<b>Volume per reaction (<math>\mu\text{L}</math>)</b>
<i>PCR-grade water</i>	14.5
<i>10x reaction buffer</i>	2.5
<i>Primer/nucleotide mix</i>	2.5
<i>Internal control DNA</i>	2.5
<i>Polymerase (1U/<math>\mu\text{L}</math>)</i>	1.0
<b>Total</b>	<b>23.0</b>

**Table 2.1. Components of a PCR master mix to assess for presence of mycoplasma**

For each reaction 23 $\mu\text{L}$  of master mix was mixed with 2 $\mu\text{L}$  of supernatant from each sample, alongside a positive control containing the provided DNA template and a negative control containing nuclease-free water instead of DNA or sample. These samples were then amplified using the settings described in Table 2.2 in a PCR thermocycler (Thermo Fisher) with the resulting solutions placed in a 1.5% agarose gel and run for 20 minutes at 100V. Mycoplasma contamination was then assessed using a DNA ladder, with a positive result equating to the detection of PCR amplicon bands at approximately 265-278 base pairs in amplicon size. Throughout the entirety of this research, no mycoplasma was detected in any culture.

<b>Phase</b>	<b>Initial denaturation</b>	<b>Denaturation and annealing</b>		
<i>Stage</i>	1	1	2	3
<i>Number of cycles</i>	1	39		
<i>Temperature (<math>^{\circ}\text{C}</math>)</i>	94	94	55	72
<i>Time</i>	2 mins	30 secs	30 secs	30 secs

**Table 2.2. PCR cycling times and temperatures to facilitate PCR reaction**

### 2.1.5. Cell line culture

All cell lines were maintained in appropriate media at 37°C in atmospheric conditions of 5% CO<sub>2</sub>. The identity of each cell line was confirmed through a multiplex PCR of mini-satellite markers that revealed a unique DNA profile. This procedure was performed by the STR genotyping service provided by Public Health England. All cell lines were also shown to be mycoplasma-free. Cell lines were maintained in continuous culture for no longer than 6 weeks.

#### 2.1.5.1. Suspension cell lines

H929, JLN3 and U937 cells were all originally obtained as frozen stocks from the ATCC and were maintained in RPMI 1640 media and kept at densities between 0.5-2x10<sup>6</sup> cells/mL. Cells were routinely split twice per week at a ratio of 1:3 following centrifugation at 300xg for 5 minutes. Cells were re-suspended in 30mL of fresh, pre-warmed media and placed back into culture in T-175 flasks.

#### 2.1.5.2. Adherent cell lines

SAOS-2 cells were originally obtained from Sigma, HS-5 cells were obtained from ATCC and CD40L-expressing murine fibroblasts were kindly donated by Dr Beth Walsby, Cardiff University. SAOS-2 and CD40L cell lines were maintained in DMEM media and HS-5 cells were maintained in M199 media. When cells became confluent, they were briefly washed with sterile PBS before the addition of 0.05% trypsin-EDTA. Cells were then incubated for 5-10 minutes at 37°C in atmospheric conditions of 5% CO<sub>2</sub> until the cells had detached from the flask, which was confirmed using a light microscope. The cells were washed in fresh FBS-containing media to deactivate the trypsin-EDTA. Detached cells were then split at a 1:3 ratio, resuspended in 20mL fresh media and placed back into culture.

### 2.1.6. Differentiation of U937 cells

U937 cells were aliquoted into 24-well plates at an initial seeding density of 5x10<sup>4</sup> cells/well. Cells were treated for 48 hours with 100nM 12-O-Tetradecanoylphorbol 13-acetate (PMA) (Sigma). Non-adhered cells were then removed by washing twice with fresh RPMI 1640 media. PMA-treated U937 cells were then incubated with 10nM

1,25(OH)<sub>2</sub>D<sub>3</sub> (Sigma). The initial time of addition of 1,25(OH)<sub>2</sub>D<sub>3</sub> to PMA-treated U937 cells will be referred to as Day 0. Treatment in this fashion continued for up to 10 days, with 1,25(OH)<sub>2</sub>D<sub>3</sub>-containing media being replaced every 2-3 days.

#### **2.1.7. U937 cell culture on ivory disks**

Slices of ivory were kindly donated by Dr Bronwen Evans, Cardiff University. These slices were soaked in sterile PBS for 2 hours before disks were cut using a 6mm hole punch. Disks were collected and placed in a sonicator for 2 minutes for a total of 10 runs, fresh water was replaced after each run. Sonicated ivory disks were placed in 100% ethanol for 10 minutes, which was followed by 2 washes with sterile PBS. PBS was then removed, and the ivory disks were left to dry until required for culture.

Sterile ivory disks were placed in each required well of a 96-well plate and were soaked for 1 hour in RPMI media containing 100nM of PMA. A working solution of U937 cells was used at a density of  $5 \times 10^4$  cells/mL in media containing 100nM PMA, around 300 $\mu$ L of this cell culture was added on top of each ivory disk being used. The ivory disks filled the vast majority of each well of a 96-well plate that they occupied, ensuring that all U937 cells would settle on the surface of the ivory disk when placed in culture. Cells were incubated in appropriate conditions for 48 hours. After this time, media was removed, cells were gently washed twice with RPMI 1640 media which was then replaced with RPMI 1640 media containing 10nM of 1,25(OH)<sub>2</sub>D<sub>3</sub>. Both media solutions were pre-warmed to 37°C. Cells were incubated in these conditions for 4 weeks, with media being changed at regular 2-3 day intervals. Once this culture period was complete, ivory disks were washed in PBS for 2 minutes and incubated in 1% sodium hypochlorite for 10 minutes. Disks were washed with sterile water and were vigorously rubbed between gloved hands for at least 2 minutes to remove any excess cells that may have remained stuck to the disk. Disks were stained with 0.5% toluidine blue for 10 minutes before finally being washed with 100% ethanol briefly, to remove excess stain.

### 2.1.8. Myeloma cell co-culture with differentiated U937 cells

H929 and JIN3 cells were washed in pre-warmed RPMI 1640 media and collected in a working culture at a density of  $5 \times 10^5$  cells/mL. U937 cells were pre-treated in 24-well plates with PMA for 2 days and  $1,25(\text{OH})_2\text{D}_3$  for a further 5 days and were subsequently washed twice in pre-warmed RPMI 1640 media to remove excess  $1,25(\text{OH})_2\text{D}_3$  from culture. Aliquots of 1mL of each myeloma cell were then added to wells containing differentiated U937 cells and were incubated at  $37^\circ\text{C}$  for up to 48 hours before being collected for further analysis. Aliquots of  $250\mu\text{L}$  of myeloma cell cultures were also added to Transwell® inserts, which were placed in wells containing differentiated U937 cells and cultured at  $37^\circ\text{C}$  for 48 hours before collection for further analysis.

### 2.1.9. Myeloma cell co-culture with adherent cell lines

HS-5, SAOS-2 cells and CD40L-expressing fibroblasts were irradiated with a dose of 60Gy (approximately 30 minutes with Caesium-137) and plated into 24-well plates at a density of  $1 \times 10^5$  cells/well in their respective media. The cells were left for a minimum of 4 hours to adhere to the tissue culture plastic. Media was removed and the cells were washed once with fresh media to remove any non-adhered cells. H929 and JIN3 cells were then cultured with these adherent cells at  $37^\circ\text{C}$  at a density of  $5 \times 10^5$  cells/mL for up to 48 hours. Myeloma cells were then collected for further analysis.

### 2.1.10. Assessment of myeloma cell migration

H929 and JIN3 cells were cultured with differentiated U937 cells for 48 hours and placed in Transwell® inserts as described in Section 2.1.8. Within the lower chamber of each well of a 24-well Transwell® plate used for cell culture, CXCL12 was added at a concentration of 100ng/mL. Myeloma cells were incubated in this fashion for a period of either 2 or 24 hours. Media was then harvested from both the upper and lower chambers of each well used for cell culture and assessed for CD138 expression using the staining procedure described in Section 2.2.2. Samples were processed using an Accuri C6 flow cytometer, with  $100\mu\text{L}$  being collected from each sample to determine the number of cells that had migrated from the upper chamber to the lower chamber.

This experiment was also performed alongside controls that did not contain a CXCL12 migratory gradient.

#### **2.1.11. Treatment of myeloma cells with bortezomib**

H929 and JJN3 cells were harvested and resuspended into a working stock solution at  $5 \times 10^5$  cells/mL in RPMI 1640 media. Cells were pre-treated with bortezomib for 1 hour at doses ranging between 20-120nM. This was to equilibrate the cellular absorbance of bortezomib, to ensure that any cytotoxic effect observed was not neutralised by co-culture with differentiated U937 cells. Aliquots of 1mL of myeloma cell working cultures were then added to differentiated U937 cells that had been treated with 10nM PMA for 48 hours followed by 100nM  $1,25(\text{OH})_2\text{D}_3$  for a further 5 days. Treated cells were incubated in this fashion for 48 hours before being harvested and assessed for viability through flow cytometry.

#### **2.1.12. Cryopreservation of cell lines**

Cells were harvested, spun down at  $300 \times g$  for 5 minutes and re-suspended in cryopreservation media at a density of between  $5-10 \times 10^6$  cells/mL, depending on the total number of cells available in culture at the point of freezing. Cell solutions were transferred to 2mL cryogenic tubes (Greiner) and placed in a Mr Frosty™ (Thermo Scientific) freezing container which contained approximately 150mL of pentane, allowing for an optimal freezing rate of  $-1^\circ\text{C}$  per minute. Cells were then left for 24 hours at  $-80^\circ\text{C}$  before being transferred to a liquid nitrogen tank for long term storage.

#### **2.1.13. Thawing of cryopreserved cells**

Cells frozen in 2mL cryogenic tubes were quickly transported from liquid nitrogen storage in a polystyrene-insulated container. Cryogenic tubes were then placed in a water bath heated to  $37^\circ\text{C}$  to aid in rapid thawing. Tubes were then sterilised with ethanol, with thawed cells being placed in a sterile 15mL falcon containing appropriate pre-warmed media and spun down at  $300 \times g$  for 5 minutes. Cells were resuspended in 10mL of their respective media and placed in a  $25\text{cm}^2$  culture flask for incubation at  $37^\circ\text{C}$ .

## 2.2. Flow Cytometry

All flow cytometry experiments were performed using Accuri C6, FACSAria™ III or LSRFortessa flow cytometers (BD Biosciences). Flow cytometers were routinely maintained in accordance with the manufacturer's instructions to eliminate the possibility of air bubbles or debris contaminating and obscuring data. Analysis of flow cytometry data was performed using either FlowJo 10 or BD Accuri C6 analysis software.

### 2.2.1. Compensation of multicolour antibody panels

To compensate multicolour fluorochrome panels, compensation particles (BD Biosciences) were used. Particles were briefly vortexed to ensure their resuspension in solution. One drop of anti-mouse Ig-kappa and one drop of negative control compensation particles were added to 100µL of sterile PBS in individual FACS tubes containing 5µL of each antibody-fluorochrome conjugate being used in every multicolour panel, alongside unstained controls. These samples were incubated at room temperature in darkness for 10 minutes before being analysed on a BD LSRFortessa. Briefly, samples were gated using forward and side scatter and were assessed for positive staining using single colour histogram plots. For each panel being used, compensation was then automatically calculated using FACSDiva software with these values being applied to future experiments involving those multicolour antibody-fluorochrome conjugate panels.

### 2.2.2. Myeloma cell staining

H929 and JJN3 cells were harvested at an approximate density of  $1 \times 10^5$  cells/mL for staining, washed in sterile PBS and centrifuged at 300xg for 5 minutes. Cell samples were then re-suspended in 5µL of each fluorochrome-conjugated monoclonal antibody in 100µL sterile PBS and were then incubated in the dark for 10 minutes at room temperature. They were then washed again in sterile PBS and re-suspended in either 200ul sterile PBS if analysis was to be performed immediately or 1% paraformaldehyde fix solution if cells were to be analysed at a later timepoint within 1 week of staining. As standard practice when constructing gates, cells were analysed using forward and

side scatter area plots to isolate whole cell populations, followed by forward scatter height vs area plots to exclude cell doublets.

#### 2.2.2.1. Determination of surface marker expression

In order to assess the expression of various markers on the surface of H929 and JIN3 myeloma cell lines, cells were stained with fluorescently-conjugated monoclonal antibodies, which are detailed in Table 2.3. The method of staining is described in Section 2.2.2. Briefly, gates were drawn around live, single cells before being assessed initially for CD138 expression. Gates were drawn around CD138<sup>bright</sup> and CD138<sup>dim</sup> populations of cells, which were then assessed further for expression of a number of other phenotypic markers. Experiments were routinely performed alongside unstained controls in order to establish cell populations that were truly positive expressors of each marker being analysed.

<b>Antigen</b>	<b>Fluorochrome</b>	<b>Manufacturer</b>	<b>Clone</b>	<b>Isotype</b>
<i>CD138</i>	APC	Biologend	MI15	Mouse IgG <sub>1</sub>
<i>CD38</i>	FITC	Biologend	HB-7	Mouse IgG <sub>1</sub>
<i>CD69</i>	PE/Cy7	Biologend	FN50	Mouse IgG <sub>1</sub>
<i>CXCR4</i>	Brilliant Violet 421	Biologend	12G5	Mouse IgG <sub>2a</sub>
<i>CD49e</i>	PE	Biologend	NKI-SAM-1	Mouse IgG <sub>2b</sub>
<i>CD45</i>	Brilliant Violet 605	Biologend	HI30	Mouse IgG <sub>1</sub>
<i>CD40</i>	Brilliant Violet 605	Biologend	5C3	Mouse IgG <sub>1</sub>
<i>CD11a</i>	PerCP	Biologend	TS2/4	Mouse IgG <sub>1</sub>

**Table 2.3. Fluorescently conjugated monoclonal antibodies selected to assess surface marker expression of myeloma cells.**

#### 2.2.2.2. CFSE assay

CellTrace™ Carboxyfluorescein succinimidyl ester (CFSE) stock was reconstituted in DMSO to a concentration of 5mM. H929 and JIN3 cells were harvested and resuspended at a density of  $5 \times 10^5$  cells/mL in PBS that had been pre-warmed to 37°C with CFSE diluted to a concentration of 1µM. This suspension was incubated in the dark at 37°C before being diluted 1:1 with fresh RPMI 1640 media containing 10% FBS to remove any unbound stain. The cells were centrifuged at 300xg for 5 minutes,

counted and resuspended to a density of  $5 \times 10^5$  cells/mL. CFSE-stained cells were then added to a 24-well plate containing U937 cells that had been treated with PMA for 48 hours and  $1,25(\text{OH})_2\text{D}_3$  for 5 days, alongside mono-culture controls. After 48 hours of incubation at  $37^\circ\text{C}$ , cells were harvested, stained with CD138-APC antibody (Table 2.3), washed in sterile PBS and analysed on an Accuri C6 flow cytometer.

#### *2.2.2.3. Cell sorting*

H929 and JIN3 cells were harvested and stained with fluorescently conjugated CD138-APC and CD38-FITC monoclonal antibodies at a concentration of  $5 \mu\text{L}$  per  $1 \times 10^6$  cells. Stained cells were then washed and resuspended in sterile PBS at a final working density of  $1 \times 10^7$  cells/mL. Cells were sorted using a FACSAria™ III (BD Biosciences). This procedure was performed at the Central Biotechnology Services (CBS) at Cardiff University, by Dr Ann Kift-Morgan and Dr Catherine Naseriyan. Briefly, cells were gated using forward and side scatter profiles to identify live cells and forward scatter height vs area profiles to exclude doublets. Expression of CD138 and CD38 was then determined and gates were drawn around CD138<sup>bright</sup>/CD38<sup>bright</sup> cells and CD138<sup>dim</sup>/CD38<sup>bright</sup> cells, with these two subpopulations being sorted into separate collection tubes, coated with warm FBS. These samples were then used for RNA extractions.

#### **2.2.3. U937 cell staining**

U937 cells treated with 100nM PMA and 10nM  $1,25(\text{OH})_2\text{D}_3$  were collected at Days 0, 3, 5 and 10 of treatment alongside a 0h control. At each time point cells were washed with sterile PBS and incubated with trypsin-EDTA (0.05%) (Gibco) for 1-2 minutes. Once all cells had detached, fresh RPMI 1640 media was added to the cells to deactivate the trypsin-EDTA, cells were then washed and resuspended in sterile PBS in preparation for staining. All samples were analysed on an Accuri C6 flow cytometer.

##### *2.2.3.1. Determination of RANK expression on U937 cells.*

U937 cell samples were harvested as described in Section 2.2.3 at each specified time point. Samples were washed and stained with RANK-PE (Table 2.4) at a concentration

of 5µL per 100µL for 10 minutes in darkness. Samples were then washed in sterile PBS and analysed using an Accuri C6 flow cytometer.

<b>Antigen</b>	<b>Fluorochrome</b>	<b>Manufacturer</b>	<b>Clone</b>	<b>Isotype</b>
<i>RANK/TNFRSF11A</i>	PE	R+D Systems	80704	Mouse IgG <sub>1</sub>

**Table 2.4. Fluorescently conjugated monoclonal antibody used to assess surface expression of RANK on U937 cells**

#### 2.2.3.2. DNA content analysis

To assess the DNA content of U937 cells in response to treatment with PMA and 1,25(OH)<sub>2</sub>D<sub>3</sub>, staining with propidium iodide was employed. Propidium iodide is a DNA intercalating agent that can be used to quantify intracellular DNA content when coupled with flow cytometry<sup>256</sup>. Once harvested, U937 cells were resuspended in 70% ethanol and stored at -20°C for at least one hour before staining, to fix the cells. Cells were washed in sterile PBS and re-suspended in 50µL of 10ug/mL RNase A (Qiagen) for 45 minutes at 37°C. Samples were then incubated with propidium iodide (Sigma) at a concentration of 50µg/mL for 15 minutes at 37°C and analysed on an Accuri C6 flow cytometer.

#### 2.2.4. Annexin V staining

An Annexin V Apoptosis Detection kit (eBioscience) was used to assess levels of apoptosis in both treated U937 cells and myeloma cell lines. Using the appropriate harvesting techniques for each of these cells outlined in Sections 2.2.2. and 2.2.3. cells were stained with 5µl of Annexin V-FITC in 100µL cell culture (1x10<sup>5</sup> cells/100µL) and incubated for around 10 minutes. Cells were then washed and resuspended in a final volume of 200µL in sterile PBS before being analysed on an Accuri C6 flow cytometer.

## 2.3. Microscopy

### 2.3.1. Tartrate resistant acid phosphatase (TRAP) Staining

Tartrate resistant acid phosphatase (TRAP) staining was performed using an acid phosphatase leukocyte (TRAP) kit (Sigma). This method utilises naphthol AS-Bi phosphates combined with diazotized fast garnet GBC salts for the detection of acid phosphatase, the latter of which rapidly forms insoluble dye deposits in the presence of acidic pH to indicate the presence of TRAP<sup>257</sup>.

<b>Component</b>	<b>Volume (mL)</b>
<i>Deionised water</i>	45
<i>Diazotised fast garnet GBC solution</i>	1.0
<i>Naphthol AS-Bi phosphate solution</i>	0.5
<i>Acetate solution</i>	2.0
<i>Tartrate solution</i>	1.0

**Table 2.5. Components of Acid phosphatase staining kit used to assess expression of TRAP in U937 cells.**

After treatment in 24-well plates with PMA for 48 hours and  $1,25(\text{OH})_2\text{D}_3$  for a further 10 days, U937 cells were washed once gently in sterile PBS pre-warmed to 37°C and fixed in a fixative solution composed of 25% citrate, 65% acetone and 10% formaldehyde (37%) for 30 seconds at room temperature before being rinsed at least 3 times in sterile deionised water. The solution described in Table 2.5 was warmed to 37°C and added to the fixed U937 cells, which were incubated for a further 60 minutes at 37°C. The cells were then thoroughly rinsed in deionised water at least three times and left to air dry before being imaged with a light microscope.

### 2.3.2. SEM imaging

Ivory disks cultured with U937 cells treated with PMA and  $1,25(\text{OH})_2\text{D}_3$  were attached to double-sided carbon tape, coated with gold in an EMscope sputter coater

(EMScope, Ashford, Kent, UK) and examined and imaged at 10kV in a Tescan VEGA3 scanning electron microscope. This procedure was performed by Dr Christopher Von Ruhland, Cardiff University.

### **2.3.3. Fluorescence microscopy**

Differentiated U937 cells were gently washed with sterile PBS and fixed in 1% paraformaldehyde for 30 minutes. They were then washed in sterile PBS and incubated in 0.5% (v/v) Triton X100 for 15 minutes. Fixed cells were stained with 4',6-Diamidino-2-phenylindole dihydrochloride (DAPI) at a concentration of 100ng/mL. Images were acquired using a Zeiss Axio Observer Z1 microscope (Carl Zeiss Microimaging, Gottingen, Germany) with a black box chamber (Solent Scientific Ltd, Segensworth, UK). The use of this equipment was kindly permitted by Professor Rachel Errington, Cardiff University.

## 2.4. Gene expression analysis

### 2.4.1. RNA sequencing

Following culture for 48 hours with differentiated U937 cells, H929 and JN3 cells were harvested in working cultures containing approximately  $10 \times 10^6$  cells in 1mL sterile PBS. These cell solutions were then flow sorted into their respective CD138<sup>bright</sup> and CD138<sup>dim</sup> subpopulations, as described in Section 2.2.2.3. As a control, H929 and JN3 cells cultured in isolation were also sorted based on CD138 positivity, with only CD138<sup>bright</sup> cells being collected in this instance. The list of samples collected is shown in Table 2.6 along with the identifiers they will be referred to throughout this thesis. Three independent biological replicates were assessed in this assay.

<b>Sample</b>	<b>Identifier</b>
<i>H929+U937 CD138<sup>bright</sup></i>	HUCB
<i>H929+U937 CD138<sup>dim</sup></i>	HUCD
<i>H929 monoculture CD138<sup>bright</sup></i>	HMCB
<i>JN3+U937 CD138<sup>bright</sup></i>	JUCB
<i>JN3+U937 CD138<sup>dim</sup></i>	JUCD
<i>JN3 monoculture CD138<sup>bright</sup></i>	JMCB

**Table 2.6. Summary of conditions and samples used to produce RNA extracts and their corresponding identifiers**

#### 2.4.1.1. RNA Isolation

Approximately  $5 \times 10^5$  cells from each condition shown in Table 2.6 were harvested following sorting, washed in ice cold PBS and re-suspended in 1mL of cold TRIzol<sup>®</sup> reagent (Thermo Fisher). These samples were frozen at  $-80^{\circ}\text{C}$  until required for RNA extraction. Upon thawing, TRIzol<sup>®</sup> lysates were mixed with 200 $\mu\text{L}$  chloroform and vortexed for 15 seconds before being centrifuged at 10,000 $\times g$  for 15 minutes at  $4^{\circ}\text{C}$ . The aqueous phase of this solution was then carefully extracted, ensuring that there was no crossover contamination from the white inter-phase layer of the solution. This aqueous solution was then thoroughly mixed with 70% ethanol. For the remainder of the RNA extraction an RNeasy mini-kit (Qiagen) was used in accordance with the

manufacturer's instructions to isolate RNA. Samples were placed in an RNeasy spin column containing a silica RNeasy membrane and centrifuged at 10,000 $\times$ g at 4°C, allowing total RNA to bind to the membrane. The addition of the provided RW1 and RPE buffers washed away contaminants within each sample. Finally, total RNA was eluted into 50 $\mu$ L of RNase-free water, this was then run back through the RNeasy column, to ensure the highest possible amount of RNA was collected. This process enabled purification of RNA molecules that are greater than 200 nucleotides in size.

#### *2.4.1.2. RNA Sample Preparation and Sequencing*

Following the generation of RNA extracts, these samples were used for RNA-sequencing, which was performed by the Wales Gene Park, Cardiff. Total RNA quality and quantity was assessed using an Agilent 2100 Bioanalyser and an RNA Nano 6000 kit (Agilent Technologies). 100-900ng of Total RNA with an RNA integrity number (RIN) >8 was depleted of ribosomal RNA, and the sequencing libraries were prepared using the Illumina® TruSeq® Stranded Total RNA with Ribo-Zero Gold™ kit (Illumina Inc.). The steps included rRNA depletion and cleanup, RNA fragmentation, 1<sup>st</sup> strand cDNA synthesis, 2<sup>nd</sup> strand cDNA synthesis, adenylation of 3'-ends, adapter ligation, PCR amplification (12-cycles) and validation. The manufacturer's instructions were followed except for the clean-up after the Ribo-Zero depletion step where Ampure®XP beads (Beckman Coulter) and 80% Ethanol were used. The libraries were validated using the Agilent 2100 Bioanalyser and a high-sensitivity kit (Agilent Technologies) to ascertain the insert size, and the Qubit® (Life Technologies) was used to perform the fluorometric quantitation. Following validation, the libraries were normalised to 4nM, pooled together and clustered on the cBot™2 following the manufacturer's recommendations. The pool was then sequenced using a 75-base paired-end (2x75bp PE) dual index read format on the Illumina® HiSeq2500 in high-output mode according to the manufacturer's instructions.

#### *2.4.1.3. RNA sequencing data analysis*

Processing of raw RNA sequencing data and subsequent differential gene expression analysis was performed by Dr Anna Evans, Wales Gene Park, Cardiff. An overview of the data processing workflow is summarised in Figure 2.1. Raw read data was converted to fastq format for all samples and reads were then trimmed of adapters

and low quality read ends using Trim Galore (v0.5.0) software. Reads were then mapped to the Gencode GRCh38 primary assembly reference genome, sourced from the Wellcome Sanger Institute server. Appropriate quality control measures were performed at each stage of read processing using FastQC and MultiQC software packages<sup>258</sup>. Read counts are directly related to gene expression levels and were calculated by inferring library strand specificity from each sequence alignment file using RSeQC software, they were then summarised by feature, specifying strandedness, using FeatureCounts (v1.5.1) software<sup>259,260</sup>. FeatureCounts was used both as part of a quality control strategy to identify outliers and batching effects and to assess read counts that were summarised at the exon, transcript and gene level. These read counts were taken forward for differential gene expression (DGE) analysis using the R package: DESeq2<sup>261</sup>. The comparisons made between samples to assess DGE are summarised in Table 2.7.

#### *2.4.1.4. Ingenuity Pathway Analysis (IPA)*

Groups of differentially expressed genes from each condition were selected for pathway analysis based on adjusted p-value ( $q < 0.05$ ), to identify cellular and molecular pathways, functions and biological processes that were overrepresented in each dataset. This analysis was performed using Ingenuity Pathway Analysis (IPA) software, version 01-07 (Qiagen). Following the compilation of significantly differentially expressed genes, fold change was then used to further filter the datasets. A  $\log_2$ [fold change] greater than 1 or less than -1 was deemed a suitable parameter to determine differential expression. Data obtained from HMCB vs HUCB and JMCB vs JUCB comparisons that met these selection criteria contained 484 and 124 differentially expressed genes. Data obtained from HMCB vs HUCD and JMCB vs JUCD comparisons consisted of 7096 and 6636 significant differentially expressed genes. Given that significant data from each HMCB vs HUCD and JMCB vs JUCD comparison was considerably larger than samples taken from HMCB vs HUCB and JMCB vs JUCB comparisons, the top 3000 most significantly differentially expressed genes in both HMCB vs HUCD and JMCB vs JUCD comparison datasets were input into IPA software for analysis. This is recommended by Qiagen as the upper limit of differentially expressed genes that can be input into IPA software.

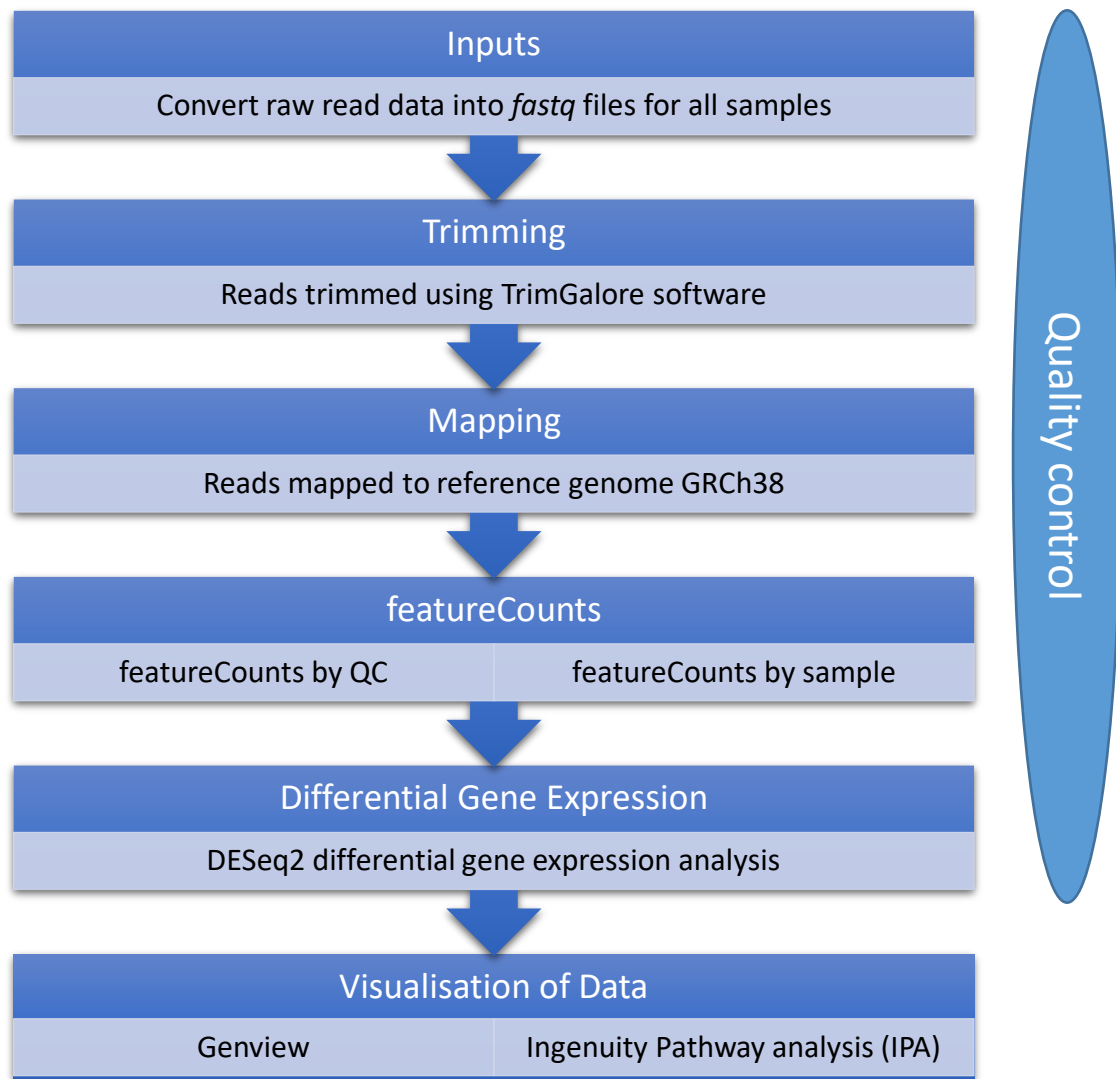


Figure 2.1. A flowchart illustrating the processes involved in the analysis of RNA sequencing data.

<i>Cell Type</i>	<b>Sample Comparison</b>
<i>H929</i>	HUCB vs HMCB
	HUCD vs HMCB
	HUCD vs HUCB
<i>JJN3</i>	JUCB vs JMCB
	JUCD vs JMCB
	JUCD vs JUCB

Table 2.7. A summary of the comparisons made to assess differential gene expression between each sample

## 2.4.2. Validation of protein expression

### 2.4.2.1. Reverse transcription reaction

In order to generate complimentary DNA (cDNA) samples suitable for use in a qPCR reaction, a reverse transcription assay was performed on RNA samples. Briefly, 250ng of RNA from each sample was converted to single stranded cDNA using a High Capacity cDNA Reverse Transcription Kit (Applied Biosystems). Each sample of RNA was made up to 10 $\mu$ l with nuclease-free water and mixed with a pre-prepared master mix containing reverse transcriptase enzyme, RT random primers and dNTPs in excess, as shown in Table 2.8. This solution was then placed in a Veriti DX (Thermo Fisher) thermocycler to facilitate the reverse transcription reaction to convert the RNA present within the sample to cDNA. The criteria for this thermocycler reaction are shown in Table 2.9. The final volume of this reaction was 20 $\mu$ L and samples were stored at -20°C until required for qPCR analysis.

<b>Component</b>	<b>Volume per sample (<math>\mu</math>l)</b>
<i>10x RT buffer</i>	2.0
<i>25x dNTP mix (100mM)</i>	0.8
<i>10x RT random primers</i>	2.0
<i>Multiscribe reverse transcriptase</i>	1.0
<i>Nuclease-free H<sub>2</sub>O</i>	4.2
<b>Total</b>	<b>15.0</b>

**Table 2.8.** Components of a High Capacity cDNA Reverse Transcription Kit used to generate cDNA from RNA extracts

	<b>Temperature (°C)</b>	<b>Time (mins)</b>
<i>Step 1</i>	25	10
<i>Step 2</i>	37	120
<i>Step 3</i>	85	5
<i>Step 4</i>	4	$\infty$

**Table 2.9.** Optimal temperature and time settings input into a Veriti DX thermocycler. This cycle was used to facilitate a reverse transcription assay as recommended by the High Capacity cDNA Reverse Transcription Kit (Applied Biosystems).

#### 2.4.2.2. Primer selection and design

In order to validate the significant differential gene expression results produced from RNA-seq analysis, a short list of target genes was selected for validation by qPCR. These genes were selected based on expression level as reported in the RNA-seq DESeq2 datasets, which were required to be high enough to ensure that detection was feasible during a qPCR experiment. Following the establishment of a gene list that fulfilled these criteria, it was important to cross-reference differential expression with absolute read count and  $\log_2$ [fold change] values from DESeq2 dataset, to ensure that there was a sufficient quantity of RNA within each sample.

Primers were designed using NCBI Primer BLAST where Primer3 software is utilised for primer design and coupled with BLAST software to determine primer specificity to the chosen target and to predict the risk of primers dimerising with one another<sup>262</sup>. There was more than one transcript variant associated with 5 out of 6 genes targeted for validation. This meant primers had to be designed to bind to and amplify common sequences between these transcript variants, the sequences of these primers are shown in Table 2.10.

It was also important to design primers that spanned an exon-exon junction of the target transcripts to ensure potential genomic DNA (gDNA) contaminants were not amplified instead of the required cDNA within each sample. Primers were then selected based on GC content (40-60%), melting temperature ( $T_m$ ) (58-63°C) and amplicon length (70-250 base pairs). Primers were generated by Eurofins Genomics and were provided in a lyophilised state. They were resuspended in nuclease-free water to make up primer solutions to 100 $\mu$ M.

<i>Gene</i>	<i>Description</i>	<i>Primer sequence (5' – 3')</i>	
<i>GAPDH</i>	Glyceraldehyde 3-phosphate dehydrogenase	Forward sequence	GTCTCCTCTGACTTCAACAGCG
		Reverse sequence	ACCACCCTGTTGCTGTAGCCAA
<i>SPP1</i>	Secreted phosphoprotein 1 (osteopontin)	Forward sequence	CGAGGTGATAGTGTGGTTTATGG
		Reverse sequence	GCACCATTCAACTCCTCGCTTTC
<i>SYK</i>	Spleen associated tyrosine kinase	Forward sequence	GAATCTGTGCTGGACATACGATG
		Reverse sequence	TGCGGGAGCGGTTAGTTC
<i>CXCL8</i>	CXC-motif chemokine ligand 8	Forward sequence	GAGAGTGATTGAGAGTGGACCAC
		Reverse sequence	CACAACCCTCTGCACCCAGTTT
<i>MMP2</i>	Matrix metalloproteinase 2	Forward sequence	AGCGAGTGGATGCCGCCTTTAA
		Reverse sequence	CATTCCAGGCATCTGCGATGAG
<i>CCL2</i>	CC-motif chemokine ligand 2	Forward sequence	CCCAAAGAAGCTGTGATCTTCA
		Reverse sequence	TCTGGGGAAAGCTAGGGGAA

**Table 2.10.** A list of target genes and corresponding forward and reverse primer pairs to be used in qPCR analysis

#### 2.4.2.3. Real-Time Polymerase Chain Reaction (qPCR)

In order to validate expression of previously selected genes, qPCR was performed. Previously generated cDNA samples were diluted 1:5 in nuclease-free water and primers were diluted to 10 $\mu$ M working stock solutions. A reaction master mix was made up for each pair of primers using SYBR® Green as shown in Table 2.11. SYBR® Green is a fluorescent dye that binds to the minor groove of double stranded DNA<sup>263</sup>. The intensity of its fluorescence increases as a result of this interaction, meaning that as more cDNA amplicon products are produced through the qPCR reaction, there is a net increase in fluorescence intensity, until the components within the reaction are eventually exhausted. Fluorescence intensity can then be quantified to determine relative levels of gene expression within a sample.

<b>Component</b>	<b>Volume per sample (<math>\mu\text{l}</math>)</b>
Power SYBR® Green PCR master mix	10.0
Forward primer (10 $\mu\text{M}$ )	1.0
Reverse primer (10 $\mu\text{M}$ )	1.0
Nuclease-free water	3.0
<b>Total</b>	<b>15.0</b>

**Table 2.11. Components of a qPCR master mix containing SYBR® Green to make a single 15 $\mu\text{L}$  reaction.** This was scaled where necessary to accommodate the appropriate number of samples in each experiment

<b>Phase</b>	<b>Initial denaturation</b>	<b>Denaturation and annealing</b>		<b>Melt Curve</b>		
<i>Stage</i>	1	1	2	1	2	3
<i>Number of cycles</i>	1	40		1		
<i>Temperature (<math>^{\circ}\text{C}</math>)</i>	95	95	60	95	60	95
<i>Time</i>	10 mins	15 secs	1 min	15 secs	1 min	15 secs

**Table 2.12. Stages of thermocycling throughout a qPCR reaction to facilitate cDNA denaturation, primer annealing and production of cDNA amplicons.**

Briefly, 15 $\mu\text{L}$  of master mix made for each primer pair was loaded into the appropriate wells of a MicroAmp Fast Optical 96-well reaction plate. These wells were then loaded with 5 $\mu\text{l}$  of each cDNA sample previously made from a reverse transcription reaction described in Section 2.4.2.1. The plates were sealed with a MicroAmp Optical Adhesive Film and centrifuged at 300 $\times g$  for 2 minutes to remove and any air bubbles that may have formed within the plate and to collect all reaction reagents at the bottom of each well. Plates were placed in a Vii7 Real-Time PCR system and the reaction was set to the thermocycler criteria outlined in Table 2.12.

#### 2.4.2.4. Analysis of qPCR data

Data collected from each qPCR experiment was initially analysed using ThermoFisher Cloud software to determine threshold cycle ( $C_t$ ) values for each gene analysed and to visualise melt curves and amplification plots. A comparative assessment of gene expression was then adopted against a GAPDH reference gene using the  $2^{-\Delta\Delta C_t}$  method<sup>264</sup>. This method compares the expression of each gene of interest against a GAPDH reference gene in CD138<sup>bright</sup> and CD138<sup>dim</sup> cells after co-culture with differentiated U937 cells in both H929 and JN3 myeloma cell lines. Gene expression within each of these samples is then compared with the corresponding monoculture CD138<sup>bright</sup> control sample in each myeloma cell line. These values were then converted to  $\log_2$  expression values to assess fold change. The calculation of  $2^{-\Delta\Delta C_t}$  for each condition as follows:

$$2^{-\Delta\Delta C_t} = 2^{-[(C_t \text{Gene of interest} - C_t \text{GAPDH}) \text{ Co-culture CD138}^{\text{bright}}] - (C_t \text{Gene of interest} - C_t \text{GAPDH}) \text{ Mono-culture CD138}^{\text{bright}}]}$$

$$2^{-\Delta\Delta C_t} = 2^{-[(C_t \text{Gene of interest} - C_t \text{GAPDH}) \text{ Co-culture CD138}^{\text{dim}}] - (C_t \text{Gene of interest} - C_t \text{GAPDH}) \text{ Mono-culture CD138}^{\text{dim}}]}$$

## **2.5. Statistical analysis**

All statistical analysis was performed using GraphPad Prism 7.0 software (GraphPad Software Inc., CA, USA), unless stated otherwise. P values <0.05 were considered statistically significant.

## CHAPTER 3: RESULTS

### Development and characterisation of an osteoclast-like *in vitro* niche

#### 3.1. Introduction

Multiple myeloma is a malignancy of terminally differentiated B-lymphocytes – known as plasma cells – that accumulate in the bone marrow<sup>265</sup>. The bone marrow microenvironment is an influential niche that is heavily involved in myeloma pathology. The cellular compartment of this niche is composed of numerous cell types that include stromal cells, osteoblasts and osteoclasts and direct cell-cell interactions between myeloma cells and these non-malignant cells of the bone marrow leads to enhanced myeloma cell survival, growth and resistance to therapy<sup>6</sup>. There is also substantial evidence that these effects are also controlled through soluble factor signalling<sup>159</sup>. These factors are responsible for myeloma cell sustenance and survival such as IL-6, osteoclast formation and function such as RANKL, inhibition of osteoblast function through OPG and bone matrix degradation such as matrix metalloproteases. Removal of myeloma cells from the bone marrow rapidly leads to apoptosis, highlighting the reliance myeloma cells have on this environment for their longevity.

Osteoclasts are highly specialised, multi-nucleated bone resorbing cells that are generated from monocytic precursor cells in response to RANK/RANKL signalling as part of normal bone remodelling<sup>196</sup>. Osteoclasts are influential in myeloma disease progression and have been shown to increase in number and activity as a result of myeloma cell interaction. This disrupts the homeostatic balance between osteoblast-induced bone formation and osteoclast-induced bone resorption in favour of the latter, which eventually results in the formation of painful bone lesions and predisposition to fracture in the majority of patients<sup>202</sup>. The exact mechanisms that lead to this phenomenon remain unresolved. In myeloma research there is currently no well-established, reproducible *in vitro* model that can effectively encapsulate the phenotype, morphology and function of human osteoclasts.

Myeloma cells are most commonly located in areas of active bone destruction. This suggests that these malignant plasma cells may preferentially interact with osteoclasts to exert these catastrophic effects. This cellular relationship has often been reported as being symbiotic, with myeloma cells contributing to an upregulation of osteoclast differentiation and subsequent activity, with osteoclasts contributing to increased myeloma cell survival and growth<sup>184,204</sup>. It was therefore of interest to investigate this relationship in an *in vitro* setting.

Primary osteoclast research *in vitro* is difficult due to the fact that osteoclasts exist in very small numbers in human bone marrow. Differentiating osteoclasts from bone marrow-derived haematopoietic precursors is efficient but not feasible due to the scarcity of such samples being available for research purposes<sup>242</sup>. It is also possible to differentiate osteoclasts from CD14<sup>+</sup> peripheral blood mononuclear cells (PBMCs) following treatment with RANKL and M-CSF<sup>266</sup>. However, it can take up to 3 weeks to differentiate these cells into functional osteoclasts *in vitro* using this procedure and this relies on the availability of peripheral blood samples from healthy donors. Again, this is potentially challenging and would also lead to considerable variation between donors in regard to age and sex, which would have to be accounted for. Taking these limitations into consideration, it was of interest to develop a humanised, reproducible *in vitro* model of human osteoclasts using a cell line.

### 3.1.1. Aims

The aim of this chapter was to develop and characterise a reproducible osteoclast-like microenvironment to be used in an *in vitro* setting. In order to do this U937 cells were treated with 100nM PMA for 48 hours followed by 10nM 1,25(OH)<sub>2</sub>D<sub>3</sub> for up to 10 days. A number of criteria were then assessed in order to determine the similarity of these cells to human osteoclasts:

1. Determine ability of treated U937 cells to form osteoclast-like cells through quantification of multinucleation, TRAP and RANK expression and ability to resorb bone material.
2. Assess the effects of myeloma cell co-culture with treated U937 cells on CD138 expression.

## 3.2. Differentiation of U937 cells into osteoclast-like cells

There is currently no cell line in existence that is representative of osteoclasts in a terminally differentiated state. However, there is evidence to suggest that cells of myelo-monocytic origin are capable of differentiating into osteoclast-like cells. The U937 cell line is a human myeloid leukaemia cell line derived from a histiocytic lymphoma and has been previously shown to respond to treatment with phorbol esters such as phorbol 12-myristate 13-acetate (PMA) or  $1,25(\text{OH})_2\text{D}_3$  – the active metabolite of vitamin D<sub>3</sub> to form multinucleated osteoclast-like cells<sup>248-250</sup>. It was important to characterise and validate U937 cells as a suitable cell line for an *in vitro* osteoclast model to use in myeloma research. Such a model could provide a foundation to investigate the mechanisms and effects of osteoclasts on myeloma cell survival, resistance to therapeutic agents and could also provide a platform for *ex vivo* primary myeloma cell research.

### 3.2.1. Treatment with $1,25(\text{OH})_2\text{D}_3$ induces morphological changes in U937 cells

To confirm previous findings, U937 cells were sequentially treated with PMA for 48 hours, followed by treatment with  $1,25(\text{OH})_2\text{D}_3$  for up to 10 days (Figure 3.1). Treatment with  $1,25(\text{OH})_2\text{D}_3$  was carried out at Day 0. Treatment with PMA caused U937 cells to become adherent to tissue culture plastic and the addition of  $1,25(\text{OH})_2\text{D}_3$  caused these adhered cells to merge with one another. This was not the case in cells treated with PMA alone, where U937 cells adhered to one another on the tissue culture plastic without merging to form larger cells (Figure 3.2A). At the final time point of treatment, it was evident that the rate of differentiation was not uniform across the entire treated population. Some treated U937 cells had adhered to one another without completely merging, whilst other treated cells appeared much larger and more mature in morphology, visually resembling conventional human osteoclasts (Figure 3.2A). Whilst both treated and untreated U937 cells continued to proliferate in culture, treatment with PMA and  $1,25(\text{OH})_2\text{D}_3$  resulted in a significant decrease in U937 cell number in comparison to untreated controls at each timepoint beyond day 3 of treatment with  $1,25(\text{OH})_2\text{D}_3$  ( $p < 0.05$ ; Figure 3.2B). This indicates that treatment also results in a decrease in the rate of proliferation in U937 cells.

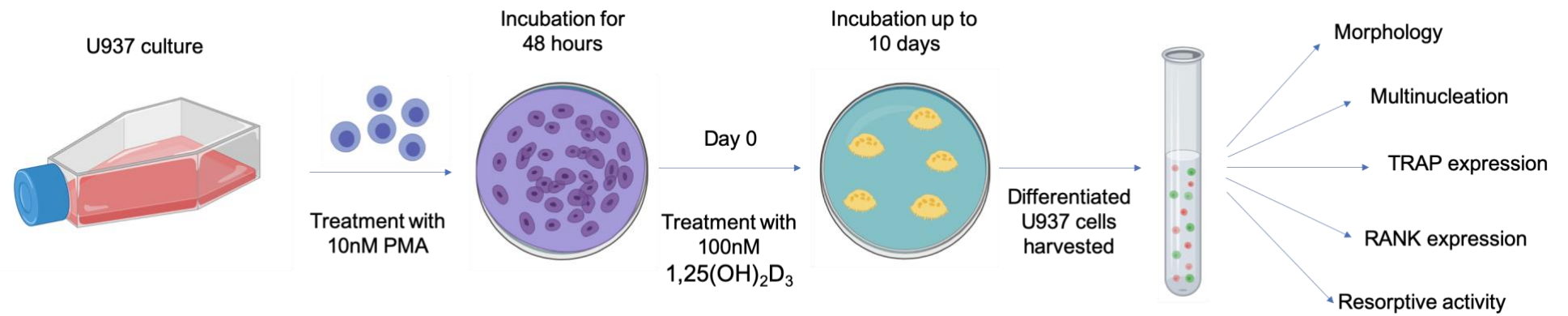
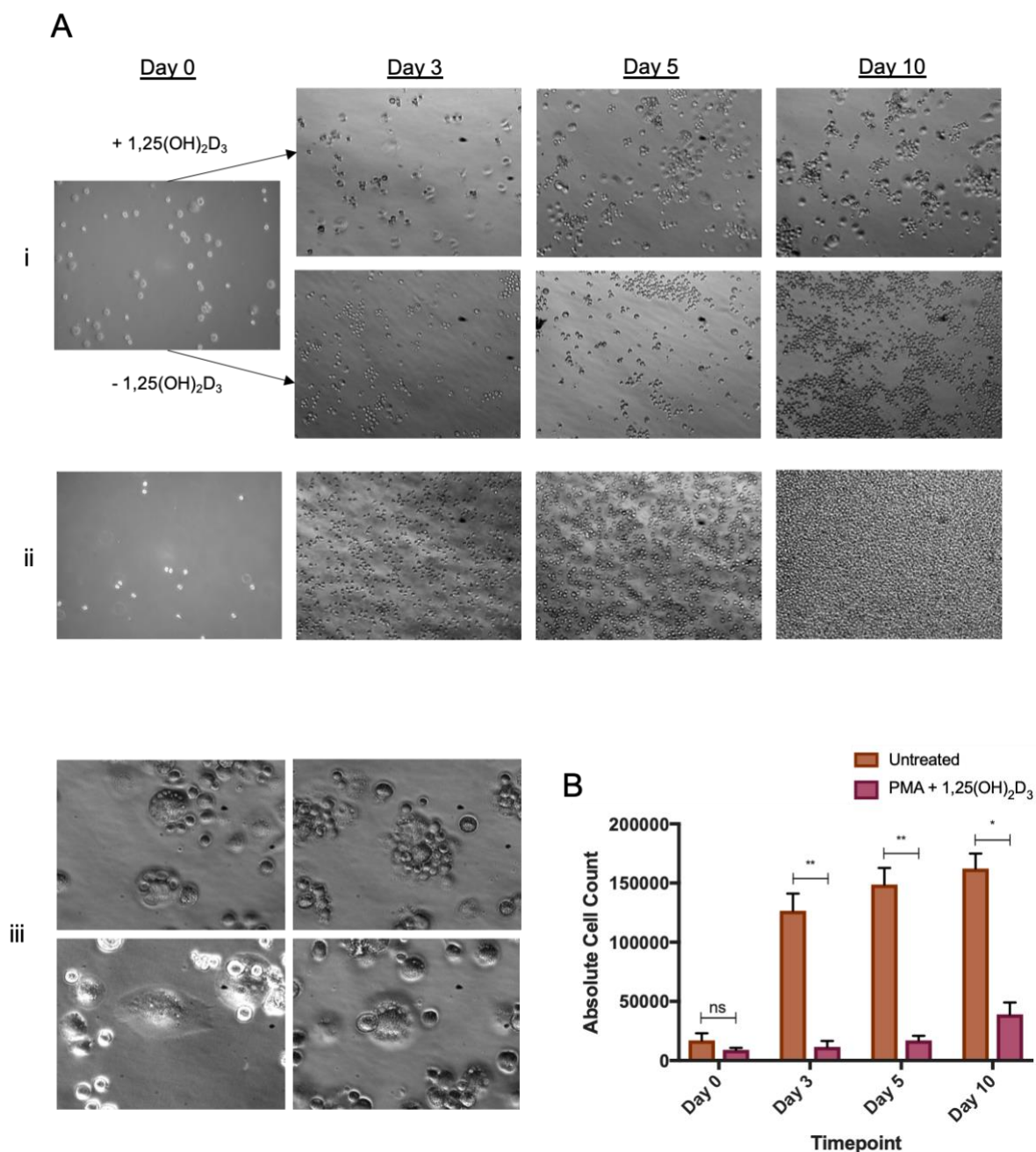


Figure 3.1. Timeline of U937 cell treatment with PMA and 1,25(OH)<sub>2</sub>D<sub>3</sub>.



**Figure 3.2. The effect of PMA and 1,25(OH)<sub>2</sub>D<sub>3</sub> on U937 cell morphology, number and viability.** (A) Representative brightfield images of U937 cells were taken after culture with 100nM PMA for 48 hours followed by culture with or without 10nM 1,25(OH)<sub>2</sub>D<sub>3</sub> for 10 days (i). Images of untreated U937 cells were also taken after concurrent culture with RPMI 1640 media alone (ii). Higher magnification images were taken of U937 cells at the final timepoint of sequential treatment with PMA and 1,25(OH)<sub>2</sub>D<sub>3</sub> (iii). (B) Absolute cell counts were recorded at each time point using an Accuri C6 flow cytometer in both treated and untreated U937 cells at the specified timepoints (n=3). A paired *t*-test was performed at each timepoint to assess statistical significance using GraphPad Prism 7.0 software (ns – not significant, \* = *p*<0.05, \*\* = *p*<0.01).

### 3.2.2. Treatment with PMA and 1,25(OH)<sub>2</sub>D<sub>3</sub> causes U937 cells to increase in size

Visually, it was clear that the process of U937 cell differentiation, as a result of treatment with PMA and 1,25(OH)<sub>2</sub>D<sub>3</sub>, was not maximally efficient. Therefore, to accommodate this during downstream analysis, U937 cells were initially gated using forward and side scatter (Figure 3.3A). Untreated U937 cells were used as a baseline to represent undifferentiated cells. Events collected from treated U937 cells that had an increased forward and side scatter profile compared with untreated U937 cells were collected in a larger cell gate. The proportion of events detected in the larger cell gate significantly increased over time in treated U937 samples ( $p < 0.01$ ; Figure 3.3B). A mean of 38.3% of treated U937 cells were detected in the larger cell gate at the final timepoint in response to treatment. This data indicates that U937 cells increase in cell size and become more morphologically complex as can be seen from the significant increase of forward and side scatter as a result of treatment with PMA and 1,25(OH)<sub>2</sub>D<sub>3</sub> in a time-dependent manner.

It was also important to establish that this increase in forward and side scatter was not as a result of treated U937 cells undergoing apoptosis. Therefore, cells were stained with annexin-V at each treatment timepoint to assess viability. There was no significant difference in cell viability over the course of treatment in U937 cells, showing that treatment with PMA and 1,25(OH)<sub>2</sub>D<sub>3</sub> was not toxic to U937 cells at the doses used throughout the entire course of treatment ( $p > 0.05$ ; Figure 3.3C).

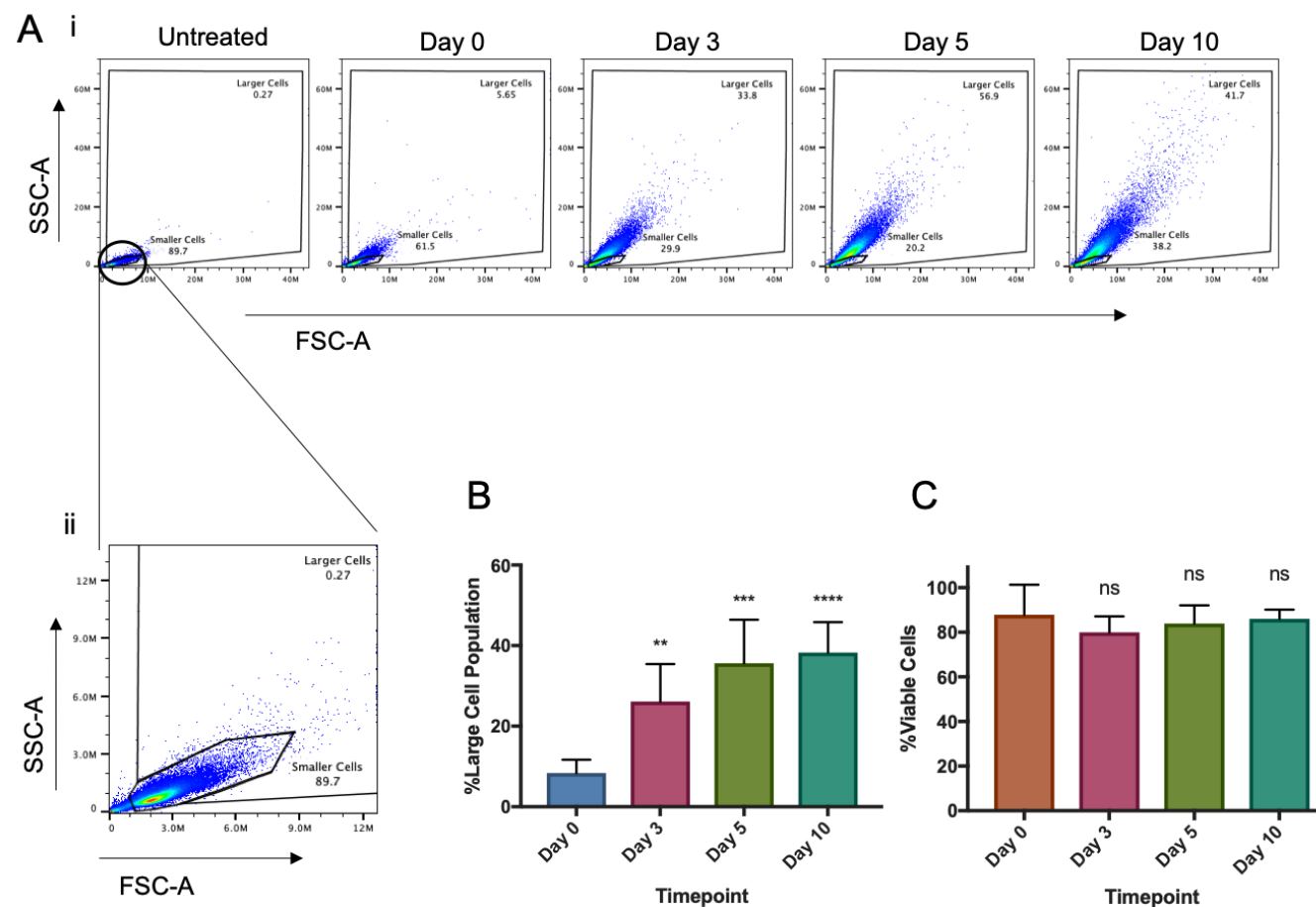


**Figure 3.3. The effect of PMA and 1,25(OH)<sub>2</sub>D<sub>3</sub> on U937 cell size.** (A) The size of U937 cells treated with PMA and 1,25(OH)<sub>2</sub>D<sub>3</sub> was assessed using an Accuri C6 flow cytometer at each specified time point. Cells were initially gated based on forward and side scatter (i). Untreated U937 cells were used as a baseline to draw a smaller cell gate (ii), with a larger cell gate encompassing the remainder of the forward and side scatter plot. (B) The proportion of U937 cells that were detected in the larger cell gate was quantified (n=6). (C) Cell viability was measured using Annexin V-FITC staining at each time point in treated U937 cells. To assess statistical significance GraphPad Prism 7.0 software was used. A one-way ANOVA was performed followed by a Dunnett multiple comparison test to compare the mean at each timepoint to Day 0 controls (ns – not significant, \*\* - p<0.01, \*\*\* - p<0.001, \*\*\*\* - p<0.0001).

### 3.2.3. Treatment with PMA and 1,25(OH)<sub>2</sub>D<sub>3</sub> increases in DNA content in U937 cells

In order to quantify the DNA content of U937 cells over time in response to treatment, staining with propidium iodide (PI) was used. The stoichiometric binding of PI to DNA enables an assessment of the DNA content of a cell based on PI fluorescence<sup>267</sup>.

From the resulting histograms, gates were drawn to determine the proportion of cells that possessed the nuclear content of a cell in G1 (2n) and G2 (4n) phase of the cell cycle. Cells that had an increased DNA content greater than 4n, were quantified in the 4n+ gate. Representative overlaid histograms of these data showed a time-dependent increase in the proportion of treated U937 cells that occupied the 4n+ gate collected in the large cell gate, compared with the small cell gate (Figure 3.4A). The collated data from treated U937 cells collected in the large cell gate indicated a significant decrease in the number of cells detected in the G1 gate ( $p < 0.0001$ ), compared with a significant increase in the number of cells detected in the 4n+ gate ( $p < 0.001$ ). This was not the case with treated U937 cells collected in the small cell gate, where no significant changes were observed in the proportion of cells collected in the G1, G2 or 4n+ gates ( $p > 0.05$ ) (Figure 3.4B). This quantitative data re-capitulates what was observed microscopically when it was visually apparent that treated U937 cells merge with one another to form larger osteoclast-like cells. This shows that treatment with PMA and 1,25(OH)<sub>2</sub>D<sub>3</sub> results in an increase in DNA content in larger U937 cells as a result of treatment-induced cellular merging to form multinucleated cells.

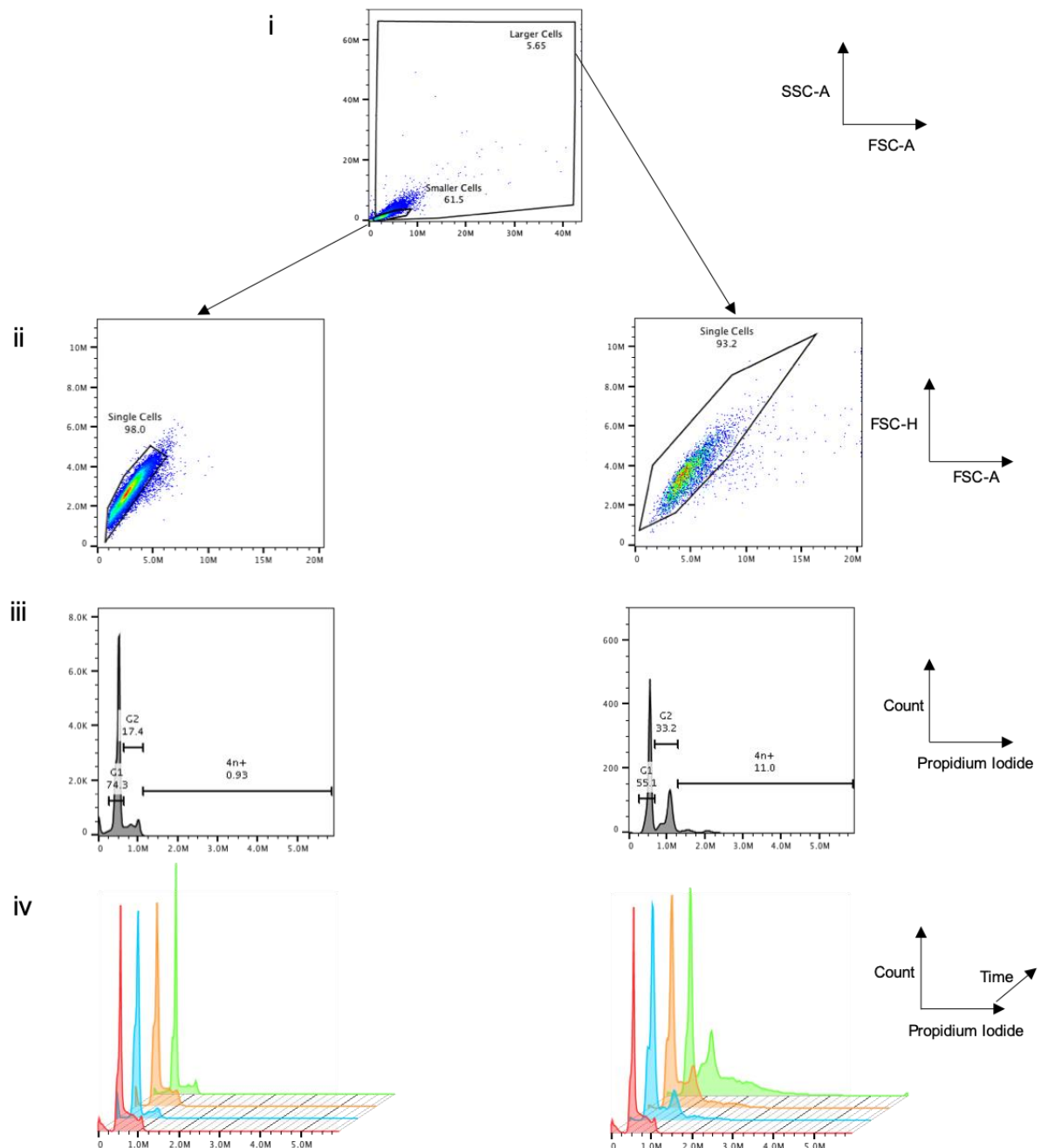


**Figure 3.4A. The effect of PMA and 1,25(OH)<sub>2</sub>D<sub>3</sub> on the DNA content of U937 cells.** Representative images of the gating strategy used to determine the DNA content of U937 cells following sequential treatment with PMA for 48 hours and 1,25(OH)<sub>2</sub>D<sub>3</sub> for up to 10 days. Cells were initially gated based on size using forward and side scatter and were separated into small and large cell populations using untreated U937 cells as a baseline reference population for gating (i). Single cell populations were then determined using a forward scatter height vs area plot (ii). Propidium iodide content was assessed within these single cell populations with gates drawn to represent G1, G2 and 4n+ populations of cells (iii). Representative overlaid histograms show PI positivity of U937 cells following treatment over a 10-day time course, representative samples were normalised to untreated controls in order to accommodate the differences in cell number in the small and large cell gates (iv).

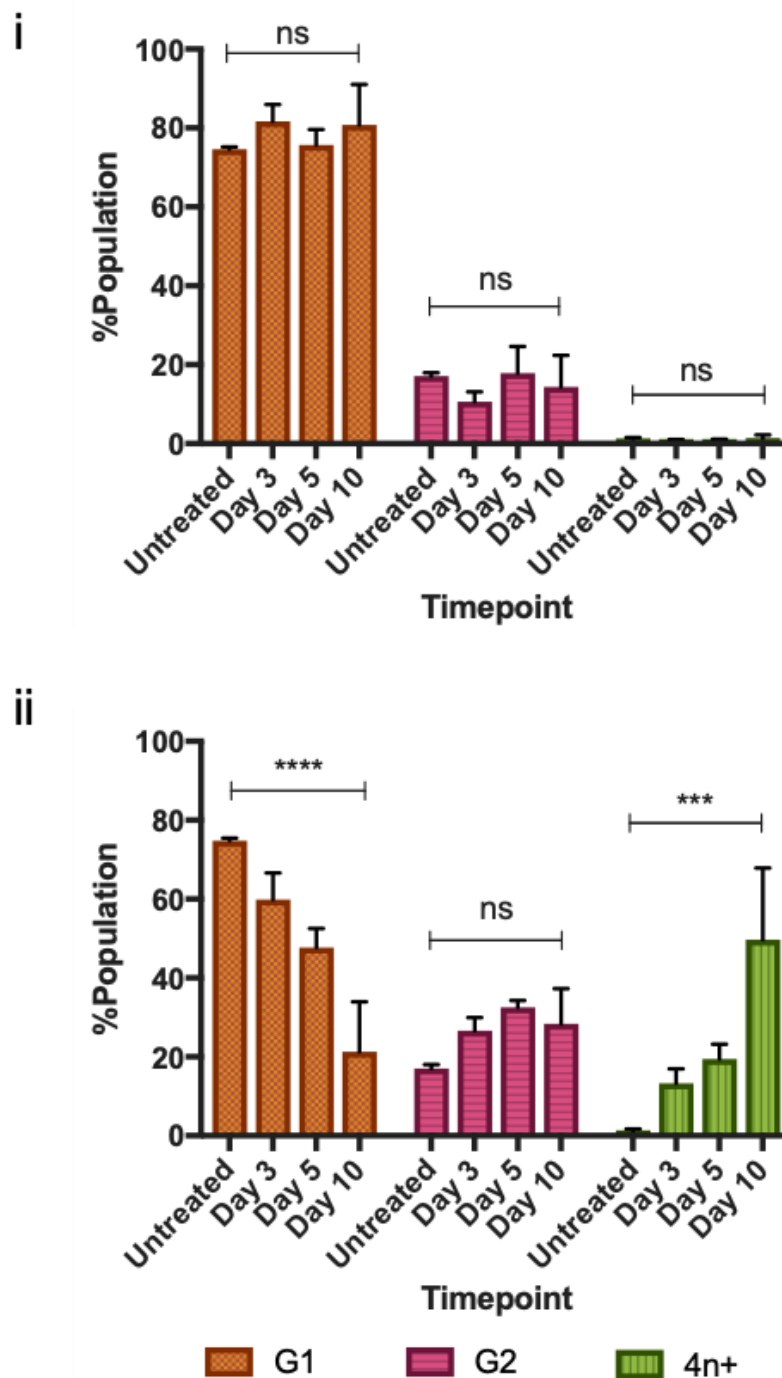


**Figure 3.4B. The effect of PMA and  $1,25(\text{OH})_2\text{D}_3$  on the DNA content of U937 cells.** The population (%) of U937 cells in either G1, G2 or 4n+ gates were assessed in both small (i) and large (ii) cell populations (n=4). To assess statistical significance GraphPad Prism 7.0 software was used. A one-way ANOVA was performed followed by a Dunnett multiple comparison test to compare the mean at each timepoint to untreated controls. (ns – not significant, \*\* -  $p < 0.01$ , \*\*\* -  $p < 0.001$ , \*\*\*\* -  $p < 0.0001$ ).

### 3.2.4. Treatment with PMA and 1,25(OH)<sub>2</sub>D<sub>3</sub> induces U937 cell multinucleation

Osteoclasts are differentiated from mononuclear haematopoietic precursor cells in response to RANK/RANKL signalling – a process which is often induced by bone-producing osteoblasts<sup>207</sup>. This feedback loop forms the basis of homeostatic bone remodelling. In response to elevated levels of RANKL binding to RANK on the surface of osteoclast precursors, these cells merge with one another to form multi-nucleated cells and adhere to calcified bone material to exert their osteolytic function<sup>268</sup>. Given that multinucleation is a fundamental characteristic of functional osteoclasts, it was of interest to establish whether this was the case in U937 cells treated with PMA and 1,25(OH)<sub>2</sub>D<sub>3</sub>.

DAPI staining was employed to visualise and enumerate the nuclei in representative U937 cells that had been treated sequentially with PMA for 48 hours and 1,25(OH)<sub>2</sub>D<sub>3</sub> for a further 10 days. Cells that had merged to visually resemble conventional human osteoclasts in each culture were imaged. Multiple nuclei within these treated U937 cells were observed after DAPI staining when compared with the same cells visualised using a brightfield filter (Figure 3.5). The number of nuclei differed between each individual cell, with a minimum of two nuclei and a maximum of 14 nuclei being observed in these particular samples, perhaps reflecting the different rates of differentiation observed in treated U937 cells.

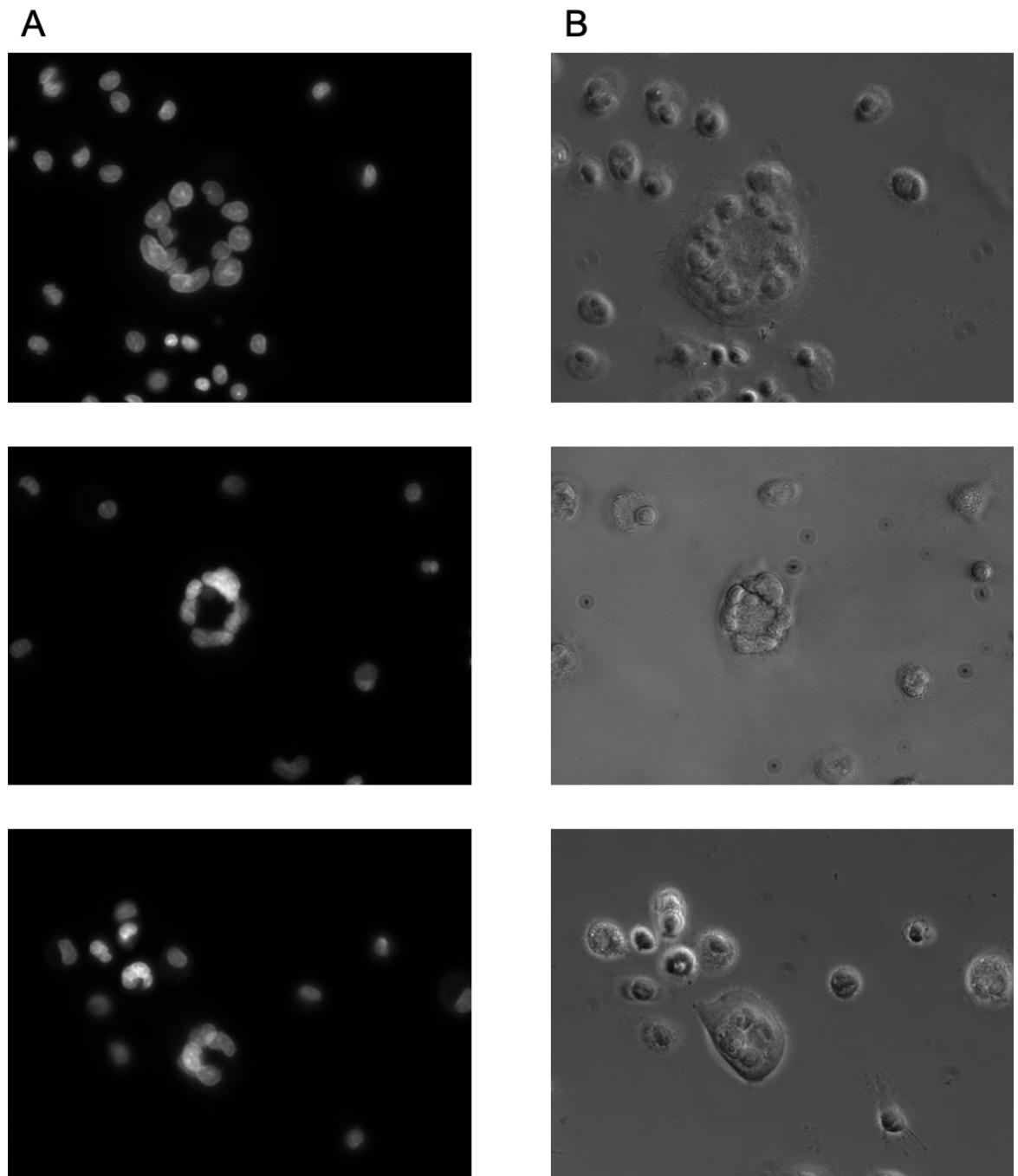


**Figure 3.5. The effect of PMA and  $1,25(\text{OH})_2\text{D}_3$  on U937 cell multinucleation.** Representative images of U937 cells following sequential treatment with PMA for 48 hours and  $1,25(\text{OH})_2\text{D}_3$  for a further 10 days. Images of the cells were taken using a DAPI filter; DAPI-stained nuclei were visualised as bright white (A). These images were then directly compared with the same samples using a brightfield filter (B) on a Zeiss Axio Observer Z1 microscope.

### 3.2.5. Tartrate resistant acid phosphatase (TRAP) expression in U937 cells

The expression and activity of tartrate resistant acid phosphatase (TRAP) is regarded as an important biochemical marker of osteoclasts and is also used as a measure of osteoclast function in relation to bone resorptive activity<sup>269,270</sup>. It was therefore of interest to determine whether U937 cells treated with PMA and 1,25(OH)<sub>2</sub>D<sub>3</sub> were expressers of TRAP. This was determined through cellular staining with a solution containing naphthol AS-BI phosphoric acid and freshly diazotized fast garnet GBC. U937 cells were treated with PMA for 48 hours, followed by 1,25(OH)<sub>2</sub>D<sub>3</sub> for a further 10 days before being assessed for TRAP activity. It was clear that the majority of these adherent cells expressed TRAP (Figure 3.6A) in response to treatment.

Upon observation at a greater magnification, it was also evident that TRAP was expressed in a granular fashion (Figure 3.6B). This was not the case in cells treated only with PMA; no purple colouration was observed in these adherent cells indicating that 1,25(OH)<sub>2</sub>D<sub>3</sub> is required to upregulate TRAP activity (Figure 3.6C). This shows that treatment with both PMA and 1,25(OH)<sub>2</sub>D<sub>3</sub> causes an increase in TRAP activity in U937 cells and provides further evidence that this treatment combination causes these cells to undergo the process of differentiation into an osteoclast-like morphology.

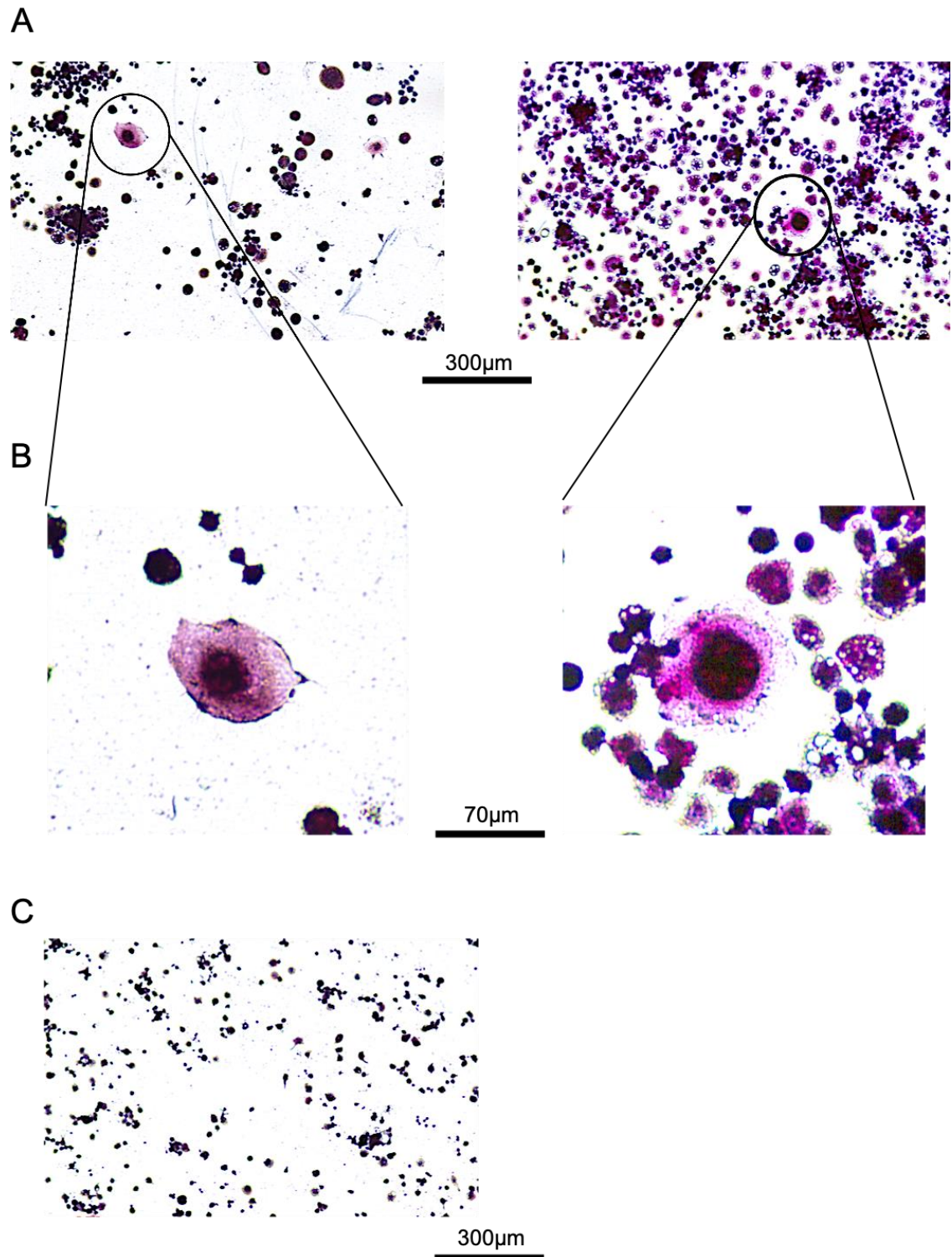


**Figure 3.6. The effect of PMA and 1,25(OH)<sub>2</sub>D<sub>3</sub> on U937 TRAP expression.** Representative images of treated U937 cells stained with TRAP stain after treatment with PMA for 48 hours and a further 10 days of treatment with 1,25(OH)<sub>2</sub>D<sub>3</sub>, with purple staining indicating the presence of TRAP. (A) A colour brightfield microscope was used to image TRAP-stained U937 cells following treatment. (B) Images at higher magnification were also taken to highlight individual cells. (C) U937 cells were treated with PMA for 48 hours and the media was replaced with 1,25(OH)<sub>2</sub>D<sub>3</sub>-free media over 10 days. Cells were then stained for TRAP activity and imaged in the same fashion as for 1,25(OH)<sub>2</sub>D<sub>3</sub> treated cells.

### 3.2.6. U937 cell expression of Receptor Activator of Nuclear Factor-kappa B (RANK)

RANK is upregulated on the surface membrane of monocytic myeloid precursor cells to initiate differentiation into multi-nucleated, bone resorbing cells in response to RANKL and continues to be expressed on mature osteoclasts<sup>207</sup>. It was therefore of interest to quantify RANK expression on U937 cells in response to treatment with PMA and 1,25(OH)<sub>2</sub>D<sub>3</sub>. RANK expression was measured using flow cytometry, with U937 cells being gated initially using forward and side scatter to distinguish between differentiated and undifferentiated cells following treatment. Representative histograms illustrating RANK expression over time show an increase in RANK expression on the surface of treated U937 cells in the larger cell gate compared to treated U937 cells in the smaller cell gate. This is also shown to be a significant phenomenon ( $p < 0.0001$ ) in cells analysed in the larger cell gate, whereas cells in the smaller cell gate did not significantly upregulate RANK ( $p > 0.05$ ; Figure 3.7). This shows that U937 cells that increase in size and nuclear content in response to treatment, also upregulate RANK. This provides further evidence that U937 cells are differentiating into cells that are representative of an osteoclast morphology and phenotype.

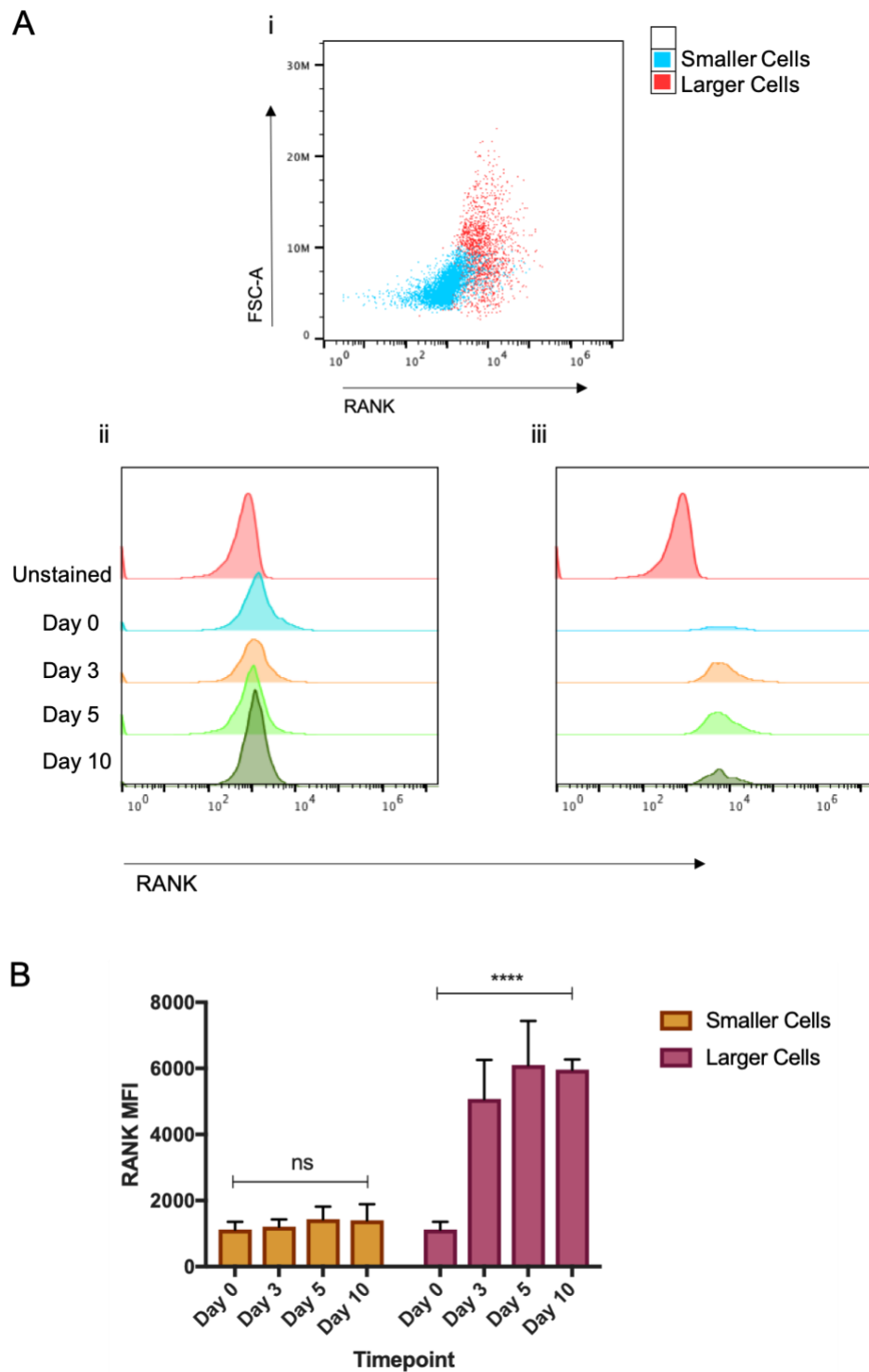


**Figure 3.7. The effect of PMA and  $1,25(\text{OH})_2\text{D}_3$  on RANK expression in U937 cells.** U937 cells were stained with PE-conjugated RANK monoclonal antibody and assessed for RANK expression using an Accuri C6 flow cytometer over a 10-day time period. (A) Representative bivariate plot showing two distinct populations of RANK positive (red) and negative cells (blue) after 10 days of treatment (i). Overlaid histograms illustrated RANK expression over time in both the (ii) smaller cell and (iii) larger cell populations of treated U937 cells against an unstained control. (B) RANK MFI was also assessed to illustrate RANK expression over time in both the smaller and larger cell populations of U937 cells over a 10-day time course of treatment with PMA and  $1,25(\text{OH})_2\text{D}_3$  ( $n=4$ ). To assess statistical significance GraphPad Prism 7.0 software was used. A one-way ANOVA was performed followed by a Dunnett multiple comparison test to compare the mean at each timepoint to Day 0 controls. (ns – not significant, \*\*\*\* -  $p<0.0001$ ).

### 3.2.7. Resorption of bone material by differentiated U937 cells

Osteoclasts play an essential role in the process of bone remodelling and have the unique capacity to resorb bone material<sup>196</sup>. It was therefore of importance to assess whether U937 cells that had differentiated in response to treatment with PMA and  $1,25(\text{OH})_2\text{D}_3$  had also developed this capability. Ivory was used as a mineralised substrate to investigate these potential resorptive properties and U937 cells were cultured and treated on sterilised ivory disks for up to 1 month. Following removal of differentiated U937 cells that had adhered to the ivory, the disks were imaged using scanning electron microscopy (SEM) alongside a control ivory disk that had not been used in culture and ivory disks that had been cultured with untreated U937 cells (Figure 3.8A). The presence of cell remnants on the disk shows that treated U937 cells had differentiated and adhered to the disk surface as a result of treatment, in a manner similar to conventional osteoclasts (Figure 3.8B). The space within the area of ivory that each cell had occupied, displayed a flatter and smoother surface compared to areas of ivory that appear to be untouched by differentiated U937 cells. Areas of positive staining with toluidine blue were also noted in Figure 3.8C where darker regions of ivory clearly outline where cells had adhered to during culture. This could indicate areas of resorption on the surface of the ivory disks as a result of U937 cell culture.

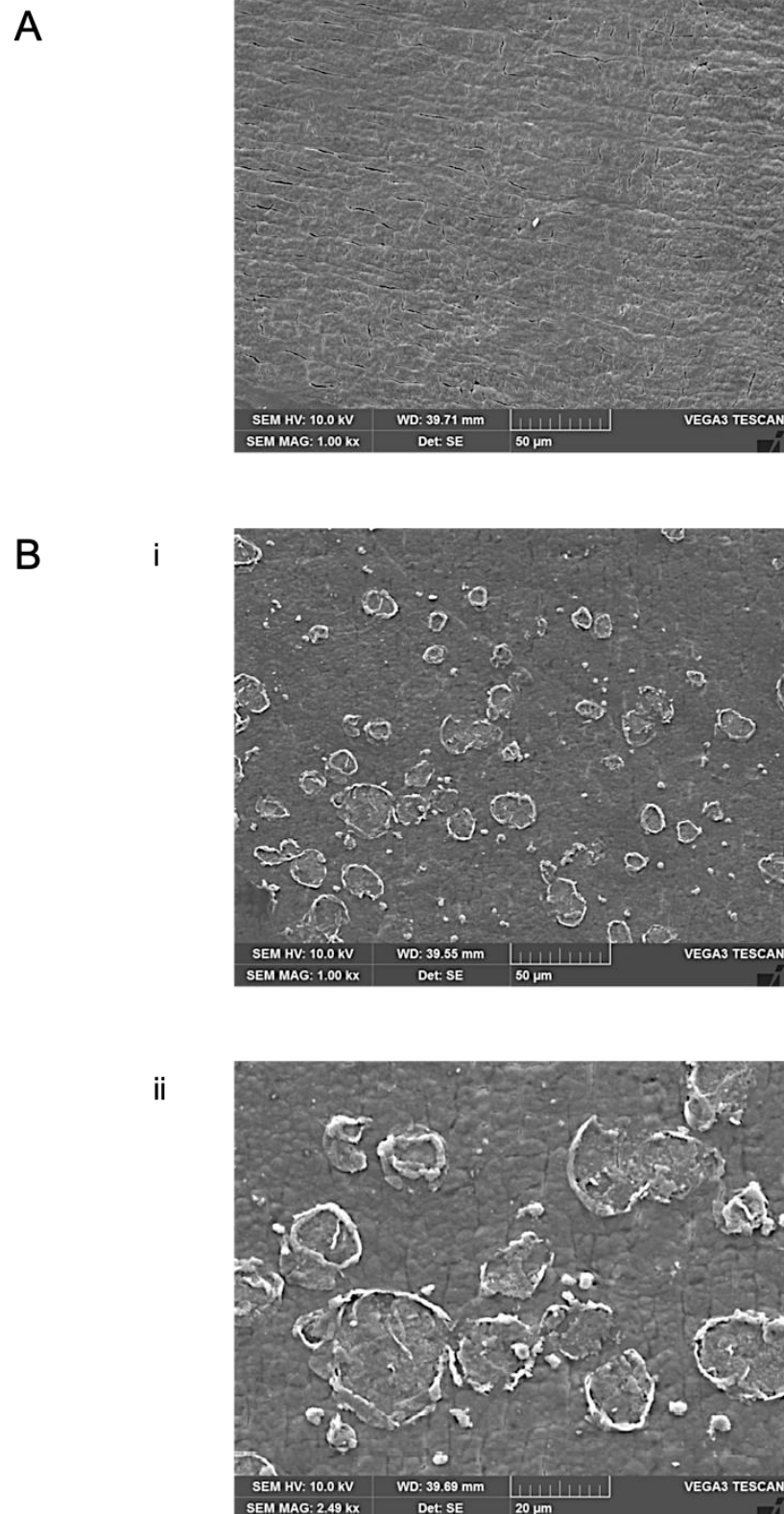


**Figure 3.8. Scanning electron microscopy (SEM) imaging of ivory disks after culture with treated U937 cells.** U937 cells were cultured on ivory in the same fashion as previously described in tissue culture plastic. However, these cells were cultured for up to one month before being imaged using SEM. (A) Representative image of ivory kept in RPMI 1640 media as a cell-free control. (B) Representative images of ivory cultured with U937 cells treated sequentially with PMA and  $1,25(\text{OH})_2\text{D}_3$  after one month at a magnification of (i) 1.00kx and (ii) 2.49kx.

C

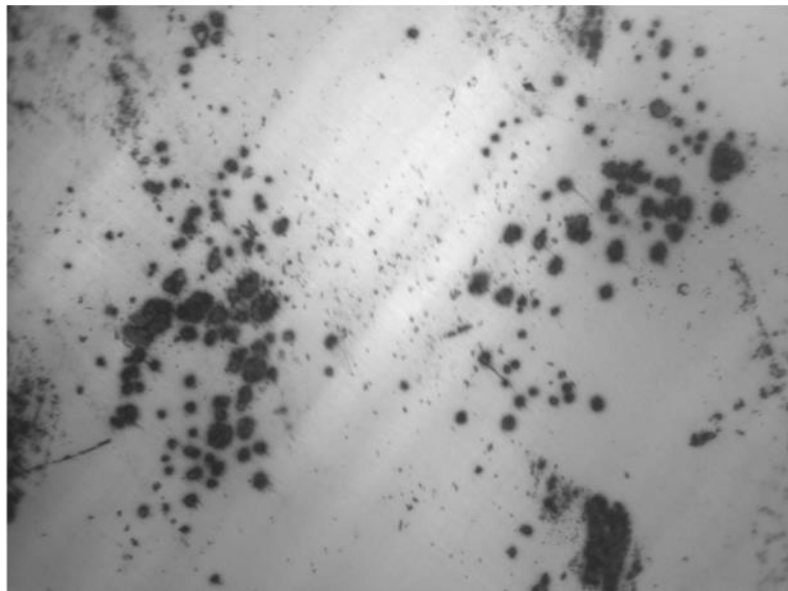
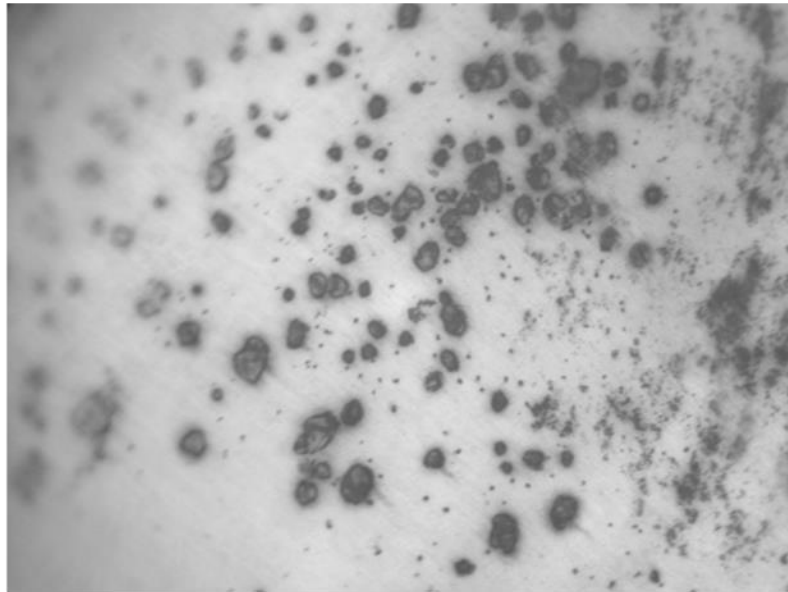


**Figure 3.8 (continued).** Image of ivory disks stained with toluidine blue following culture with treated U937 cells. U937 cells were cultured on ivory in the same fashion as previously described in tissue culture plastic. However, these cells were cultured for up to one month before being removed and the disks stained with toluidine blue. (C) Representative images were taken of these disks using a light microscope.

### 3.3. CD138 expression in myeloma cells

Having established that U937 cells can be differentiated into multi-nucleated cells that possess morphological and phenotypic features of osteoclasts, it was of interest to determine how these osteoclast-like cells could influence myeloma cell phenotype and function. CD138, also known as syndecan-1, is a cell surface marker almost exclusively expressed by plasma cells, following terminal differentiation from their B-cell precursors<sup>34</sup>. As a result, CD138 continues to be expressed by myeloma cells and can be used in diagnostics and myeloma cell purification from clinical samples<sup>271</sup>. Plasma cells, both normal and malignant, also express high levels of CD38 in comparison with other haematopoietic cells of either lymphoid or myeloid origin<sup>272</sup>. Co-expression of these two surface antigens provides a useful identification strategy for myeloma plasma cells, with CD38 in particular also proving to be a promising therapeutic target through treatment with daratumumab<sup>273</sup>.

H929 and JJN3 cells are myeloma cell lines that are both known to express CD138 and CD38<sup>241</sup>. Therefore, flow cytometric analysis of these antigens was used to positively identify myeloma cells in these experiments. Initial analysis of H929 cells revealed a subpopulation of CD138<sup>dim</sup> cells, which confirmed previous findings from a number of reports<sup>41,42,274</sup>. To my knowledge, there have been no previous reports explicitly highlighting the presence of a similar subpopulation of CD138<sup>dim</sup> cells in the JJN3 cell line. However, this was uniquely confirmed in the data presented in this research. Therefore, both CD138<sup>bright</sup> and CD138<sup>dim</sup> cells were taken into consideration in the gating strategies of subsequent experiments (Figure 3.9).

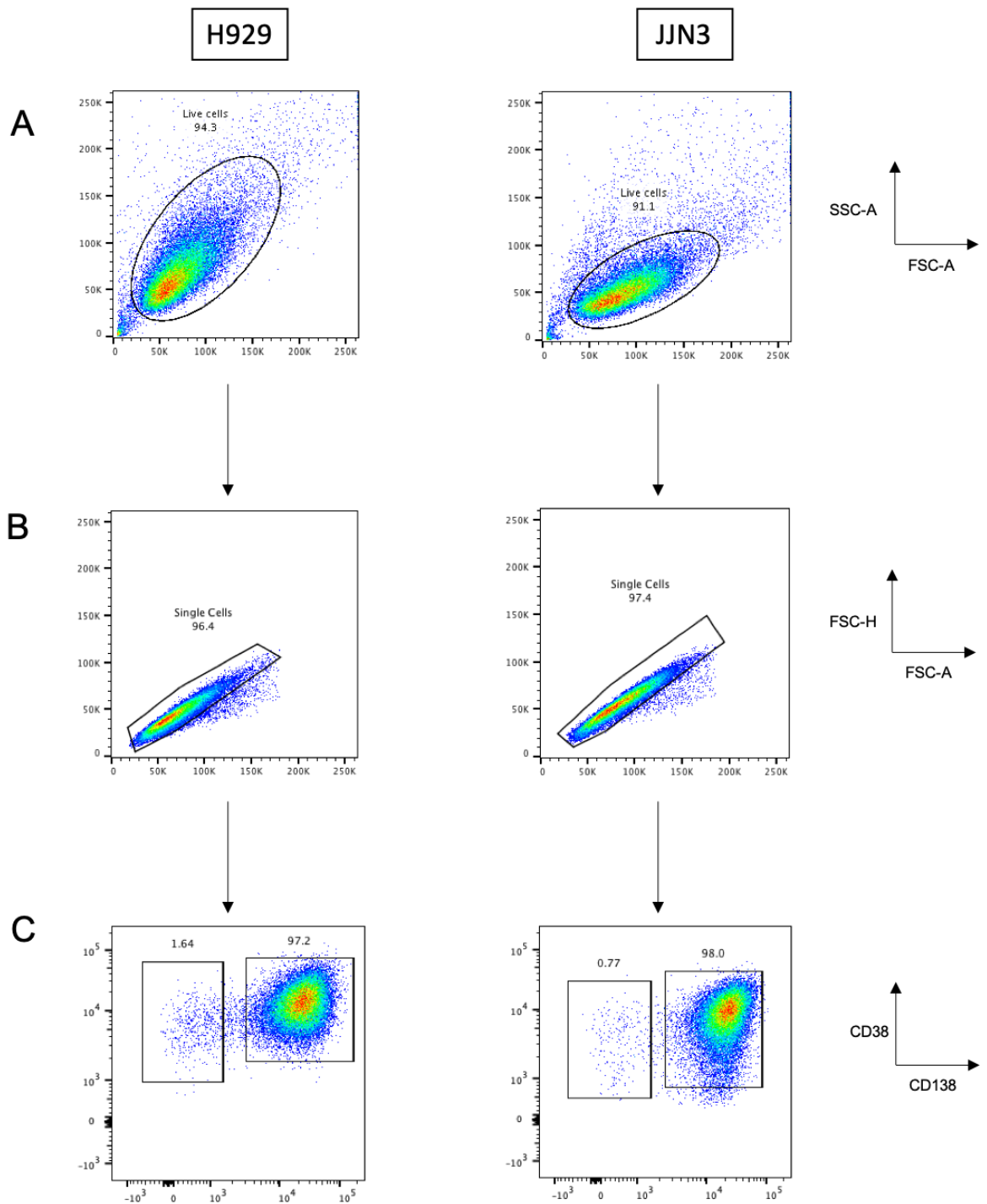


**Figure 3.9. Gating strategy to assess the expression of CD138 and CD38 in myeloma cells lines.** H929 and JJN3 cells were assessed for CD138 and CD38 expression using an Accuri C6 flow cytometer. Representative images were taken from mono-culture samples. (A) Cells were initially gated through forward and side scatter profiles. (B) Single cell populations were determined through gating with forward scatter height vs area. (C) Cells were then gated using CD138 and CD38 positivity, where two gates were drawn to determine cells that were CD138<sup>bright</sup>/CD38<sup>bright</sup> or CD138<sup>dim</sup>/CD38<sup>bright</sup>.

### 3.3.1. Identification of a CD138<sup>dim</sup> population of myeloma cells

Having identified a CD138<sup>dim</sup> sub-population in both H929 and JLN3 cells in monoculture, it was of interest to then investigate whether this phenotype was altered as a result of co-culture with other cells that are found in the bone marrow microenvironment.

The proportion of myeloma cells that possessed a CD138<sup>dim</sup> phenotype did not alter as a result of co-culture with HS-5, SAOS-2 or CD40-ligand expressing fibroblasts. This meant the vast majority of these myeloma cells continued to express a CD138<sup>bright</sup> phenotype. Under these conditions, the proportion of cells that were CD138<sup>dim</sup> did not alter significantly in H929 cells but significantly decreased in JLN3 cells ( $p < 0.05$ ). However, when H929 and JLN3 myeloma cells were cultured on U937 cells, which had been differentiated with PMA for 48 hours and  $1,25(\text{OH})_2\text{D}_3$  for a further 5 days, there was a distinct and significant expansion in the proportion of H929 ( $p < 0.01$ ) and JLN3 ( $p < 0.05$ ) myeloma cells that were CD138<sup>dim</sup> (Figure 3.10). This indicates that differentiated U937 cells are capable of influencing the surface phenotype of myeloma cells as a result of co-culture.

It was also of interest to determine whether this significant expansion of CD138<sup>dim</sup> myeloma cells as a result of co-culture with differentiated U937 cells could also be influenced by soluble factor signalling. Both myeloma cells were cultured in Transwell® chambers placed directly above cultures of differentiated U937 cells to ensure that no direct cell-cell contact could take place between these two cell types. Media within these cultures was shared through the permeable membrane of the Transwell® chambers, meaning the influence of soluble factor signalling could be determined with regard to CD138 expression.

This revealed a significant increase in the proportion of CD138<sup>dim</sup> cells in H929 cells after 48 hours of culture in a Transwell® chamber ( $p < 0.01$ ). However, it is clear that this difference wasn't numerically as great as H929 cells cultured in direct contact with differentiated U937 cells. Conversely, JLN3 cells did not elicit a significant expansion in the same fashion as H929 cells after co-culture in a Transwell® chamber ( $p > 0.05$ ) (Figure 3.11).

### 3.3.2. CD138<sup>dim</sup> myeloma cells represent a live population

It is been previously reported that myeloma cells shed CD138 from their surface as a consequence of undergoing apoptosis<sup>275</sup>. To investigate whether this was the case in each CD138<sup>dim</sup> subpopulation identified in this project, myeloma cells were assessed for viability using annexin V staining following co-culture with differentiated U937 cells. The combined mean proportions of annexin V<sup>negative</sup> cells in both CD138<sup>bright</sup> and CD138<sup>dim</sup> subpopulations of myeloma cells was 99.1% in H929 cells and 99.6% in JLN3 cells (Figure 3.12). This clearly showed that both CD138<sup>bright</sup> and CD138<sup>dim</sup> cells were negative for annexin V binding and were not undergoing apoptotic cell death. This demonstrates that the genesis of CD138<sup>dim</sup> myeloma cells was not as a consequence of CD138<sup>bright</sup> cells undergoing apoptosis and subsequently shedding CD138 from their surface.

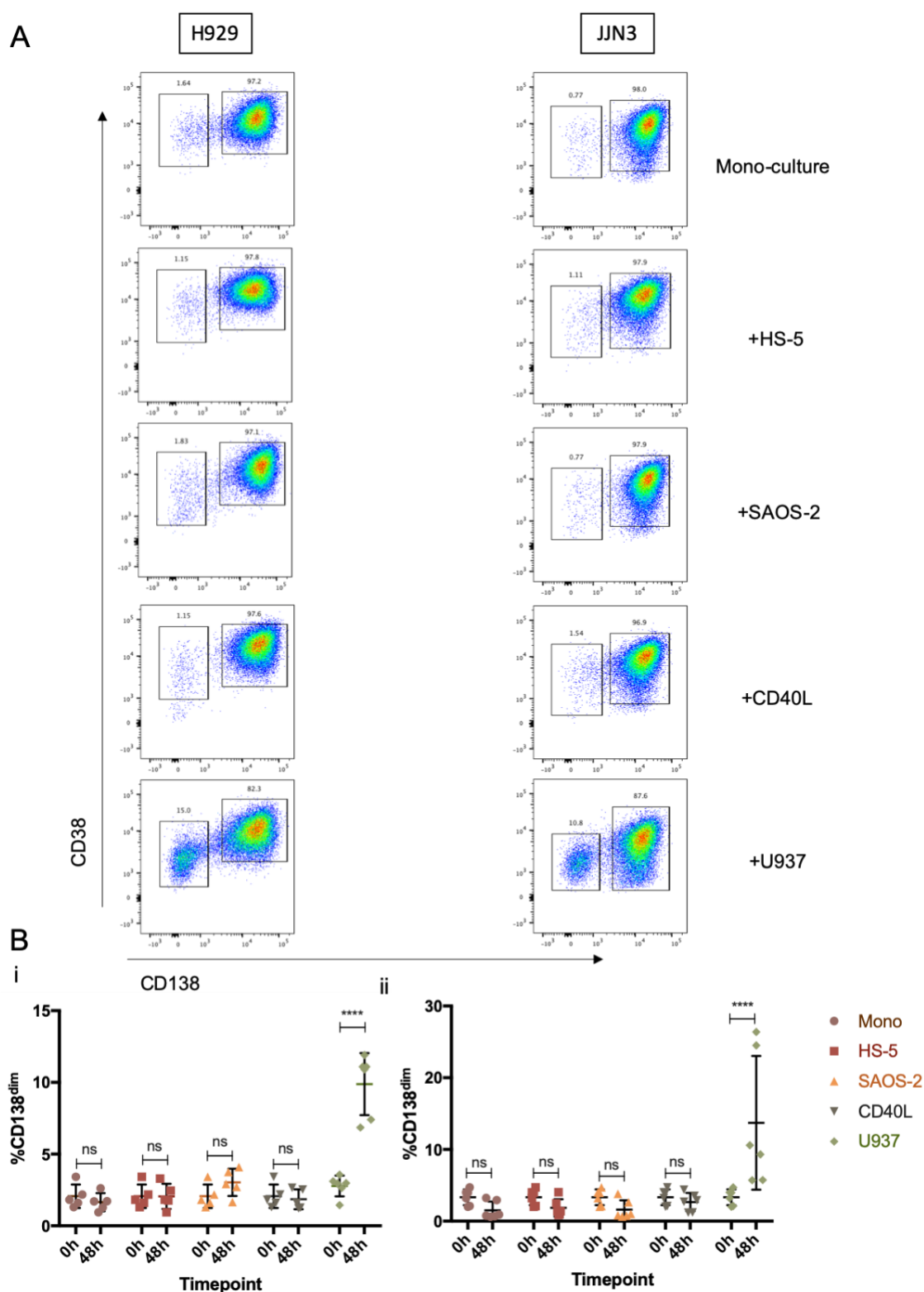


**Figure 3.10. Identification and quantification of a subpopulation of CD138<sup>dim</sup> myeloma cells.** H929 and JJN3 cells were cultured for 48 hours in monoculture or with HS-5, SAOS-2, CD40L or U937 cells that had been treated with PMA for 48 hours and 1,25(OH)<sub>2</sub>D<sub>3</sub> for a further 5 days. Myeloma cells were harvested and gated using forward and side scatter and were then assessed for CD138 and CD38 positivity using an Accuri C6 flow cytometer. (A) Two gates were drawn to assess the proportions of cells that were either CD138<sup>bright</sup>/CD38<sup>bright</sup> or CD138<sup>dim</sup>/CD38<sup>bright</sup>. (B) The proportion (%) of CD138<sup>dim</sup>/CD38<sup>bright</sup> H929 (i) and JJN3 (ii) cells was quantified and plotted with the mean shown for each culture condition. Standard deviation was used to plot error bars (n=6). A two-way ANOVA and Sidak multiple comparison test were performed to assess statistical significance between timepoints for each co-culture condition using GraphPad Prism 7.0 software (ns – not significant, \*\*\*\* - p<0.0001).

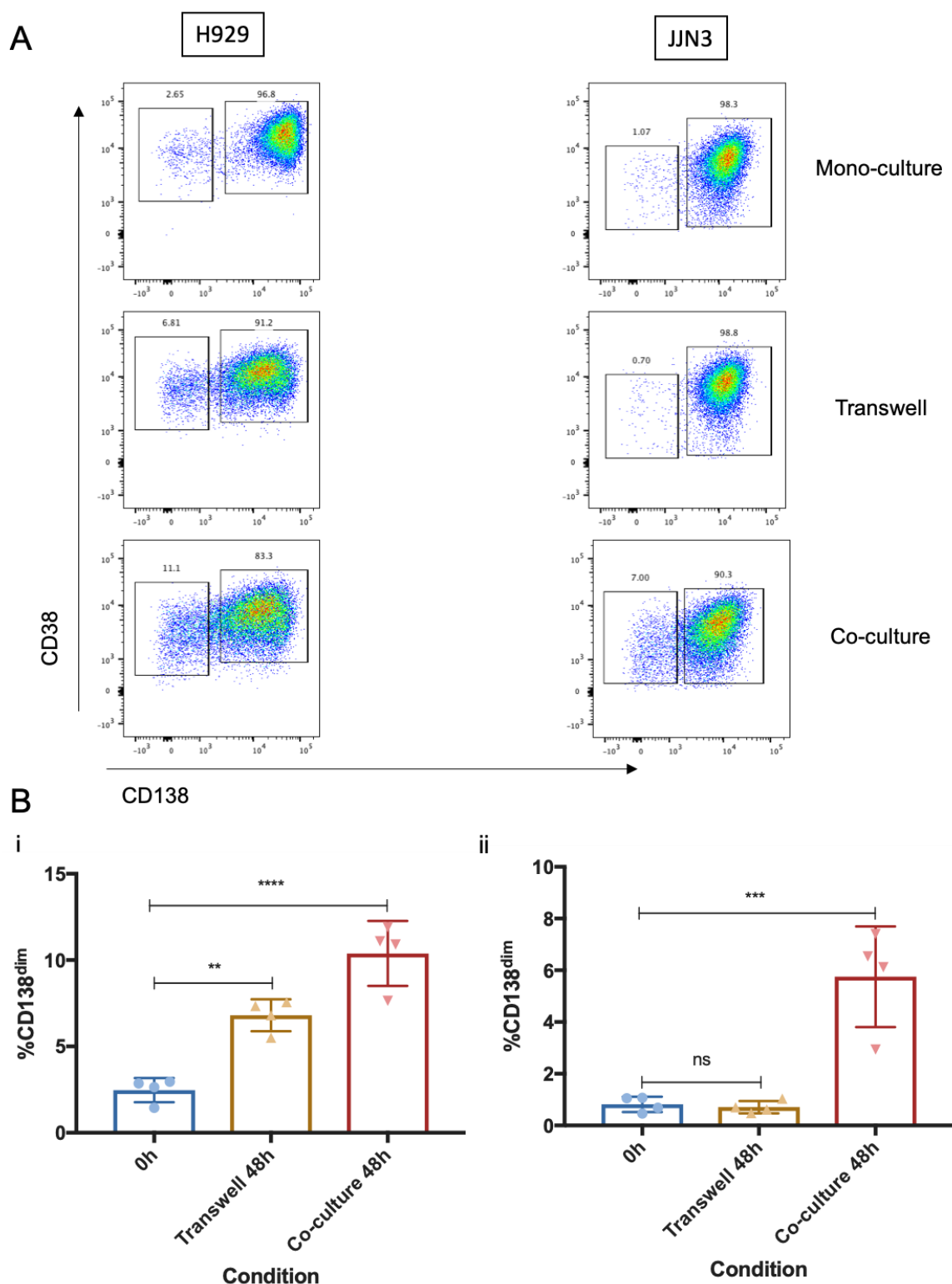


**Figure 3.11: Identification of CD138<sup>dim</sup> myeloma cells after Transwell® co-culture with differentiated U937 cells.** H929 and JLN3 myeloma cells were cultured in Transwell® chambers and also in direct cell-cell contact with differentiated U937 cells. (A) Gates were drawn around CD138<sup>bright</sup> and CD138<sup>dim</sup> subpopulations of myeloma cells after 48 hours of monoculture or co-culture in Transwell® chambers or in direct cell-cell contact with differentiated U937 cells. (B) Proportions of CD138<sup>dim</sup> H929 (i) and JLN3 (ii) cells were evaluated for each of these conditions. Standard deviation was used to plot error bars (n=4). A one-way ANOVA followed by a Dunnett multiple comparison test was used to determine statistical significance using GraphPad Prism 7.0 software (ns – not significant, \*\* - p<0.01, \*\*\* - p<0.001, \*\*\*\* - p<0.0001).

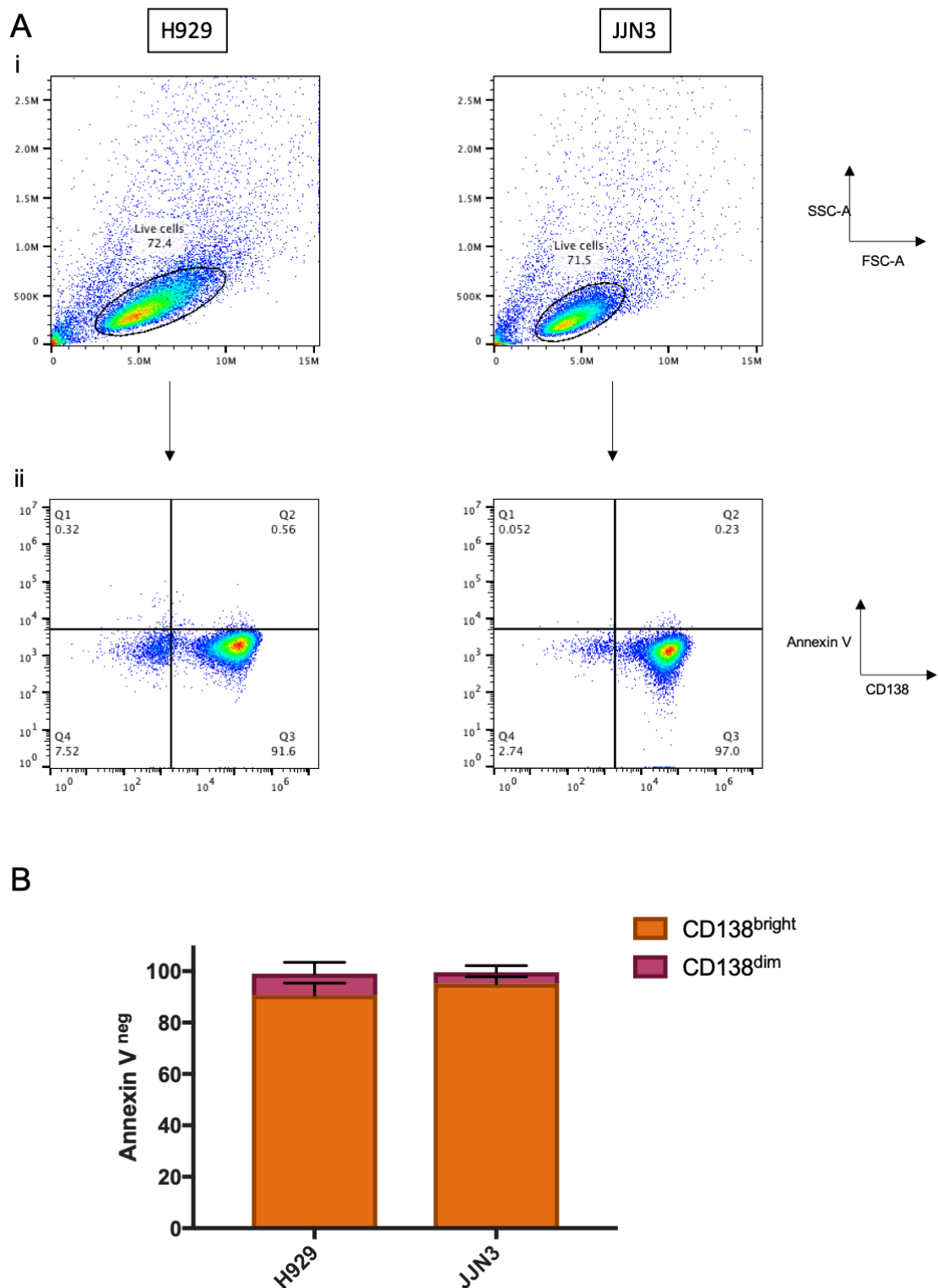


**Figure 3.12. Viability of CD138<sup>dim</sup> myeloma cells after co-culture with differentiated U937 cells.** H929 and JJN3 cells were incubated for 48 hours with U937 cells that had been differentiated with PMA for 48 hours and 1,25(OH)<sub>2</sub>D<sub>3</sub> for a further 5 days. Myeloma cells were harvested and stained with APC-conjugated CD138 antibody and FITC-conjugated annexin V. (A) H929 and JJN3 cells were gated using forward and side scatter with a gate drawn around the live population of cells (i) H929 and JJN3 cells were then assessed for CD138 and annexin V expression (ii). (B) Data was then compiled to illustrate the proportion of live cells that were CD138<sup>dim</sup>/annexin-V<sup>negative</sup>. Standard deviation values were used to construct error bars and were calculated from n=3 separate experiments.

### 3.3.3. CD138<sup>dim</sup> cells represent a true subset of myeloma cells

To confirm that the expansion of the proportion of myeloma cells that possessed a CD138<sup>dim</sup> phenotype represented a true subpopulation of myeloma cells, pre-labelling of H929 and JN3 cells with CellTrace™ carboxyfluorescein succinimidyl ester (CFSE) was employed. This revealed that CFSE<sup>bright</sup> myeloma cells also possessed the same CD138 phenotypic profile under the same culture conditions described in Section 3.2.1, where an expansion of CD138<sup>dim</sup> myeloma cells was observed after co-culture with differentiated U937 cells. There was also a small population of cells that appeared to possess a CD138<sup>dim</sup>/CFSE<sup>dim</sup> phenotype in both cell lines after co-culture with differentiated U937 cells. However, these cells were above the threshold for CFSE positivity set by unstained control cells as indicated by the U gate in Figure 3.13A, thus indicating that these CD138<sup>dim</sup>/CFSE<sup>dim</sup> cells are not contaminants from co-culture with differentiated U937 cells.

There was a small, yet significant expansion of CD138<sup>dim</sup>/CFSE<sup>bright</sup> H929 cells ( $p < 0.05$ ) and no significant overall change in proportion of JN3 cells ( $p > 0.05$ ) in this subpopulation after 48 hours of isolated culture (Figure 3.13A). There was also a significant expansion of CD138<sup>dim</sup>/CFSE<sup>bright</sup> H929 ( $p < 0.0001$ ) and JN3 cells ( $p < 0.05$ ) after 48 hours of co-culture with differentiated U937 cells. Crucially however, the proportion of CD138<sup>dim</sup>/CFSE<sup>bright</sup> cells was significantly greater after co-culture with differentiated U937 cells in comparison to monoculture after 48 hours in both H929 and JN3 cells ( $p < 0.01$ ; Figure 3.13B). This indicates that CD138<sup>dim</sup> cells are a true subpopulation of myeloma cells and not a cellular contaminant from co-culture with differentiated U937 cells.

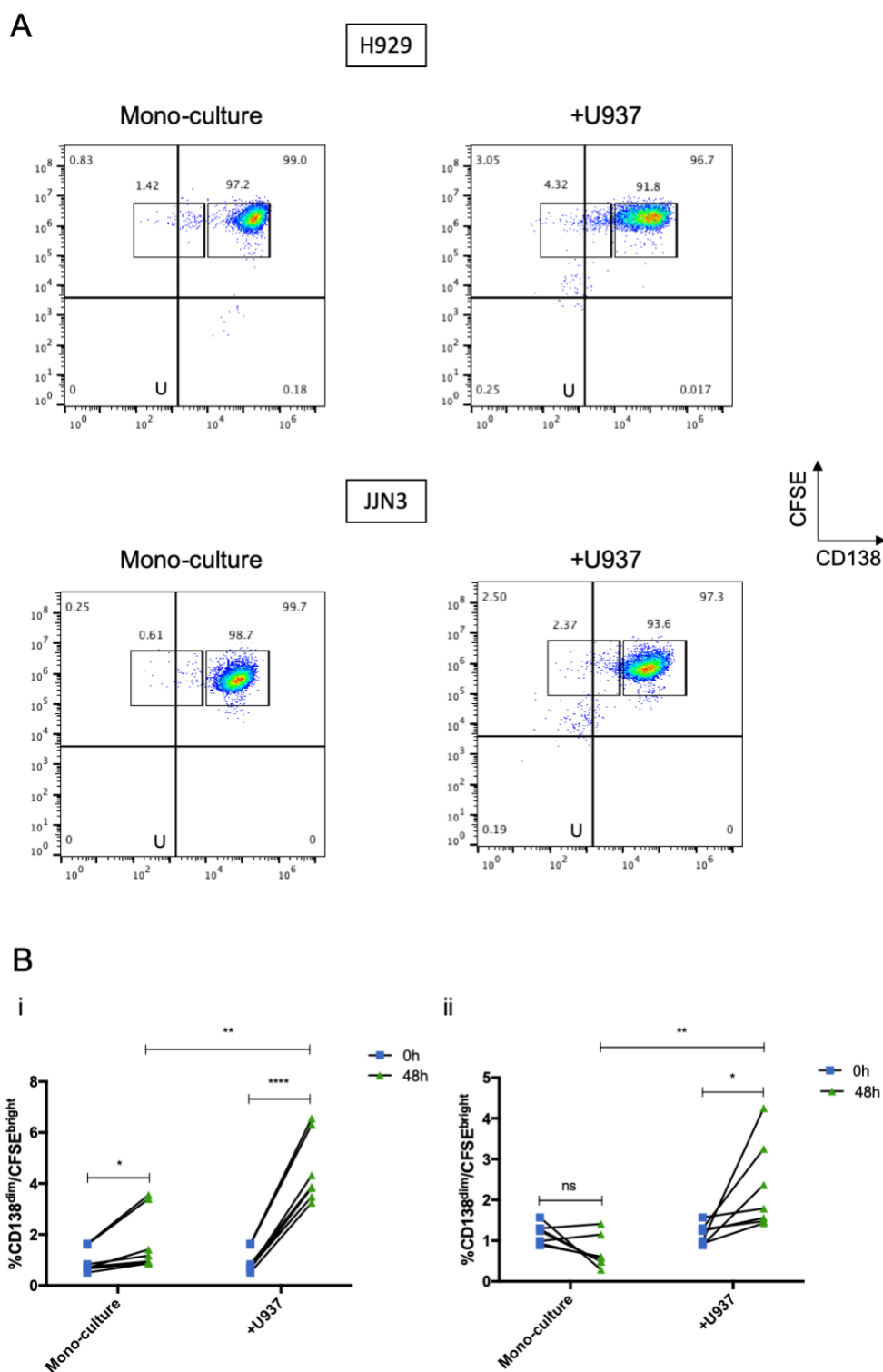


**Figure 3.13. CFSE labelling of CD138<sup>dim</sup> myeloma cells.** H929 and JJN3 cells were pre-stained for 30 minutes with CellTrace™ CFSE before being cultured for 48 hours with U937 cells that had been treated with PMA for 48 hours followed by 1,25(OH)<sub>2</sub>D<sub>3</sub> for a further 5 days, prior to co-culture. H929 and JJN3 cells were harvested from culture and gated using forward and side scatter and assessed for CD138 and CFSE positivity alongside mono-culture controls. (A) CFSE and CD138 positivity was assessed in both H929 and JJN3 myeloma cells after 48 hours of monoculture or co-culture with differentiated U937 cells. Gates were drawn around CD138<sup>bright</sup>/CFSE<sup>bright</sup> and CD138<sup>dim</sup>/CFSE<sup>bright</sup> populations of cells. (B) The proportion of CD138<sup>dim</sup>/CFSE<sup>bright</sup> cells was assessed in both monoculture and co-culture with differentiated U937 cells against controls taken at a 0-hour time point. Individual values are plotted from each condition (n=5). Paired and unpaired *t*-tests were performed to assess statistical significance using GraphPad Prism 7.0 software (ns – not significant, \* - p<0.05, \*\* - p<0.01, \*\*\*\* - p<0.0001).

### 3.4. Discussion

#### 3.4.1. Development of an *in vitro* osteoclast-like model

Multiple myeloma is an incurable plasma cell malignancy with only 30% of patients surviving for more than 10 years<sup>4</sup>. The bone marrow microenvironment is crucial to the survival, proliferation and growth of these malignant plasma cells and has also been heavily implicated in drug resistance<sup>6,276</sup>. Therefore, therapeutic targeting of the microenvironment has gained interest in conjunction with targeting myeloma cells themselves<sup>277</sup>. This highlights the importance of the microenvironment in supporting disease pathogenesis and progression<sup>165</sup>. Osteoclasts are influential cells found within this environment that exist in greater numbers as a result of myeloma cell-induced manipulation of RANK/RANKL/OPG signalling<sup>213</sup>. This leads to a catastrophic upregulation of resorptive activity in the majority of myeloma patients resulting in bone lesions, severe myalgia and spontaneous fractures in patients as well as other complications such as hypercalcaemia<sup>278</sup>.

This study aimed to develop and characterise a reproducible *in vitro* model representative of osteoclast function and behaviour and to investigate the influence that this *in vitro* osteoclast-like microenvironment has on myeloma cells. U937 cells were chosen for this study due to previous research indicating that they are able to form multi-nucleated cells that upregulate osteoclast-specific genes such as tartrate resistant acid phosphatase (TRAP), cathepsin K and RANK in response to appropriate stimuli in the form of PMA and  $1,25(\text{OH})_2\text{D}_3$ <sup>249,250</sup>.

Treatment with PMA significantly inhibited U937 cell growth and induced cells to adhere to both tissue culture plastic and ivory. Sequential treatment with  $1,25(\text{OH})_2\text{D}_3$  then caused these cells to adhere to one another and merge to form large multi-nucleated cells, as demonstrated by DAPI staining (Figures 3.2 and 3.5). These cells were also shown to have a greater nuclear DNA content than a typical cell in the G2 phase of the cell cycle (Figure 3.4). These data indicate that treatment in this fashion caused U937 cells to form larger cells that contain multiple distinct nuclei, collectively sharing cytoplasmic material, much like conventional human osteoclasts<sup>268</sup>. This is also

reflective of human osteoclasts as the number of nuclei within an individual osteoclast can vary dramatically, with some reports showing osteoclasts containing up to 20 nuclei. Nuclei number has also been directly associated with an increase in resorptive function<sup>279,280</sup>.

The treatment protocol used in these experiments was adapted from previous research that used U937 cells to create an *in vitro* osteoclast model. The methods described in these papers were used as a template to adapt an appropriate method for the experiments presented in this thesis. A range of incubation times and densities were investigated until the protocol stated in Section 2.1.6 was deemed most appropriate. This was because incubation for any longer than 10 days did not seem to result in further differentiation of osteoclast-like cells but led to a greater expansion of adherent mononuclear cells that would have likely diluted the effect of differentiated osteoclasts on myeloma cells within the co-culture. This was likely because treatment with PMA and  $1,25(\text{OH})_2\text{D}_3$  was sequential, meaning that cells that proliferated at a later time point would not have experienced the effect of PMA prior to treatment with  $1,25(\text{OH})_2\text{D}_3$ . A range of cell densities was also investigated, with an optimal starting density of  $5 \times 10^4$  cells/ml being decided upon due to the fact that fewer cells than this led to a lack of differentiation, likely because cells were too far apart in culture. Conversely, higher cell densities resulted in difficulties in identifying distinct, individual multinuclear cells within the culture, as cells seemed to form clumps as opposed to clearly merged multinuclear cells. Whilst the density that was used for these experiments was deemed appropriate for osteoclast formation to take place, it is clear that as more cells differentiate, the distance between each individual cell inevitably increases. This could have affected the efficiency of osteoclast formation as the treatment time spent in culture progresses.

Despite this promising data that shows U937 cells can reflect osteoclast behaviour, the true *in vivo* mechanisms that induce osteoclastogenesis rely on M-CSF and RANKL, as discussed in section 1.2.4. It is curious that treatment with these two soluble factors did not induce osteoclastogenesis in U937 cells (data not shown), which indicates that these cells are differentiating using alternative mechanisms through treatment with PMA and  $1,25(\text{OH})_2\text{D}_3$  instead. PMA is commonly used for the differentiation of

monocytic cells into macrophages. Macrophages in an *in vivo* setting are subsequently capable of terminally differentiating into osteoclasts. It could be speculated that this is the sequential process that is being promoted in these experiments. The protein kinase C family of kinases are responsible for a vast number of cellular functions that are known to be induced by PMA. Whilst it is of course difficult to ascertain the exact mechanisms of osteoclastogenesis as a result of PMA treatment shown in this chapter, it is interesting to speculate what mechanisms are responsible for inducing this process. For example, previous research has shown that one PKC isoenzyme, PKC- $\beta$ , has been implicated in osteoclastogenesis. Direct inhibition of this particular isoenzyme was also shown to inhibit osteoclast formation and bone resorbing activity in murine bone marrow cultures<sup>281</sup>. Given that it is known that PMA is an activator of the PKC family of kinases, it could be speculated that treatment with PMA in this scenario could induce PKC- $\beta$  activity which could be utilised in the process of osteoclastogenesis seen in U937 cells. Furthermore to this, it has also been reported that PMA induces NF- $\kappa$ B function, which has been linked to causing monocytic cells to differentiate into macrophage-like cells<sup>282</sup>.

TRAP is a well-established marker of human osteoclasts<sup>270</sup>. Treatment with PMA and 1,25(OH)<sub>2</sub>D<sub>3</sub> resulted in an exclusive and distinct upregulation of TRAP expression in U937 cells (Figure 3.6). Receptor Activator of Nuclear Factor kappa-B (RANK) is another surface marker expressed by osteoclasts. It is initially expressed on the surface of monocytic myeloid precursors prior to the induction of osteoclastogenesis and continues to be expressed by mature osteoclasts<sup>207</sup>. Whilst U937 cells did not demonstrate any RANK expression in an untreated state, treatment with PMA and 1,25(OH)<sub>2</sub>D<sub>3</sub> induced a significant increase in RANK expression in U937 cells. However, it is also important to recognise that RANK is expressed in macrophages prior to terminal differentiation to osteoclasts<sup>283</sup>. Therefore, investigations into additional osteoclast-specific biomarkers could have further improved this model. One such marker would be the calcitonin receptor (CTR). Calcitonin acts as a negative regulator of osteoclast activity in normal bone physiology, it is therefore a trademark of osteoclasts to express the receptor for calcitonin in order for the homeostatic regulation of bone re-modelling to take place<sup>284,285</sup>. Expression of this receptor could have improved the validity of the model further. However, given the data that has

been presented so far in this thesis, the expression of TRAP and RANK in this context provides further evidence that these cells are capable of differentiating into cells that possess key phenotypic features of human osteoclasts.

The primary function of osteoclasts is to resorb bone as part of the homeostatic process of bone remodelling, which is deregulated in myeloma in favour of osteolysis<sup>203</sup>. It is also clear that U937 cells strongly adhere to a bone-like material in the form of ivory in response to treatment with PMA and 1,25(OH)<sub>2</sub>D<sub>3</sub>. Cell remnants were still clearly visible on the surface of ivory disks despite a vigorous cell removal process before visualisation with SEM. There are methods that can be used in the removal of adherent cells from a particular culture surface that include enzymatic removal using trypsin or Accutase or through cellular degradation using bleach-like substances such as ammonium hydroxide or sodium hypochlorite. The main aim of this is to completely remove the cells from the surface of the ivory in order to observe potential resorption pits that may have formed beneath the cells during prolonged culture. It is of course difficult to determine whether the U937 cells used here are any more or less adherent than alternative cell types such as differentiated PBMCs, but what is clear is that these cells were firmly adherent to the ivory used in these experiments.

There was a disparity between areas of the ivory that had been inhabited by treated U937 cells and areas of disk that were seemingly untouched by these cells, with the former appearing to have a smoother surface (Figure 3.8B). This smoothing could be indicative of osteoclast function through the secretion of osteolytic enzymes, as well as an increased concentration of H<sup>+</sup> ions that occurs *in vivo*. Whilst the mechanisms of bone resorption were not explored here, it could be speculated that this could be the cause of the smoothing effect that can be seen on the ivory disks as a result of U937 cell activity. Staining with toluidine blue also revealed significant staining around the areas of cell adherence (Figure 3.8C). This is indicative of resorption pit formation and could also indicate that these cells are imbedding themselves within the ivory, thus making cell removal considerably more difficult. However, there are more investigations that could be pursued in order to both qualify and quantify this phenomenon. Confocal microscopy is a powerful tool that has been previously utilised

to assess pit depth in studies relating to osteoclast formation and function. It would be a useful confirmatory experiment to quantify the depth of these resorption pits<sup>286,287</sup>. It would also be fascinating to observe the effects of myeloma cell culture on pit depth, which to an extent it could be speculated that you would expect to see an increase in pit depth and thus an increase in osteoclast activity in U937 cells as a result of myeloma cell influence. Additionally, quantifying the expression of secreted enzymes such as cathepsin k in this instance would have further characterised this model. Cathepsin K is a cysteine protease secreted by osteoclasts to facilitate normal bone degradation<sup>288</sup>. It is also known to be upregulated in osteoclasts following interactions with myeloma cells<sup>289</sup>. If this was found to be the case in the model I have presented here, that would further validate U937 cells as being representative of functional osteoclasts and this could also act as a marker of osteoclast function following co-culture with myeloma cell lines.

Collectively these data show that U937 cells treated with PMA and  $1,25(\text{OH})_2\text{D}_3$  are capable of forming large multi-nucleated cells that express TRAP and RANK and are also able to resorb a bone-like matrix in the form of ivory. These features are characteristic of conventional human osteoclasts and provide a suitable rationale to use these cells for an *in vitro* model representative of osteoclasts.

#### **3.4.2. Characterisation of myeloma cells cultured with differentiated U937 cells**

The next aim of this study was to investigate how this *in vitro* osteoclast-like model could influence the behaviour of myeloma cells. The cell surface marker CD138 (syndecan-1), is an exclusive marker of plasma cells following terminal differentiation from B-lymphocytes<sup>36,290</sup>. Consequently, CD138 is a well-established marker for myeloma cell identification and classification during diagnosis and subsequent monitoring of patients<sup>272</sup>. H929 and JN3 are myeloma cell lines that predominantly express CD138 on their surface<sup>241</sup>. H929 cells have also been previously shown to incorporate a small, yet distinct population of CD138<sup>dim</sup> cells along with RPMI-8226, U266 and MM1S cells, this was also confirmed in primary material<sup>39,41,42,274</sup>. This phenomenon was confirmed in this project (Figure 3.9). Interestingly, this has not previously been reported in JN3 cells. However, in a unique finding, the data

presented in this project clearly shows the presence of CD138<sup>dim</sup> cells in JN3 cell cultures.

Whilst primary cells were not used in this research, the proportions of CD138<sup>dim</sup> cells in primary material has been previously reported and appears to vary to a much greater extent in comparison with immortalised cells. Reid *et al.* reported up to 97% of myeloma cells in some patients were CD138<sup>dim</sup>, although the mean figure in this article was reported at 19.6%. This research also showed that there was a significant increase in the proportion of primary myeloma cells that were CD138<sup>dim</sup> at more advanced stages of disease, thus highlighting a potential role for CD138<sup>dim</sup> cells in the progression of myeloma<sup>39</sup>.

The initial identification of this subpopulation of CD138<sup>dim</sup> cells outlined in this thesis lead to further novel observations. The proportion of CD138<sup>dim</sup> cells significantly and exclusively increased after H929 and JN3 cells were cultured with differentiated U937 osteoclast-like cells. This was not the case following co-culture with HS-5, SAOS-2 or CD40L-expressing fibroblasts (Figure 3.10). Myeloma cells are capable of manipulating cells of the bone marrow microenvironment to positively support myeloma function through soluble factor signalling and direct cell-cell contact<sup>291</sup>. Myeloma cells are known to exert their influence on osteoclasts through these distinct mechanisms, with osteoclasts being known to reciprocally support myeloma cells in paracrine fashion<sup>204</sup>. H929 and JN3 myeloma cells are evidently dependent on both of these signalling mechanisms to influence CD138 surface expression. The expansion of CD138<sup>dim</sup> cells in both myeloma cell lines is clearly dependent on direct cell-cell contact, however in H929 cells this effect can also be replicated in Transwell® chambers, thus highlighting that this particular myeloma cell line is also responsive to soluble factor signalling to expand the proportion of CD138<sup>dim</sup> cells within that population. However, this was not the case in JN3 cells where it appears that the expansion of CD138<sup>dim</sup> cells is solely mediated through direct cell-cell contact (Figure 3.11).

It is known that CD138 is shed from the surface of myeloma cells as a result of cells undergoing apoptosis<sup>275</sup>. This has led to a suggestion that CD138<sup>dim</sup> cells identified from H929 and JN3 cell lines are in fact apoptotic artefacts<sup>292</sup>. Despite this speculation

it is clear from the data presented in this project that CD138<sup>dim</sup> myeloma cells are negative for annexin V staining, thus indicating that they are viable populations of cells and regulate CD138 expression through alternative mechanisms (Figure 3.12).

Confirmation was also required to show that CD138<sup>dim</sup> cells are a true subpopulation of myeloma cells and were not U937 contaminants resulting from co-culture with differentiated U937 osteoclast-like cells. Pre-labelling of myeloma cells with fluorescent CFSE prior to co-culture with differentiated U937 cells, demonstrated that the CD138<sup>dim</sup> population originated from myeloma cells. The use of CFSE also allowed identification of a small CD138<sup>dim</sup>/CFSE<sup>dim</sup> subpopulation that produced a greater fluorescent signal than an unstained control. CFSE staining is often used to assess cellular proliferative capacity<sup>293</sup>. Thus, this phenomenon could be explained by a subpopulation of CD138<sup>dim</sup> cells that had undergone more extensive proliferation (Figure 3.13).

It would also be interesting to explore the effect of myeloma cell co-culture on differentiated U937 cells. I have already alluded to the hypothesis that these malignant cells may cause an increase in osteoclast activity that may result in increased bone resorption, which could be confirmed through the quantitative technique of confocal microscopy, or even through further toluidine blue staining which may result in a greater number of resorption pits observed throughout the ivory disk. It would also be interesting to observe whether culture with myeloma cells, or in media conditioned from myeloma cells would lead to a higher rate of osteoclast formation from U937 cells.

#### **3.4.3. The role of CD138<sup>dim</sup> cells in myeloma**

The function of CD138 and the subsequent role of malignant plasma cells lacking the surface expression of this antigen is still widely unknown, with limited evidence currently available<sup>294</sup>. It is well-established that the expression of CD138 is exclusive to plasma cells following their differentiation from non-CD138 expressing B-lymphocytes<sup>290</sup>. It has, however, been speculated that a CD138<sup>dim</sup> population could be representative of a myeloma stem cell phenotype<sup>42,276</sup>. The origin of myeloma is of course still subject to highly contested debate and the point of initiation of malignant

transformation is currently unknown. It has therefore been hypothesised that prior to terminal differentiation into CD138-expressing plasma cells, plasmablasts or B-cells at an earlier stage of differentiation could be representative of myeloma stem cells.

It is known that CD138 is primarily responsible for both cell-cell adhesion and adhesion to type-1 collagen and it has been previously demonstrated that plasma cells lacking in CD138 expression display more invasive properties<sup>295</sup>. Levels of shed CD138 in patients have also been correlated with poor prognosis<sup>38</sup>. However, the mechanisms responsible for this shedding in myeloma are still disputed. Matrix metalloproteinases are a class of enzymes that are capable of cleaving CD138 from the surface of plasma cells, with MMP-9 in particular being highlighted as having an affinity for cleaving CD138<sup>296</sup>. MMP-9 has also been shown to be significantly upregulated in myeloma which could be linked to higher levels of shed CD138 and therefore greater proportions of malignant plasma cells that exhibit lower expression levels of CD138<sup>297</sup>.

Previous research has also shown that CD138<sup>dim</sup> myeloma cells also have a reduced sensitivity to lenalidomide, dexamethasone and bortezomib<sup>42,43,298</sup>. Myeloma is currently an incurable disease; throughout which patients nearly always experience an eventual relapse after treatment<sup>299</sup>. This has led to further speculation that CD138<sup>dim</sup> cells could be the root cause of drug resistance in patients<sup>44</sup>. This phenomenon will be explored further in this project.

#### **3.4.4. Final conclusions**

Collectively, this research confirms that U937 cells, treated with PMA and 1,25(OH)<sub>2</sub>D<sub>3</sub>, are capable of forming large, multi-nucleated, cells that upregulate TRAP and RANK on their surface. Furthermore, these cells acquired the ability to resorb a bone-like matrix in the form of ivory. Therefore, these data provide further evidence that treatment of U937 cells with the regimen detailed in this chapter, can generate a reproducible humanised *in vitro* model of human osteoclasts. Co-culture with myeloma cells yielded some novel results that led to the identification and expansion of a subpopulation of CD138<sup>dim</sup> myeloma cells. Given the current interest in the field into the role of CD138<sup>dim</sup> cells in the pathology of myeloma, it is of interest to investigate further transcriptional and functional differences between these two subsets of myeloma

cells. This could reveal information about the purpose that these cells serve in the origin and progression of myeloma, the mechanisms that contribute to increased osteolytic activity and their role in the culmination of relapsed disease.

## CHAPTER 4: RESULTS

### Assessment of the global changes of the myeloma transcriptome in an osteoclast-like microenvironment

#### 4.1. Introduction

Syndecan-1, also known as CD138, is almost exclusively expressed on the surface of both malignant and normal plasma cells<sup>34</sup>. This characteristic has facilitated the unique clinical classification of myeloma cells in patient diagnostics. Determination of CD138 expression has also enabled the classification of myeloma cells using gene expression profiling<sup>46,300</sup>. The role of CD138 in myeloma has been primarily attributed to myeloma cell survival, proliferation and adherence to the bone marrow<sup>301-303</sup>. Whilst the biological and clinical significance of malignant plasma cells that are low-expressors of CD138 has yet to be fully established, it has been previously shown that lower levels of CD138 surface expression and higher levels of serum CD138 being infers poorer prognoses in patients<sup>38</sup>.

Previous research has identified the presence of potential myeloma stem cells that lack CD138 surface expression in both myeloma cell lines and primary myeloma cells<sup>39,41-43</sup>. These cells have been shown to acquire enhanced clonogenicity, the ability to engraft in murine models and possess greater levels of chemoresistance against commonly used myeloma therapies. Interestingly, there is also evidence to suggest that myeloma cell interaction with cells of the bone marrow, drives CD138 expressing myeloma cells towards a CD138<sup>dim</sup> phenotype<sup>304</sup>. This effect has also been found to be specifically induced by osteoclast co-culture<sup>305</sup>. However, there is also evidence that demonstrates that CD138<sup>bright</sup> myeloma cells – derived from both primary tissue and human cell lines – are also highly clonogenic and can successfully engraft in murine models<sup>306,307</sup>. These data add to the complexity of the disease and the difficulty in identifying the roles of each of these plasma cell subsets in the pathogenesis, pathophysiology and progression of myeloma.

Having confirmed the presence of CD138<sup>dim</sup> myeloma cells and the subsequent expansion of these cells when cultured in an osteoclast-like *in vitro* microenvironment with differentiated U937 cells, it was of interest to further investigate the behaviour of these cells. The first characteristics that will be evaluated in these cells are their transcriptional properties. There have been a number of studies utilising gene expression profiling technology to assess a variety of transcriptional characteristics in myeloma cells, using CD138 expression as a selection strategy for sample collection<sup>308-310</sup>. However, there are a very limited number of studies that have utilised this technique to investigate the transcriptional differences between CD138<sup>bright</sup> and CD138<sup>dim</sup> myeloma cells. One study in particular showed that there were very few Differentially Expressed (DE) genes between CD138<sup>bright</sup> and CD138<sup>dim</sup> myeloma cells on a transcriptional level. However, this research was performed in the absence of a co-culture model and simply purified these cells from monoculture<sup>274</sup>. It was therefore of interest to determine the transcriptional differences that occur in CD138<sup>bright</sup> and CD138<sup>dim</sup> myeloma cells following co-culture within an osteoclast-like environment with differentiated U937 cells. In order to investigate this, RNA-seq was performed on these two subsets of cells before and after culture with differentiated U937 cells. RNA-seq enables the identification of genes that are transcriptionally activated or repressed, which could provide valuable information into corresponding proteins that are subsequently translated. This means that understanding the transcriptomic profile of cells provides critical information to the basis of how their behaviour, function and potential role in disease.

RNA-sequencing (RNA-seq) is a high-throughput, quantitative technique that utilises next generation sequencing to determine the expression levels of each individual gene within the entire transcriptome of a cell, or group of cells<sup>311</sup>. RNA-seq has quickly grown in popularity and is now established as one of the most frequently used sequencing methods to quantify gene expression. A number of intrinsic advantages over other forms of sequencing has led to this. RNA-seq does not require previous knowledge on the transcriptome being sequenced, therefore this can provide a mechanism to identify novel transcripts, variants and isoforms that were previously unknown<sup>312</sup>. RNA-seq is also a more reproducible technique, with fewer technical

replicates required to produce reliable results in comparison with microarrays, for example<sup>313</sup>.

Critically, RNA-seq is an incredibly powerful sequencing tool used to assess DE genes between selected variables<sup>314</sup>. It is this experimental trait that has led to the selection of this technique to be used in this study. The research presented in this project has confirmed the existence of a subset of previously identified CD138<sup>dim</sup> myeloma cells in H929 and JIN3 myeloma cell lines. Investigation into the effects of myeloma cell co-culture in an osteoclast-like *in vitro* microenvironment led to the novel discovery of an expansion of CD138<sup>dim</sup> cells as a result of direct cell-cell contact and soluble factor influence from differentiated U937 cells. This phenomenon coupled with previous research highlighting the potential pathological and clinical significance of CD138<sup>dim</sup> myeloma cells has provided a suitable rationale to determine the global transcriptional profile of these two subsets of CD138<sup>dim</sup> cells in both H929 and JIN3 myeloma cell lines following co-culture with differentiated U937 cells. This will provide a strategy to investigate differential gene expression signatures in each subset of myeloma cells which could reveal further information about the influence of culture within an osteoclast-like environment as well as indicate potential roles of each cell subset in the pathology of myeloma.

#### 4.1.1. Aims

This chapter aimed to investigate the global transcriptomic changes that occur in CD138<sup>bright</sup> and CD138<sup>dim</sup> myeloma cells following co-culture with differentiated U937 cells. This analysis strategy set out to answer the following questions:

1. What is the effect of osteoclast-like U937 co-culture on the gene expression profiles of CD138<sup>bright</sup> and CD138<sup>dim</sup> myeloma cells?
2. What are the distinct differences in gene expression between CD138<sup>bright</sup> and CD138<sup>dim</sup> myeloma cells?

In order to address these aims this chapter will describe and discuss:

- i. Experimental design, data collection and analysis strategy of RNA-sequencing
- ii. Assessment of global transcriptional changes in each myeloma subpopulation
- iii. Determination of DE gene signatures between myeloma cell subpopulations
- iv. Selection and validation of candidate gene expression by qPCR

## 4.2. Assessing changes in the global transcriptome of CD138<sup>bright</sup> and CD138<sup>dim</sup> myeloma cells

### 4.2.1. Experimental design and rationale

H929 and JIN3 myeloma cell lines were cultured for 48 hours either in isolation or with U937 cells that had been differentiated into osteoclast-like cells following treatment with PMA for 48 hours and 1,25(OH)<sub>2</sub>D<sub>3</sub> for 5 days. These cells were then harvested and sorted using FACS based on CD138 and CD38 surface expression. This led to the isolation of myeloma cells that possessed a phenotype that was either CD138<sup>bright</sup> or CD138<sup>dim</sup>. However, due to the small proportion of CD138<sup>dim</sup> myeloma cells in monoculture (no U937 cells), it was not feasible to sort a sufficient quantity of these cells to produce the appropriate amount of RNA required to perform an RNA-seq experiment. Mono-culture samples of myeloma cells were therefore only sorted for CD138<sup>bright</sup> cells, which were used as the control comparators during downstream transcriptomic analysis. Sample preparation was performed in three independent biological replicates. Purity checks of these samples were also performed after CD138-expression based sorting, with all sorted samples showing >95% purity. Representative examples of the gating strategy used for sorting are shown in Supplementary Figure I.

There was a combined total of 18 samples, from which RNA was extracted to be used in this RNA-seq experiment. Prior to RNA-sequencing, samples were assessed for RNA quality and integrity through the evaluation of 18S and 28S ribosomal ratios with each sample producing a RIN value >9.5 (Supplementary Figure II)<sup>315</sup>. This demonstrated the successful isolation of high-quality RNA which was suitable to be used for RNA-sequencing. Complimentary DNA (cDNA) libraries were then generated to be used for sequencing by the Wales Gene Park, Cardiff. Sequencing was performed in duplicate with replicates being performed approximately four weeks apart. This strategy helped to ensure that data produced from this technique are representative of true biological events and not artefacts from sequencing discrepancies. Processed data was then used to determine the differential expression of genes in each sample. There are a number of software programmes and analysis strategies that can facilitate this procedure including Cufflinks-Cuffdiff2, edgeR and DESeq2. There is, however, no optimal method reported in the literature for widespread use under all circumstances when assessing

DE genes, meaning the selection of an appropriate analysis strategy is dependent on the requirements from each individual experiment<sup>316-318</sup>. DESeq2 is a well-established and frequently cited analysis strategy to assess differential gene expression and was the strategy chosen to analyse this dataset as it provides a good false discovery rate control for experiments containing more than two samples, produces a low number of false positive results and the software has a short runtime to process data<sup>261</sup>.

Processing of the raw data and initial differential expression analysis using a DESeq2 differentiation gene expression analysis strategy was performed by Dr Anna Evans, Wales Gene Park, Cardiff. A schematic of this experimental workflow is shown in Figure 4.1.

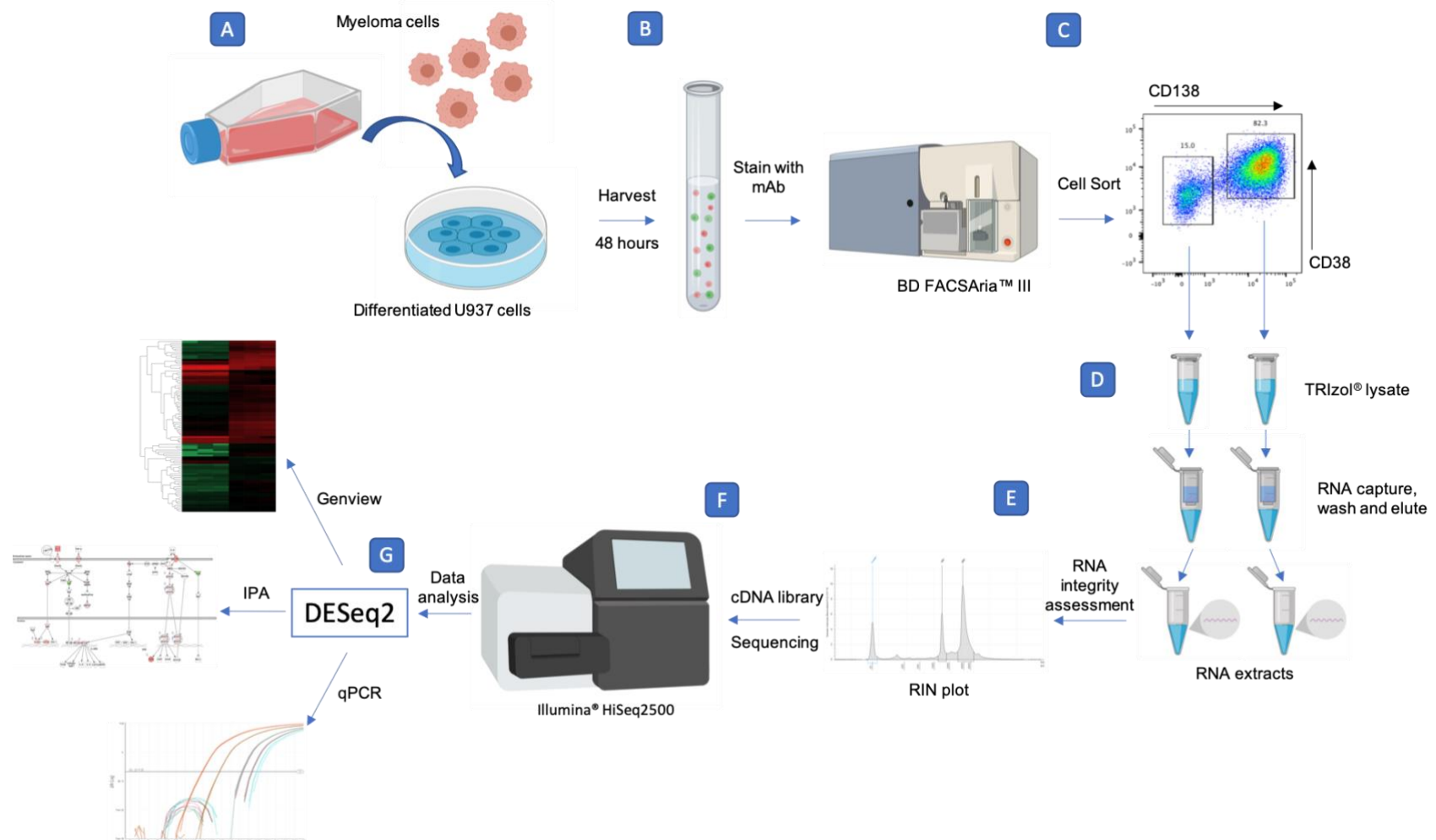


**Figure 4.1. A schematic flowchart illustrating the experimental design and workflow of an RNA-seq experiment.** H929 and JN3 myeloma cells were separately cultured for 48 hours with U937 cells treated with PMA for 48 hours and  $1,25(\text{OH})_2\text{D}_3$  for a further 5 days (A). Myeloma cells were harvested, stained with CD138 and CD38 fluorescence-conjugated monoclonal antibodies (B) and sorted into CD138<sup>bright</sup> and CD138<sup>dim</sup> subpopulations (C). Sorted cell pellets were lysed in TRIzol® reagent and RNA was extracted (D). RNA extracts were assessed for integrity and quality, producing a RIN score (E). A cDNA library was generated for each sample to be used for sequencing using an Illumina® HiSeq 2500 sequencer (F). Reads were trimmed and mapped to a reference genome to assess differential gene expression using the DESeq2 method. Differentially expressed genes were then visualised using Ingenuity Pathway Analysis and Genview2, with candidate genes being validated using qPCR (G). Figure was compiled using BioRender online software.

#### 4.2.2. RNA-seq data processing and quality control

Raw read data was trimmed to remove adapters and low read counts, these trimmed reads were mapped to the hg38 human reference genome. The number of reads determined in this instance equates to the transcriptional activity of individual genes. In order to assess read distribution between each sample and corresponding replicate, density plots were constructed to assess the count distribution of each dataset from both H929 and JN3 cells. Total read counts that amassed to values  $<1$  were removed and DESeq2 library depth normalised counts were plotted against density in a histogram format. Normalisation is an essential process in the RNA-seq workflow that allows the correct inference of gene expression, ensuring that outliers are not incorporated into the analysis which could potentially skew true results, which of course generates a more accurate representation of the data in downstream analysis. This visualisation provides a comparative analysis within and between sample replicates to identify potential outliers, which appear as distinctly different graphical distributions in comparison with other samples. The data illustrated here clearly shows that biological replicates for each sample follows the same graphical trend, demonstrating that normalisation of this dataset was successful and that no obvious outliers were present within this part of the analysis (Figure 4.2A). The data was then transformed using a variance stabilising transformation (VST) to remove the dependence on the variance on the mean in each dataset<sup>261</sup>. In order to compare distribution of transformed data between each sample, box plots of VST counts were constructed (Figure 4.2B). These plots clearly show a uniform distribution of transformed data across each sample in both H929 and JN3 myeloma cells, indicating that the transformation was effective and there is a comparative and equal distribution of reads across each sample.

It is also important to state here that the conditions for each of the samples used in these experiments and displayed within the figures for the remaining chapters will be abbreviated. The abbreviations can be found in Methods Section 2.4.1 in Table 2.6. This table will also be placed below for the convenience for the reader to determine the meaning of the abbreviations used in the following chapters.

<b>Sample</b>	<b>Identifier</b>
<i>H929+U937 CD138<sup>bright</sup></i>	HUCB
<i>H929+U937 CD138<sup>dim</sup></i>	HUCD
<i>H929 monoculture CD138<sup>bright</sup></i>	HMCB
<i>JJN3+U937 CD138<sup>bright</sup></i>	JUCB
<i>JJN3+U937 CD138<sup>dim</sup></i>	JUCD
<i>JJN3 monoculture CD138<sup>bright</sup></i>	JMCB

**Table 2.6. Summary of conditions and samples used to produce RNA extracts and their corresponding identifiers**

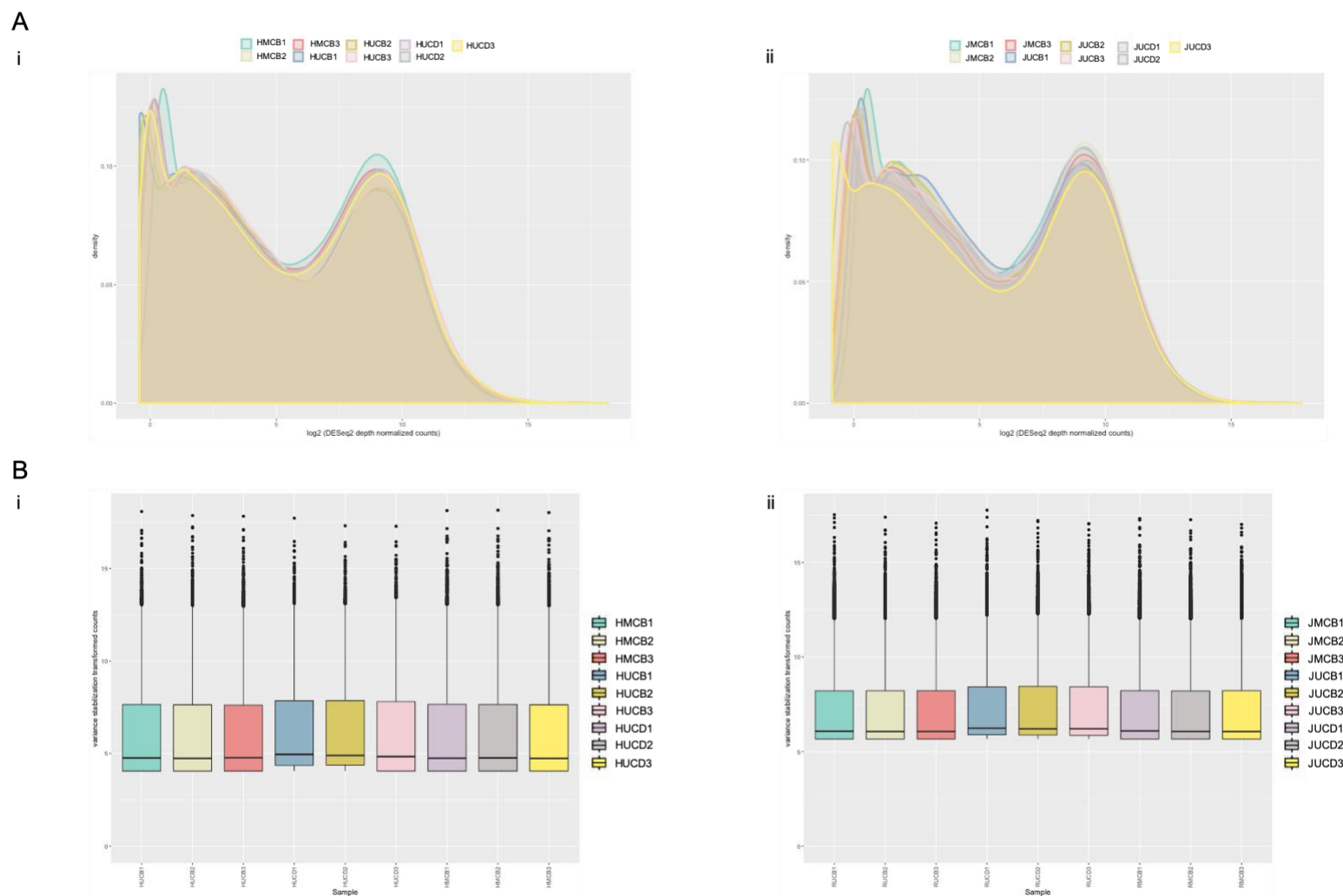


**Figure 4.2. Quality control of raw and transformed data.** (A) Histograms of DESeq2 normalised counts were plotted against density for each sample and corresponding biological triplicate, each box is a compilation of each technical sequencing duplicate for each individual sample. (B) Variance stabilising transformed counts showing lower, median and upper quantiles and counts were plotted for each sample to assess distribution of transformed data between samples in H929 (i) and JN3 (ii) myeloma cells. Biological triplicates were compiled for each cell line and experimental condition ( $n=3$ ).

### 4.2.3. Assessment of sample correlation and hierarchical clustering

Following the normalisation and transformation of each dataset to assess quality and distribution of the data, it was of interest to assess the transcriptomic correlation between each dataset. A Pearson's correlation test was performed using variance stabilising transformation (VST) data to assess transcriptional similarities and differences between sequencing duplicates, biological triplicates and each experimental condition. From this plot strong correlation is indicated by yellow colouration and weak correlation is indicated by blue coloration. What is apparent from this dataset is the clear correlation between both sequencing duplicates and biological triplicates across each sample analysed in this dataset, as shown by the similarity in colour in each 6x6 sample block. Thus, indicating that each biological and technical replicate was successful in regard to producing comparable and uniform data. It is also evident that each sample extracted from CD138<sup>bright</sup> cells after culture in isolation or with differentiated U937 cells share high levels of correlation in both H929 and JN3 cells. Interestingly, despite the weaker correlation observed between corresponding samples of CD138<sup>bright</sup> cells in each cell line, there is a fairly strong correlation between CD138<sup>dim</sup> samples from each cell line (Figure 4.3A).

Similar observations were also recapitulated during the process of unsupervised hierarchical clustering. This process facilitates the identification of groups or clusters of samples that possessed similarities with each other relating to global gene expression. The process was performed in an unsupervised fashion to ensure no prior assumptions were made about the data, removing any bias from the analysis. Here, two primary branches of samples were identified, one of which formed a CD138<sup>bright</sup> cluster and the second forming a CD138<sup>dim</sup> cluster. These were each followed by another two sub-branches, making a total of four sub-branches. Groups of samples within these sub-branches are highlighted by coloured boxes (Figure 4.3B). This data illustrates the similarities in global gene expression between CD138<sup>bright</sup> cells in each culture condition and the differences in global gene expression observed in CD138<sup>dim</sup> myeloma cells when compared with CD138<sup>bright</sup> cells in each myeloma cell line. This highlights the fact that H929 and JN3 cells have gene expression profiles that are substantially different and independent from one another and also shows that CD138<sup>bright</sup> and CD138<sup>dim</sup> cells are transcriptionally different from each other.

Overall, this data simply demonstrates that culture with differentiated U937 cells does not substantially alter the global transcriptome of CD138<sup>bright</sup> myeloma cells in each myeloma cell line. In contrast, this data also shows that CD138<sup>dim</sup> cells in both H929 and JN3 myeloma cells display significantly different global transcriptomic features, in comparison with CD138<sup>bright</sup> cells under the same co-culture conditions with differentiated U937 cells. This provides an indication that culture with differentiated U937 cells has a preferential influence on the transcriptional profile of CD138<sup>dim</sup> myeloma cells.

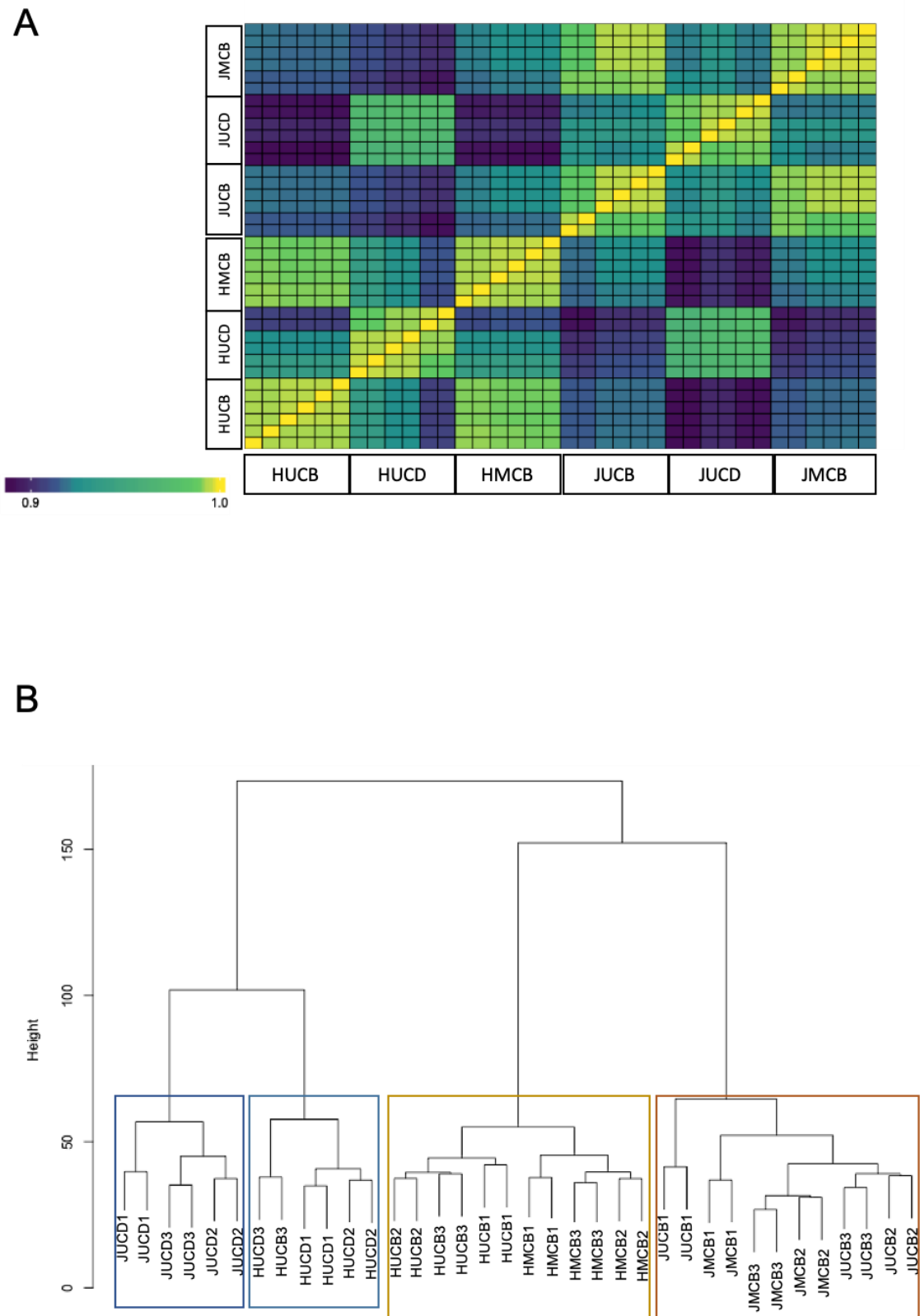


**Figure 4.3. Pearson's correlation and unsupervised hierarchical clustering.** (A) A Pearson's correlation grid containing data from each biological triplicate and sequencing duplicate to highlight similarities and differences in global gene expression between samples. Correlation is annotated by colour with yellow/green indicating stronger correlation and blue indicating weaker correlation. (B) An unsupervised hierarchical clustering plot showing four sub-branches that are highlighted by coloured boxes, orange boxes are indicative of CD138<sup>bright</sup> samples and blue boxes are indicative of CD138<sup>dim</sup> samples from each myeloma cell line.

#### 4.2.4. Principal component analysis of RNA-seq data

Principal component analysis is a technique used to reduce the dimensionality of large datasets by transforming potentially correlated data into uncorrelated variables called principal components. This makes data easier to interpret and enables the identification of groups of data that share commonalities and differences, in this case relating to transcriptional profiling<sup>319</sup>. This technique was used to simply identify samples that were either associated or different to one another and to ascertain the relative differences in variance between each of those samples.

The first observation to make about this data is the clear clustering of replicates from each sample which are highlighted by black ovals in Figure 4.4. Here, it is shown that in both H929 and JJN3 cells the largest differences in variance, as indicated along the PC1 axis, are between both subsets of CD138<sup>bright</sup> and CD138<sup>dim</sup> myeloma cells. It is also evident that in H929 cells there is a greater distinction along the PC2 axis between CD138<sup>bright</sup> cells cultured alone compared with cultured with CD138<sup>bright</sup> cells cultured with differentiated U937 cells. This observation is not as distinct between the same subsets of JJN3 cells. There is also greater variation along the PC2 axis in JJN3 cells, however variation along this axis is not as significant as variation along the PC1 axis, meaning there is still a highly significant correlation between each of the clusters highlighted. It is also important to note that the JMCB cluster in Figure 4.4B is composed of two overlapping data points, meaning that there are in fact 3 data points within that cluster. Overall this supports the data shown in the Pearson's correlation plot and hierarchical clustering shown in Figure 4.3.

In conclusion, the data presented so far in this chapter has revealed that CD138<sup>bright</sup> and CD138<sup>dim</sup> myeloma cells produced distinctly different transcriptomic profiles. This seems to be preferentially induced in CD138<sup>dim</sup> cells as a result of co-culture with differentiated U937 cells and conversely there appeared to be no overwhelming changes in the transcriptomic profile of CD138<sup>bright</sup> cells as a result of co-culture in the same fashion.

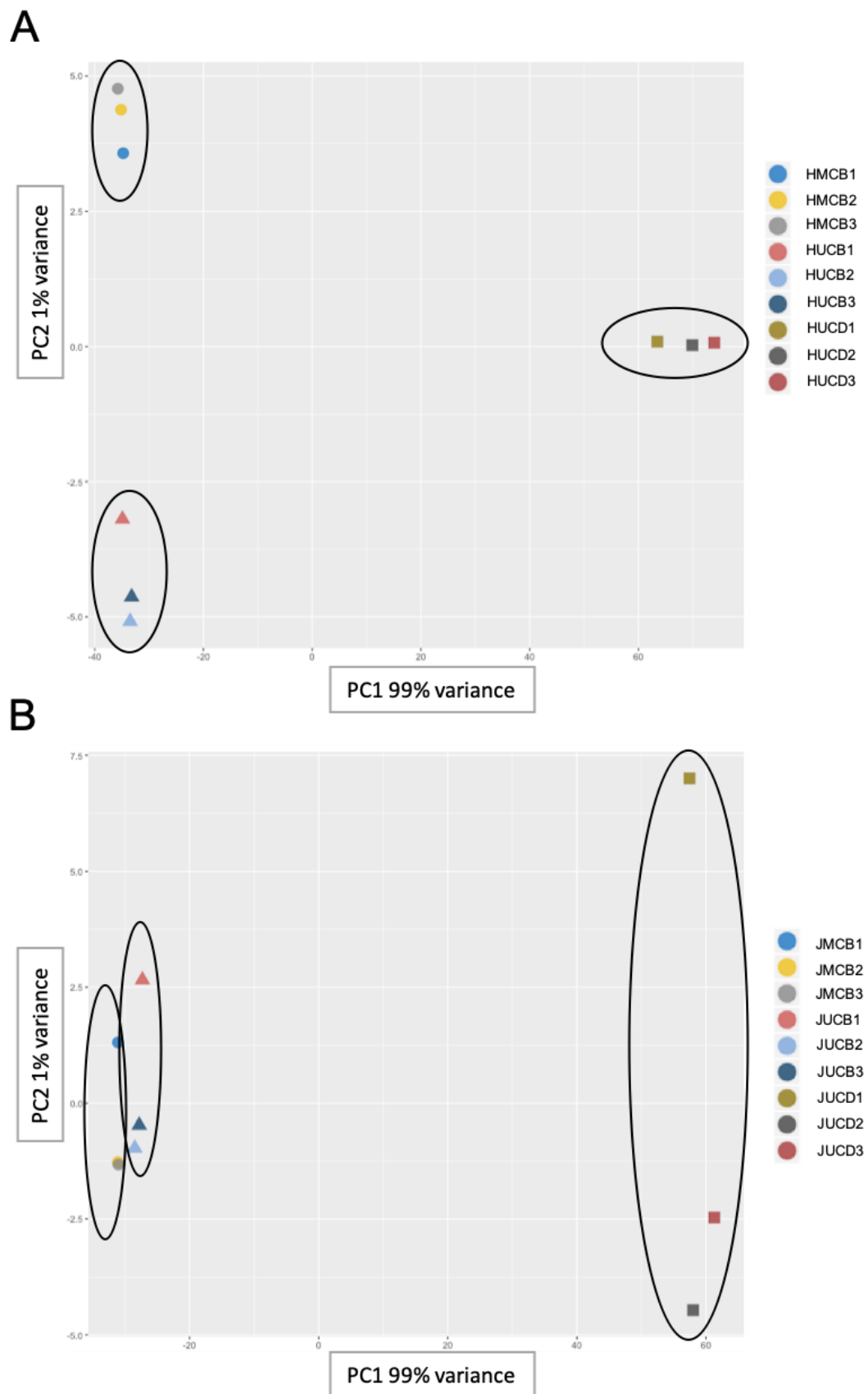


**Figure 4.4. Principal component analysis of variance stabilising transformed counts.** VST counts from the top 500 DE genes in regard to highest variance were used to create PCA plots in both H929 (A) and JJN3 (B) myeloma cells. CD138<sup>bright</sup> cells from monoculture and co-culture with differentiated U937 cells are represented by circles and triangles, respectively. CD138<sup>dim</sup> cells from each cell line are represented by squares. Data shown is representative of three biological replicates (n=3).

### 4.3. Establishment of differentially expressed (DE) genes between CD138<sup>bright</sup> and CD138<sup>dim</sup> myeloma cells

#### 4.3.1. Comparison strategy to determine DE genes

As shown in Section 4.2, correlation analysis, unsupervised hierarchical clustering and principal component analysis revealed distinct patterns of global transcriptional differences between each cell line and subpopulation of myeloma cells. This complimented the phenotypic analysis, which identified these two subpopulations of myeloma cells and supports the hypothesis that these two distinct subpopulations exhibited clear differences in gene expression in response to co-culture with differentiated U937 cells. The aim of this section of analysis was to assess differences in transcriptional activity between CD138<sup>bright</sup> and CD138<sup>dim</sup> cells co-cultured with differentiated U937 cells in H929 and JN3 myeloma cells against a respective CD138<sup>bright</sup> mono-culture control. This would reveal the impact of this co-culture model on the transcriptional activity of CD138<sup>bright</sup> and CD138<sup>dim</sup> cells. In turn, this information could be used to highlight clusters of genes that are transcriptionally altered in response to co-culture, which could provide a platform to determine the biological influence of differentiated U937 osteoclast-like cells on myeloma cells and also elucidate the roles of CD138<sup>bright</sup> and CD138<sup>dim</sup> myeloma cells in human disease. In order to further assess these differences, DE genes between each sample will be determined. This comparative strategy is outlined in Figure 4.5.

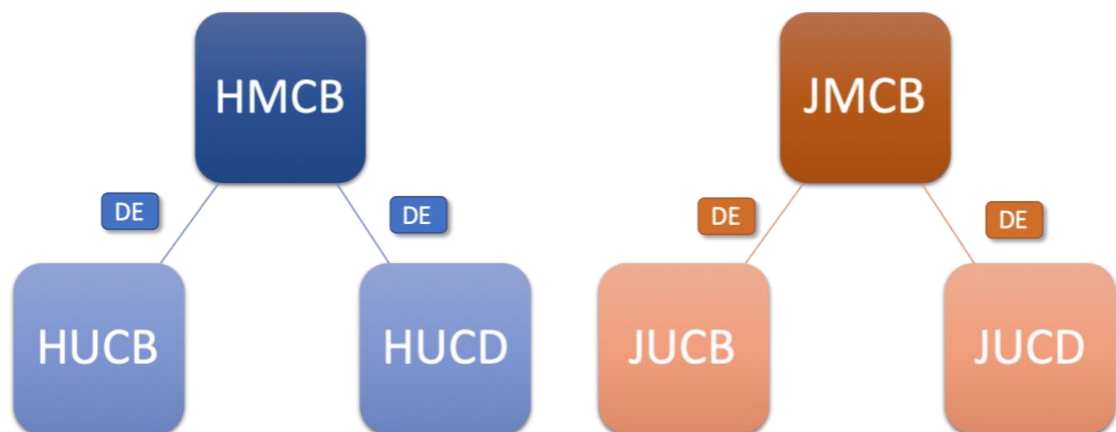


**Figure 4.5. A diagram illustrating the comparisons made between each sample to investigate differential gene expression. DE = Differentially expressed genes.**

### 4.3.2. Visualisation of DE genes in each dataset

#### 4.3.2.1. MvA plots

In order to visualise the comparisons outlined in Figure 4.5, MvA plots were constructed. These plots were originally proposed by Bland and Altman as a means to compare clinical measurement techniques to assess statistical agreement as to whether a new technique was effective enough to replace another<sup>320</sup>. Since its original publication, this technique has been adopted and widely used to visualise gene expression data to observe differences in expression between two conditions, where the  $\log_2(\text{fold change})$  is plotted against the  $\log_{10}(\text{mean of normalised counts})$ . In order to assess statistical significance an adjusted p-value, known as a q-value, was used. This statistical assessment measures significance in conjunction with the false discovery rate and is recommended for larger datasets, such as those created from genome-wide studies, in order to avoid the inevitably higher rate of false positive results<sup>321</sup>. Initially an adjusted p value of  $q < 0.1$  was applied as an initial selection criterion to visualise as many significant differentially expressed genes as possible.

As this experiment utilised triplicate biological measurements, each data point represents the mean of each DE gene accumulated from each replicate. The first observation to make from these comparisons is that co-culture with differentiated U937 cells causes a change in the transcriptional activity of both CD138<sup>bright</sup> and CD138<sup>dim</sup> cells. This is shown by the presence of red points highlighted in the MvA plots in Figure 4.6, meaning that co-culture in this fashion results in clear changes in the up or downregulation of gene expression in both subpopulations of cells, in each myeloma cell line. The second observation to make here is the distinction in the number of DE genes between CD138<sup>bright</sup> and CD138<sup>dim</sup> cells in both myeloma cell lines. Visually it appears that there is a much greater number of DE genes, indicated by the large increase in the number of red data points presented on the MvA plots when the number of DE genes from CD138<sup>dim</sup> cells is compared with CD138<sup>bright</sup> mono-culture control cells, in comparison with CD138<sup>bright</sup> cells co-cultured with differentiated U937 cells. Thus, indicating that there is an increase in transcriptional activity in CD138<sup>dim</sup> cells compared with CD138<sup>bright</sup> cells after co-culture with differentiated U937 cells.

#### 4.3.2.2. Heatmaps

Having established that co-culture with differentiated U937 cells induced substantial changes in the transcriptional behaviour of both CD138<sup>bright</sup> and CD138<sup>dim</sup> myeloma subpopulations, it was of interest to identify these DE genes and quantify their transcriptomic regulation as a result of co-culture with differentiated U937 cells. This could aid the establishment of cellular pathways that could be overrepresented in each dataset. The significance threshold was further reduced here from  $q < 0.1$  to  $q < 0.05$ . The top 200 most significant DE genes were then arranged in a heatmap to compare similarities between groups of DE genes. Data collated from H929 cells showed that the majority of these significant DE genes were downregulated in CD138<sup>bright</sup> cells and upregulated in CD138<sup>dim</sup> cells when compared with a CD138<sup>bright</sup> monoculture control. There also appears to be a darker shading of red from each CD138<sup>dim</sup> heatmap which indicates higher fold changes occurring in the DE genes from these CD138<sup>dim</sup> datasets compared with CD138<sup>bright</sup> cells (Figure 4.7A). Data collated from JJN3 cells replicates this observation, however in contrast to CD138<sup>bright</sup> H929 cells, CD138<sup>bright</sup> JJN3 cells co-cultured with differentiated U937 cells are mostly upregulated in comparison with a mono-culture control (Figure 4.7B).

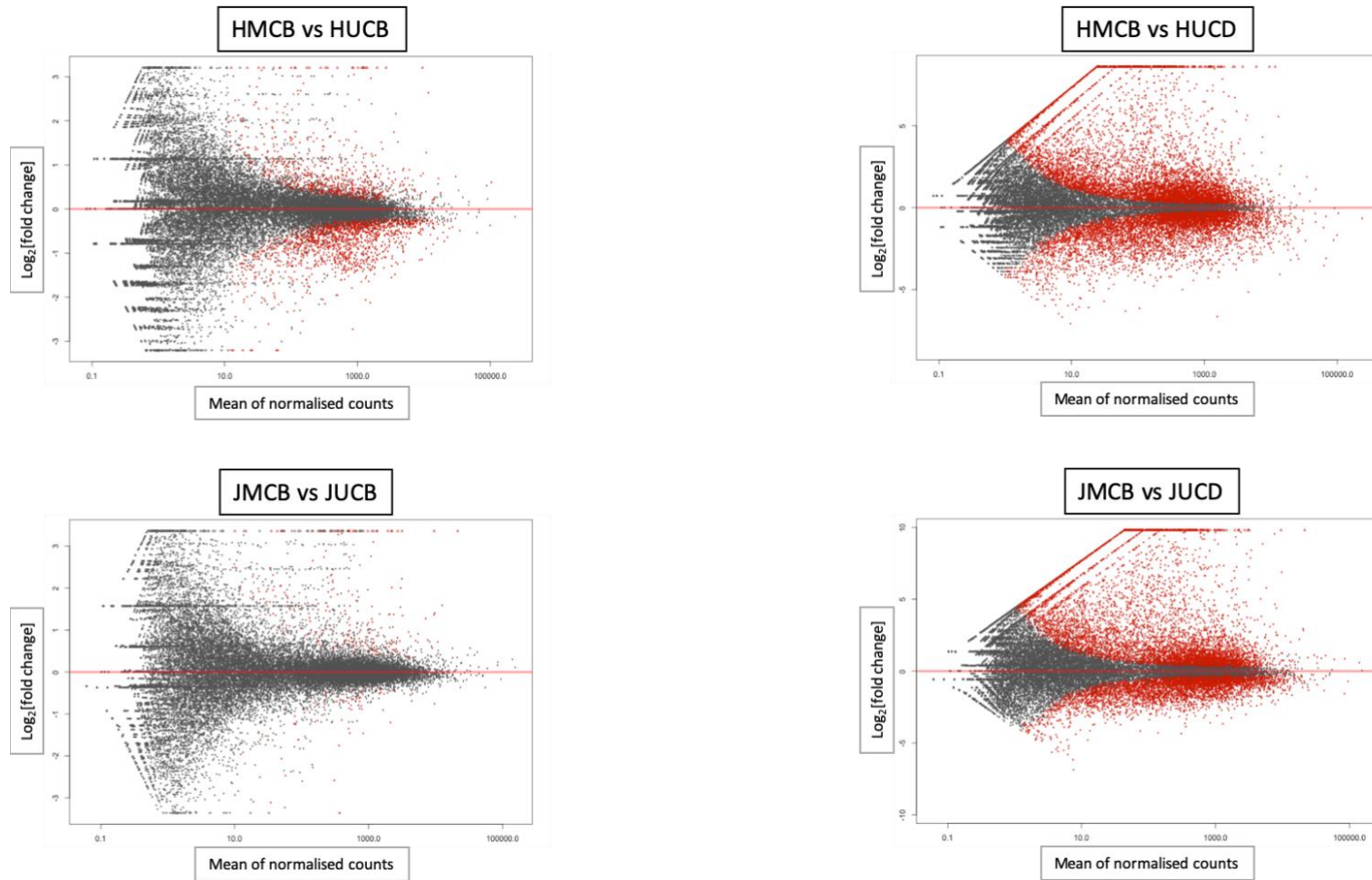


**Figure 4.6. MvA plots facilitating the visualisation of differentially expressed genes.** Differentially expressed genes from mono-culture controls in both H929 and JIN3 cell lines were compared with CD138<sup>bright</sup> and CD138<sup>dim</sup> cells after co-culture with differentiated U937 cells. Genes with similar levels of expression between conditions centre around the horizontal red line on each plot. Genes that have an increased expression in comparison are positioned above this red line and conversely, genes that have lower differential expression are positioned below the red line. Red points indicate differentially expressed genes with an adjusted p-value < 0.1. Points falling outside of the plotting area are represented by triangles. HMCB - H929 monoculture CD138<sup>bright</sup>, HUCB - H929+U937 CD138<sup>bright</sup>, HUCD - H929+U937 CD138<sup>dim</sup>, JMCB - JIN3 monoculture CD138<sup>bright</sup>, JUCB - JIN3+U937 CD138<sup>bright</sup>, JUCD - JIN3+U937 CD138<sup>dim</sup>.

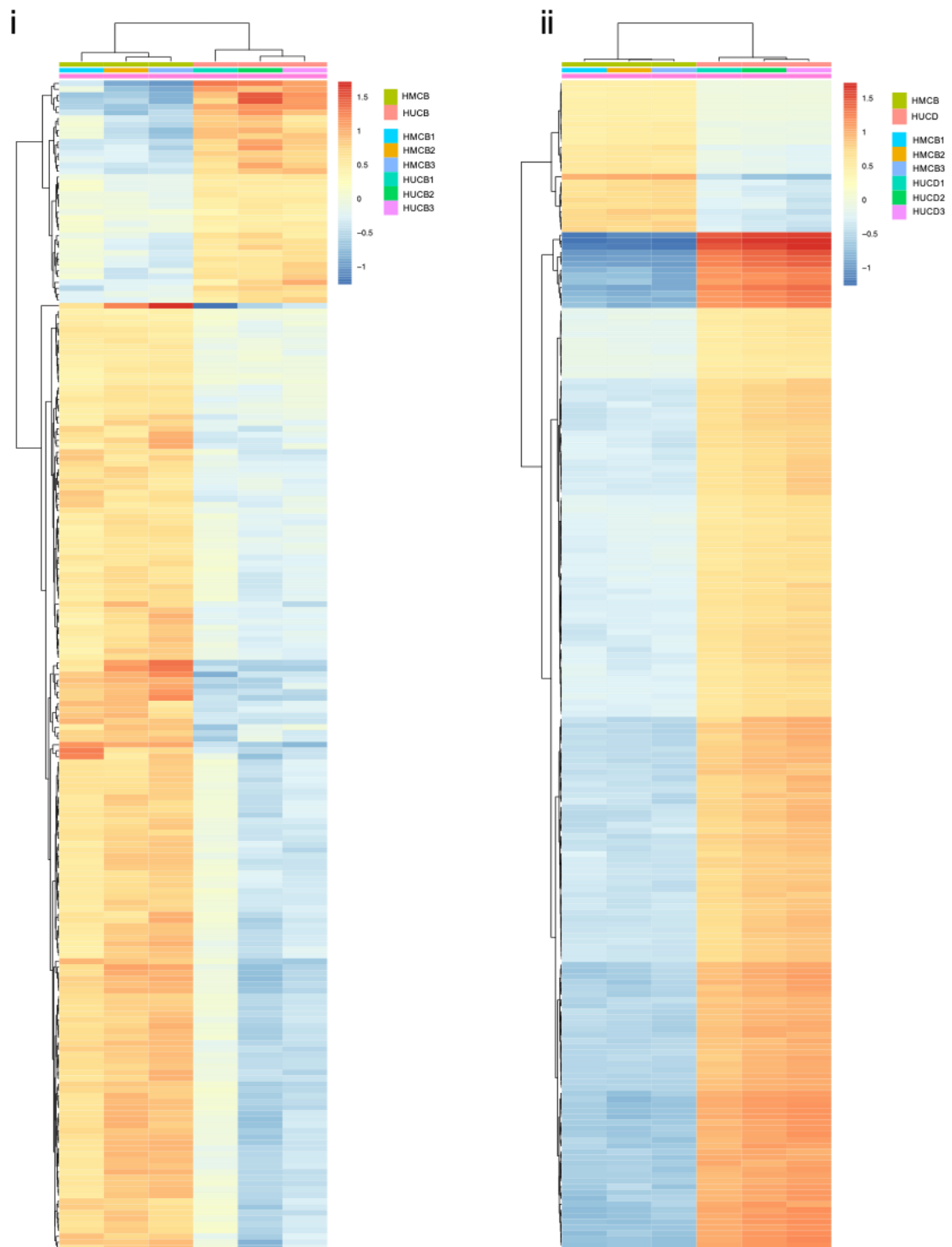


**Figure 4.7A. Heatmap illustrating the top 200 differentially expressed genes in H929 cells.**

Differentially expressed genes from HMCB vs HUCB (i) and HMCB vs HUCD (ii) comparisons were sorted in order of significance using adjusted p-value ( $q < 0.05$ ). Relative fold changes of the 200 most differentially expressed genes are shown in the form of a heatmap to compare upregulated (red) or downregulated (blue) genes. HMCB - H929 monoculture CD138<sup>bright</sup>, HUCB - H929+U937 CD138<sup>bright</sup>, HUCD - H929+U937 CD138<sup>dim</sup>, JMCB - JN3 monoculture CD138<sup>bright</sup>, JUCB - JN3+U937 CD138<sup>bright</sup>, JUCD - JN3+U937 CD138<sup>dim</sup>.

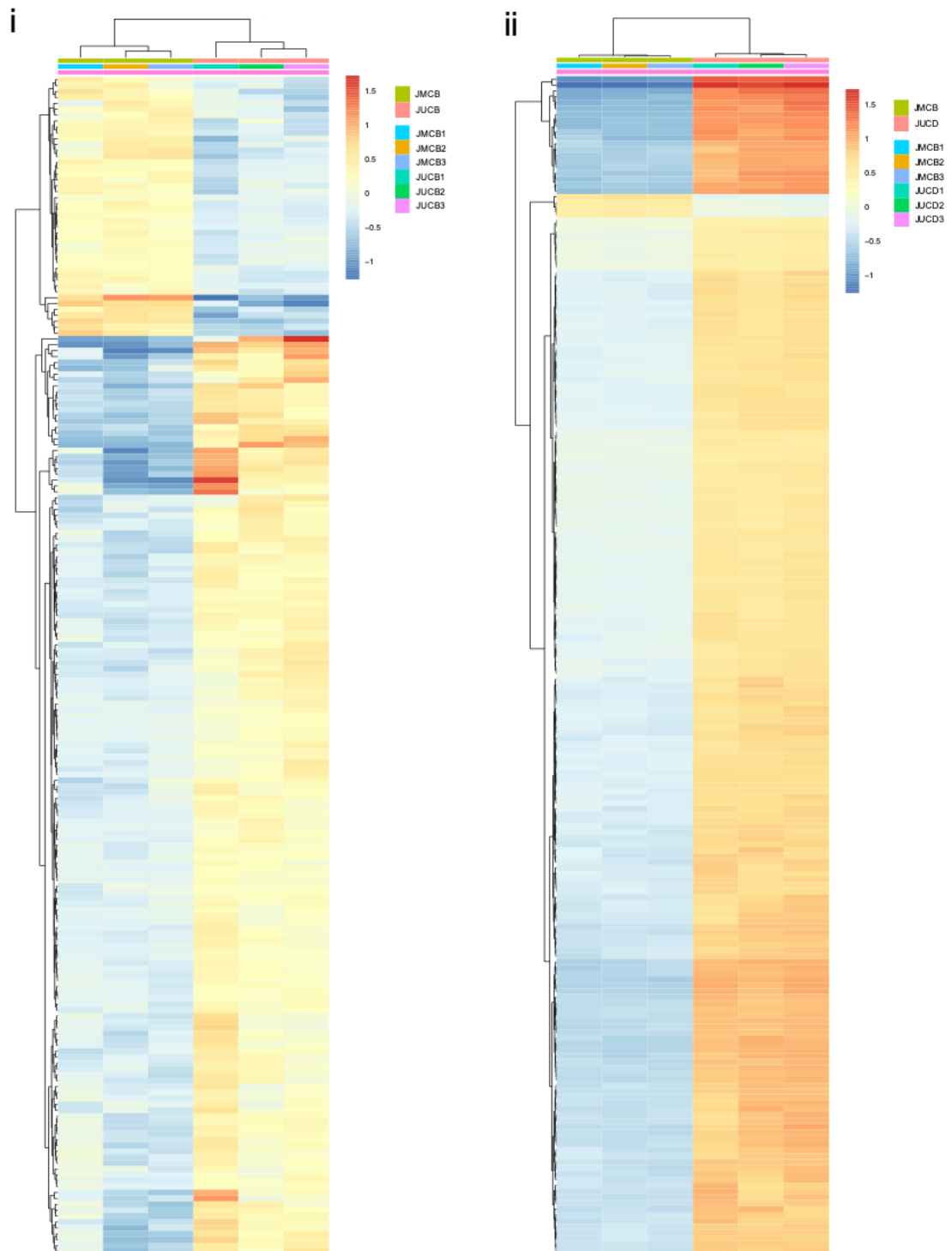


**Figure 4.7B. Heatmap illustrating the top 200 differentially expressed genes in JN3 cells.**

Differentially expressed genes from JMCB vs JUCB (i) and JMCB vs JUCD (ii) comparisons were sorted in order of significance using adjusted p-value ( $q < 0.05$ ). Relative fold changes of the 200 most differentially expressed genes are shown in the form of a heatmap to compare upregulated (red) or downregulated (blue) genes. HMCB - H929 monoculture CD138<sup>bright</sup>, HUCB - H929+U937 CD138<sup>bright</sup>, HUCD - H929+U937 CD138<sup>dim</sup>, JMCB - JN3 monoculture CD138<sup>bright</sup>, JUCB - JN3+U937 CD138<sup>bright</sup>, JUCD - JN3+U937 CD138<sup>dim</sup>.

#### 4.3.2.3. Venn Diagrams

In order to quantify and visualise these data further, Venn diagrams were constructed to provide a means of comparing commonly up or down-regulated genes from each comparison made within the dataset. In order to further reduce the number of DE genes in the dataset a  $\log_2$  fold change threshold of  $>1$  or  $<-1$  was applied in addition to a significance of  $q < 0.05$ .

Firstly, it is apparent that the absolute number of DE genes is much higher in HUCD and JUCD datasets, when compared with respective HMCB and JMCB datasets. This is in contrast to HUCB and JUCB datasets which produced a much smaller number of differentially expressed genes when compared with the same respective monoculture controls. The HMCB vs HUCB and JMCB vs JUCB comparisons produced 484 (157 upregulated and 327 downregulated) and 124 (104 upregulated and 20 downregulated) DE genes, respectively. In contrast, the HMCB vs HUCD and JMCB vs JUCD comparison produced 7096 (4213 upregulated and 2883 downregulated genes) and 6636 (4473 upregulated and 2163 downregulated genes) DE genes, respectively. It is also interesting that there are some discrepancies between both H929 and JIN3 myeloma cells, which indicated that CD138<sup>bright</sup> cells co-cultured with differentiated U937 cells produced a higher proportion of upregulated genes in JIN3 cells and conversely, a higher proportion of downregulated genes in H929 cells when compared with respective monoculture controls. This was not the case in CD138<sup>dim</sup> cells in either cell line, where the majority of DE genes were upregulated (Figure 4.8A).

In order to draw further comparisons from these data and determine whether there was commonality between these DE genes in each condition, a four-way Venn diagram was constructed. From this analysis, there appeared to be very little commonality between DE genes from CD138<sup>bright</sup> cells between both myeloma cell lines, with only one DE gene being exclusively shared, as shown by the blue vs orange overlap. The remainder of DE genes are shown to be exclusive to each cell line. In contrast, there appears to be a much higher level of commonality between DE genes from HUCD and JUCD datasets, where a total of 3296 (2366 upregulated and 930 downregulated) genes are exclusively shared between these two cell lines as shown by the orange vs green overlap. There are also a number of DE genes shared between both CD138<sup>bright</sup>

and CD138<sup>dim</sup> cells from each myeloma cell line, although the number of DE genes shared here are not as substantial as those exclusively shared between each CD138<sup>dim</sup> subset. This indicates that co-culture with differentiated U937 cells has a common influence on the transcriptional profile of CD138<sup>dim</sup> cells but not CD138<sup>bright</sup> myeloma cells. This further supports the data shown in Section 4.2 and clearly demonstrates a significant change in the transcriptomic profile of CD138<sup>dim</sup> cells in response to co-culture with differentiated U937 cells.

Whilst there are certainly some distinct changes in DE genes in CD138<sup>bright</sup> cells that will be subject to further investigation, there are more substantial changes in the number of DE genes present in CD138<sup>dim</sup> myeloma cells after co-culture in this osteoclast-like *in vitro* model. The next steps of analysis are to produce a functional assessment of these DE genes to assess the biological effects of osteoclast co-culture and to examine the potential roles of each subset of myeloma cells in the pathology and progression of this malignancy.

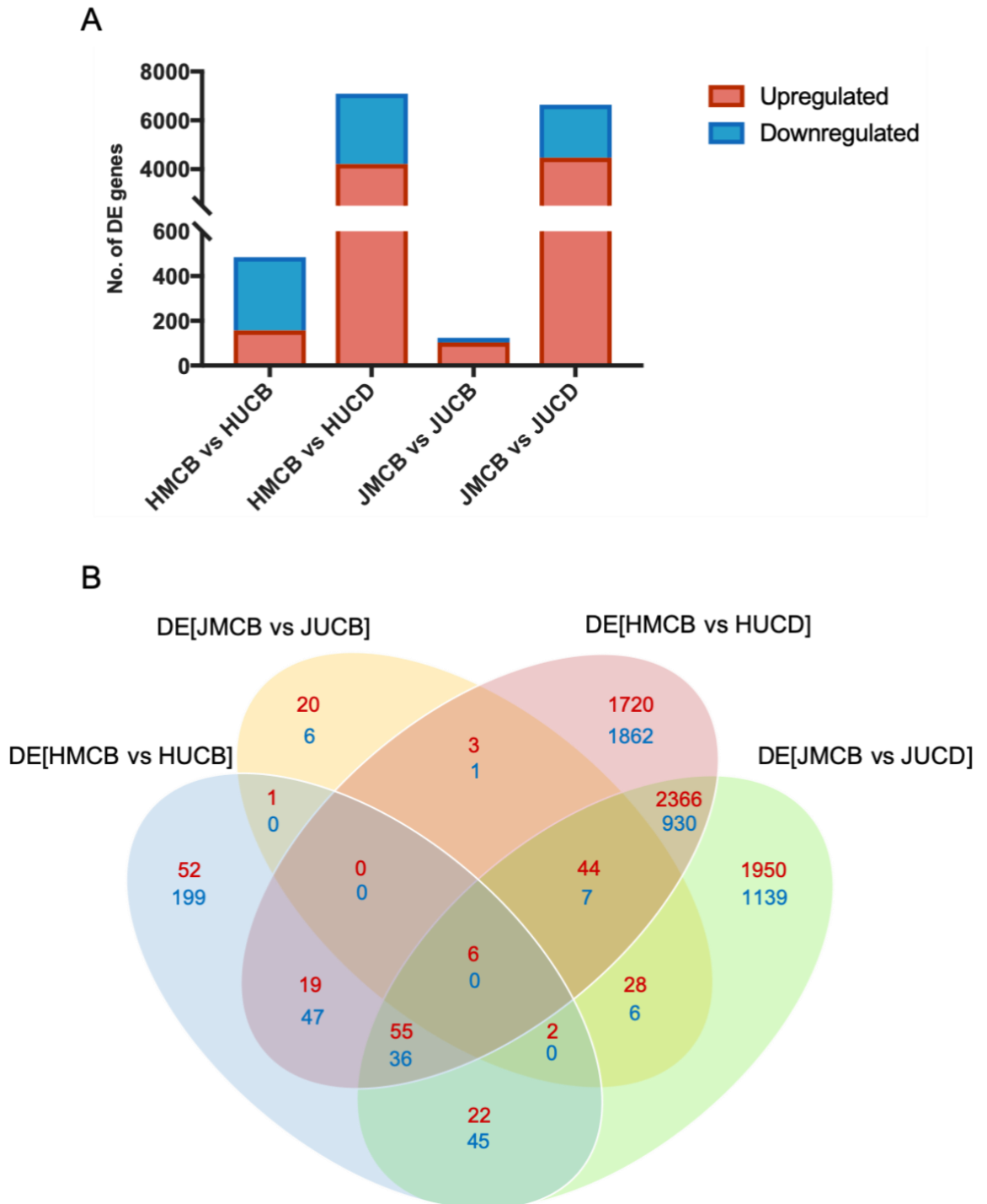


**Figure 4.8. Venn diagrams highlighting the number of significant differentially expressed genes ( $q < 0.05$ ) that have  $\log_2$  fold changes  $> 1$  and  $< -1$ .** (A) The absolute number of differentially expressed genes from each comparison, this data is divided into genes that are significantly upregulated (red) and downregulated (blue). (B) A Venn diagram illustrating the number of commonly upregulated or downregulated genes from each comparison, which are represented by coloured ovals. HMCB – H929 monoculture CD138<sup>bright</sup>, HUCB – H929+U937 CD138<sup>bright</sup>, HUCD – H929+U937 CD138<sup>dim</sup>, JMCB – JN3 monoculture CD138<sup>bright</sup>, JUCB – JN3+U937 CD138<sup>bright</sup>, JUCD – JN3+U937 CD138<sup>dim</sup>.

## 4.4. Over-representation of differentially expressed genes

Having established lists of DE genes between CD138<sup>bright</sup> and CD138<sup>dim</sup> myeloma cells in both H929 and JJN3 cell lines, it was then of interest to construct a functional assessment of these gene lists to determine cellular functions and overrepresented pathways within each dataset. In order to assess this, Ingenuity Pathway Analysis (IPA) was employed.

Ingenuity Pathway Analysis is a software application that can be used to interpret genomics data, including data generated from RNA-seq experiments, to establish a functional overview of overrepresented functions and pathways within a dataset. It does so by building on a manually developed knowledge base to relate specific genes to specific pathways and functions<sup>322</sup>. This could potentially reveal information about key regulators involved in biological processes and mechanisms that contribute to disease propagation and progression. It was therefore of interest to assess each DE gene list produced from CD138<sup>bright</sup> and CD138<sup>dim</sup> cells in each myeloma cell line using IPA to investigate these processes.

DE gene lists produced from each sample comparison (Figure 4.8) were input into IPA. All DE genes determined between HMCB vs HUCB (484 genes) and JMCB vs JUCB (124 genes) comparisons were input into IPA. However, the IPA-recommended upper limit for the number of genes to be included in each gene list is 3000. Therefore, DE gene lists produced from HMCB vs HUCD (7096 genes) and JMCB vs JUCD (6636 genes) comparisons were sorted in order of significance, with the 3000 most significant ( $q < 0.05$ ) DE genes being input into IPA. Each list of DE genes was then found to be significantly associated with a number of overrepresented cellular functions and pathways following analysis using IPA.

### 4.4.1. Overrepresentation of cellular functions

Lists of cellular functions that were overrepresented in each dataset were produced along with corresponding quantification of statistical significance following analysis of each dataset in IPA. The pathways produced were assessed for commonality between CD138<sup>bright</sup> and CD138<sup>dim</sup> cells in both myeloma cell lines, with the top 5 most

significantly overrepresented cellular functions being presented in Figure 4.9. It is clear here that each function in CD138<sup>dim</sup> cells is overrepresented at a much higher level of significance compared with CD138<sup>bright</sup> cells. The two lists also share similar functions including cell movement, cell death and survival and cellular function and maintenance. Interestingly, cell movement is the most significant overrepresented cellular function in CD138<sup>dim</sup> myeloma cells.

The next stage of analysis was to determine the pathways that were overrepresented in these datasets that could lead to further elucidation of the mechanisms behind cellular function, which could infer more information relating to the potential roles that these cells may possess in human disease.

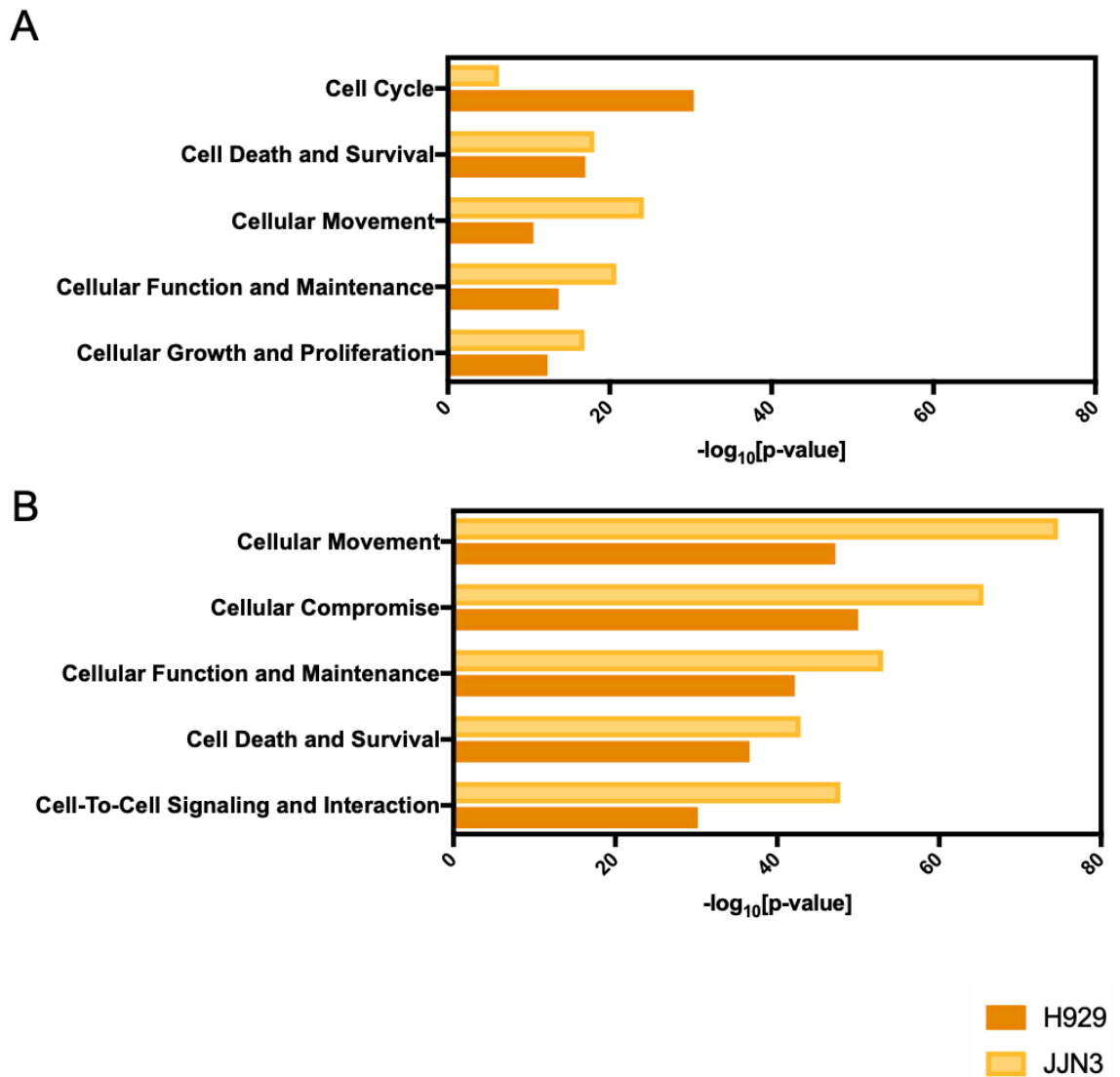


**Figure 4.9. Summary of overrepresented cellular functions determined by IPA analysis.** Significant cellular functions that were overrepresented in each dataset were assessed for commonality between each myeloma cell line in both (A) CD138<sup>bright</sup> and (B) CD138<sup>dim</sup> cell subsets. The top 5 most significant functions were then plotted in a bar chart which illustrates their statistical significance.

#### 4.4.2. Quantification of overrepresented pathways

The same datasets used to analyse cellular functions in Section 4.3.1 were used to assess overrepresentation of cellular pathways. Pathway lists were accompanied by p-values to assess significance and z-scores to determine the difference between the expected and observed relationship between overrepresented pathways and gene expression. Pathway lists were therefore further sorted based on significance ( $p < 0.05$ ) and z-score ( $-2 < z < 2$ ). The z-score limits that were chosen represent values that are two standard deviations above or below the mean which are considered significant in relation to determining whether a pathway is activated or inhibited. This strategy produced lists of overrepresented pathways that are illustrated in Figure 4.10. Here, it is shown that when assessing the impact of co-culture on H929 or JN3 CD138<sup>bright</sup> cells, there were few overrepresented pathways. So, the HMCB vs HUCB and JMCB vs JUCB comparisons produced only 2 (1 activated and 1 inhibited) and 5 (all activated) significant overrepresented pathways, respectively.

In contrast, there were over a hundred different overrepresented pathways produced when comparing monoculture CD138<sup>bright</sup> vs co-culture CD138<sup>dim</sup> cells. e.g. HMCB vs HUCD and JMCB vs JUCD comparisons produced 131 (128 activated and 3 inhibited) and 140 (135 activated and 5 inhibited) significant overrepresented pathways, respectively (Figure 4.10A). This shows that the impact of co-culture with differentiated U937 cells on transcriptional activity is much greater in CD138<sup>dim</sup> cells in comparison to CD138<sup>bright</sup> cells in both myeloma cell lines. It is also apparent that the majority of significant overrepresented pathways produced from both HMCB vs HUCD and JMCB vs JUCD comparisons are shared, with 104 (62.2%) activated pathways being common to both sample comparisons as indicated by the green vs red Venn diagram overlap (Figure 4.10B). This is further evidence to suggest that co-culture with differentiated U937 cells induces a preferential influence on the transcriptomes of CD138<sup>dim</sup> myeloma cells when compared with CD138<sup>bright</sup> myeloma cells, thus inferring that these cells are more transcriptionally active in the presence of an osteoclast-like microenvironment, compared with CD138<sup>bright</sup> cells.



### 4.4.3. Evaluation of overrepresented pathways

Having established that there is a substantial difference in the number of significant DE genes and overrepresented pathways between CD138<sup>bright</sup> and CD138<sup>dim</sup> myeloma cells, when compared with CD138<sup>bright</sup> mono-culture controls, it was of interest to further dissect this information to investigate which molecular pathways are overrepresented in each dataset. This would reveal information about what biological functions are influenced by co-culture with differentiated U937 cells which could also potentially allude to the function of each subset of myeloma cells in relation to disease pathophysiology and progression.

There were just 2 and 5 overrepresented pathways amassed from CD138<sup>bright</sup> H929 and JN3 cells, respectively. These pathways were exclusive to each cell line within each CD138<sup>bright</sup> comparison (Figure 4.10). The majority of these pathways are well-established in the pathological composition of myeloma. In H929 cells there was an overall activation of interferon signalling and an inhibition of cell cycle regulation. Whereas in JN3 cells there was an overall activation of leukocyte extravasation signalling, IL-8 signalling and NF- $\kappa$ B signalling (Figure 4.11A).

Given the vast increase in the number of pathways that were overrepresented in the both H929 and JN3 CD138<sup>dim</sup> datasets, a more selective approach was adopted to narrow down the number of pathways to a more manageable size and investigate which pathways are more relevant to myeloma biology. In order to do this, the 104 commonly shared pathways between H929 and JN3 CD138<sup>dim</sup> cells were selected for further assessment. The pathways within this dataset ranged a wide array of cellular functions, many of which were not entirely relevant to myeloma biology. This entire list of pathways is shown in Supplementary Table 4.2. These overrepresented pathways were cross-referenced with the literature and current knowledgebase to manually select pathways that were more specifically relevant to myeloma biology. This produced a list of 31 pathways that were both common to both H929 and JN3 CD138<sup>dim</sup> cells and also bears relevance to the pathophysiology of myeloma. Of these pathways, there were 30 pathways that were significantly activated and 1 pathway that was significantly inhibited. The trends observed in each cell line are comparable

between both H929 and JJN3 cell lines, albeit with marginally different z-scores being produced for each overrepresented pathway (Figure 4.11B).

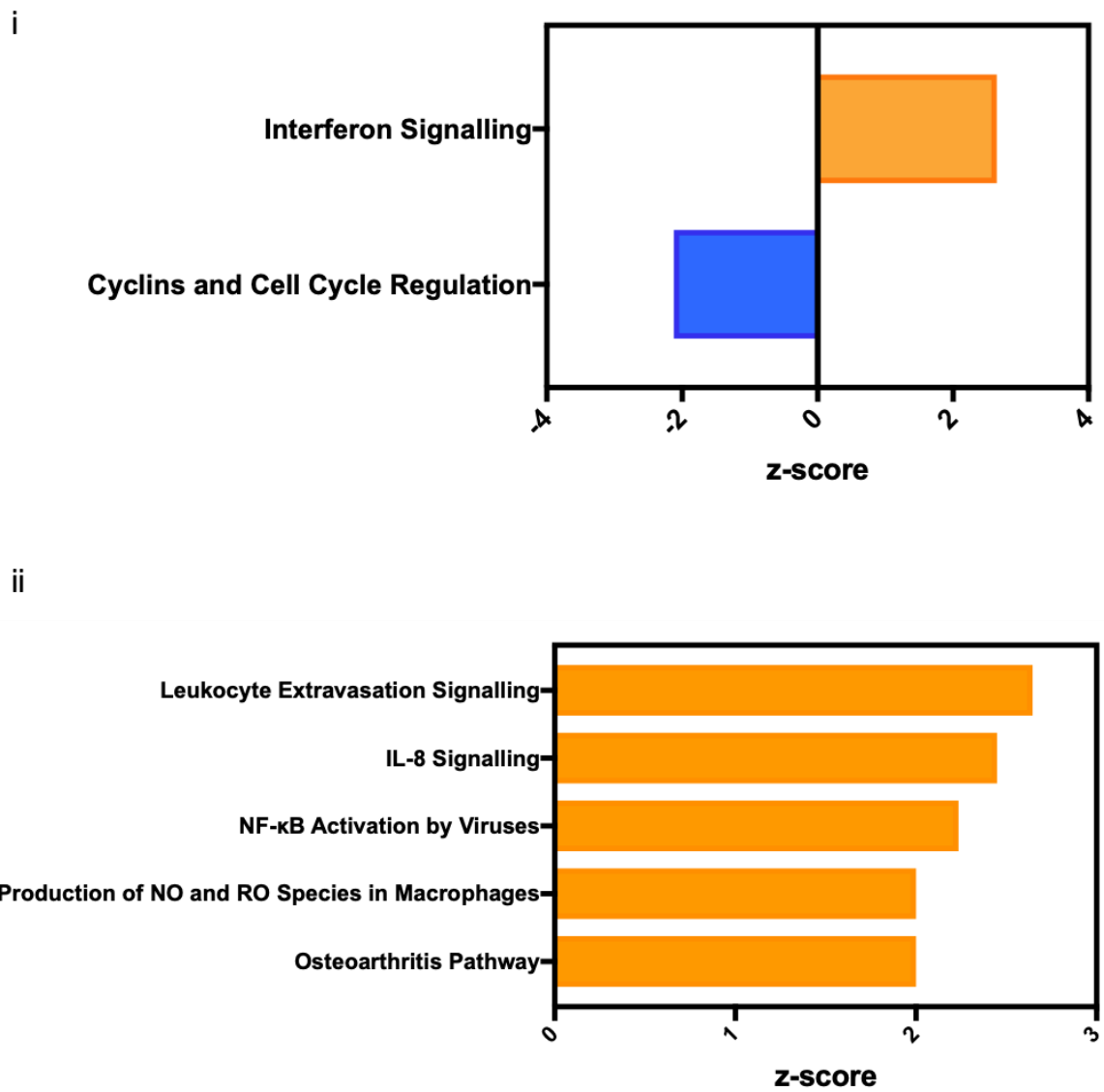


**Figure 4.11A. Summary of significantly overrepresented pathways in CD138<sup>bright</sup> comparisons.** Each significant ( $p < 0.05$ ) overrepresented pathway is shown for HMCB vs HUCB (i) and JMCB vs JUCB (ii) sample comparisons. Pathways that were either activated ( $z > 2$ ) or inhibited ( $z < -2$ ) are coloured orange and blue, respectively.

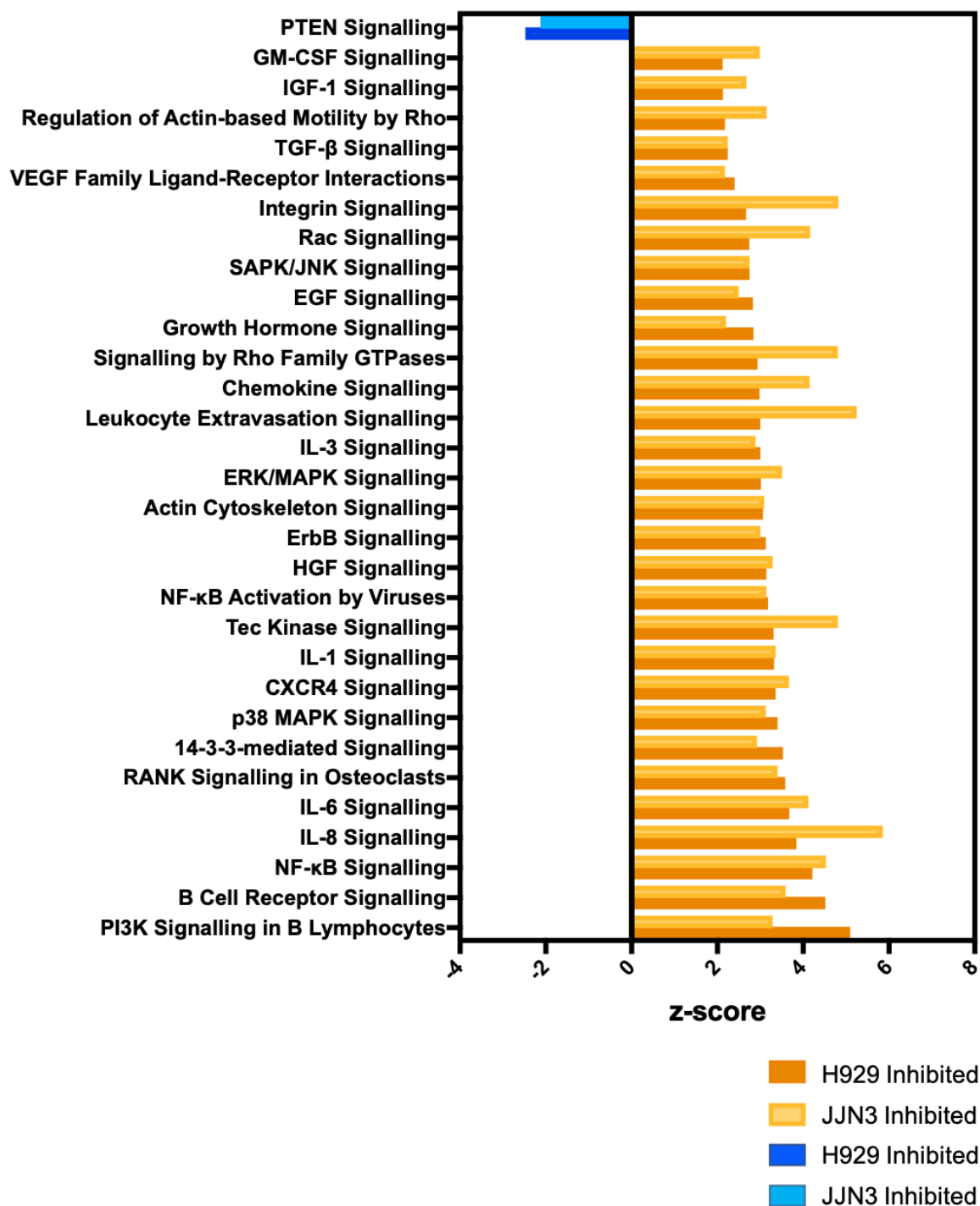


**Figure 4.11B. Summary of significantly overrepresented pathways in CD138<sup>dim</sup> comparisons.** Significant ( $p < 0.05$ ) overrepresented pathways that were common to both H929 and JJN3 CD138<sup>dim</sup> datasets were further filtered for pathways relating to myeloma pathophysiology. Pathways in this illustration that are activated ( $z > 2$ ) are coloured orange and pathways that are inhibited are coloured blue.

## 4.5. Validation of DE genes using qPCR

### 4.5.1. Selection of targets to be used for validation

RNA-sequencing revealed that culture with differentiated U937 cells induced massive changes in the transcriptional behaviour of CD138<sup>dim</sup> myeloma cells, compared with CD138<sup>bright</sup> cells in both H929 and JLN3 cell lines. In order to validate these findings, to ensure that the results obtained from RNA-sequencing are representative of true-positives, qPCR was employed to assess gene expression.

The variety of enriched pathways that were overrepresented from DE analysis in CD138<sup>dim</sup> myeloma cells spanned a wide range of molecular and cellular functions. Given the extremely large number of DE genes and subsequent pathways that were overrepresented in this analysis it was impractical to use an extensive gene list, relating to each of these pathways, to be used for validation by qPCR. It was therefore important to employ a logical selection strategy when choosing candidate genes to be used for validation. It was of interest to choose genes that were not restricted to any single pathway that was overrepresented in the pathway analysis and to select genes that spanned a wide range of functions and are of particular interest in the pathophysiology of myeloma. Therefore, candidate genes were chosen based on their relation to functions in survival, influence in bone resorption, angiogenesis, migration, and adhesion.

It was important to select genes that were commonly overrepresented and upregulated in CD138<sup>dim</sup> myeloma cells from both H929 and JLN3 cells. It was also crucial to confirm that these genes were highly expressed in each of the CD138<sup>dim</sup> samples used in RNA-sequencing as this would produce a better chance of detecting gene expression using qPCR. Therefore, genes were selected on the basis of; baseline expression being high enough to ensure qPCR detection, and fold change, in comparison with CD138<sup>bright</sup> monoculture controls, was also suitably high ( $\log_2$  fold change  $>1$ ). Having established the selection criteria for candidate genes to be used in qPCR validation, a list of genes that fulfil these criteria is shown in Table 4.1 alongside a general description of gene function, which also highlights the role of each candidate gene in relation to the pathophysiology of myeloma.

#### 4.5.2. Expression of genes selected for validation

Read counts obtained from RNA-sequencing are directly comparable to gene expression of each individual gene in the genome. Normalised read counts for each candidate gene selected for qPCR were highlighted in each of the samples used in this experiment and were transformed using a  $\log_2(n+pseudo-number)$  calculation. In this case the *pseudo-number* used was 1. This calculation normalises extreme outliers in the dataset and also accounts for genes that have no reads, indicating a transcriptionally inactive gene, which therefore facilitates the numerical quantification of this data. The  $\log_2$  values of these normalised read counts are plotted in Figure 4.12. It is clear that each gene selected for qPCR validation is very highly expressed in each CD138<sup>dim</sup> sample in both myeloma cell lines. The fold change of gene expression is also significantly greater in CD138<sup>dim</sup> cells in comparison to CD138<sup>bright</sup> cells cultured in isolation or with differentiated U937 cells. This also confirmed that these genes fulfilled the criteria outlined in Section 4.4.1. for the selection of candidate genes to be used for validation to demonstrate both a high level of baseline expression and a high fold change in comparison to CD138<sup>dim</sup> cells.

	<b>Candidate Gene</b>	<b>Description of function</b>
<b>SPP1</b>	<b>Secreted phosphoprotein 1/osteopontin</b>	Osteopontin is a secreted phosphoglycoprotein that is a critical regulator of bone homeostasis. Previous research has demonstrated its involvement in facilitating the adhesion of osteoclasts to bone, enabling them to carry out their resorptive function <sup>323</sup> . Osteopontin is secreted by numerous cell types, including plasma cells, with an increasing level of secretion being found to derive from myeloma cells at each stage of disease progression <sup>324</sup> . These characteristics have established osteopontin as a marker of osteoclast activity and angiogenesis <sup>325</sup> .
<b>SYK</b>	<b>Spleen-associated tyrosine kinase</b>	Syk is a cytosolic protein tyrosine kinase first identified by Kobayashi <i>et al</i> <sup>326</sup> . Syk has been recognised as a key component to B-cell receptor signalling and has been found to be upregulated in a number of haematological cancers, including myeloma. Activation of Syk results in the transduction of downstream signals through PI3K and BTK propagation <sup>327</sup> . Inhibition of Syk has also been shown to induce apoptosis and inhibit proliferation in myeloma cells, thus demonstrating a promising therapeutic strategy <sup>328</sup> .
<b>CXCL8</b>	<b>C-X-C motif chemokine ligand 8/Interleukin 8</b>	CXCL8 is associated with the CXC family of chemokines. It's expression and subsequent secretion is rapidly induced by pro-inflammatory cytokines, which can be induced within the microenvironment of a number of cancers, including myeloma <sup>329,330</sup> . CXCL8 has been related to a number of functions including angiogenesis, cell motility and apoptosis, meaning it provides a promising therapeutic target to tackle metastasis and chemoresistance <sup>331</sup> .
<b>MMP2</b>	<b>Matrix metalloproteinase 2</b>	MMP2 belongs to the larger family of MMP proteins which are secreted proteolytic endopeptidase enzymes that are responsible to the degradation of multiple components within the extracellular matrix <sup>332</sup> . MMP2 has been found in elevated quantities in myeloma patients and has a role in the degradation of collagen IV. This is a major component of the basement membrane, which has led to MMP2 being associated with aberrant bone remodelling and metastasis <sup>297</sup> .
<b>CCL2</b>	<b>C-C motif chemokine ligand 2/monocyte chemoattractant protein-1 (MCP-1)</b>	Not normally expressed in the bone marrow microenvironment, CCL2 has been found to be secreted in larger quantities in myeloma patients, playing an important role in the process of angiogenesis. Secretion of this chemokine has been shown to derive from myeloma cells themselves in response to IL-6 <sup>333</sup> .

Table 4.1. A summary and description of genes selected for validation using qPCR.

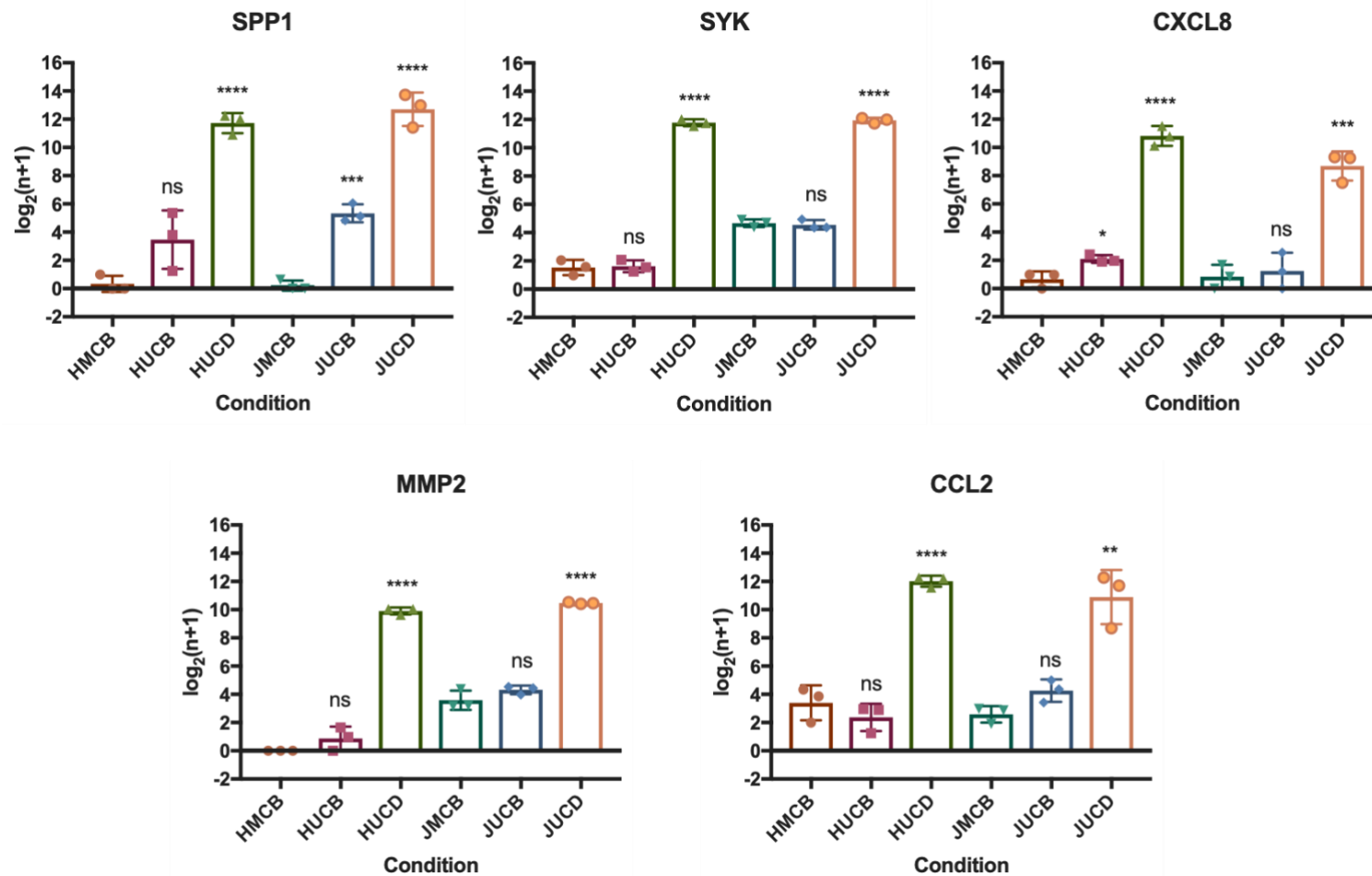


**Figure 4.12. Expression of differentially expressed genes selected for qPCR validation in H929 and JN3 cells.** The  $\log_2(n+1)$  expression values for each DE gene selected for qPCR validation is plotted for each sample used in RNA-seq analysis, where n represents normalised gene expression and 1 represents a pseudo-number applied to account for genes that have an expression value of zero. Selection criteria for these genes was based on significance ( $q < 0.05$ ) and fold change ( $\log_2 FC > 1$ ) of CD138<sup>dim</sup> cells in both H929 and JN3 cells. Error bars are representative of standard deviation and all three biological replicates were used to compile this data ( $n=3$ ). Significant changes in expression were assessed and graphs were constructed using GraphPad Prism 7.0. A one-way ANOVA followed by a Dunnett multiple comparison test was performed to compare expression against a CD138<sup>bright</sup> monoculture control in each cell line (ns – not significant, \*\*\* =  $p < 0.001$ , \*\*\*\* =  $p < 0.0001$ ).

### 4.5.3. Validation of candidate genes using qPCR

A real-time polymerase chain reaction (qPCR) was selected to validate the expression of the candidate genes outlined in Table 4.1. The RNA samples used in this experiment were the exact samples that were also used for the RNA-seq experiment, thus providing a more robust and comparable experimental strategy to validate gene expression data through the quantification of expression of these candidate genes. RNA from each sample was converted to cDNA through the process of reverse transcription, which was subsequently used in a qPCR experiment.

Primer pairs were designed to target each candidate gene as well as a GAPDH endogenous control using NCBI Primer-Blast software. The melt curves for each of these primer pairs are displayed in Supplementary Figure III. This data shows a single peak curve produced from each primer used in this experiment, ensuring that primer dimers were not formed during this validation procedure. This confirms the quality of this experiment in producing data that is truly representative and reflective of gene expression through the amplification of cDNA.

Data produced from the qPCR experiment was analysed using the  $2^{-\Delta\Delta C_t}$  method, with CD138<sup>bright</sup> mono-culture samples from each myeloma cell line being used as a control comparator to assess gene expression from CD138<sup>bright</sup> and CD138<sup>dim</sup> cells co-cultured with differentiated U937 cells. Thus, both HMCB and JMBCB samples produced a mean expression value of zero for each gene analysed in this qPCR experiment. This data also shows the significant upregulation of expression of every gene in both HUCD and JUCD samples ( $p < 0.0001$ ) (Figure 4.13). It is also important to note that whilst the raw gene expression data for MMP2 produced for H929 samples demonstrated a large upregulation of expression in HUCD samples, because there was no quantifiable expression of MMP2 in the HMCB samples, the relative expression of MMP2 in the HUCD sample was therefore calculated as zero when using the  $2^{-\Delta\Delta C_t}$  method.

Finally, it is also demonstrable that gene expression calculated in the RNA-seq dataset correlates with fold change, calculated through qPCR. This is shown in Figure 4.14, where  $\text{Log}_2(\text{Expression})$  is plotted against  $\text{Log}_2(2^{-\Delta\Delta C_t})$ . This clearly shows that there is a defined relationship between these two parameters, primarily indicating that using

qPCR to measure the expression of a selection of candidate genes was a successful method to validate this RNA-seq experiment.

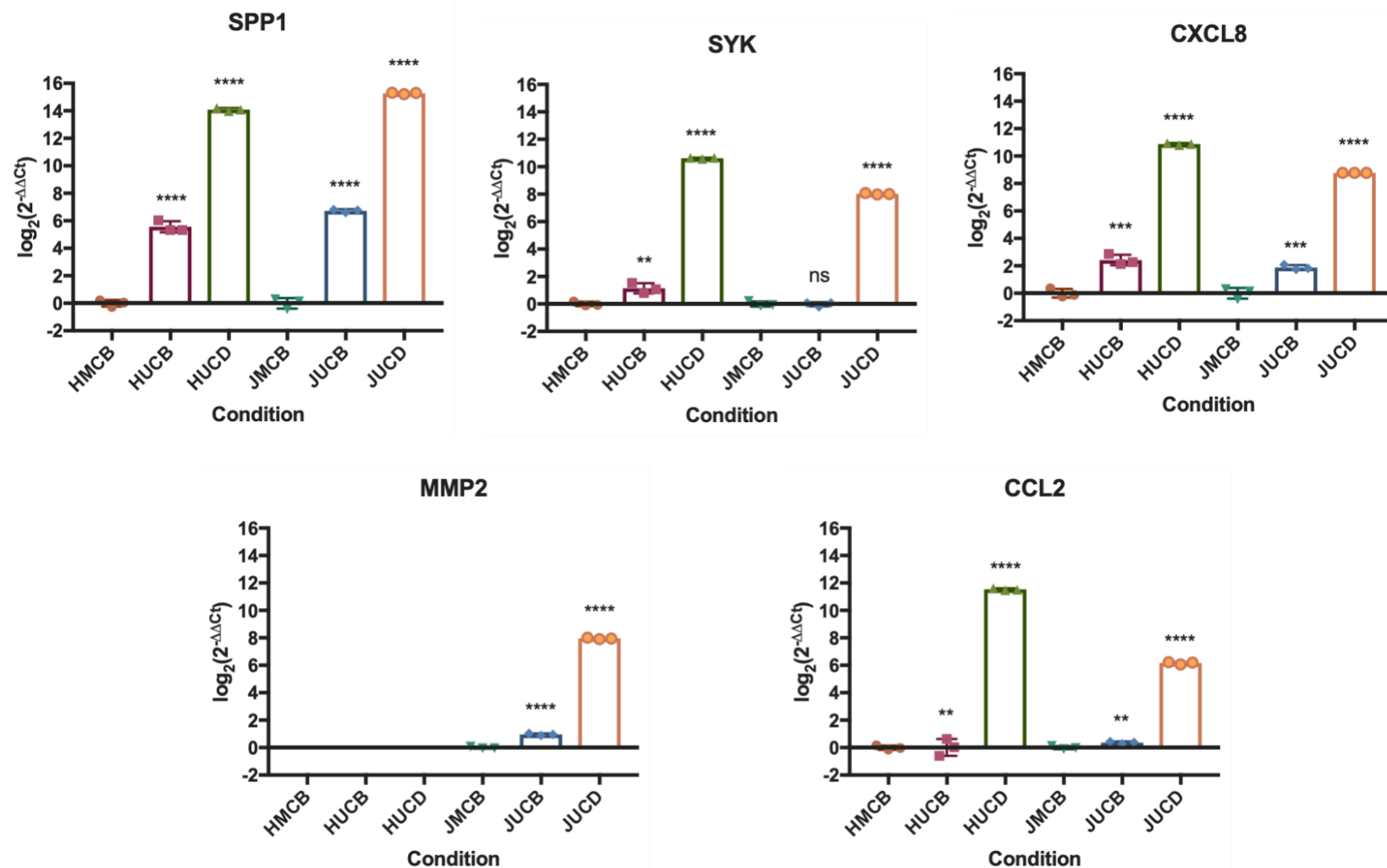


**Figure 4.13. Validation of differentially expressed genes in H929 and JN3 cells using qPCR.** Fold changes of gene expression were calculated and compared to respective CD138<sup>bright</sup> monoculture controls using the  $2^{-\Delta\Delta Ct}$  method, these values were  $\log_2$  transformed. Error bars are representative of standard deviation and triplicate measurements were used to compile this data (n=3). Significant changes in expression were assessed and graphs were constructed using GraphPad Prism 7.0. A one-way ANOVA followed by a Dunnett multiple comparison test was performed to compare expression against a CD138<sup>bright</sup> monoculture control (ns – not significant, \*\* = p<0.01, \*\*\* = p<0.001, \*\*\*\* = p<0.0001).

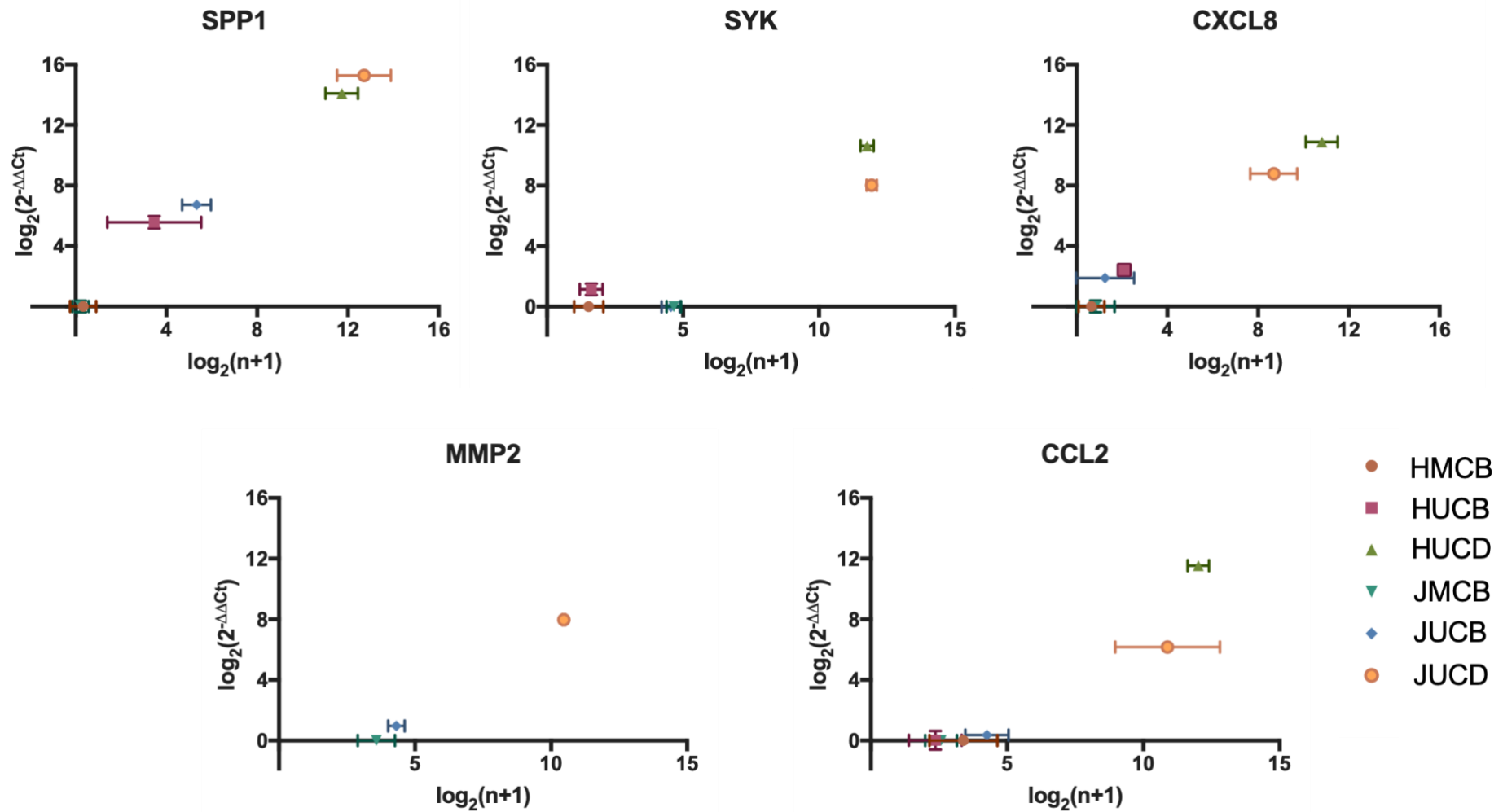


**Figure 4.14. Correlation between gene expression and fold change in each condition assessed using qPCR or each gene selected for validation.** In order to assess correlation between gene expression and fold change in each cell line and subpopulation of CD138<sup>bright</sup> and CD138<sup>dim</sup> cells,  $\log_2(\text{Expression})$  was plotted against  $\log_2(2^{-\Delta\Delta Ct})$  for each gene selected for validation. Error bars are representative of standard deviation and triplicate measurements were used to compile this data ( $n=3$ ). GraphPad Prism 7.0 software was used to compile graphs.

## 4.6. Discussion

The presence of a low frequency subset of CD138<sup>dim</sup> cells in both H929 and JN3 myeloma cells was confirmed in this project. This was coupled with the novel discovery that co-culture with osteoclast-like differentiated U937 cells led to the preferential expansion of this subpopulation of myeloma cells. This study aimed to elucidate changes in transcriptomic behaviour in both CD138<sup>bright</sup> and CD138<sup>dim</sup> myeloma cells in response to this novel co-culture method and to determine DE gene signatures that occurred as a result. This could reveal the impact of osteoclast-like U937 cells on each of these subpopulations of myeloma cells and allude to specific roles they may have in the pathogenesis and progression of the disease.

### 4.6.1. Assessment of differentially expressed genes through RNA-seq

Following the isolation and extraction of RNA from each subset of myeloma cells in both cell lines, RNA-seq analysis revealed a clear distinction in the transcriptional profile between CD138<sup>bright</sup> and CD138<sup>dim</sup> cells. Initial analysis through unsupervised hierarchical clustering and principle component analysis revealed that CD138<sup>dim</sup> cells were transcriptionally distinct from CD138<sup>bright</sup> cells in both H929 and JN3 cell lines. Interestingly, despite being placed under exactly the same culture conditions with differentiated U937 cells, CD138<sup>bright</sup> cells isolated from each myeloma cell line clustered with the respective mono-culture control. This indicated that differentiated U937 cells had a preferential effect on the global transcriptional activity of CD138<sup>dim</sup> cells.

Whilst some of the treatments that are currently used in myeloma patients are capable of eliminating the vast majority of malignant plasma cells from the bone marrow, patients inevitably experience relapse. This points to a drug-resistant subtype of malignant plasma cell that can further propagate disease and contribute to relapse. Therefore, identifying these cells and using them as potential targets for treatment would be highly beneficial to develop a treatment strategy that can more effectively eradicate the disease. There is some evidence that alludes to CD138<sup>dim</sup> cells being representative of this subpopulation, with a reduction of CD138 expression correlating with poorer sensitivity to therapeutic intervention<sup>42,43</sup>. The identification and

expansion of CD138<sup>dim</sup> myeloma cells as a result of co-culture with osteoclast-like cells in this project could be representative of a drug resistant subclone that is responsible for post-treatment relapse, as has been previously discussed in this thesis. Therefore, understanding the transcriptional differences that characterise these CD138<sup>dim</sup> cells in response to co-culture conditions could reveal novel molecular targets and provide important information about their role in disease, thus potentially providing new therapeutic strategies to more completely eradicate malignant plasma cells from patients.

The next step in the analysis workflow was to establish lists of DE genes in both CD138<sup>bright</sup> and CD138<sup>dim</sup> myeloma cells after culture with differentiated U937 cells, compared with respective CD138<sup>bright</sup> monoculture controls. Despite clustering with their respective mono-culture controls, CD138<sup>bright</sup> cells from both H929 and JN3 cell lines still produced a large number of DE genes after co-culture with differentiated U937 cells that were both significant ( $q < 0.05$ ) and had fold change  $> 1$  or  $< -1$ , when compared with respective CD138<sup>bright</sup> monoculture controls. These conditions resulted in the identification of 484 and 124 DE genes in H929 and JN3 cells respectively. The most striking data was produced from CD138<sup>dim</sup> cells in both myeloma cell lines, where 7096 and 6636 DE genes were identified following comparison with respective CD138<sup>bright</sup> mono-culture controls (Figures 4.6, 4.7 and 4.8). Clearly, this vast difference in the number of DE genes identified between these two subtypes after co-culture with differentiated U937 cells is another layer of evidence to suggest that these osteoclast-like cells have a preferential influence on the transcriptional behaviour on CD138<sup>dim</sup> myeloma cells.

#### 4.6.2. Evaluation of overrepresented pathways

The next stage of analysis was to ascertain overrepresented pathways and functions from these DE gene lists. This would reveal information relating to the biological behaviour of these two subpopulations and could perhaps point to their roles in disease pathology and progression, as well as also highlighting the influence of osteoclast-like cells on these functions. The relative number of over-represented pathways that were determined from CD138<sup>dim</sup> H929 and JN3 cells when compared with their respective CD138<sup>bright</sup> monoculture controls was yet another indicator that

co-culture with differentiated U937 cells drastically and preferentially affects the transcriptional behaviour of CD138<sup>dim</sup> cells compared with CD138<sup>bright</sup> cells. The sheer number of overrepresented pathways in each CD138<sup>dim</sup> sample highlights the influential effect that osteoclasts have on these cells, that preferentially induce transcriptomic changes that could contribute to myeloma pathology.

#### 4.6.2.1. CD138<sup>bright</sup> overrepresented pathways

Despite the small number of overrepresented pathways determined from CD138<sup>bright</sup> myeloma cells after co-culture with differentiated U937 cells, there were still some pathways of interest to interpret. The majority of these pathways were significantly activated, as shown by their positive z-score of >2 (Figure 4.11A). Overrepresented pathways in CD138<sup>bright</sup> cells were also unique to each myeloma cell line. However, interestingly all overrepresented pathways from JN3 CD138<sup>bright</sup> cells were also shared by CD138<sup>dim</sup> cells, with 4 of these pathways being shared in CD138<sup>dim</sup> cells from both cell lines and 1 pathway being shared with just CD138<sup>dim</sup> JN3 cells. Each activated pathway in this particular dataset has collectively been shown to influence myeloma survival, proliferation, angiogenesis, metastasis and induction of osteoclast activity<sup>159,331,334,335</sup>. This indicates that an osteoclast-like *in vitro* microenvironment can induce transcriptional changes in CD138<sup>bright</sup> myeloma cells associated with aberrant cellular responses and disease pathology.

Curiously, it appeared that H929 cell co-culture with differentiated U937 cells also led to an inhibition of cell cycle regulation ( $z < -2$ ). It is of course well established that myeloma cells possess aberrant mutations to key genes that regulate cell cycle progression. This leads to increased activation of those signals that drive myeloma cells through the cell cycle, allowing them to become more proliferative<sup>82</sup>. For example, it has been previously found that H929 cells harbour the t(4,14) translocation which leads to overactivation of fibroblast growth factor receptor 3 (FGFR3) and MMSET and is associated with poorer prognosis in patients<sup>336,337</sup>. It is therefore curious that co-culture with differentiated U937 cells leads to an inhibition of proliferative signalling. To functionally assess the effect of osteoclast-like co-culture on the proliferative capacity of these cells, propidium iodide staining coupled with flow cytometric analysis could be adopted in order to determine the cell cycle stage that these cells are at

under these co-culture conditions. Relative cell number could also be assessed in conjunction with this data to determine proliferative capacity.

#### 4.6.2.2. *CD138<sup>dim</sup> overrepresented pathways*

In order to provide a disease context to the data analysis, the 104 commonly shared overrepresented pathways (see Supplementary Table I) were reduced to 31 that were more specifically associated with myeloma. Of these 31 pathways, 30 were found to be activated and it was apparent that there were a range of physiological processes and functions that are implicated in the dataset. These will be discussed in more detail in the remainder of this chapter.

The first of which that will be discussed is the activation of cytokine signalling. In this list, there are a number of cytokine and chemokine-related pathways that are activated, including GM-CSF, TGF- $\beta$ , IL-1, IL-3, IL-6 and IL-8 signalling as well as general activation of chemokine signalling (Table 4.2a). The function of these markers in relation to osteoclast differentiation and activity is also described in Table 4.2b. It is well established that the cytokine profile in the bone marrow microenvironment of myeloma patients is drastically altered with each of the aforementioned signalling pathways being heavily implicated in a number of critical processes that facilitate myeloma cell survival, proliferation, growth, manipulation of angiogenesis and metastasis and ability to influence osteoclast activity<sup>338-341</sup>. The IL-6 and IL-8 signalling pathways in particular are established as master regulators of these processes and have the ability to initiate a number of signalling pathways that directly contribute to the pathological behaviour of these malignant plasma cells<sup>331,342</sup>. Whilst not all pathways relating to cytokines and chemokines are overrepresented here, there are clearly a substantial number of critical cytokine-related pathways that are represented in this dataset. This shows that osteoclast-like U937 cells are able to induce these signals exclusively in CD138<sup>dim</sup> myeloma cells. It is known that the alteration of the cytokine microenvironment is beneficial to both the survival of myeloma cells and in reciprocation, the continued osteoclastogenesis, and subsequent activity, that is a characteristic feature of myeloma. Given that IL-6 and IL-8 are such influential cytokines it could be proposed that the upregulation of these pathways in CD138<sup>dim</sup> cells could result in a knock-on effect on the upregulation of the other associated

pathways described here. It would also be interesting to investigate whether CD138<sup>dim</sup> cells could even be described as ‘feeder’ cells for CD138<sup>bright</sup> cells by providing an additional supply of IL-6 and IL-8.

In addendum to the data presented here it would of course be of interest to investigate the effects that myeloma cells also have on these osteoclast-like U937 cells in relation to cytokine secretion. This would provide further information into the molecular mechanisms behind increased osteoclast genesis and activity and potentially identify targets that could inhibit this from occurring in patients. For example, an interesting experiment might involve culturing U937 cells using the same method described in this assay but in the presence of conditioned media from myeloma cells lines, to investigate whether their osteoclastogenic and osteolytic capabilities are enhanced as a result.

<i>Pathway</i>	<i>z-score</i>	
	HMCB vs HUCD	JMCB vs JUCD
<i>Chemokine Signalling</i>	2.98	4.15
<i>GM-CSF Signalling</i>	2.12	2.99
<i>IL-1 Signalling</i>	3.32	3.36
<i>IL-3 Signalling</i>	3.00	2.89
<i>IL-6 Signalling</i>	3.68	4.12
<i>IL-8 Signalling</i>	3.84	5.86
<i>TGF-<math>\beta</math> Signalling</i>	2.24	2.24

**Table 4.2a. Overrepresented pathways produced from CD138<sup>dim</sup> H929 and JN3 myeloma cells that are directly related to cytokine and chemokine signalling.**

Another group of pathways that were found to be overrepresented in this dataset are directly related to growth and proliferation. Here, it can be observed that in addition to the cytokines and chemokines that influence myeloma cell growth and proliferation, there are also pathways that include IGF-1<sup>343,344</sup>, EGF<sup>345</sup>, HGF<sup>346</sup> and VEGF<sup>347</sup> signalling, as well as collective activation of growth hormone signalling, which are more directly influential in these processes (Table 4.3). This is another indicator that co-culture with differentiated U937 cells uniquely upregulated the expression of genes and corresponding pathways that contribute to the growth and proliferation of CD138<sup>dim</sup> myeloma cells.

<b>Pathway</b>	<b>Function</b>
<i>GM-CSF Signalling</i>	Granulocyte-macrophage colony stimulating factor is a cytokine that has been found to be responsible for osteoclast differentiation through promoting fusion of pre-osteoclasts <sup>348</sup> . It has been found to specifically drive monocytic differentiation away from a macrophage phenotype towards an osteoclast phenotype in conjunction with M-CSF and RANKL <sup>349</sup> .
<i>IL-1 Signalling</i>	The IL-1 family of cytokines contains 11 isotypes, of which IL-1 $\beta$ , a pro-inflammatory cytokine, has been arguably most closely associated with multiple myeloma pathology. IL-1 $\beta$ is known to have potent osteoclast activating factor influence and also induces IL-6 secretion that functions through both autocrine and paracrine signalling <sup>350</sup> . It has also been identified as a cytokine involved in the progression from MGUS to symptomatic myeloma and as a result has been previously investigated for targeted therapy <sup>351</sup> . Whilst unable to directly induce osteoclast differentiation, it has been shown to possess synergistic activity with RANKL to aid in osteoclast differentiation and activation <sup>352,353</sup> .
<i>IL-3 Signalling</i>	IL-3 has been found to exhibit a dual function in relation to bone resorption and has inhibitory effects on osteoblast function, whilst also promoting osteoclast fusion and activation. In a similar fashion to IL- $\beta$ it has also been shown to function in a synergistic fashion with RANKL and MIP-1 $\alpha$ to promote osteoclast activation in myeloma <sup>203</sup> . As well as increased secretion from cells within the bone marrow that can be induced by myeloma cells, IL-3 has also been shown to be directly secreted from myeloma cells themselves <sup>341</sup> .
<i>IL-6 Signalling</i>	IL-6 signalling has long been associated with the prolonged survival of myeloma cells and can act in both autocrine and paracrine fashion to continually sustain malignant plasma cell activity. It has also been heavily associated with promoting osteolytic activity both directly and also in conjunction with influencing osteoblast behaviour <sup>354,355</sup> . This has been shown to occur through increasing RANKL secretion and contributing to OPG inhibition to promote a net increase in osteoclast differentiation and activity.
<i>IL-8 Signalling</i>	IL-8 has been previously shown to be secreted by myeloma cells, this secretion also increases in response to stromal cell interaction and treatment with anti-myeloma therapies <sup>356</sup> . IL-8 has interestingly been shown to directly contribute to the growth of osteoclast precursors whilst also directly stimulating osteoclastogenesis through mechanisms that are independent of RANKL signalling <sup>356,357</sup> .
<i>TGF-<math>\beta</math> Signalling</i>	Transforming growth factor $\beta$ signalling has been previously found to inhibit the maturation of terminally differentiated osteoblasts. This of course contributes to the osteolytic nature of myeloma through inhibiting osteoblast-mediated matrix secretion <sup>358</sup> . These late-stage osteoblasts have also been found to contribute to pro-apoptotic signals that affect myeloma cell survival, therefore enhancement of TGF- $\beta$ signalling in myeloma can also contribute to prolonging the survival of these malignant plasma cells <sup>359</sup> .

**Table 4.2b. Functional descriptions of overrepresented pathways produced from CD138<sup>dim</sup> H929 and JN3 myeloma cells that are directly related to cytokine and chemokine signalling.**

<b>Pathway</b>	<b>z-score</b>	
	HMCB vs HUCD	JMCB vs JUCD
<i>EGF Signalling</i>	2.83	2.50
<i>Growth Hormone Signalling</i>	2.84	2.20
<i>HGF Signalling</i>	3.14	3.29
<i>IGF-1 Signalling</i>	2.13	2.68
<i>VEGF Family Interactions</i>	2.40	2.18

**Table 4.3. Overrepresented pathways produced from CD138<sup>dim</sup> H929 and JN3 myeloma cells that are directly related to growth and proliferation signalling.**

Another clear overrepresentation is the activation of pathways relating to adhesion, angiogenesis, motility and metastasis. Activated pathways that are related to these processes appear to lead to increased Rho and Rac signalling as well as mobilisation of actin, which are directly related to cell motility<sup>360</sup>. These pathways are known to be upregulated in myeloma, with Rho signalling contributing to cell motility and Rac signalling being shown to contribute to myeloma cell adhesion to the extracellular matrix of the bone marrow microenvironment<sup>361</sup>. It is also well-established that increased actin activity is the driving force for cell motility and migration<sup>362</sup>. Another well-established signalling pathway related to adhesion is initiated by chemokine receptor CXCR4 and its chemoattractant ligand CXCL12/SDF-1, this signalling pathway has also been heavily linked with the promotion of myeloma cell homing and migration<sup>166</sup>. Coupled with the increased activation of IL-8 signalling which is known to promote angiogenesis, this list of pathways could allude to two interesting phenomena, i) differentiated U937 osteoclast-like cells have the capability of exclusively inducing the upregulation of genes responsible for cell motility and migration in CD138<sup>dim</sup> myeloma cells and ii) these CD138<sup>dim</sup> myeloma cells could be the cells responsible for infiltrating new areas of bone marrow through the manipulation of these angiogenic and migratory signals. The latter of which has been hinted at in previous research where CD138<sup>dim</sup> cells have been found to possess greater migratory potential<sup>363</sup>.

<b>Pathway</b>	<b>z-score</b>	
	HMCB vs HUCD	JMCB vs JUCD
<i>Actin Cytoskeleton Signalling</i>	3.06	3.09
<i>CXCR4 Signalling</i>	3.36	3.67
<i>IL-8 Signalling</i>	3.84	5.86
<i>Integrin Signalling</i>	2.67	4.82
<i>Leukocyte Extravasation Signalling</i>	3.00	5.25
<i>Rac Signalling</i>	2.74	4.16
<i>Regulation of Actin Motility by Rho Signalling by Rho Family GTPases</i>	2.18	3.15
	2.94	4.81

**Table 4.4. Overrepresented pathways produced from CD138<sup>dim</sup> H929 and JN3 myeloma cells that are directly related to adhesion, angiogenesis, motility and metastasis signalling.**

Overall these data illustrate that differentiated osteoclast-like U937 cells influence a number of biological characteristics specifically in CD138<sup>dim</sup> myeloma cells in each cell line. These transcriptional changes have the potential to affect these cells' ability to grow, proliferate, adhere, mobilise and potentially metastasise to new areas of bone marrow. Given the reliance of primary myeloma cells on the human bone marrow microenvironment and the interest of the role of CD138<sup>dim</sup> cells within the pathology and progression of the disease, these data could indicate that these CD138<sup>dim</sup> cells may represent a subpopulation of myeloma cells that possess greater migratory and metastatic potential. This could result in further spread of malignant cells throughout the bone marrow or facilitate the aggressive late-stage transition to the infiltration of the peripheral circulation as observed in patients with plasma cell leukaemia.

It is well-known that myeloma cells have a clear affinity for osteoclasts, which directly leads to the most debilitating symptoms observed in patients. This is a result of direct cellular contact between myeloma cells and osteoclasts, soluble factor signalling and the preferential proximity to osteoclasts within the bone marrow that myeloma cells reside in<sup>204</sup>. The data presented in this thesis could allude to the osteoclast-influenced mechanisms behind myeloma cell disease propagation through the assessment of transcriptomic changes that occur particularly in CD138<sup>dim</sup> cells as a direct result of interactions with osteoclast-like cells.

### 4.6.3. Validation of gene expression through qPCR

This RNA-sequencing experiment has shown that co-culture with differentiated U937 cells induces substantial changes in gene expression in both CD138<sup>bright</sup> and CD138<sup>dim</sup> myeloma cells, with CD138<sup>dim</sup> myeloma cells demonstrating a much higher number of DE genes and overrepresented pathways as a result of these co-culture conditions. It was therefore desirable to further validate these gene expression changes through qPCR. This quantitative gene expression technique has been recommended as the gold standard for validation of gene expression data produced from microarray experiments<sup>364,365</sup>. More recently qPCR has also been used as the recommended technique for validating gene expression data produced from RNA-seq experiments which was the rationale for selecting qPCR as the appropriate technique to validate the gene expression data presented in this thesis<sup>366</sup>.

Five DE genes were selected for validation that fulfilled a number of selection criteria that were true for both H929 and JIN3 cells, as follows: high level of normalised gene expression in CD138<sup>dim</sup> cells, high level of fold change in CD138<sup>dim</sup> cells compared with monoculture control ( $\log_2$  FC>1), relevance to overrepresented pathways and association with myeloma pathology. It was also taken into consideration that as a collective gene list there shouldn't be an association with any single function related with myeloma pathology, but instead genes selected should span a range of different functions (Table 4.1).

Overall the validation of the observations demonstrated from the RNA-seq dataset was successful using qPCR. For each gene selected for validation there was a reliable level of gene expression in all samples when compared with the RNA-seq dataset. There was also a significant increase of fold change in each CD138<sup>dim</sup> sample when compared with respective mono-culture controls, which again replicates the observations shown in the RNA-seq dataset. Overall this demonstrates that validation using qPCR was a successful method in confirming that the increases in gene expression of these selected genes was in fact due to the direct influence of differentiated U937 cells on the transcriptional behaviour of CD138<sup>dim</sup> myeloma cells.

#### 4.6.4. Limitations to the study

Whilst the data presented in this chapter are accurately described, there are experimental limitations that must be discussed. In order to isolate cell samples for RNA preparation and RNA-seq, cell samples were required to be sorted based on CD138 expression after culture with differentiated U937 cells. Every effort was made to ensure that there was no contamination between either myeloma subpopulation or from differentiated U937 cells used in each co-culture experiment. Gates used in the flow cytometry plots were drawn a suitable distance apart in order to eradicate potential contamination from adjacent myeloma subpopulations. Despite these efforts and the calculated sorting purity being greater than 95% in every sample, there was still minor potential for cellular contamination. This is due to inherent sorting inefficiencies that can occur when separating subpopulations of cells through flow cytometry.

In order to investigate this further, a more sensitive technique was adopted to confirm whether co-culture samples were contaminated with cell types of another phenotype or lineage. Replicates from each sorted sample was sent to the short tandem repeat (STR) genotyping facility at Public Health England. This technique is normally used to determine the true identity of cultured cell lines, however in this instance the experimental setup was adapted to assess whether there was any cellular contamination in the samples used for RNA-seq.

The results of this confirmed that CD138<sup>bright</sup> and CD138<sup>dim</sup> JN3 samples and H929 CD138<sup>bright</sup> samples were pure, thus indicating that no cellular contamination had taken place from co-culture with differentiated U937 cells. However, there was an indication that H929 CD138<sup>dim</sup> samples contained some cellular contamination from U937 cells after co-culture. The assay used to genotype samples is very sensitive and is able to detect DNA at picogram levels, however the data produced does not explicitly quantify the level of contamination, meaning that there is no way to use this data to assess the proportion of contamination. Given that there was no indication from the flow cytometry data that the samples were contaminated, it is reasonable to suggest that the level of contamination was very small.

Unfortunately, as no RNA samples from U937 cells were produced to be used for RNA-seq analysis, no direct comparison could be made between U937 cells and co-cultured myeloma cells regarding similarities between differentially expressed genes. Whilst of course a direct comparison in this regard could not be made to infer the level of potential U937 cell contamination, an NCBI GEO dataset search was performed and an RNA-seq dataset was found from U937 cells that had been treated with PMA in a similar fashion as had been described in the experimental set-up demonstrated in this thesis<sup>367</sup>. This was deemed as a suitable comparator to compare differentially expressed genes between the U937 dataset and the H929 and JN3 datasets produced in this study. The top 500 most highly expressed genes were then compared between the U937 dataset as well as the CD138<sup>dim</sup> datasets from H929 and JN3 cells. These lists were plotted in a heatmap to compare expression profiles and are shown in Supplementary Figure IV. Here, it is clear that there is very little similarity in the top 500 highest expressed genes between the U937 dataset and the two myeloma cell datasets. Most of the similarity observed is between CD138<sup>dim</sup> cells from H929 and JN3 cells. Of course, whilst this is not the ideal comparison to make in this scenario by using dataset from two different experiments, it is encouraging that there is little similarity between the datasets presented in the chapter and the RNA-seq data from U937 cells treated with PMA. Thus, indicating that any contamination that could have occurred was minimal and undetectable through flow cytometry during cell sorting and would have very little impact on the subsequent data analysis and results shown in this chapter.

#### 4.6.5. Final conclusions

Overall these data demonstrated that differentiated osteoclast-like U937 cells preferentially influenced the transcriptional behaviour in CD138<sup>dim</sup> cells of both H929 and JN3 myeloma cells. This, in turn, resulted in a huge increase in the number of DE genes in CD138<sup>dim</sup> cells when compared with CD138<sup>bright</sup> cells. These DE genes are representative of numerous functions that have the potential to influence adhesion, migration, responses to cytokines, angiogenesis, growth and proliferation of CD138<sup>dim</sup> myeloma cells. Having presented these novel data, the next phase of experimentation and analysis is to determine the functional capacity of these transcriptional changes on the behaviour of CD138<sup>dim</sup> cells in this co-culture model. This could lead to further

elucidation of the role of these cells in myeloma and lead to the identification of novel therapeutic targets that could prevent these cells from propagating their malignant effects in patients.

## CHAPTER 5: RESULTS

### Assessment of CD138<sup>bright</sup> and CD138<sup>dim</sup> myeloma cell functionality in response to co-culture with osteoclast-like cells.

#### 5.1. Introduction

Multiple myeloma is an extraordinarily complex haematological malignancy in regard to the mechanisms of disease pathogenesis, progression and its ability to manipulate the cells of the bone marrow microenvironment. The reliance that malignant plasma cells have on the bone marrow microenvironment for their survival, proliferation and capacity to manipulate angiogenic processes that ultimately facilitate metastasis and dissemination throughout the bone marrow, is well established in the literature. Although the specific mechanisms responsible for these processes are still widely questioned. There are also many unanswered questions relating to the exact subset of myeloma cells that are responsible for these processes and the mechanisms through which they carry out these aberrant functions. Myeloma has been found to demonstrate intra-clonal heterogeneity, meaning that in addition to the heterogeneity observed between different patients, there is also substantial potential for genetic and phenotypic heterogeneity within an individual patients' malignancy<sup>368</sup>. This of course further complicates the ability to tailor treatments that would be most effective for patients on an individual basis.

One particular subset of myeloma cells that have been of recent interest are CD138<sup>dim</sup> myeloma cells. As has already been discussed throughout this thesis, these CD138<sup>dim</sup> cells have been previously shown to be responsible for increased resistance to chemotherapeutic intervention, they have the capacity to engraft in myeloma NOD/SCID murine models and also have high clonogenic capacity. In addition to these factors, this research has so far established that these CD138<sup>dim</sup> cells exhibit substantial changes in gene expression in comparison to CD138<sup>bright</sup> cells following co-culture with differentiated U937 osteoclast-like cells. Pathway analysis revealed a number of different cellular and biological processes that could be influenced by these

differentially expressed genes including adhesion, survival, migration and ability to manipulate angiogenesis. Therefore, it was of interest to evaluate this further by assessing the differential expression of specific genes related to these functions and to perform functional assays to determine whether expression of these genes resulted in an alteration in the biological behaviour of these cells. This could provide another step to ultimately establish the potential role of CD138<sup>dim</sup> myeloma cells in the propagation and progression of myeloma.

### **5.1.1. Aims**

In order to assess the role of specific DE genes, they will be discussed in accordance with their function. The aims of this chapter are to therefore, within each of these functions:

1. Determine expression of genes of interest from RNA-seq data
2. Validate gene expression through qPCR and flow cytometry
3. Assess, where possible, the functional influence of these upregulated genes by assessing cell survival, adhesion and migratory capacity.

## 5.2. Evaluation of transcriptional activity of myeloma markers

There are a wide variety of phenotypic markers that are frequently used to determine the identity of malignant plasma cells<sup>369</sup>. Strategies to identify these cells must fulfil specificity criteria that firstly separate these malignant cells from healthy plasma cells and also distinguish them from other cell types<sup>370</sup>. This has made immunophenotyping a useful tool to aid diagnosis and subsequently monitor disease progression and patient response to treatment. Immunophenotyping has revealed information about the stage of a particular cells' development through the process of differentiation, in this case the terminal differentiation of B-lymphocytes into plasma cells<sup>371</sup>.

Given the speculation surrounding the identity and function of CD138<sup>dim</sup> cells in myeloma it was of interest to investigate whether there was a transcriptional alteration in the plasma cell-specific phenotypic markers they express in comparison with CD138<sup>bright</sup> cells. This could reveal more information about whether CD138<sup>dim</sup> cells represent a subset of myeloma cells that are less developmentally mature than their CD138<sup>bright</sup> counterparts.

### 5.2.1. Loss of CD138 is a transcriptionally regulated event

CD138 is widely used as a phenotypic marker to identify myeloma cells, due to its relative exclusivity of expression on the plasma cell surface membrane<sup>34</sup>. Given the unique establishment of an expansion of CD138<sup>dim</sup> myeloma cells in response to co-culture with differentiated U937 cells in this project, it was of interest to investigate the transcriptional regulation of this specific antigen under these experimental conditions, using expression data produced by RNA-seq.

It has been previously established that CD138 can be shed from the surface of both normal and malignant plasma cells in response to apoptosis<sup>275</sup>. Data demonstrating the presence of Annexin V-negative CD138<sup>dim</sup> myeloma cells was presented in Figure 3.12, which phenotypically confirmed that CD138<sup>dim</sup> cells were not representative of an apoptotic population of myeloma cells. However, it was also of further interest to determine whether the lack of CD138 expression was a transcriptionally regulated

event and was not shed through any other post-translational mechanism. This was determined using the normalised gene expression values from DESEQ2 analysis of the RNA-seq data presented in Chapter 4. A  $\log_2(n+1)$  formula was applied to these values which are plotted in Figure 5.1. This clearly showed a significant reduction in the expression of the SDC1 gene, which encodes CD138, in both H929 and JLN3 myeloma cells ( $p < 0.0001$ ) in response to co-culture with differentiated U937 osteoclast-like cells. The MFI values for CD138 expression as determined by flow cytometry were also determined, which emulate this trend.

It is important to note that the exact same samples were used in the compilation of both RNA-seq and flow cytometry data here to ensure appropriate consistency and comparability. A  $\log_2$  transformation was applied to each dataset to facilitate visualisation of correlation of expression between samples. What is clear is that in both H929 and JLN3 cells, there is firstly a significant reduction in SDC1 transcriptional activity and secondly that this is mirrored in the surface expression data determined by flow cytometry ( $p < 0.0001$ ). This confirms that the lack of CD138 expression observed throughout this thesis is regulated at the transcriptional level and is not simply a result of shedding from the surface membrane.

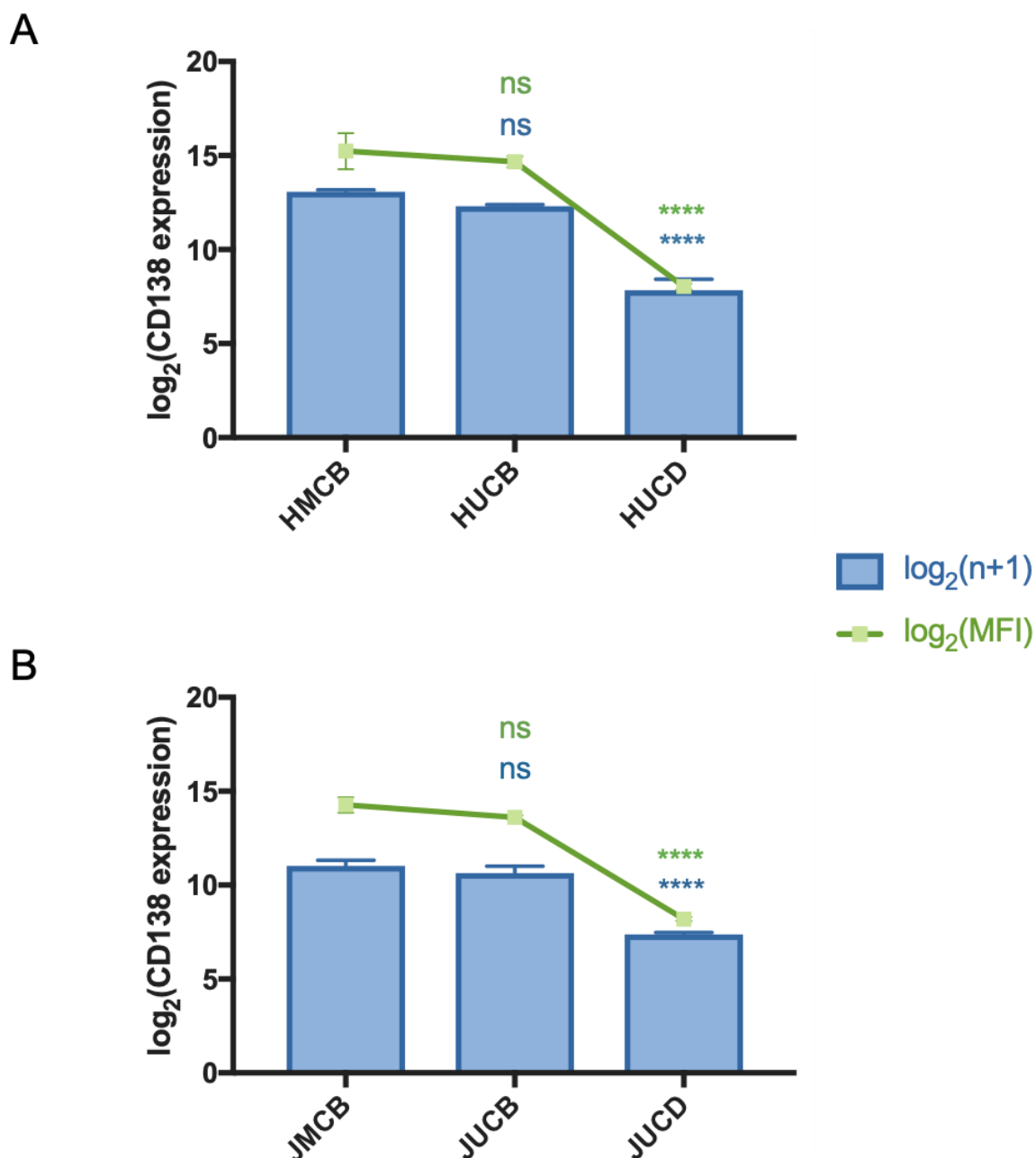


**Figure 5.1. Expression of CD138 in H929 and JJN3 cells determined by RNA-seq and flow cytometry.** Normalised DESEQ2 expression values for SDC1 (CD138) were compiled from each sample used in this RNA-seq experiment. The  $\log_2(n+1)$  formula was used to normalise any negligible values, where  $n$  represents DESEQ2 normalised gene expression and 1 represents a pseudo-number applied to account for genes that have an expression value of zero, these are represented by blue bars. The  $\log_2(\text{MFI})$  values for CD138 expression determined by flow cytometry from each sample used in this RNA-seq experiment were also compiled and are represented by the green line plot for both (A) H929 and (B) JJN3 myeloma cells. Statistical significance was assessed using a 2-way ANOVA followed by a Tukey multiple comparison test. Data was compiled using Prism 7.0 software and error bars were constructed using standard deviation (ns – not significant, \*\*\*\* -  $p < 0.0001$ ).

### 5.2.2. Transcriptional overview of myeloma phenotypic identifiers

Whilst CD138 and CD38 are almost exclusively expressed on the surface of plasma cells, both normal and malignant, it is still widely accepted that no single surface marker can uniquely identify these cells. Therefore, a number of other surface markers have been utilised in the identification of plasma cells in myeloma patients which provides greater specificity of identification and also provides further functional information in regard to cellular properties that relate to adhesion, migratory capacity, stage of differentiation and disease prognosis.

It was therefore of interest to determine the gene expression of a number of these commonly utilised antigens to firstly establish any differences in their expression between CD138<sup>bright</sup> and CD138<sup>dim</sup> cells and then to also relate this expression information to cellular function and potential stage of differentiation. The markers chosen for this section of analysis are shown in Table 5.1 and are provided with a brief description to their function and relation to malignant plasma cells. A list of these markers was created using Genview2 software (Peter Giles, Wales Gene Park, Cardiff) which facilitates the visualisation of gene expression data through heatmaps and hierarchical clustering.

The first comparison made here was between CD138<sup>bright</sup> cells that had been cultured in isolation against CD138<sup>bright</sup> cells that had been co-cultured with differentiated U937 cells, derived from both H929 and JLN3 cells. Here, it is clear that there are very few changes in the expression of these antigens between these two culture conditions in either cell line (Figure 5.2A). This is in contrast to the comparison made between CD138<sup>bright</sup> myeloma cells cultured in isolation and CD138<sup>dim</sup> cells co-cultured with differentiated U937 cells, in both H929 and JLN3 cells. This comparison shows clear changes in the expression of some of these antigens. There are some commonalities in these gene expression changes between both cell lines. For example, there is a subtle, yet clear downregulation of CD38, CD81 and CD307 coupled alongside upregulation of CD19 and CD45 in CD138<sup>dim</sup> cells when compared with CD138<sup>bright</sup> cells in both myeloma cell lines. Thereafter, the remaining gene expression changes observed appear to be exclusive to each cell line during this particular comparison. H929 CD138<sup>dim</sup> cells exclusively downregulated CD28 and CD56 in response to co-culture

with differentiated U937 cells, whereas no changes were then observed in the expression of CD54 and CD117. JJN3 CD138<sup>dim</sup> cells appeared to exclusively display a contrast in this trend, where CD54 was upregulated and CD117 downregulated. There were also no apparent changes in the gene expression of CD28 and CD56 in this comparison.

These observations could indicate that these CD138<sup>dim</sup> cells are at an earlier stage of differentiation in comparison to CD138<sup>bright</sup> cells, which could especially be implied through the upregulation of CD19 in both cell lines. The expression of CD45 has also been linked to earlier stages of plasma cell development, with a decrease in expression occurring through to terminal differentiation<sup>372</sup>. This characteristic could imply that these cells are more representative of a cancer stem cell-like phenotype, which has been previously suggested as a chemo-resistant subpopulation of myeloma cells responsible for disease relapse in patients<sup>373,374</sup>.

	<b>Gene Identity</b>	<b>Function and relation to plasma cell phenotype</b>
<i>CD19</i>	B-lymphocyte antigen CD19	Expressed by B-lymphocytes and is lost as a result of terminal differentiation to plasma cells. Evidence has reported CD19 <sup>+</sup> cells being representative of cancer stem-like cells <sup>373</sup> , with CAR T-cell therapy also being developed against CD19 to be used in treatment <sup>374</sup> .
<i>CD200</i>	OX-2 membrane glycoprotein	Transmembrane receptor that has been highlighted as an independent prognostic marker in myeloma, where increased expression resulted in lower event-free survival rates <sup>375</sup> .
<i>CD28</i>	T-cell antigen CD28	Involved in T-cell activation and is found to be upregulated on malignant plasma cells in comparison with normal plasma cells <sup>376</sup> . It is also associated with more aggressive disease, with increased expression being noted throughout myeloma disease progression from MGUS to symptomatic disease <sup>377</sup> .
<i>CD38</i>	Cyclic ADP ribose hydrolase	Surface receptor that is uniformly expressed on the surface of plasma cells and is used extensively in the identification of myeloma cells alongside CD138 <sup>46</sup> . Novel immunotherapies have been designed to target this antigen in the treatment of myeloma, namely daratumumab <sup>45</sup> .
<i>CD81</i>	Target of the Antiproliferative Antibody 1 (TAPA-1)	Associated with CD19 expression, CD81 possesses important roles in cell growth, motility and plasma cell homing. Whilst little is currently known about its role in myeloma pathology, there have been studies that have implicated CD81 expression in disease prognosis <sup>378</sup> .
<i>FCRL5 (CD307)</i>	Fc receptor-like protein 5	Found to be expressed at increasing levels throughout B-lymphocyte development and differentiation, eventually reaching maximal expression in plasma cells, both normal and malignant <sup>370,379</sup>
<i>ICAM1 (CD54)</i>	Intracellular adhesion molecule 1	Adhesion marker found to be constitutively expressed on the surface of myeloma cells and is also found to be present in increased levels along the B-lymphocyte differentiation process. Expression of CD54 is also found to be strictly regulated by the transcription factor NF- $\kappa$ B <sup>380</sup> .
<i>KIT (CD117)</i>	Mast/stem cell growth factor receptor	Growth factor receptor found to be expressed on a proportion of malignant plasma cells, which surprisingly infers good prognosis in patients and is used as a marker to distinguish between normal and malignant plasma cells <sup>381</sup> .
<i>NCAM1 (CD56)</i>	Neural cell adhesion molecule	Adhesion marker used to distinguish identity of malignant plasma cells from normal plasma cells <sup>370</sup> . Loss of expression could also be linked with late stage disease, with CD56 expression being found to be inversely correlated with the number of myeloma cells in peripheral circulation <sup>48</sup> .
<i>PTPRC (CD45)</i>	Protein tyrosine phosphatase, receptor type, C	Marker related to adhesive function that is variably expressed on plasma cells. Increased expression is more commonly associated with plasma cells at an earlier stage of differentiation, an observation which is also replicated with disease stage <sup>382</sup> .
<i>SDC1 (CD138)</i>	Syndecan-1	Extracellular surface glycoprotein with adhesion-related roles, almost exclusively expressed on plasma cells and is used as the primary marker in the identification of malignant plasma cells. Correlates with loss of CD19 during B-lymphocyte terminal differentiation <sup>34</sup> .

Table 5.1. Summary of the identity and function of surface markers used in immunophenotyping of myeloma cells

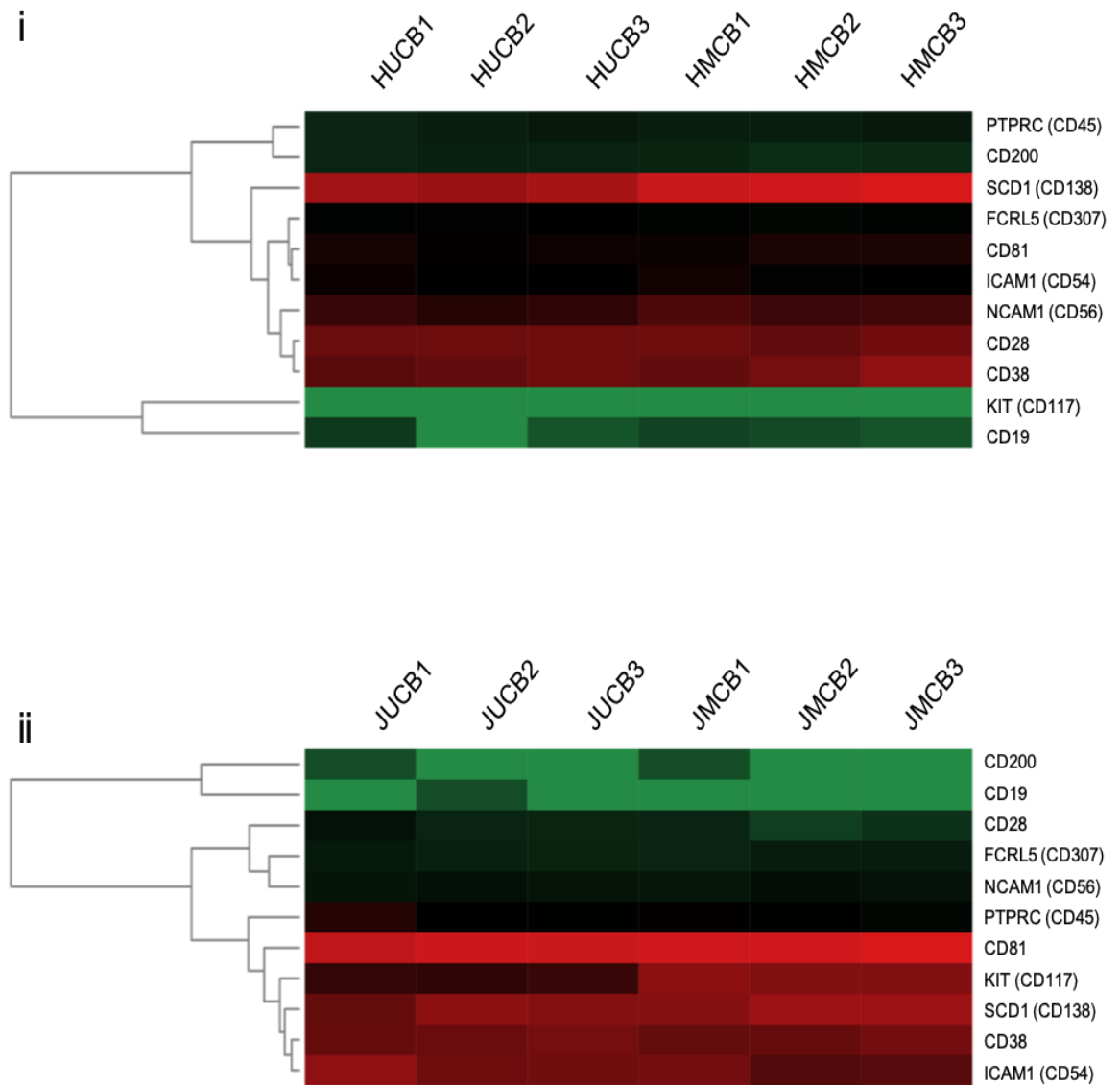


**Figure 5.2A. Heatmap illustrating the expression of genes involved in the phenotypic identification of myeloma cells.** Genview2 software was used to compare the expression of 11 genes that are used in the phenotypic identification of myeloma cells. The expression of these genes is presented in a heatmap following hierarchical clustering. Each biological replicate from CD138<sup>bright</sup> H929 (i) and JJN3 (ii) cells co-cultured with differentiated U937 cells was compared with a corresponding CD138<sup>bright</sup> mono-culture control in each myeloma cells line. Green colouration indicates low gene expression and red colouration indicates high gene expression.

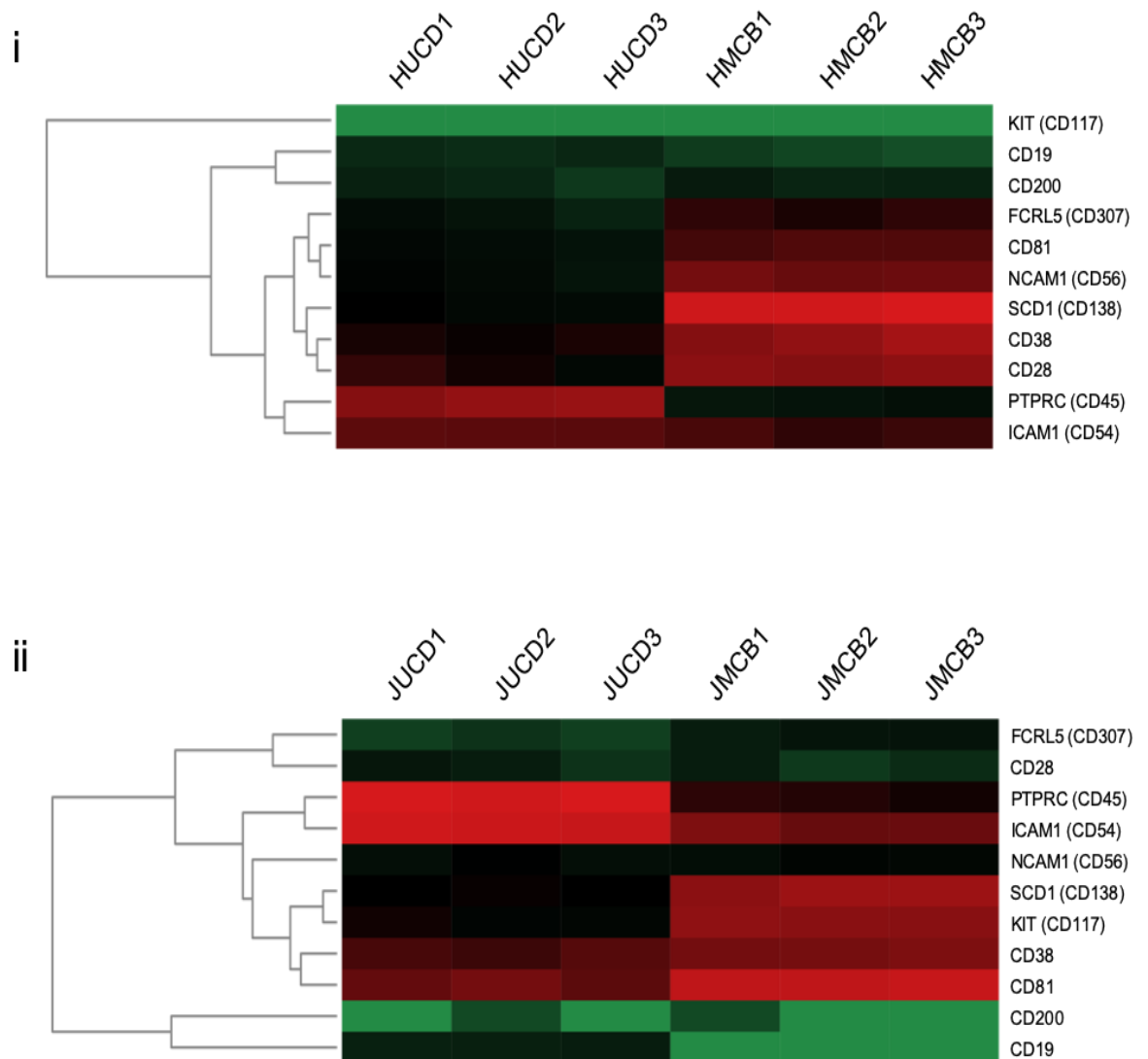


**Figure 5.2B. Heatmap illustrating the expression of genes involved in the phenotypic identification of myeloma cells.** Genview2 software was used to compare the expression of 11 genes that are used in the phenotypic identification of myeloma cells. The expression of these genes is presented in a heatmap following hierarchical clustering. Each biological replicate from CD138<sup>dim</sup> H929 (i) and JN3 (ii) cells co-cultured with differentiated U937 cells was compared with a corresponding CD138<sup>bright</sup> mono-culture control in each myeloma cells line. Green colouration indicates low gene expression and red colouration indicates high gene expression.

### 5.2.3. Assessment of immunoglobulin gene expression

One of the key functions of plasma cells is to secrete monoclonal antibodies. These cells increase their capacity for antibody secretion as they progress through the differentiation process from B-lymphocytes to terminally differentiated plasma cells<sup>23</sup>. Such is the increased capacity and commitment to using the cells' transcriptional and translational mechanisms for antibody production that plasma cell growth is significantly stunted<sup>383</sup>. This of course means that genes associated with immunoglobulin (Ig) are upregulated throughout this process, thus resulting in an enhancement of antibody secretion. It was therefore of interest to determine whether there were any transcriptional changes to the expression of Ig genes in response to co-culture with differentiated U937 cells between CD138<sup>bright</sup> and CD138<sup>dim</sup> cells.

From each sample comparison in the RNA-seq dataset Ig-related genes were identified and their fold changes and significant q-values were quantified. Only genes that were significantly differentially expressed were included in this section of analysis ( $q < 0.05$ ). CD138<sup>bright</sup> myeloma cells cultured with differentiated U937 cells upregulated just two Ig-related genes when compared with CD138<sup>bright</sup> cells cultured in isolation in both H929 and JJN3 cells. There were no Ig-related genes that were downregulated. In contrast, when the same comparison was made with CD138<sup>dim</sup> cells, there were 18 and 11 Ig-related genes that were downregulated in H929 and JJN3 cells, respectively (Figure 5.3). This repression of Ig-related gene transcription could potentially indicate that CD138<sup>dim</sup> cells are less functionally capable of producing immunoglobulin, which could in turn infer that they are less mature and are more representative of B-lymphocyte or plasmablast functionality, two precursor cells prior to terminal plasma cell differentiation.

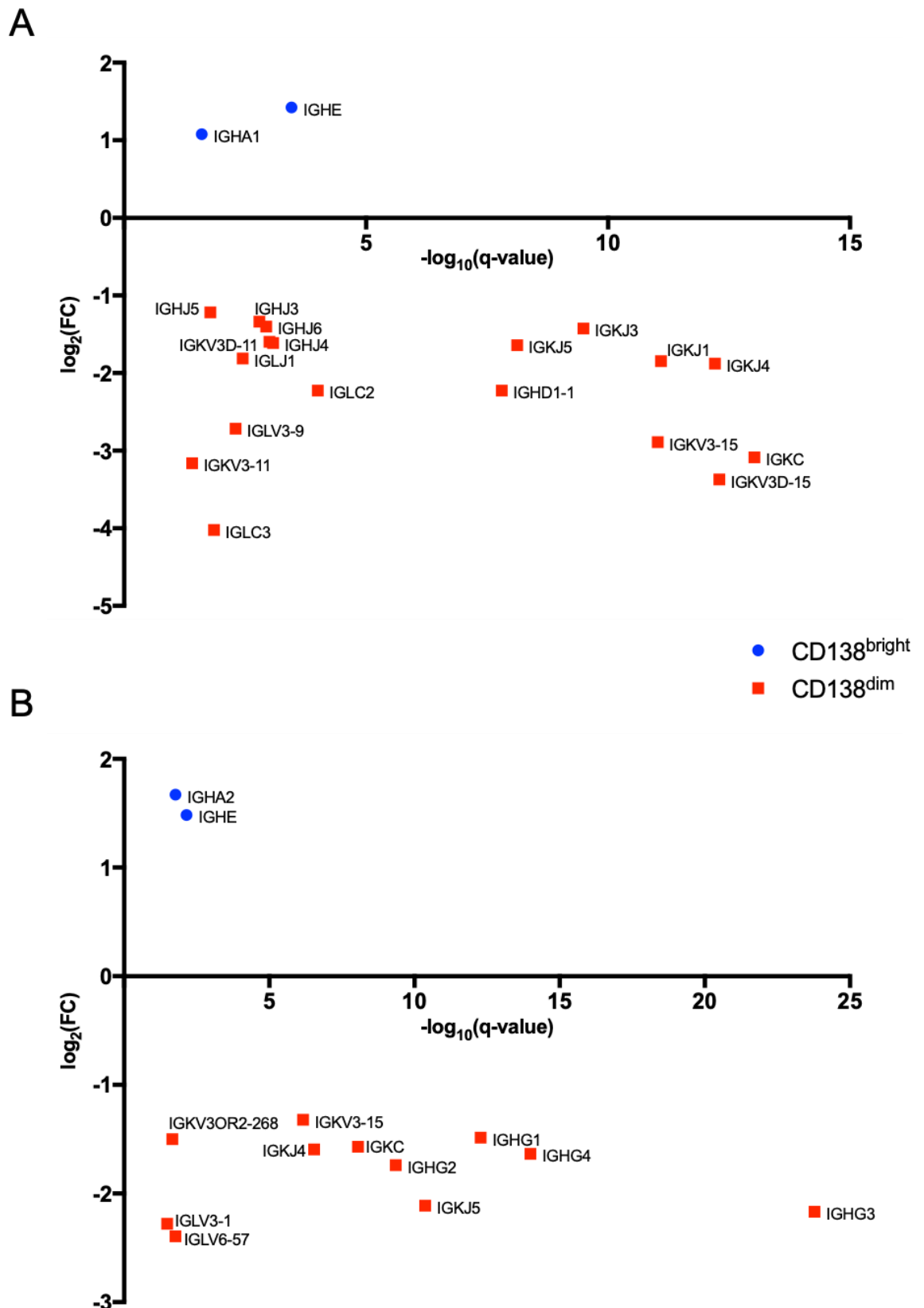


**Figure 5.3. Expression changes of immunoglobulin genes in CD138<sup>bright</sup> and CD138<sup>dim</sup> myeloma cells.** Fold changes in expression of immunoglobulin genes that were significantly altered in (A) H929 and (B) JN3 cells in response to co-culture with differentiated U937 cells were plotted alongside corresponding transformed q-values. DE genes from CD138<sup>bright</sup> cells are represented by blue points and DE genes from CD138<sup>dim</sup> cells are represented by red points.

#### 5.2.4. Assessment of CD138<sup>dim</sup> cell activation through expression of CD69

It was also of interest to determine whether there was any indication of increased cellular activation in CD138<sup>dim</sup> cells compared with CD138<sup>bright</sup> cells using both RNA-seq data and subsequent validation through flow cytometry. Whilst the ligand and exact function of the CD69 receptor has not been fully established, it has been widely used as a marker of cellular activation. This is because it was first identified on the surface of T-cells following stimulation of the T-cell receptor (TCR)<sup>384</sup>.

This data shows that there was no significant change in CD69 expression in CD138<sup>bright</sup> cells after co-culture with differentiated U937 cells, when compared with a CD138<sup>bright</sup> mono-culture control. There was however a significant increase in the level of CD69 expression in CD138<sup>dim</sup> myeloma cells in both H929 and JN3 cell lines ( $p < 0.0001$ ). This gene expression data was also re-capitulated at the protein level, with flow cytometric analysis confirming that this transcriptional increase in CD69 gene expression also resulted in a significant increase in the surface expression of the CD69 receptor in CD138<sup>dim</sup> cells in both myeloma cell lines, with no corresponding significant increase in CD69 expression in CD138<sup>bright</sup> myeloma cells (Figure 5.4). This therefore indicates that CD138<sup>dim</sup> myeloma cells could represent a more active subpopulation of myeloma cells following co-culture with differentiated U937 osteoclast-like cells.

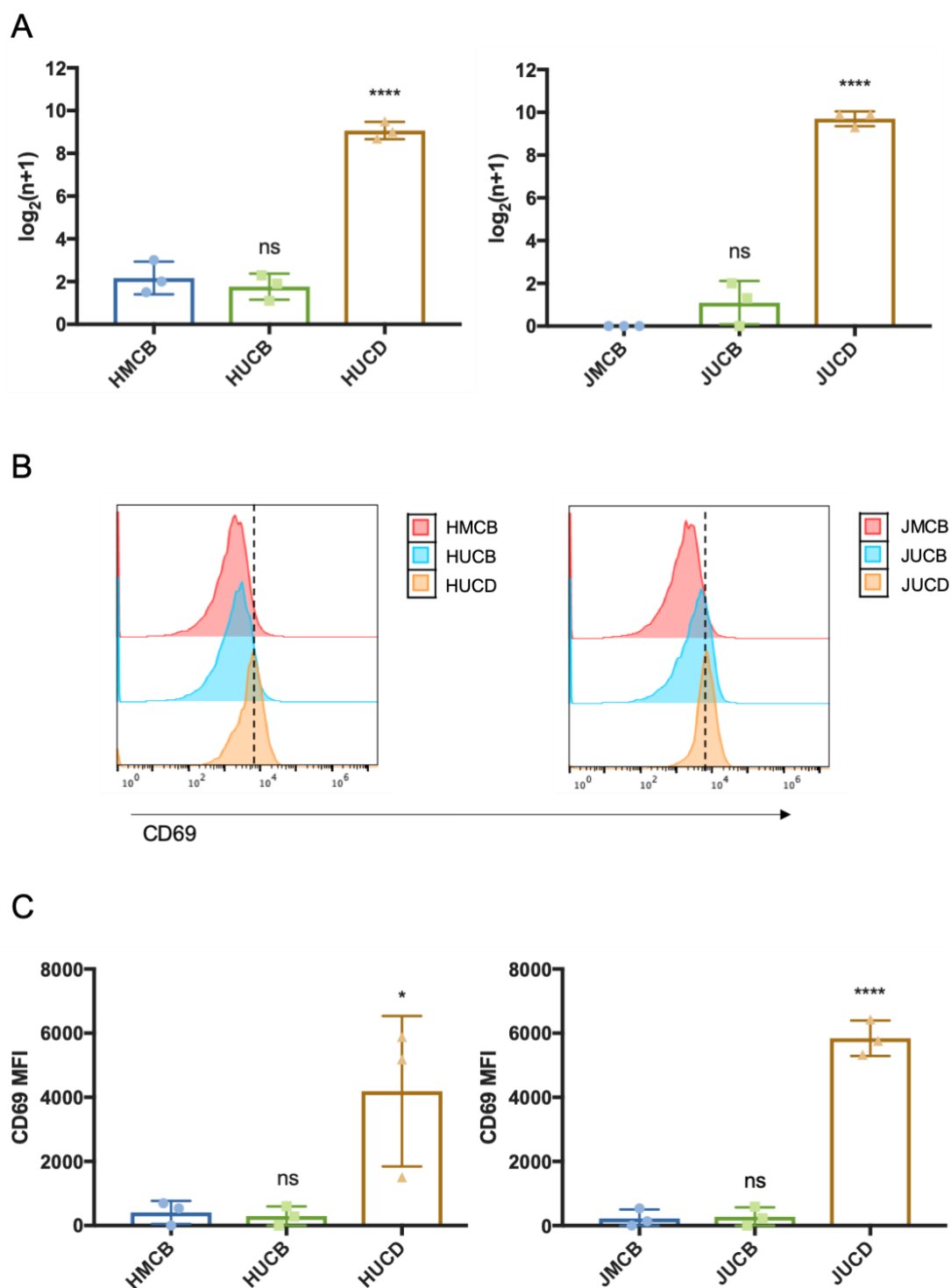


**Figure 5.4. Expression of CD69 in CD138<sup>bright</sup> and CD138<sup>dim</sup> myeloma subsets.** (A) Expression of CD69 was determined at the transcriptional level using normalised DESEQ2 values obtained from RNA-seq data analysis. The  $\log_2(n+1)$  formula was used to normalise any negligible values, where  $n$  represents DESEQ2 normalised gene expression and 1 represents a pseudo-number applied to account for genes that have an expression value of zero. (B) Representative histograms obtained from flow cytometry illustrating CD69 expression in CD138<sup>bright</sup> and CD138<sup>dim</sup> cells in both myeloma cell lines. A dotted line has been drawn to separate the mono-culture control samples from each myeloma sample cultured with differentiated U937 osteoclast-like cells. (C) Compilation of CD69 expression data obtained by flow cytometry for each sample used. Statistical significance was assessed using a one-way ANOVA followed by a Dunnett multiple comparison test comparing each sample against a CD138<sup>bright</sup> mono-culture control. Data was compiled using Prism 7.0 software and error bars were constructed using standard deviation (ns – not significant, \* -  $p < 0.05$ , \*\*\*\* -  $p < 0.0001$ ).

### 5.3. Evaluation of the adhesive, angiogenic and migratory capacity of myeloma cells

#### 5.3.1. Assessment of adhesion markers in CD138<sup>dim</sup> myeloma cells

Adhesion to the bone marrow is a fundamental characteristic of myeloma cells, especially during the processes of homing, migration and eventual metastasis to secondary tumour sites or peripheral circulation. It was interesting that of a number of over-represented pathways described in Section 4.6.2.2, there were a number of pathways relating to adhesion and metastasis, namely CXCR4 signalling, integrin signalling and leukocyte extravasation signalling. It was therefore of interest to investigate the genes that could be responsible for the overrepresentation of these pathways. The genes selected for adhesion-related analysis are described in Table 5.2.

Firstly, the normalised DESEQ2 values from each sample were obtained for each of these genes from RNA-seq analysis and transformed using a  $\log_2(n+1)$  transformation (Figure 5.5). It is clear that CD138<sup>dim</sup> cells co-culture with differentiated U937 cells in each myeloma cell line distinctly upregulated the expression of CD49e, CD45 and CXCR4 in comparison with a corresponding CD138<sup>bright</sup> mono-culture control. Conversely, whilst the expression of CD11a was clearly very high across all samples, there was a small yet significant downregulation of expression in the HUCD sample and no significant change of expression in the JUCD sample. The expression of CD40 also followed this same trend, although the expression of this particular antigen was much lower in comparison with CD11a.

Secondly, it was of interest to determine the post-translational expression of these antigens which was achieved through flow cytometry. This in-part validated the results from the RNA-seq analysis and also alluded to the potential functionality that these gene expression changes could infer in these cells. The expression of CD49e and CD45 as determined by flow cytometry, almost exactly replicated what was observed at the gene expression level, shown in the RNA-seq analysis, where CD138<sup>dim</sup> cells clearly upregulated this particular antigen in response to co-culture with differentiated U937 cells, in both myeloma cell lines. Interestingly, the expression of CD11a and CD40, as determined by flow cytometry, showed a clear upregulation in CD138<sup>dim</sup> cells

compared with CD138<sup>bright</sup> cells. Although this was not significant in H929 cells, it was clearly significant in JJN3 cells, which contrasts the gene expression data determined by RNA-seq where no upregulation of expression was observed in CD138<sup>dim</sup> cells. Finally, the expression of CXCR4 was replicated at the protein level in H929 cells, where CD138<sup>dim</sup> cells significantly upregulated the expression of this antigen when compared with CD138<sup>bright</sup> cells. However, there was no significant change in JJN3 cells when this comparison was made. However, an additional comparison was made between JUCB and JUCD samples which showed a very significant upregulation of CXCR4 in CD138<sup>dim</sup> cells compared with CD138<sup>bright</sup> cells. This interestingly demonstrates that whilst co-culture with differentiated U937 cells seemingly downregulated the expression of CXCR4 in CD138<sup>bright</sup> cells, its expression is maintained in CD138<sup>dim</sup> cells under the same culture conditions (Figure 5.6).

	<b>Gene Identity</b>	<b>Function</b>
<i>ITGA5 (CD49e)</i>	Integrin alpha 5	Alpha subunit on the VLA-5 adhesion antigen known to bind to fibronectin <sup>385</sup> . Found to be upregulated on malignant plasma cells and possesses strong correlation of expression with CD11a <sup>386</sup> .
<i>ITGAL (CD11a)</i>	Integrin alpha L/Lymphocyte function associated antigen 1	Adhesion molecule found to be expressed on malignant plasma cells. Previous research has shown that expression correlates with proliferation and myeloma cell growth <sup>387</sup> .
<i>CD40</i>	Cluster of differentiation 40	Important adhesion marker that has been shown to induce migration through NF- $\kappa$ B signalling in myeloma cells <sup>388</sup> . Also shown to induce IL-6 secretion in myeloma cells and BMSCs <sup>389</sup> .
<i>PTPRC (CD45)</i>	Protein tyrosine phosphatase, receptor type, C	Coupled with immunophenotypic use, CD45 serves as an adhesion marker that has been shown to be expressed in early stage plasma cells. Lack of expression has also been associated with increased myeloma cell migration <sup>372</sup> .
<i>CXCR4</i>	C-X-C chemokine receptor type 4	Critical regulator of myeloma cell homing and migration to the bone marrow and extramedullary sites <sup>166</sup> . Expression decreases in response to CXCL12, although increased expression has been inferred with more favourable prognosis <sup>390</sup> .

**Table 5.2. A functional summary of adhesion-related antigens.**

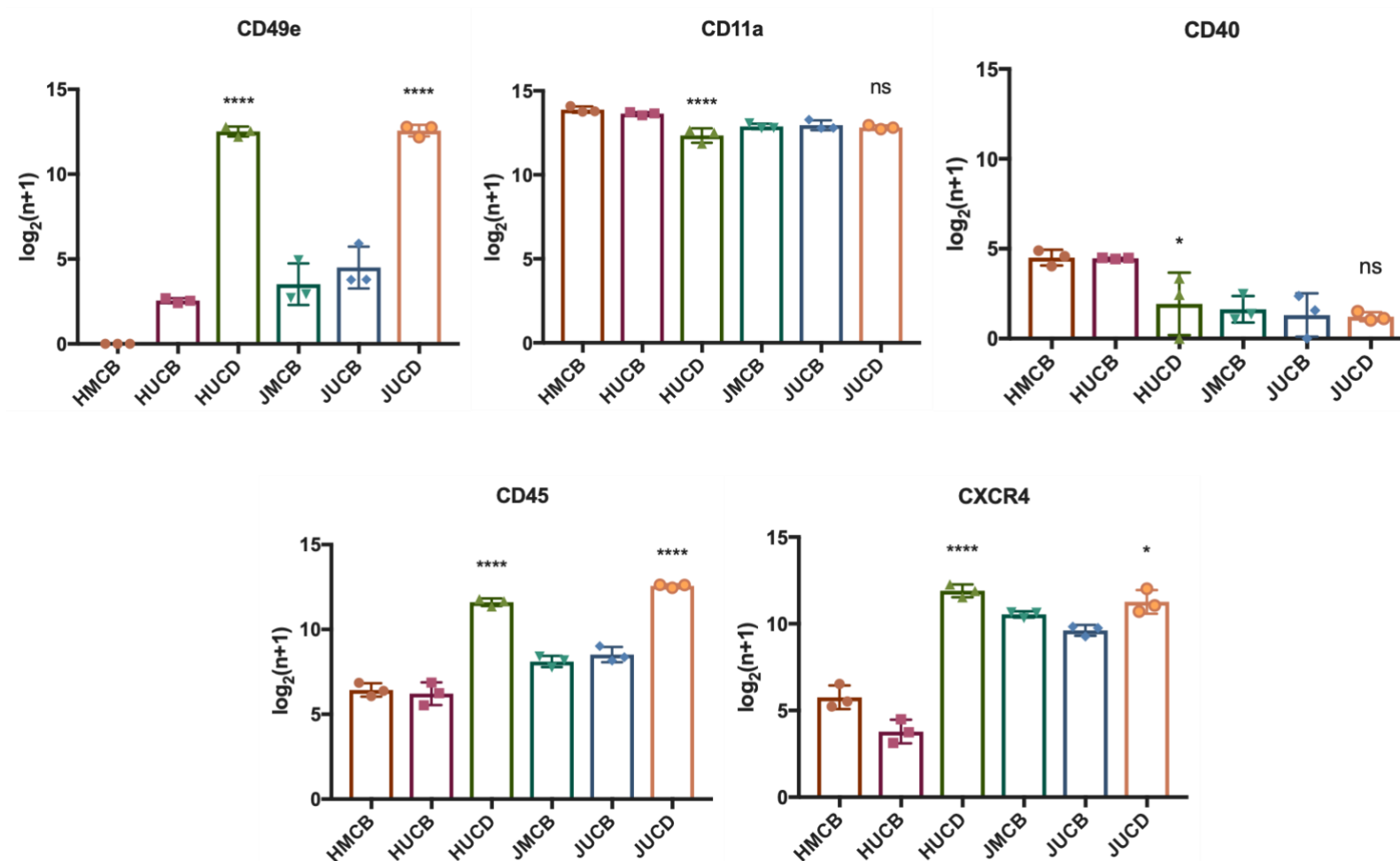


**Figure 5.5. Expression of genes associated with cell adhesion in H929 and JJN3 cells as determined by RNA-seq.** The  $\log_2(n+1)$  formula was used to normalise any negligible values, where  $n$  represents DESEQ2 normalised gene expression and 1 represents a pseudo-number applied to account for genes that have an expression value of zero. These expression values were plotted for 5 adhesion-related genes for each sample used in both H929 and JJN3 cells during RNA-seq analysis. Significance was determined using a one-way ANOVA followed by a Tukey multiple comparison test (ns = not significant, \* -  $p > 0.05$ , \*\*\*\*= $p < 0.0001$ ).

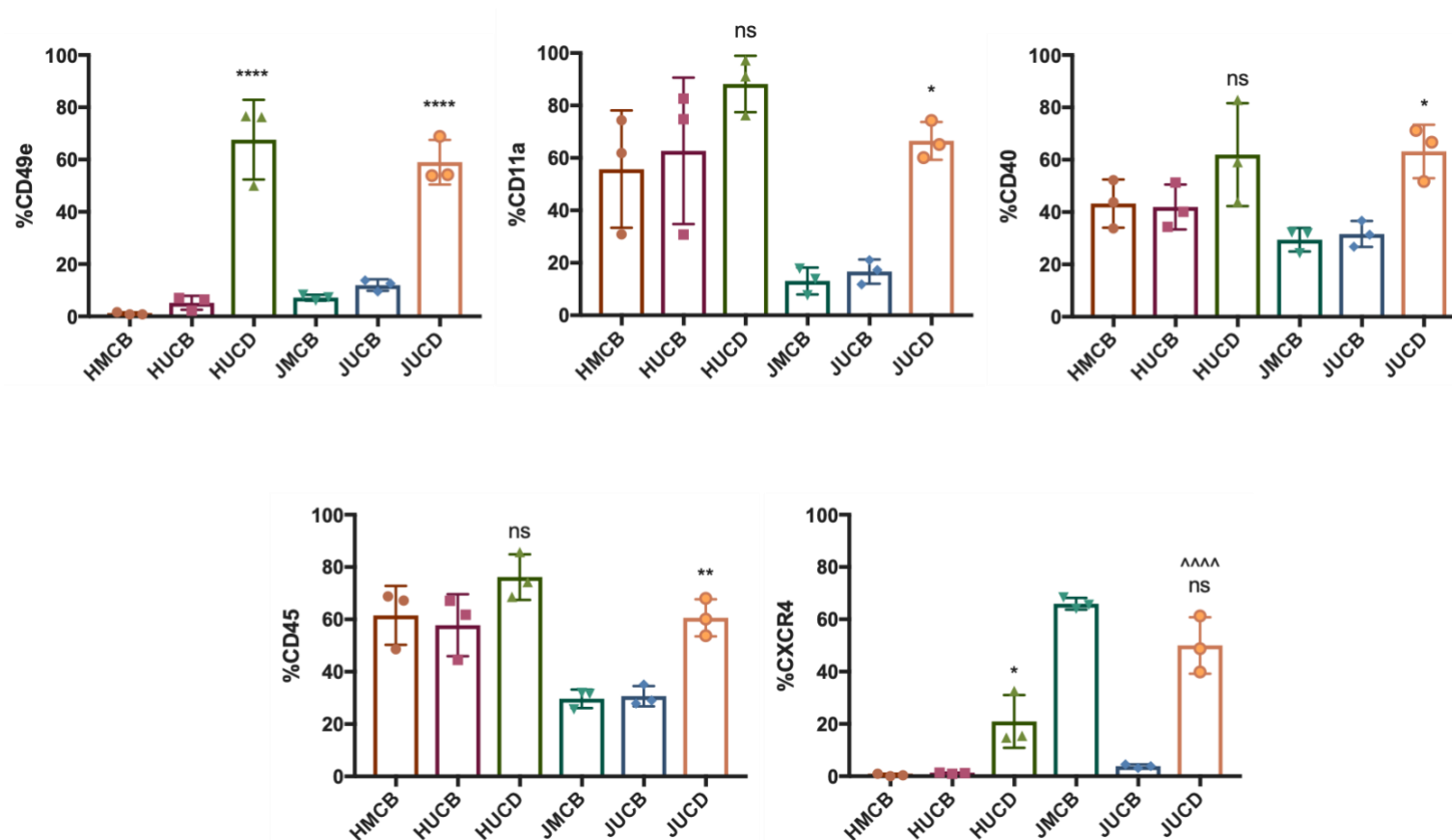


**Figure 5.6. Validation of differentially expressed adhesion markers using flow cytometry.** H929 and JJN3 cells were co-cultured with differentiated U937 cells for 48 hours, harvested and stained with a multicolour flow panel that contained CD138 and CD38 as well as the adhesion markers displayed. Expression positivity was determined in both CD138<sup>bright</sup> and CD138<sup>dim</sup> cells in both H929 and JJN3 cells and compared with a respective CD138<sup>bright</sup> mono-culture control. Statistical significance was determined using a one-way ANOVA followed by a Tukey multiple comparison test. The significance values illustrated are for comparisons between CD138<sup>dim</sup> cells with the corresponding CD138<sup>bright</sup> mono-culture control in each cell line, with the exception being with CXCR4 positivity in JJN3 cells, where an additional statistical comparison between CD138<sup>dim</sup> and CD138<sup>bright</sup> JJN3 cells that had been co-cultured with differentiated U937 cells, significance in this comparison is represented with a '^' symbol (ns = not significant, \* -  $p < 0.05$ , \*\* -  $p > 0.01$ , \*\*\*\* =  $p < 0.0001$ , ^^^ -  $p < 0.0001$ ).

### 5.3.2. Determination of angiogenic potential of myeloma cells

The CXCL8 signalling pathway contributes to the propagation of a number of cellular functions in a number of different cells of both haematopoietic and solid tumour origin<sup>391</sup>. One of the more established effects this signalling cascade has, is the ability to enhance the angiogenic capacity of these cells<sup>392</sup>. Myeloma is a cancer that has strong associations with CXCL8 activation. This correlates with the ability of myeloma cells to manipulate the process of angiogenesis within the bone marrow microenvironment and also relates to a number of other processes such as migration and metastasis, as highlighted in Section 4.6.2.2<sup>393</sup>.

Real-time PCR data presented in Figure 4.13 clearly showed a significant upregulation of CXCL8 in CD138<sup>dim</sup> cells in both myeloma cell lines, thus emulating the expression data determined from the RNA-seq experiment. Given that CD138<sup>dim</sup> cells have also been shown to upregulate genes associated with, angiogenesis, motility and migration, it was therefore of interest to further explore the CXCL8 pathway and the genes associated with signal transduction. IPA was used to assess the DE genes associated with CXCL8 signalling in both myeloma cell lines from a CD138<sup>bright</sup> vs CD138<sup>dim</sup> comparison. The upstream regulator function was used to firstly predict activation or inhibition of the pathway. This function relays prior evidence of molecular associations between different members of signalling pathways and subsequently draws conclusions as to whether these known associations are being replicated in the dataset being analysed. From this analysis, IPA then predicts whether particular signalling transducers and corresponding pathways are being activated or inhibited. In both H929 and JJN3 cells, CXCL8 signalling was predicted to be activated. Sets of 23 (20 upregulated, 3 downregulated) and 30 (26 upregulated, 4 downregulated) genes that were associated with CXCL8 signalling were found to be significantly differentially expressed in H929 and JJN3 cells respectively. The predicted links between CXCL8 and these DE genes associated with this pathway are shown in Figure 5.7. Of the genes that were upregulated, 16 of them were common to both myeloma cell lines. Of these are a number of key regulators of CXCL8 signalling that include the receptor of CXCL8 binding, CXCLR2. Adhesion markers such as ITGA5 (CD49e) and ITGB2 are also upregulated, as well as key matrix metalloproteinases MMP2 and MMP9, which heavily contribute to extracellular matrix degradation and are known to be secreted by

myeloma cells, the expression of the former has also been confirmed at protein level in both myeloma cell lines. IL1- $\beta$  is also a key transducer of CXCL8 signalling and is another commonly upregulated gene determined from CD138<sup>dim</sup> cells in both cell lines and plays a key role in CXCL8 signal regulation in multiple myeloma<sup>394</sup>.

It is also widely accepted that CXCL8 acts as a potent neutrophil and tumour-associated macrophage chemoattractant, in addition to promoting osteoclastogenesis. This heavily implies that CXCL8 has an innate ability to dramatically alter the composition of the tumour microenvironment within the bone marrow. Neutrophils in particular are known to secrete lytic enzymes in response to CXCL8-induced chemotaxis that can contribute to remodelling within the extracellular matrix of the bone marrow microenvironment that can directly contribute to the enhancement of angiogenesis<sup>391,395</sup>.

Collectively, these results suggest that CD138<sup>dim</sup> myeloma cells have an increased capacity for CXCL8 signalling and angiogenic activity.

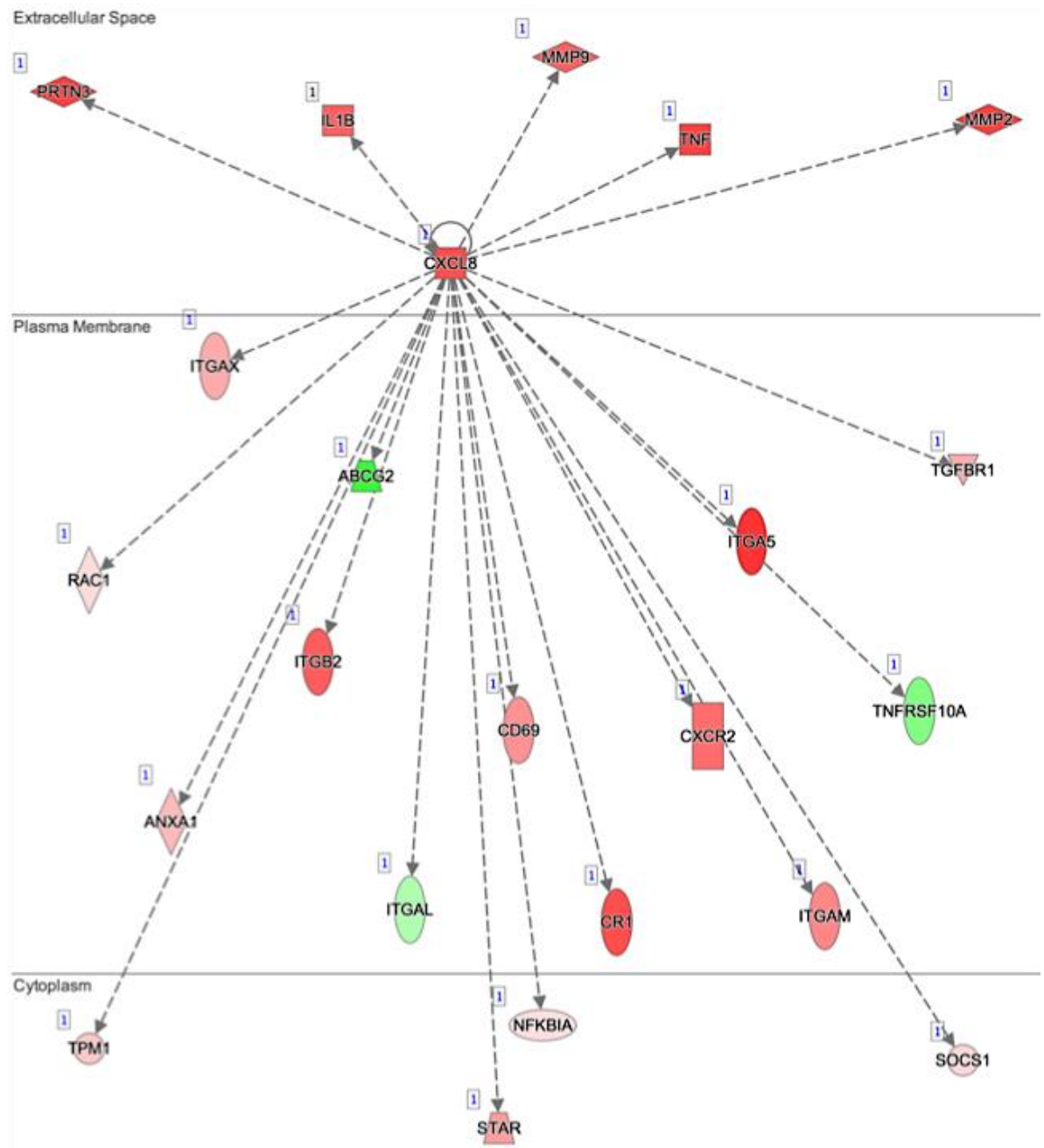


**Figure 5.7A.** A schematic of CXCL8 signalling and associated DE genes from CD138<sup>dim</sup> H929 cells. IPA software was used to construct this diagram using the upstream regulator tool to display the functional associations between CXCL8 and other members of this signalling pathway. Upregulated genes are coloured red and conversely genes that are downregulated are coloured green. Each gene is positioned in accordance with their relative functional location within the cell.

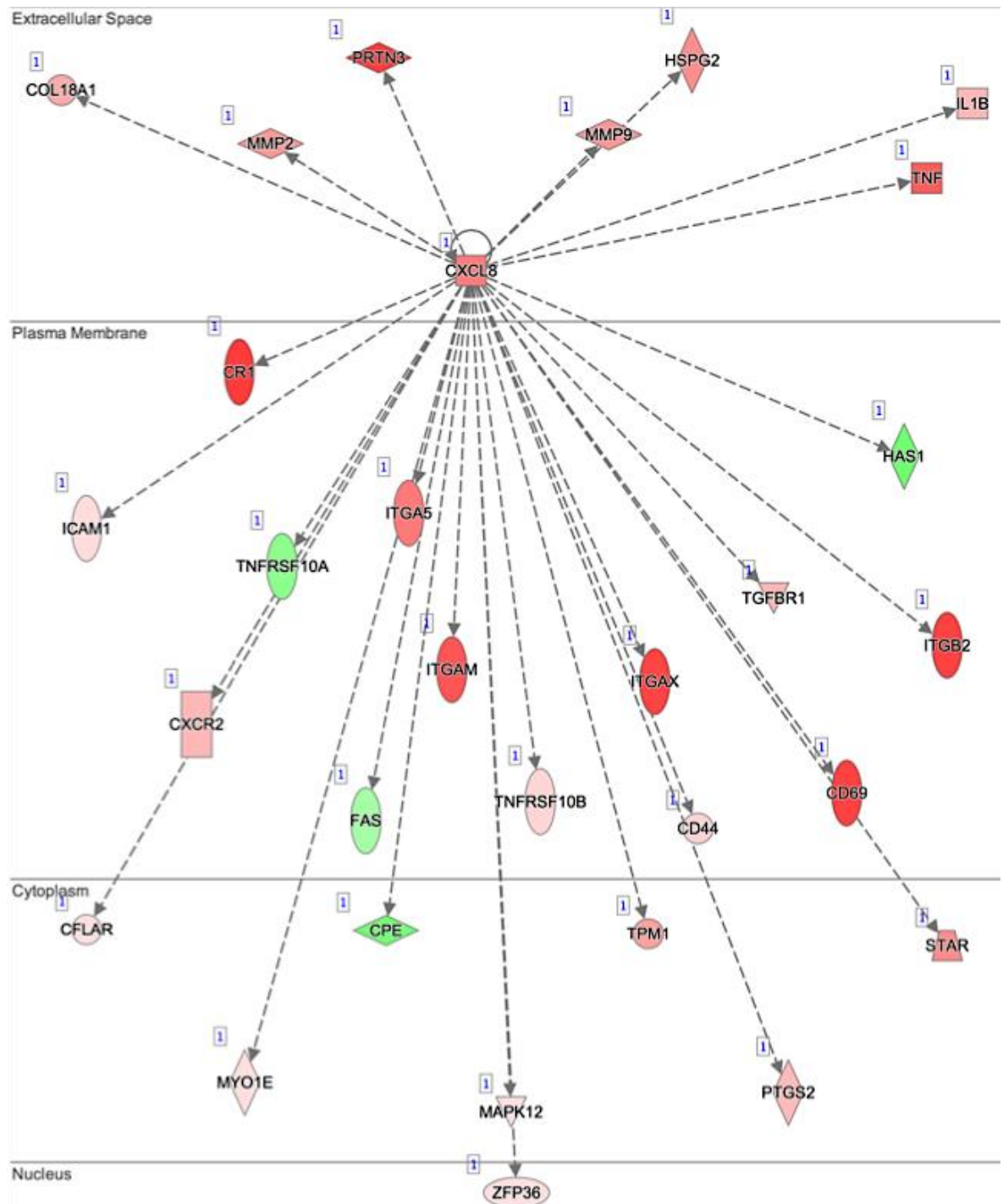


**Figure 5.7B.** A schematic of CXCL8 signalling and associated DE genes from CD138<sup>dim</sup> JN3 cells. IPA software was used to construct this diagram using the upstream regulator tool to display the functional associations between CXCL8 and other members of this signalling pathway. Upregulated genes are coloured red and conversely genes that are downregulated are coloured green. Each gene is positioned in accordance with their relative functional location within the cell.

### 5.3.3. Functional assessment of migratory potential of myeloma cells

Thus far, I have established that CD138<sup>dim</sup> myeloma cells have the capacity to upregulate the expression of genes associated with adhesion, extracellular matrix degradation and angiogenesis. These are key mechanisms that are related to the process of cellular migration. Migration is an essential process that facilitates the dissemination of malignant plasma cells throughout the bone marrow<sup>396</sup>. Whilst the complete mechanistic landscape of this process is still contested, it is clear that myeloma cells are able to manipulate the angiogenic capacity of endothelial cells to produce micro blood vessels within the bone marrow, which subsequently facilitates their migratory capacity<sup>347</sup>.

There has also been speculation revolving around the identity of these migratory myeloma cells and whether it is a capability that all malignant plasma cells possess, or if there are particular subsets of myeloma cells that have an increased migratory potential. Previous evidence has suggested that malignant plasma cells that are low expressors of CD138 are present in the peripheral circulation of myeloma patients and that these cells demonstrate greater migratory capabilities<sup>41,363</sup>. Given this prior information and the inference of CD138<sup>dim</sup> cells as potentially possessing greater migratory capacity than CD138<sup>bright</sup> cells in this research, it was of interest to determine the migratory potential of CD138<sup>dim</sup> H929 and JN3 cells following co-culture with differentiated U937 cells. CXCR4, as previously discussed is an essential regulator of myeloma cell homing and is heavily implicated in migration. Given that the data presented in this thesis show its expression to be upregulated in CD138<sup>dim</sup> cells, migration was assessed in both the presence and absence of a CXCL12 gradient – the ligand of CXCR4<sup>166</sup>.

Myeloma cells were co-cultured with differentiated U937 cells for 48 hours before being harvested and placed in Transwell® chambers in either the presence or absence of a CXCL12 (100ng/mL) gradient. After 24 hours of Transwell® culture, the level of overall migration and the ratio of CD138<sup>bright</sup> and CD138<sup>dim</sup> migrated cells was determined. The first observation to make here is that it is evident that both H929 and JN3 cells are capable of migrating along a CXCL12 gradient, indicating that the

CXCR4/CXCL12 signalling cascade is at least in-part responsible for influencing the migratory capacity of these cells.

H929 cells were incapable of migrating in the absence of a CXCL12 gradient, with very few cells being detected in the lower chamber of the Transwell® plate under these conditions. Whilst this was not a statistically significant phenomenon, it is numerically evident that there are a much greater number of H929 cells that have migrated through the Transwell® membrane in response to a CXCL12 gradient when in comparison to an absence of CXCL12. What is also interesting is that JLN3 cells have the capability of migrating in both the presence and absence of a CXCL12 gradient, indicating that the CXCR4/CXCL12 signalling axis is not solely responsible for the migratory capacity of cells from this particular cell line. Although, as highlighted by the two y-axes in Figure 5.8A, there was a lower total proportion of migrated JLN3 cells compared with H929 cells.

The next step of analysis was to determine the proportions of CD138<sup>bright</sup> and CD138<sup>dim</sup> H929 and JLN3 cells that had migrated. What is clear here is that CD138<sup>bright</sup> H929 cells were the dominant population of migrated cells, with only a small proportion of CD138<sup>dim</sup> H929 cells having migrated in response to a CXCL12 gradient. In contrast however, there was a relatively equal proportion of CD138<sup>bright</sup> and CD138<sup>dim</sup> JLN3 cells that had migrated in response to a CXCL12 gradient, with an apparently larger proportion of CD138<sup>dim</sup> JLN3 cells that had migrated in the absence of a CXCL12 gradient (Figure 5.8B). This was further confirmed statistically where the proportion of migrated CD138<sup>bright</sup> and CD138<sup>dim</sup> H929 cells did not significantly alter in comparison with the proportion of these subpopulations determined at a 0h timepoint. Whereas there was a clear and significant representation of CD138<sup>dim</sup> JLN3 cells that had migrated in the presence ( $p < 0.001$ ) and absence ( $p < 0.0001$ ) of a CXCL12 gradient (Figure 5.8C). This shows that whilst there are differing migratory characteristics between both cell lines, CD138<sup>dim</sup> cells obtained from JLN3 cells clearly have the capacity to preferentially migrate when compared with CD138<sup>bright</sup> cells.

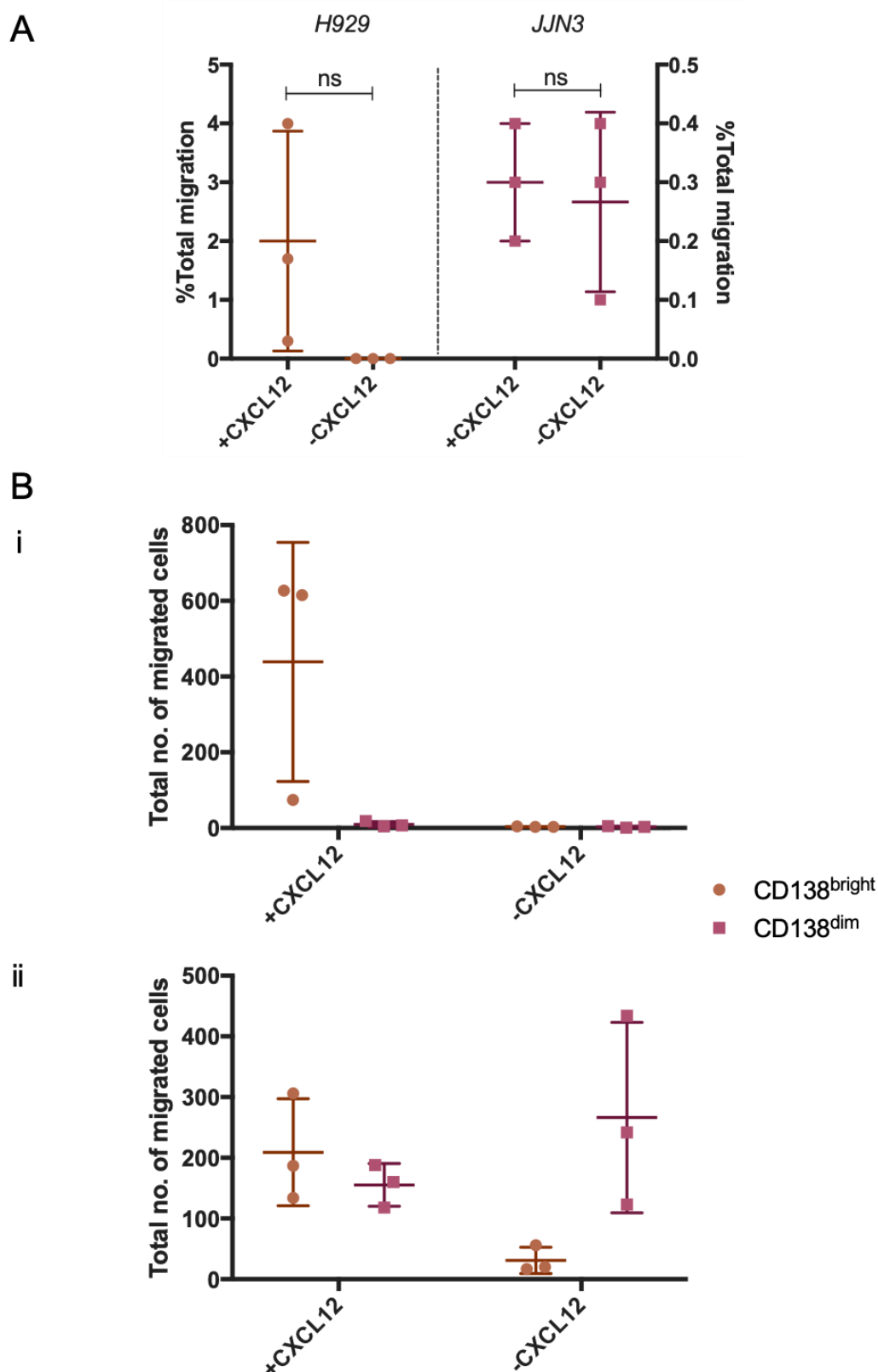
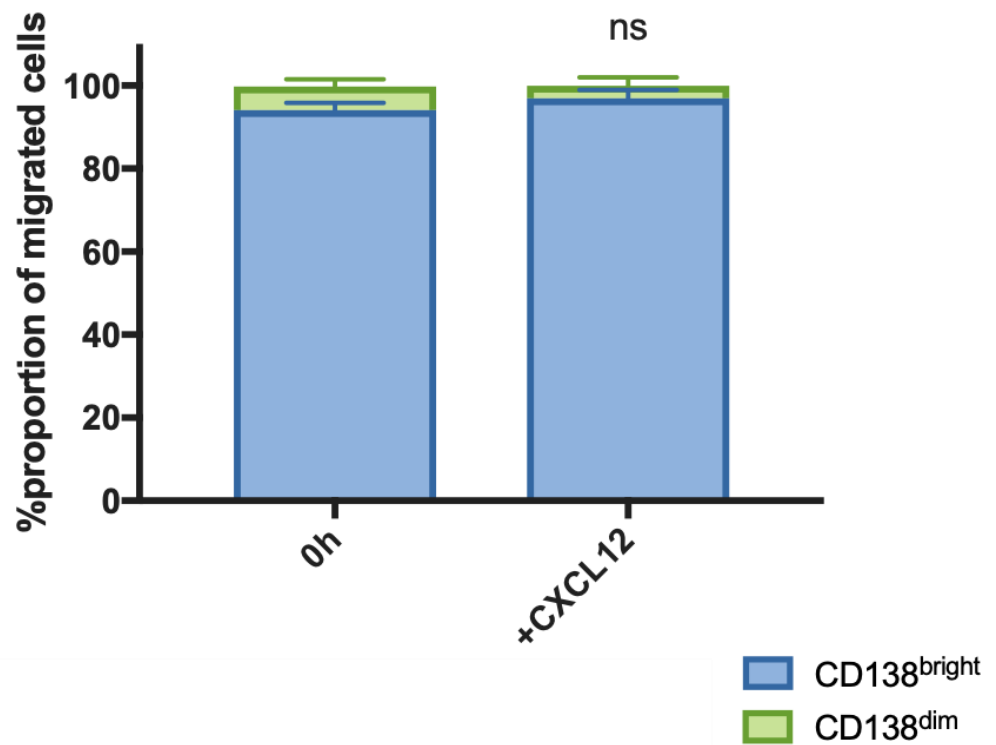


**Figure 5.8. Migration of myeloma cell lines following co-culture with differentiated U937 cells.** Following co-culture with differentiated U937 cells for 48 hours, H929 and JLN3 cells were placed in Transwell® chambers in the presence or absence of a CXCL12 (100ng/mL) gradient. After 24 hours cells were then harvested from the upper and lower chambers of the Transwell® to assess migration. (A) The total proportion of migrated H929 and JLN3 cells were assessed with and without a CXCL12 gradient. (B) the total absolute number of migrated CD138<sup>bright</sup> and CD138<sup>dim</sup> cells were then assessed in H929 (i) and JLN3 (ii) cells, with and without a CXCL12 gradient. Statistical significance was assessed using a 2-way ANOVA followed by a Tukey multiple comparison test. Graphs were plotted using GraphPad Prism 7.0 software (ns – not significant).

C

i



ii

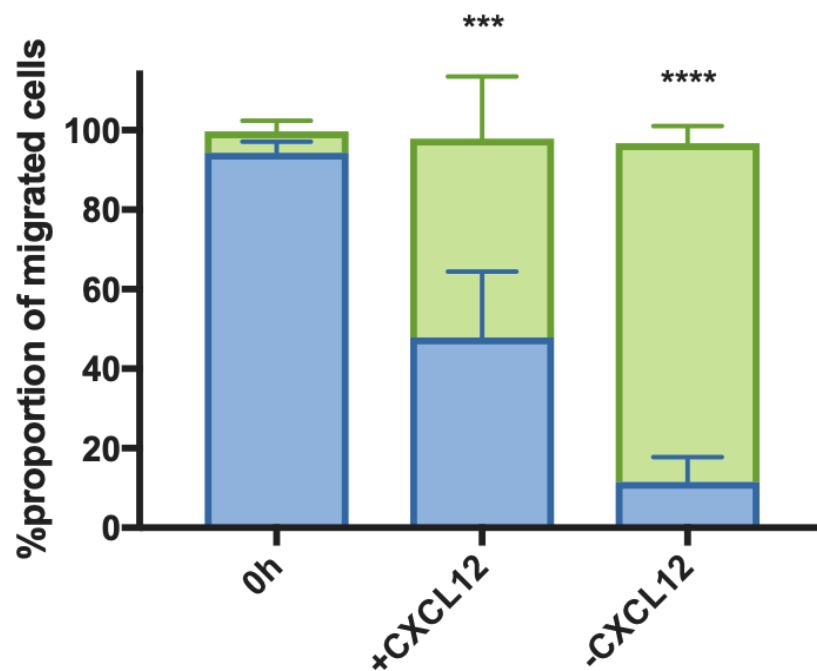


**Figure 5.8 (continued). Migration of myeloma cell lines following co-culture with differentiated U937 cells.** (C) The proportion of CD138<sup>bright</sup> (blue) and CD138<sup>dim</sup> (green) H929 (i) and JN3 (ii) cells that had migrated after 48 hours of co-culture with differentiated U937 cells and 24 hours of culture in a Transwell® chamber in the presence or absence of a CXCL12 gradient were plotted. However, due to the negligible number of H929 cells that had migrated in the absence of a CXCL12 gradient, no data was plotted for this particular experimental condition. Statistical significance was determined using GraphPad Prism 7.0 software, a 2-way ANOVA followed by a Dunnett multiple comparison test was performed against a 0h control, prior to Transwell® culture (ns – not significant, \*\*\* -  $p < 0.001$ , \*\*\*\* -  $p < 0.0001$ ).

## 5.4. Assessment of myeloma cell activation and chemoresistance

Multiple myeloma is a malignancy heavily associated with disease relapse following treatment<sup>136</sup>. The strong dependence malignant plasma cells have on the bone marrow microenvironment makes it extremely difficult to effectively treat this disease, with a small residual population of drug-resistant myeloma cells remaining within the bone marrow after nearly all cases of treatment<sup>397</sup>. It is evident that these chemo-resistant, malignant plasma cells are ultimately responsible for the eventual propagation of disease that causes inevitable relapse. There is plenty of evidence demonstrating the contribution of numerous non-malignant cells within the bone marrow to myeloma cell resistance against chemotherapeutic intervention, with osteoclasts also being highlighted as culprits for this phenomenon<sup>204</sup>.

This also raises questions into the role and identity of chemo-resistant myeloma cells and how they functionally differ from other intra-heterogeneous subsets within the malignant plasma cell cohort. There is evidence to suggest that these drug-resistant malignant plasma cells are low expressors of CD138, having been previously detected in circulation in late stage disease<sup>38,398,399</sup>. It was therefore of interest to investigate the influence of osteoclast-like culture on the survival of myeloma cells and also assess the functional chemo-resistant potential of CD138<sup>dim</sup> cells identified in H929 and JN3 cells in this research after culture with differentiated U937 cells.

### 5.4.1. Assessment of chemoresistance in CD138<sup>dim</sup> myeloma cells

It is well established that the bone marrow microenvironment contributes to drug resistance in multiple myeloma<sup>400</sup>. This phenomenon has been previously shown to occur through both cell adhesion-mediated (CAM-DR) and soluble factor-mediated (SF-DR) resistance mechanisms<sup>401</sup>. Osteoclasts have also been shown to directly contribute to drug resistance in myeloma through cell-cell contact<sup>204</sup>. It was therefore of interest to determine firstly whether differentiated U937 cells were able to provide a protective effect to myeloma cells in response to treatment with a chemotherapeutic drug and to additionally determine whether CD138<sup>bright</sup> and CD138<sup>dim</sup> myeloma cells displayed different chemo-resistant properties.

#### 5.4.1.1. Differentiated U937 cells provide a protective effect against bortezomib

Myeloma cells were treated with bortezomib (20-120nM), a proteasome inhibitor in clinical use for the treatment of myeloma patients<sup>123,402</sup>, in the presence or absence of differentiated U937 cells and assessed for viability after 48 hours. As previously discussed CD138 is shed from the surface of myeloma cells in response to apoptosis, therefore making the assessment of viability and distinguishing between both CD138<sup>bright</sup> and CD138<sup>dim</sup> cells difficult using Annexin V staining. Therefore, forward and side scatter were used as parameters to determine populations of live and dead cells. A live cell gate was drawn with CD138 and CD38 positivity being determined within those populations of viable cells (Figure 5.9).

Treatment with bortezomib, revealed a significant increase in LD<sub>50</sub> (nM) in both H929 (44nM vs 35nM; p<0.001) and JJN3 (73nM vs 52nM; p<0.001) myeloma cells as a result of culture with differentiated U937 cells when compared with myeloma cells cultured in isolation (Figure 5.10). Thus, indicating that these osteoclast-like cells have the capability of providing a level of protection to myeloma cells against chemotherapeutic intervention. It is also evident that JJN3 cells are more chemo-resistant to bortezomib in comparison with H929 cells under the same monoculture (p<0.001) or co-culture conditions with differentiated U937 cells (p<0.0001).

#### 5.4.1.2. CD138<sup>dim</sup> myeloma cells are more chemo-resistant than CD138<sup>bright</sup> cells

Myeloma patients inevitably experience clinical relapse due to the expansion of a sub-clonal population of malignant cells that are resistant to previously used therapeutics<sup>127</sup>. It has been hypothesised that the population of cells responsible for this could be CD138<sup>dim</sup> myeloma cells<sup>42</sup>. Therefore, having established that differentiated U937 cells significantly expand the proportion of CD138<sup>dim</sup> cells *in vitro*, it was then of interest to investigate whether this significant differential toxicity observed between culture conditions could be inferred by CD138<sup>dim</sup> myeloma cells.

Using the gating strategy outlined in Figure 5.9, proportions of CD138<sup>bright</sup> and CD138<sup>dim</sup> myeloma cell populations were quantified within the live cell gate as determined by forward and side scatter at each dose of bortezomib treatment. Significant changes in cell number in both CD138<sup>bright</sup> and CD138<sup>dim</sup> cells were

determined at the doses immediately above and below previously determined LD<sub>50</sub> values. The absolute number of H929 CD138<sup>dim</sup> cells did not significantly change ( $p>0.05$ ) and the absolute number of JJN3 CD138<sup>dim</sup> cells significantly increased ( $p<0.0001$ ) at these respective treatment doses. Conversely there was a significant decrease in absolute cell number of both H929 ( $p<0.01$ ) and JJN3 ( $p<0.0001$ ) CD138<sup>bright</sup> cells at both doses immediately above and below previously determined LD<sub>50</sub> values. There was also a significant increase in CD138<sup>bright</sup>:CD138<sup>dim</sup> ratio in both H929 ( $p<0.01$ ) and JJN3 ( $p<0.0001$ ) cells at both of these doses, highlighting that CD138<sup>dim</sup> cells were more resistant to treatment with bortezomib when compared with CD138<sup>bright</sup> cells (Figure 5.11).

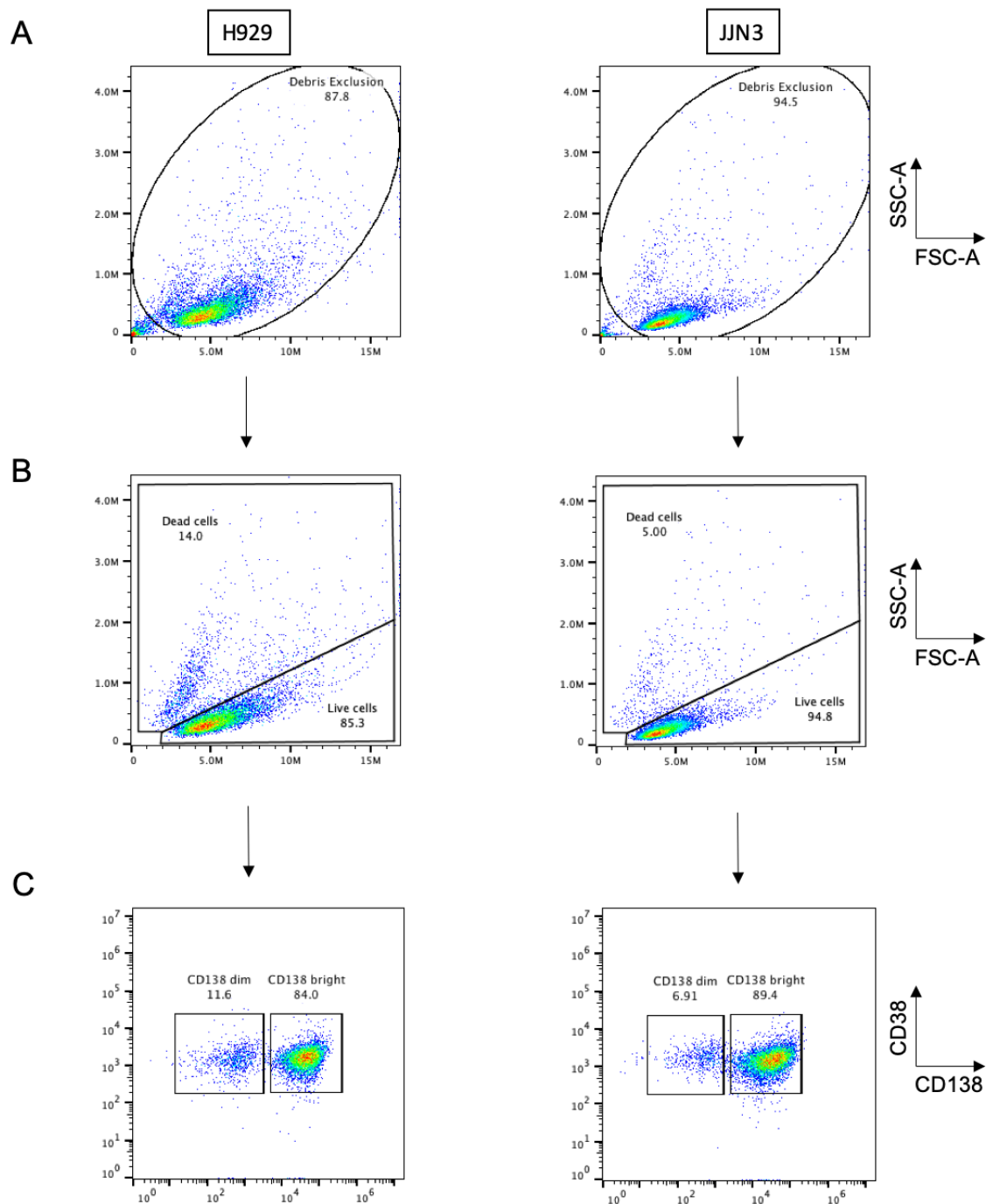


**Figure 5.9. Gating strategy to assess myeloma cell viability following treatment with bortezomib.**

H929 and JN3 cells were pre-treated with bortezomib for 1 hour prior to their addition to culture with or without U937 cells that had been treated with PMA for 48 hours and  $1,25(\text{OH})_2\text{D}_3$  for a further 5 days. Myeloma cells were then incubated for 48 hours before being harvested. Viability in this experiment was determined using forward and side scatter following the exclusion of debris from the plots<sup>403</sup>. (A) Debris was excluded from forward and side scatter plots with the resulting events being separated by (B) live and dead cell gates. (C) Within the live cell population CD138 positivity was determined with two gates being drawn around each CD138<sup>bright</sup> and CD138<sup>dim</sup> subpopulation.

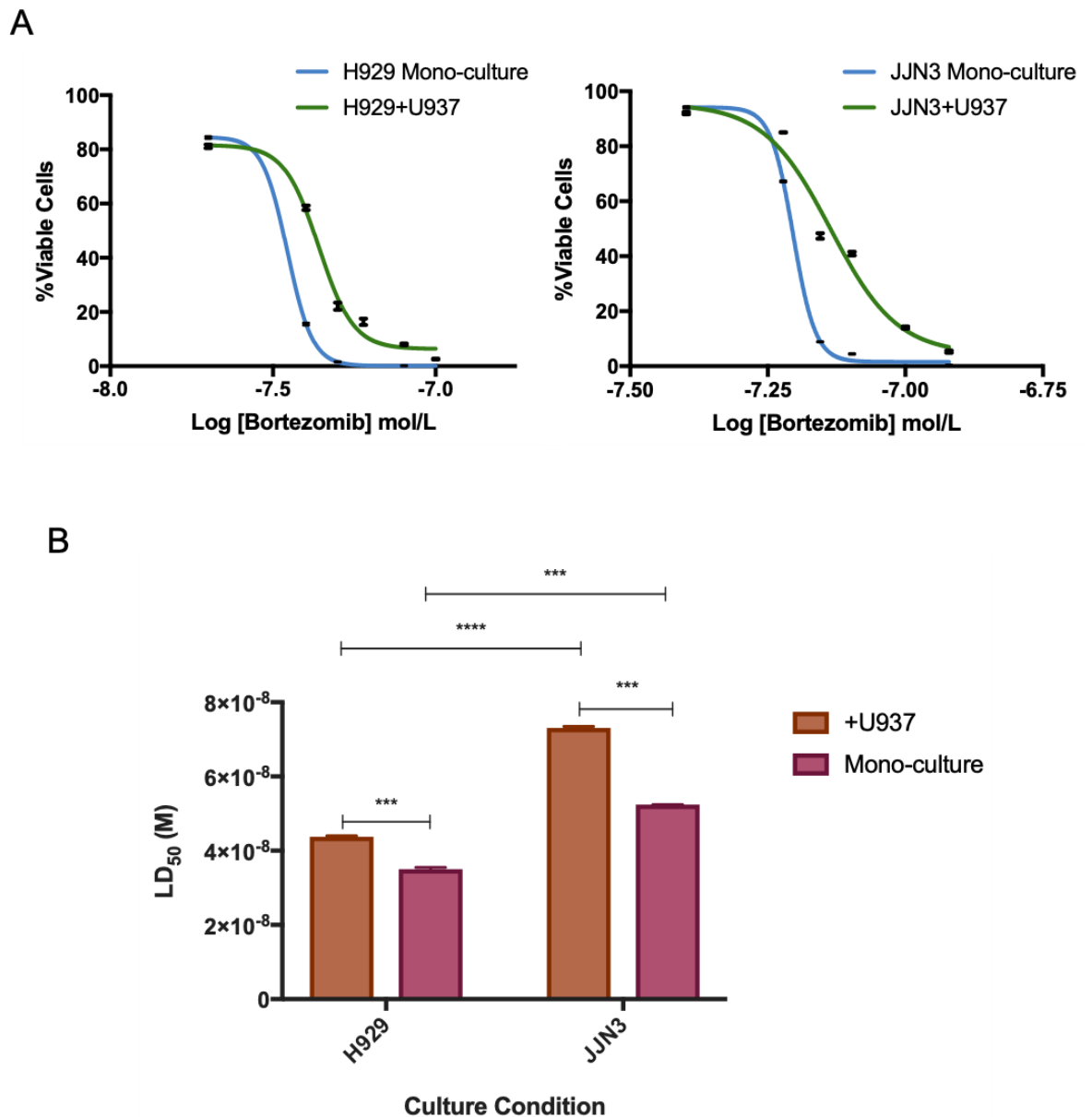


**Figure 5.10. The toxicity of bortezomib in myeloma cells cultured with differentiated U937 cells.** (A) The percentage of viable cells at each treatment dose was plotted for each culture condition against the log of the dose to create sigmoidal dose response curves. (B) From these curves LD<sub>50</sub> values were calculated for each culture condition, with standard error of the mean being used to plot error bars (n=3). Paired *t*-tests were applied to assess statistical significance using GraphPad Prism 7.0 software (\*\*\*) -  $p < 0.001$ , \*\*\*\* -  $p < 0.0001$ ).

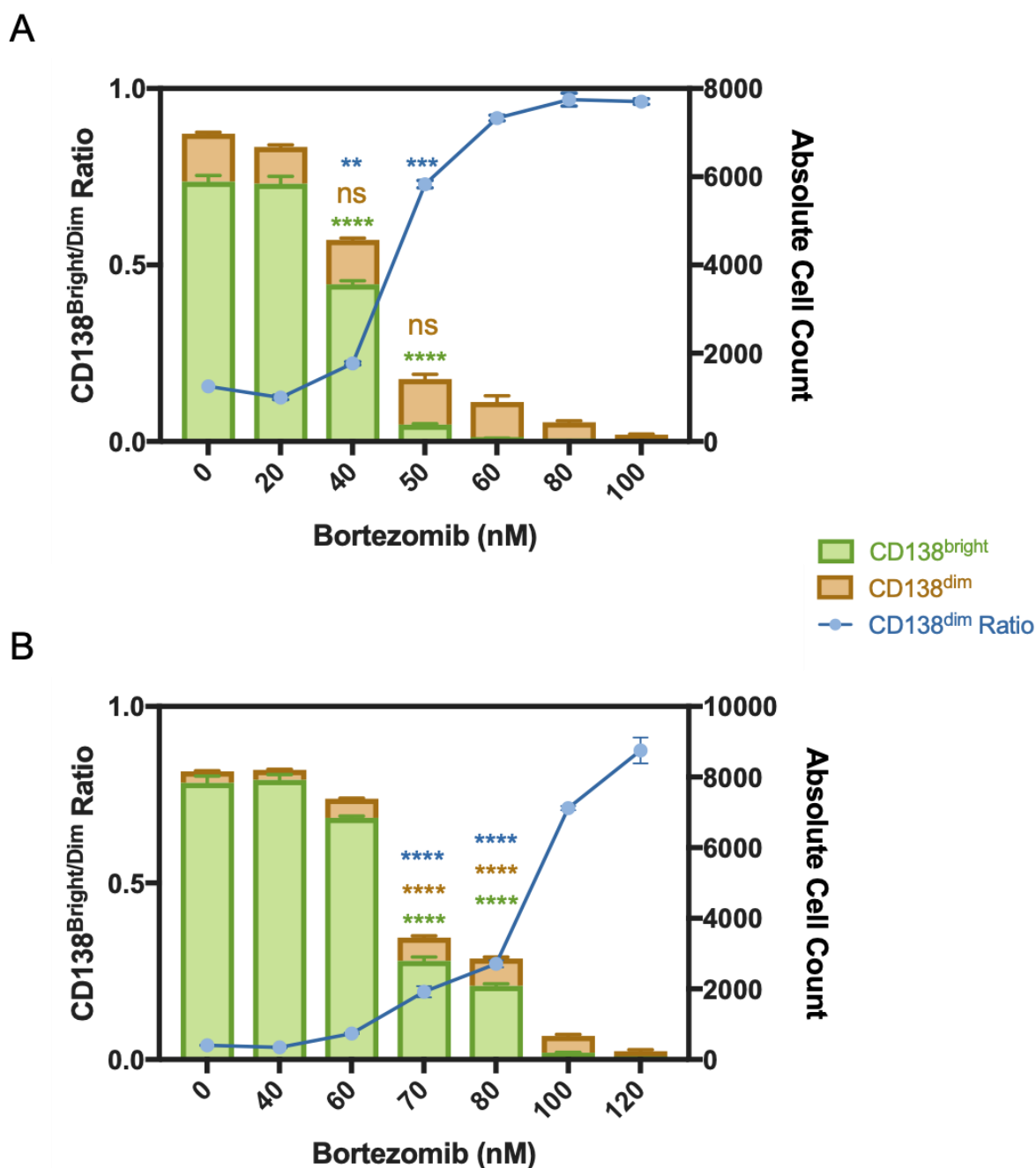


**Figure 5.11. The toxicity of bortezomib in CD138<sup>bright</sup> and CD138<sup>dim</sup> myeloma cells.** The absolute cell counts of CD138<sup>bright</sup> (green) and CD138<sup>dim</sup> (orange) (A) H929 and (B) JN3 myeloma cells were plotted on the right y-axis. The ratio of CD138<sup>dim</sup> cells compared with CD138<sup>bright</sup> H929 and JN3 myeloma cells were plotted on the left y-axis. The doses of treatment immediately above and below the calculated LD<sub>50</sub> values for each cell line were used to assess statistical significance in comparison with an untreated control. Error bars were plotted as standard error of the mean and statistical significance was determined by using Graphpad Prism 7.0 software to perform a two-way ANOVA followed by a Dunnett multiple comparison test using the untreated sample in each cell line as a comparative control (ns = not significant, \*\* -  $p > 0.01$ , \*\*\*= $p < 0.01$ , \*\*\*\*= $p < 0.0001$ ).

## 5.5. Discussion

Multiple myeloma is a complex haematological malignancy that is heavily reliant on the bone marrow microenvironment for survival and disease propagation. The cells of this environment are manipulated to facilitate the biological processes which in turn contribute to the pathophysiology and progression of myeloma. Inevitably, in a post-treatment scenario, myeloma patients nearly always experience relapse which is primarily due to the physiological protection provided by a number of different cell types within the bone marrow microenvironment. However, given the heterogeneity observed between patients and the intra-clonal heterogeneity even within the same patient, it poses the question as to whether there are particular clonal subsets of myeloma cells that are inherently more chemo-resistant and have greater migratory potential than others. Such cells could emerge in the post-treatment scenario, ultimately causing treatment failure and patient relapse.

Intra-clonal heterogeneity has been highlighted in a number of malignancies and poses a serious problem in the consideration of cancer treatment, including myeloma<sup>368,404</sup>. This phenomenon has been shown at all stages of myeloma disease progression and has been hypothesised to be an early initiating event in the pathogenesis of this malignancy<sup>405</sup>. It has also been previously identified in some myeloma cell lines which replicated the intra-clonal heterogeneity observed in patients before treatment, with chemo-resistant subclones being shown to emerge in a post-treatment scenario<sup>406</sup>. This forms the basis of disease evolution through treatment-induced selection pressure.

Myeloma cells that are low expressors of CD138 are one subset of myeloma cells that have been previously speculated to be reminiscent of a myeloma sub-clonal population that are representative of these features<sup>41-43</sup>. The research presented in this thesis has demonstrated an exclusive increase in the proportion of myeloma cells that are CD138<sup>dim</sup>, specifically after culture with osteoclast-like cells. Having established that the transcriptional profile between CD138<sup>bright</sup> and CD138<sup>dim</sup> cells is significantly altered after culture with differentiated U937 cells, it was of interest to

establish the functional differences that were inferred from transcriptomic analysis between these two subsets of myeloma cells.

### 5.5.1. Identification of CD138<sup>dim</sup> cells

The first functional assessment performed was to determine whether loss of CD138 was a transcriptionally influenced event, or if it was due to another post-translational shedding mechanism. RNA-seq analysis conclusively determined that loss of CD138 was due to transcriptional alteration in both myeloma cell lines as a result of culture with differentiated U937 cells and was not as a result of shedding through apoptosis or any other post-translational mechanism (Figure 5.1). Whilst difficult to conclusively determine in this research, it is reasonable to hypothesise two mechanisms of CD138<sup>dim</sup> cell expansion as a direct result of osteoclast-like co-culture. The first could be a result of preferential proliferative expansion of CD138<sup>dim</sup> cells that were already present in these cell lines prior to culture with differentiated U937 cells. The second could be as a result of co-culture-induced 'switching' of myeloma cells from a CD138<sup>bright</sup> phenotype to a CD138<sup>dim</sup> phenotype.

Some studies have previously speculated whether mature, terminally differentiated plasma cells have the capability to de-differentiate to a more immature phenotype with altered functional properties. This has been previously shown to occur in CD138<sup>bright</sup> primary myeloma cell cultures upon interaction with osteoclasts, causing these cells to de-differentiate to a more immature CD138<sup>dim</sup> phenotype<sup>305</sup>. There is also some evidence to suggest that there is a level of plasticity that can occur between mature and immature plasma cells. Studies have demonstrated that it is possible for plasma cells to revert between mature and immature phenotypes, with immature plasma cells exhibiting higher levels of chemoresistance<sup>407</sup>.

The unique expansion of CD138<sup>dim</sup> cells observed here goes some way to emulate these previous findings and suggests that differentiated U937 osteoclast-like cells are capable of inducing similar changes in the two myeloma cell lines used in this project. However, having identified CD138<sup>dim</sup> H929 and JN3 cells and establishing significant transcriptomic differences compared with CD138<sup>bright</sup> cells in response to osteoclast

co-culture it was of interest to further investigate the potential functional capacity that these cells possess.

A literature review established a list of immunophenotypic markers that span a range of biological functions that also have the potential to identify the stage of differentiation of each subset of myeloma cells. What was interesting was that no clear changes were observed in the transcriptional expression of any of the genes used in this analysis in CD138<sup>bright</sup> cells as a result of co-culture with differentiated U937 cells. However, there were some obvious changes in the expression of markers such as CD19 and CD45, both of which were transcriptionally activated, in CD138<sup>dim</sup> cells. Previous research has alluded to the fact that during the process of terminal differentiation from B-lymphocytes to antibody-secreting plasma cells, the expression of each of these markers is lost, with lack of CD19 expression being reported as a phenotypic hallmark of terminally differentiated malignant plasma cells<sup>408,409</sup>. This could indicate that these CD138<sup>dim</sup> cells are more immature in phenotype in comparison with CD138<sup>bright</sup> cells and are representative of cells that are not as advanced in differentiation as mature plasma cells are. Another study also demonstrated phenotypic plasticity between plasma cells by measuring CD19 expression, again inferring that plasma cells are capable of altering their phenotype. Functionally, this alludes to alterations in the alleged maturity of these cells, with patients found to have a less mature plasma cell phenotype having severely poorer prognosis compared with those with a classically defined mature phenotype<sup>410</sup>.

To supplement this, the widespread transcriptional repression of Ig-related genes is evident in CD138<sup>dim</sup> cells in both H929 and JIN3 cells also highlights the potential functional inhibition of antibody secretion that is most commonly associated with mature plasma cells. Thus, supporting the concept that CD138<sup>dim</sup> cells are representative of a subset at an earlier stage of cellular differentiation. This data could also infer an increased level of intra-clonal heterogeneity within the CD138<sup>dim</sup> subpopulation, compared with the CD138<sup>bright</sup> cells.

### 5.5.2. CD138<sup>dim</sup> cells are representative of a more migratory subpopulation of myeloma cells

The next functional assessment to be performed was relating to the potential migratory capacity of CD138<sup>dim</sup> cells. It has been speculated that myeloma cells lacking CD138 expression possess greater migratory potential which, when coupled with chemo-resistance following therapy and disease management, could lead to advanced disease dissemination throughout the bone marrow and to extramedullary sites post-treatment, thus accumulating in patient relapse. Cell surface adhesion molecules are critical mediators of migration, and signalling pathways related to adhesion were highlighted during IPA analysis. It was therefore of interest to investigate this further by analysing the expression of specific markers that are known to be key to adhesion and migration. It has been shown in Figure 5.4 that a number of the markers chosen for this portion of analysis were exclusively upregulated in CD138<sup>dim</sup> cells from both myeloma cell lines. This indicates that these cells possess greater adhesive capacity, which in terms of CD49e, CD45 and CXCR4 expression, is regulated at the transcriptional level and is detectable at the protein level through flow cytometry. The expression of CD11a and CD40 was not significantly upregulated in CD138<sup>dim</sup> cells as determined from RNA-seq data analysis but was significantly upregulated as determined through flow cytometry. The expression of CD11a in particular was high across each sample used in RNA-seq data analysis, which could indicate a post-transcriptional preference for CD11a protein expression in CD138<sup>dim</sup> cells compared with CD138<sup>bright</sup> myeloma cells.

Of the markers used in this section of analysis, CXCR4 is known to be a crucial regulator of migration in a number of cells of haematological origin, including myeloma<sup>166,411</sup>. Malignant plasma cells are known to upregulate CXCR4 to enhance their migratory capabilities. Surface CXCR4 is internalised in response to CXCL12 binding, thus reducing the surface expression of this marker to initiate a downstream signalling cascade. It is widely accepted that the CXCR4/CXCL12 signalling axis is a crucial regulator of myeloma cell migration<sup>166</sup>. Here, I have shown that CXCR4 expression is exclusive to CD138<sup>dim</sup> cells in both myeloma cell lines after co-culture with differentiated U937 cells. Interestingly CD138<sup>bright</sup> JN3 cells already have high levels of CXCR4 expression as determined by flow cytometry (Figure 5.5). Curiously,

this was eradicated in these cells upon co-culture with differentiated U937 cells, however its expression was maintained in CD138<sup>dim</sup> cells. Whilst this was an interesting anomaly, it is clear that there is a significant increase in CXCR4 expression in CD138<sup>dim</sup> cells in both myeloma cell lines when compared with CD138<sup>bright</sup> cells that have been cultured under the same conditions, with differentiated U937 cells. This was the basis to further pursue the migratory capabilities of both CD138<sup>bright</sup> and CD138<sup>dim</sup> H929 and JJN3 cells.

CXCL12 is the natural ligand that initiates the CXCR4 signalling cascade. This results in the activation of a number of intracellular proteins that leads to enhancement of the machinery that ultimately contributes to migration. These primarily include, JAK/Stat, p38/MAPK, Rho and Rac signalling, all of which have also been found to be exclusively upregulated in CD138<sup>dim</sup> myeloma cells in both H929 and JJN3 cell lines, as shown in Figure 4.11B<sup>412</sup>. Here I have shown that CD138<sup>dim</sup> cells, specifically from JJN3 origin, are capable of migrating in proportionally greater numbers when compared with CD138<sup>bright</sup> cells. This effect is surprisingly accentuated in the absence of a CXCL12 gradient, where CD138<sup>dim</sup> cells migrated in even greater numbers, in comparison with CD138<sup>bright</sup> cells. This indicated that CXCR4 signalling, whilst clearly critical in facilitating migration in these cells, is not the sole mechanism responsible for migration in these cells. The origin of both myeloma cell lines used in this research is comparable to the migratory effects we see here. For example, H929 cells were derived from the bone marrow of a myeloma patient at a plasmacytoma site<sup>239</sup>, whereas JJN3 cells were derived from the bone marrow of a patient with plasma cell leukaemia<sup>240</sup>. This could allude to the differences in migratory capacity that occurs between these two cell lines, as plasma cell leukaemia is a critically advanced myeloma-related malignancy where malignant plasma cells migrate to the peripheral circulation. This means that these cells could be more capable of migrating when compared with H929 cells, which were isolated from a patient with a less aggressive state of malignancy.

This migratory data was also complimented with the significant upregulation of CXCL8 expression and over-representation of its corresponding signalling pathway. This cytokine is a key signalling molecule that has been previously described as a master-regulator of the process of angiogenesis<sup>329</sup>. Angiogenesis is a critically important

process relating to the dissemination of myeloma cells throughout the bone marrow during early-stage disease propagation and also in a post-treatment/relapse setting, where drug resistant myeloma cells are actively redistributed throughout the bone marrow. As shown in Figure 5.7, there are a number of proteins associated with this pathway that are significantly differentially expressed that contribute to an overall prediction of activation for CXCL8 signalling. The proteins within this pathway that are common and exclusive to either cell line are shown in Supplementary Figure V. Myeloma cells are known to biologically influence the cells of their surrounding microenvironment within the bone marrow and have been shown to increase the secretion of CXCL8 from endothelial cells, which in turn results in local angiogenic enhancement<sup>180</sup>. Both primary myeloma cells and myeloma cell lines have been shown to be directly capable of secreting CXCL8<sup>356</sup>. This shows that culture with osteoclast-like cells induces transcriptional upregulation of CXCL8, which interestingly has also been shown to influence osteoclast activity<sup>356</sup>. Within this *in vitro* microenvironment, this could hint at the potential capabilities of these two cell types to directly influence one another in symbiotic fashion. Finally, coupled with CXCL8 upregulation, the receptor that initiates CXCL8 signalling, CXCR2, is also upregulated in CD138<sup>dim</sup> cells in both H929 and JJN3 cells. This also supports the hypothesis that CXCL8 signalling in this context could be performed in a both an autocrine and paracrine fashion, which has been previously alluded to in a number of studies<sup>413,414</sup>.

### 5.5.3. CD138<sup>dim</sup> cells are a more chemo-resistant subset of myeloma cells

The inevitable relapse that myeloma patients experience after treatment has been a long-standing issue that makes the curability of myeloma close to impossible in the current clinical climate. The presence of drug-resistant cells that are strongly reliant on the cells of the bone marrow microenvironment are responsible for re-populating this environment in a post-treatment scenario. Determination of the presence and load of minimal residual disease is directly associated with time until a patient's next relapse<sup>415</sup>. The identification of these chemo-resistant cells has been of interest in order to tackle the small number of malignant plasma cells that remain in the bone marrow after treatment, in order to fully eradicate the malignancy.

Whilst CD19 is not widely expressed on malignant plasma cells, it has been thought that a small population of CD19 expressing cells reside in the bone marrow after patient treatment. Some studies have shown promising clinical responses using CAR T-cell therapy against CD19<sup>374,416</sup>. A recent study also showed that the proportion of CD19 expressing myeloma cells is actually much greater than first thought, with up to 80% of myeloma cells isolated being shown to express CD19 at the reduced threshold being discussed in the study. Though the level of expression is exceptionally small and required super-resolution microscopy in order to determine quantifiable levels of CD19 expression, it was that CAR T-cell treatment against CD19 successfully and selectively destroyed these cells<sup>417</sup>. The data shown in this thesis also shows a significant and exclusive upregulation of CD19 in CD138<sup>dim</sup> cells in both H929 and JLN3 cell lines. This observation coupled with the fact that these CD138<sup>dim</sup> cells show much greater levels of resistance against bortezomib treatment provides another indication that these cells could be good candidates for treatment in a post-relapse scenario. Of course, lack of expression of CD138 means that this does not exclusively provide a specific therapeutic target that can be utilised against these cells. However, the data presented here coupled with the recent research demonstrating the success of CD19 as an anti-myeloma target, could provide further rationale to target these cells.

#### 5.5.4. Final conclusions

To summarise the findings of this final results chapter, I have demonstrated that loss of CD138 expression on the surface of two myeloma cell lines is a transcriptionally regulated event which is influenced by culture with osteoclast-like U937 cells. This is coupled with the inference that CD138<sup>dim</sup> myeloma cells could be representative of a more immature phenotype, given the upregulation of CD19 and CD45 and repression of immunoglobulin gene expression. Functionally I have also shown that CD138<sup>dim</sup> cells have greater adhesive and migratory capacity which is seemingly facilitated by both CXCR4 dependent and independent mechanisms. This is coupled with a significant upregulation of CXCL8 expression and subsequent signalling which can be related with a high potential to induce angiogenesis. In addition to this, it is evident that CD138<sup>dim</sup> cells are a more chemo-resistant subset of myeloma cells after treatment with bortezomib in comparison with CD138<sup>bright</sup> cells. Overall this functional assessment of CD138<sup>dim</sup> cells in H929 and JLN3 cells could implicate these cells as a phenotypically

distinct and relatively immature subset of myeloma cells. This subset has the potential to resist therapeutic intervention and disseminate further throughout the bone marrow in a post treatment scenario to ultimately cause disease relapse in patients. Further investigation of these unique cells would be highly beneficial to treat residual disease in myeloma patients and further understand the mechanisms behind osteoclast-induced disease activity which could lead to the identification of new therapeutic markers for future treatments.

## CHAPTER 6: GENERAL DISCUSSION

### 6.1. Summary of key findings

- ⇒ U937 cells, a myelomonocytic cell line derived from a histiocytic lymphoma, are capable of forming large, multinucleated osteoclast-like cells in response to treatment with PMA and  $1,25(\text{OH})_2\text{D}_3$ . These adherent cells were capable of expressing TRAP and RANK, and were able to resorb bone material, much like conventional osteoclasts.
- ⇒ H929 and JJN3 myeloma cell co-culture with differentiated osteoclast-like U937 cells induced an exclusive proportional expansion of  $\text{CD138}^{\text{dim}}$  myeloma cells.
- ⇒ Transcriptomic analysis between  $\text{CD138}^{\text{bright}}$  and  $\text{CD138}^{\text{dim}}$  myeloma cells in each cell line revealed substantial differences in their global transcriptomes with a vast number of differentially expressed genes being found in response to co-culture with differentiated U937 cells in  $\text{CD138}^{\text{dim}}$  myeloma cells.
- ⇒ Pathways that were over-represented within the  $\text{CD138}^{\text{dim}}$  dataset were related to a number of critical processes that are heavily involved in myeloma disease pathophysiology. These include clear associations with migration, survival, adhesion and angiogenesis.
- ⇒ Validation of 5 genes selected for analysis by qPCR were found to directly replicate the gene expression changes observed from RNA-seq data analysis.
- ⇒ Functional investigation of  $\text{CD138}^{\text{dim}}$  cells revealed that they are a more adhesive and chemo-resistant subset of myeloma cells with greater potential to induce angiogenesis and migrate through a Transwell® chamber than  $\text{CD138}^{\text{bright}}$  cells, after co-culture with differentiated U937 cells.

## 6.2. Final discussion

The work carried out in this project uniquely combined two valuable fields of research that have not yet been investigated in the literature: 1) The development of an *in vitro* osteoclast model and 2) the investigation of the impact that this model has on the behaviour of myeloma cells. Whilst the development of *in vitro* osteoclast models have been previously described before, some of which have become well-established, there have not been any reports in the literature of a cell line-based osteoclast model designed to specifically investigate osteoclast:myeloma cell interactions, function and role in disease pathology.

Firstly, I will discuss the development and characterisation of the *in vitro* osteoclast model used in this project. There are a number of methods that have been reported to successfully induce osteoclastogenesis in an *in vitro* setting. The majority of these methods have been developed using primary tissue obtained from human donors, where CD14<sup>+</sup> monocytes are isolated from peripheral circulation and induced to differentiate into osteoclasts using M-CSF and RANKL<sup>243,266,286,418,419</sup>. Whilst these methods are clearly well-established and have been successfully published in peer-reviewed journals, there are still limitations to using them. These include donor availability, biological variability between donors and the fact that these are time consuming procedures, often taking up to three weeks to differentiate osteoclasts from monocytic CD14<sup>+</sup> precursors.

There have also been reports of various cell lines that have osteoclastogenic capabilities and whilst these methods address some of the limitations associated with differentiating osteoclasts from primary human tissue. Arguably the most well established osteoclastogenic cell line is in fact derived from a murine source, RAW 264.7<sup>244-247</sup>. This is of course not entirely relatable to human physiology and makes the co-culture of cell lines derived from different species a less physiologically relevant model to use for the research of human disease. There are a small number of human cell lines that have previously been reported as having potential to differentiate into osteoclast-like cells, one of which was the U937 cell line that was chosen for this research. This cell line has been previously shown to exhibit osteoclast-like properties

upon treatment with PMA and  $1,25(\text{OH})_2\text{D}_3$ <sup>249,250</sup>. Cells treated in this fashion have also been shown to resorb dentine, much like conventional human osteoclasts. This was the rationale for choosing these cells in this research.

The role of vitamin D was also interesting in this *in vitro* scenario. In normal human physiology vitamin D is responsible for RANKL expression from osteoblasts through the vitamin D receptor (VDR). However, in the model discussed in this chapter, the formation of these osteoclast-like cells is induced in a monoculture setting. It would therefore be interesting to investigate whether the action of  $1,25(\text{OH})_2\text{D}_3$  is mediated through VDR binding and also whether this could induce RANKL expression in U937 cells. Given that I have shown that RANK expression is induced through treatment with PMA and  $1,25(\text{OH})_2\text{D}_3$ , it could be speculated that this could result in an autocrine signalling mechanism that causes RANKL to be secreted and reciprocally activate these cells, leading to the formation of osteoclast-like cells. Whilst the addition of M-CSF and RANKL did not induce osteoclastogenesis in U937 cells, the addition of RANKL following treatment with PMA was not explored. Therefore, this treatment strategy could infer whether RANKL is effective in inducing osteoclastogenesis in U937 cells treated with PMA and could also infer whether  $1,25(\text{OH})_2\text{D}_3$ -induced osteoclastogenesis could also be mediated through autocrine RANKL signalling. It is also important to recognise that in patients who are vitamin D deficient, this model would not be wholly representative of their osteoclast-related pathology. This is because vitamin D deficiency results in hyperparathyroidism, increased levels of serum parathyroid hormone, which subsequently causes negative regulation of bone mineralisation<sup>223</sup>.

Whilst this thesis focuses on the effects of a U937 osteoclast model on the behaviour of myeloma cells, conversely it would also be fascinating to investigate the effect of myeloma cells on this osteoclast model. It has been previously reported that myeloma cells are capable of secreting RANKL to promote the formation of osteoclasts<sup>420</sup>. It would therefore be an interesting experiment to perform to investigate whether this could also be the case in the osteoclast model I have presented here. Whilst direct treatment with RANKL did not lead to the formation of osteoclast-like U937 cells, the upregulation of RANK induced by PMA and  $1,25(\text{OH})_2\text{D}_3$  could indicate an autocrine

signalling mechanism that could lead to RANKL-induced osteoclastogenesis. If the addition of myeloma cells, or conditioned media from myeloma cell lines also contains higher concentrations of RANKL, it could be hypothesised that one might expect to see further activation of the osteoclastogenic process. This could manifest in greater numbers of U937 osteoclast-like cells, more nuclei within each individual osteoclast or an increase in resorptive activity.

The development of a reproducible osteoclast model using U937 cells presented in this thesis provided a unique and novel basis for investigating the biological effects of osteoclasts on myeloma cells. Osteoclasts are known to be critical mediators of myeloma pathogenesis and progression and have been shown to contribute heavily to myeloma cell survival and eventual migration<sup>204,254,421</sup>. Whilst the alterations in the cytokine composition of the bone marrow microenvironment are primarily influenced by stromal cells, there is evidence to suggest that osteoclasts are also mediators of cytokine secretion, and have been shown to influence secretion of cytokines such as IL-6 as a result of myeloma cell interaction in a viscous cycle of reciprocal cytokine signalling<sup>203</sup>. Co-culture between differentiated U937 osteoclast-like cells and H929 and JJN3 myeloma cells revealed a distinct and exclusive expansion of a subpopulation of CD138<sup>dim</sup> cells in both myeloma cell lines. The presence of CD138<sup>dim</sup> cells has been reported numerous times in the H929 cell line, however this was a unique observation in the JJN3 cell line<sup>41,42,274</sup>. The expansion of these cells was found to be exclusive to co-culture with osteoclast-like cells, which shows that there is seemingly a preferential influence that these osteoclast-like cells are able to exert on CD138<sup>dim</sup> myeloma cells. Given the close proximity of myeloma cells to osteoclasts in the bone marrow microenvironment of patients and the well-established effects that these two cell types exert upon one another, it was an interesting observation to explore further on both a basis of myeloma gene expression and subsequent functionality.

RNA-seq revealed substantial changes in the transcriptome of CD138<sup>dim</sup> cells after co-culture with differentiated U937 cells, with very few changes noted in comparison with CD138<sup>bright</sup> cells. Further analysis of these differentially expressed genes revealed a number of over-represented pathways from IPA analysis that linked these genes to a

number of pathways, that if activated or inhibited could potentially contribute to catastrophic aberrant signalling that could lead to propagation of disease progression. A vast number of pathways were found to be over-represented in the CD138<sup>dim</sup> dataset of both myeloma cell lines, with 104 pathways being commonly activated or inhibited in H929 and JJN3 cells. Validation using qPCR was also performed on five key genes that have been previously related to myeloma disease propagation, which demonstrated significant correlation between gene and protein expression determined in this fashion.

Functionally it was of interest to explore a number of key characteristics that were highlighted as a result of IPA pathway analysis. It is known that adhesion is a critical characteristic of myeloma cells that enables them to home to the bone marrow microenvironment. This is also a mechanism that heavily contributes to myeloma cell survival through the process of cell adhesion-mediated drug resistance (CAM-DR)<sup>161,276</sup>. Interestingly CAM-DR is also known to be associated with NF- $\kappa$ B signalling, which was another pathway found to be over-represented in the CD138<sup>dim</sup> dataset<sup>422</sup>. Adhesion to a number of specific cells within the bone marrow also induces the secretion and subsequent alteration of the cytokine milieu within this environment. For example, myeloma cell adhesion to bone marrow stromal cells induces a significant increase in a number of varying cytokines and chemokines that are secreted into the surrounding microenvironment<sup>159</sup>. It is clear that the CD138<sup>dim</sup> cells identified in this project significantly upregulate a number of adhesion markers which was further validated by flow cytometry. These markers are integrins that are known to contribute to myeloma cell homing, which is thought to be influenced by CXCR4 signalling<sup>276</sup>. Crucially, this signalling pathway was found to be upregulated at both the transcriptional and protein level, as determined by RNA-seq, IPA pathway analysis and flow cytometry. Given that CXCR4 has been previously shown to upregulate integrin activity to facilitate cancer cell homing in other malignancies, it would be reasonable to hypothesise that the upregulation of CXCR4 demonstrated here could be linked with the upregulation of integrin expression of the surface of these malignant plasma cells<sup>412,423</sup>. This would mean that CD138<sup>dim</sup> myeloma cells are representative of a more adhesive subset of malignant cells, a process which is known to enhance the ability of myeloma cells to survive within the bone marrow and resist therapeutic intervention

through CAM-DR. CXCR4 signalling has also been directly implicated in the upregulation of matrix metalloproteinase secretion, which again adds to the evidence that correlates this signalling pathway with migration and metastasis<sup>424</sup>. This was also a phenomenon that was noted in CD138<sup>dim</sup> cells both through RNA-seq, qPCR and IPA pathway analysis, where MMP2 and MMP9, two mediators of extracellular matrix degradation known to be secreted by myeloma cells was significantly enhanced.

CXCR4 signalling is arguably the most well-established pathway responsible for homing in a variety of cancers, including multiple myeloma<sup>166,411</sup>. Given that it was found to be upregulated in CD138<sup>dim</sup> myeloma cells in this project, coupled with what is already known about the capabilities of this pathway in directly influencing adhesion, extracellular matrix degradation, survival and migration, it was of interest to explore this functionally and investigate whether these cells possessed greater migratory capacity in comparison with CD138<sup>bright</sup> cells. This was indeed found to be the case, particularly in CD138<sup>dim</sup> cells derived from JJN3 cells. The migratory capacity of H929 cells did not significantly alter between either subset of CD138<sup>bright</sup> or CD138<sup>dim</sup> cells, with the same proportions of each subset being identified before and after migration. There was also no indication that either subset of H929 cells could migrate in the absence of a CXCL12 gradient, thus highlighting CXCR4/CXCL12 signalling is required to induce migration in these cells. In contrast, JJN3 cells were able to migrate in the absence and presence of a CXCL12 gradient. What was most fascinating about this experiment was that in approximation, equal proportions of CD138<sup>bright</sup> and CD138<sup>dim</sup> cells were able to migrate along a CXCL12 gradient. Considering that the proportion of CD138<sup>dim</sup> cells was only 5.4% before addition to a Transwell® chamber, this shows that there is a significant increase in the preferential migratory capacity of CD138<sup>dim</sup> JJN3 cell compared with CD138<sup>bright</sup> JJN3 cells. In addition to this there was an even greater proportion of CD138<sup>dim</sup> cells able to migrate in the absence of CXCR4/CXCL12 signalling. CXCR4 signalling has also been subject to therapeutic intervention, based on the concept of removing the reliance myeloma cells have on this signalling pathway for CAM-DR, adhesion and migration<sup>425</sup>. This data could provide a rationale for targeting this subset of myeloma cells with a CXCR4 inhibitor that could reduce their capabilities of resisting therapeutic intervention.

There is interest around the potential of CD138<sup>dim</sup> myeloma cells to be the cells responsible for disease dissemination across the bone marrow in a post-treatment setting. The data presented in this thesis certainly supports that hypothesis given that the CD138<sup>dim</sup> myeloma cells presented in this thesis are a more adhesive, migratory and chemo-resistant subset of myeloma cells. Despite being demonstrated in the reductionist setting of an *in vitro* microenvironment, this however does present the rationale for targeting these cells in a therapeutic strategy that could potentially deepen patient responses and prolong time until relapse.

### 6.2.1. Limitations to this study

Whilst this research presents a number of novel findings there are inevitably some limitations that must be discussed. The first of which are the limitations surrounding the use of cell lines in *in vitro* research. Cell lines are an incredibly valuable research tool that have been frequently used in research for many decades. However, there are limitations to their use, given that each cell line is derived from a single source, and are thus not capable of replicating the diverse and heterogenous nature of particular malignancies between patients. For example, in the case of myeloma research, virtually all known myeloma cell lines are derived from patients who possess IgH translocations. This means that patients who present with hyperdiploidy in myeloma are not represented in cell line research. These cell lines are also derived from patients who have experienced end-stage extramedullary disease, meaning that whilst they are capable of surviving outside of a bone marrow microenvironment and are thus suitable cells for immortalising in an *in vitro* setting, it could also be argued that these cells are not representative of the myeloma cells that are found within the tumour microenvironment of the bone marrow<sup>426</sup>.

The bone marrow is of course an extremely complex microenvironment composed of numerous cell types and non-cellular material. It is impossible to replicate this complexity in an *in vitro* setting and can therefore be regarded as a limitation in this research. Despite the positive results gained from differentiating U937 cells into cells that are capable of emulating a number of biological osteoclast features, there are a number of other cells within the bone marrow microenvironment that influence their

behaviour during the pathogenesis and progression of multiple myeloma. This of course could not be replicated in these experiments, meaning *in vitro* research must, by definition, be carried out in a reductionist fashion. However, attempts were made to add to the complexity of this *in vitro* bone marrow microenvironment in regard to incorporating an osteoblast and bone-like calcified matrix to these experiments.

Osteoblasts are a key cell type involved in the homeostatic regulation of bone remodelling and are found to be inhibited in multiple myeloma biology<sup>427</sup>. These cells are also primarily responsible for the production of the calcified matrix that ultimately forms bone tissue<sup>428</sup>. SAOS-2 cells are a well characterised cell line derived from an osteosarcoma that are known to have capabilities in secreting a bone-like calcified matrix<sup>429</sup>. Lutter *et al.* were able to demonstrate this phenomenon and culture osteoclasts, derived from CD14<sup>+</sup> monocytes and RAW264.7 cells, on the surface of this matrix to measure levels of bone resorption<sup>247</sup>. As part of an initial plan of experiments I was able to culture these cells and produce calcified matrices after treatment with ascorbic acid and glycerol  $\beta$ -phosphate that stained positively for calcium using a von kossa stain (Supplementary Figure VI). Whilst this was an initially interesting and positive result to incorporate into this *in vitro* microenvironment, it quickly became apparent that U937 cells were unable to adhere and differentiate into osteoclast-like cells on this surface, in the same manner as they were able to do so on tissue culture plastic. Therefore, this particular experiment was not investigated further.

One feature of myeloma cells that again adds to the difficulty of researching this disease in an *in vitro* setting, is that given their heavy reliance on the bone marrow microenvironment for survival, malignant plasma cells are very difficult to sustain in an *ex vivo* setting. It was an aim of this project to determine whether culture with differentiated U937 cells could sustain the survival of primary myeloma cell in an *ex vivo* setting. However, despite ethical approval being obtained for such experiments the availability of suitable samples was scarce. The samples that were received had been derived from patients who had already been previously treated. Therefore, the initial viability and plasma cell concentration of these samples was very low, meaning

that the determination of the influence of these osteoclast-like cells on primary myeloma cells was difficult to establish.

Another limitation that has already been alluded to is the potential for cellular contamination involving the RNA-seq experiment described in Chapter 4. Flow cytometry is deemed a sufficiently sensitive technique that has very good capabilities of identifying distinct populations of cells and is the method of choice that is used during quantification of minimal residual disease in a number of malignancies including myeloma. However, there are some inherent inefficiencies when it is coupled with cell sorting that could lead to cellular contamination of sorted samples. In order to investigate this further to ensure that no contamination was taking place in these experiments, sorted samples were isolated and sent for STR genotyping, which was performed by Public Health England. The results of this concluded that there was no cellular contamination present in any sorted sample used for RNA-seq, except for CD138<sup>dim</sup> H929 cells (HUCD). This was of course a cause for concern as the cellular contaminant in this case was from U937 cells that were present in the co-culture. The limitation within this particular assay was that there was no way to quantify the extent of contamination as the assay was performed using PCR. Therefore, any amount of contaminant DNA present within the sample at quantities higher than a picogram would be sufficient to be amplified and detected. Given the fact that there was no contamination detected in any other co-culture sample and the fact that there were no obvious cellular contaminants detected by flow cytometry, it is fair to suggest that the level of contamination detected in CD138<sup>dim</sup> H929 cells was minimal.

As a further layer of evidence to imply that the subsequent RNA-seq data analysis was not affected by this, an RNA-seq dataset obtained from U937 cells that had been treated with PMA was obtained from NCBI GEO<sup>367</sup>. The 500 most highly expressed genes from this U937 dataset were compared with the corresponding CD138<sup>dim</sup> datasets from H929 and JN3 cells. Of course, if the contamination of U937 cells within these samples was very high, there would be a high level of similarity between these datasets. However, that was not the case, with only 31 genes being found to be common to all three cell lines and the majority of common genes being shared between both myeloma cell lines. Whilst of course, performing this analysis with RNA-

seq data obtained from the U937 cells used in this project would have been the ideal comparison to make, this was unfortunately not possible. However, given the data presented and the evidence discussed here, it is reasonable to imply that any contamination detected was minimal and that would not have substantially affected any subsequent RNA-seq analysis as a result.

### 6.2.2. Future work and clinical impact

Multiple myeloma is still an incurable malignancy during which patients always relapse after treatment. This is due to a resistant subset of myeloma cells that are capable of evading treatment-induced apoptosis and ultimately re-disseminating throughout the bone marrow. The identity of these cells has long been debated, with CD138<sup>dim</sup> cells being proposed as a subtype of myeloma cells that could be responsible for this phenomenon. Targeting these cells could then potentially lead to a deeper treatment response, prolonged survival and even eradicate the inevitable relapse seen in so many patients.

The data presented in this thesis has shown that CD138<sup>dim</sup> myeloma cells are a chemo-resistant subtype of myeloma cells that have greater adhesive and migratory properties than CD138<sup>bright</sup> cells. According to RNA-seq analysis these cells also appear to upregulate a vast array of molecular pathways that could contribute to a more aggressive pathophysiology. This makes a suitable rationale for investigating these cells further as targets for treatment. Of course, the mechanisms by which these cells demonstrate these characteristics have not been widely explored in this project. However, future work that could be performed to configure these mechanisms will be suggested here.

There is continued speculation around the number, proportions, origin and role of CD138<sup>dim</sup> cells in myeloma. Previous research has shown that the proportions of these cells *in vivo* can vary dramatically, it also raises the question as to why these cells do not become the dominant clone in myeloma. It can be speculated perhaps that this subclonal population are feeder cells for CD138<sup>bright</sup> malignant plasma cells. Given that I have shown the significant upregulation of numerous pathogenic markers through

RNA-seq analysis, it could be speculated that expression of these markers could contribute to enhancing the ability of mature CD138<sup>bright</sup> myeloma cells to exert their malignant effects within the bone marrow. These CD138<sup>dim</sup> cells are also found in greater numbers in more advanced stages of disease. Could this be a result of CD138 shedding from the surface of mature myeloma cells, or could this be a stage of disease during which the underlying CD138<sup>dim</sup> cells begin to propagate and become a more dominant clone? Another interesting piece of research would be to investigate the secretory profile of these cells through the analysis of co-culture supernatants. This could lead to an assessment into the secretory pattern of enzymes such as MMPs. Given that I have shown through qPCR that MMP2 is upregulated it would be interesting to see if there are other MMP enzymes that are also upregulated which could add to previous data showing that an upregulation of MMP's in myeloma leads to enhanced degradation of the extracellular matrix, thus contributing to the increased osteolytic effects that are seen in patients. This could also reveal a potential mechanism behind the reduction of CD138 expression in these myeloma cells and help to answer the question as to whether these cells are in fact an immature stem-like plasma cell or whether they are more mature malignant plasma cells that have had CD138 proteolytically cleaved.

Currently it is still difficult to determine the origin and exact role of these cells *in vivo*, but these are interesting questions that could lead to greater understanding of the evolution of the disease course of myeloma and could also lead to the discovery of new therapeutic targets that could hinder disease progression.

It is evident that CD138<sup>dim</sup> cells are capable of migrating in the presence and absence of CXCR4 and determining the additional mechanisms that lead to this would be a valuable addition to this research. Myeloma cells that have an enhanced migratory capacity are able to disseminate throughout the bone marrow and are also able to spread to extramedullary sites in late stage disease, which results in a very poor patient prognosis. I have shown that CD138<sup>dim</sup> cells are capable of migrating in the presence of a CXCL12 gradient, indicating that CXCR4 signalling is a key mediator of migration in these cells. This is coupled with the fact that these cells display significantly higher levels of chemoresistance against the frontline myeloma therapy,

bortezomib. It would therefore be of interest to investigate whether these two characteristics could be intrinsically linked. Especially given the fact that inhibition of CXCR4 has been shown to increase the sensitivity of myeloma cells to currently established therapy<sup>425</sup>. It is also interesting that CD138<sup>dim</sup> JN3 cells are capable of migrating in the absence of CXCL12 induced CXCR4 signalling. Given that I have also shown that these cells are capable of upregulating adhesion markers such as CD49e, CD40, CD45 and CD11a in addition to CXCR4, this could be speculated as an alternative mechanism through which these cells are capable of migrating in the absence of a CXCL12 gradient. It would be interesting to explore whether these adhesion markers contribute to the alternative migratory mechanisms that are present in JN3 CD138<sup>dim</sup> cells.

I have also shown that CXCL8 signalling is significantly upregulated, which is well-established as an angiogenesis-inducing pathway. There have also been reports that correlate increased angiogenesis with an increased load of circulating myeloma cells, thus inferring poorer prognosis in patients<sup>430</sup>. Whilst it is clear that the expression of a number of proteins associated with CXCL8 signalling and angiogenesis are upregulated in CD138<sup>dim</sup> cells described in this research, it would be of further interest to establish whether this could functionally be the case. For example, there are commercially available functional *in vitro* assays that are capable of measuring the angiogenesis-inducing capabilities of various cell types. Such assays have been previously used to measure the capabilities of myeloma cells to induce angiogenesis in the presence of osteoclastic microenvironments<sup>431</sup>. It would be interesting to explore whether the enhancement of CXCL8 signalling as a result of osteoclast co-culture contributes to an acquired preferential ability of CD138<sup>dim</sup> cells to induce angiogenesis. This would provide further evidence to implicate CD138<sup>dim</sup> cells in the propagation of migration and bone marrow niche alteration, in comparison with CD138<sup>bright</sup> cells.

The model I have presented in this thesis is robust, reproducible and representative of human osteoclasts. Although, there is of course scope for improvement. The bone marrow microenvironment is incredibly complex and replicating that level of complexity within an *in vitro* model would be impossible. However, the current inability to sustain primary myeloma samples in long term cultures also presents an

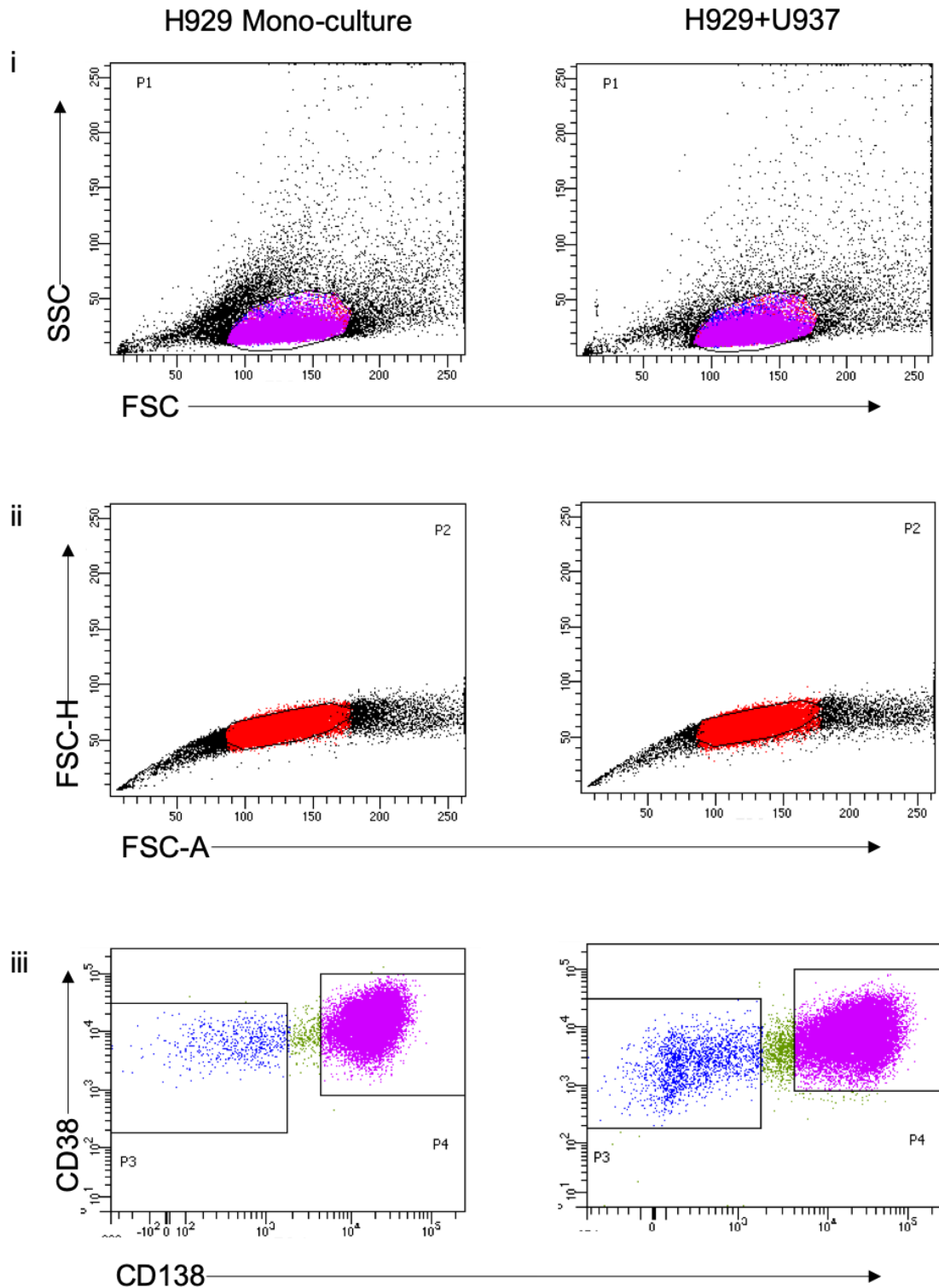
opportunity to sufficiently enhance the complexity of *in vitro* models to try to accommodate this. It would therefore be interesting to investigate and develop this model to incorporate a higher level of physiological complexity, for example using 3D modelling to further emulate the physiological structure of the bone marrow microenvironment. There have been attempts to create such *in vitro* models using 3D cell culture technology, but with a general lack of reproducible osteoclast representation<sup>432,433</sup>. One model, however, has utilised osteoclasts in a 3D model such as this, however the dilemma still arises as to whether the bone marrow cells used within such a model should be patient-derived or whether cell lines should be used, which would improve reproducibility<sup>434</sup>.

Expanding the model presented in this thesis to become more physiologically relevant in this way could positively impact on its ability to be used in the wider context of patient care. This could provide a foundation for use in pre-clinical testing with innovative therapies such as immunotherapy (CAR-T cell therapy), which could reveal more information about the mechanisms behind chemoresistance in myeloma and also be used as a predictor of a patient's response to therapy. Another benefit of developing this approach, if such a model were capable of sustaining long term myeloma cell culture, would be the direct incorporation of the patients' own normal immune cell composition. Although of course the immune composition of most myeloma patients is compromised, there is evidence to suggest that patients with long-term disease experience some level of immune recovery<sup>435</sup>. This would also provide more physiological relevance and address issues related to the use of immunodeficient *in vivo* murine models in myeloma research.

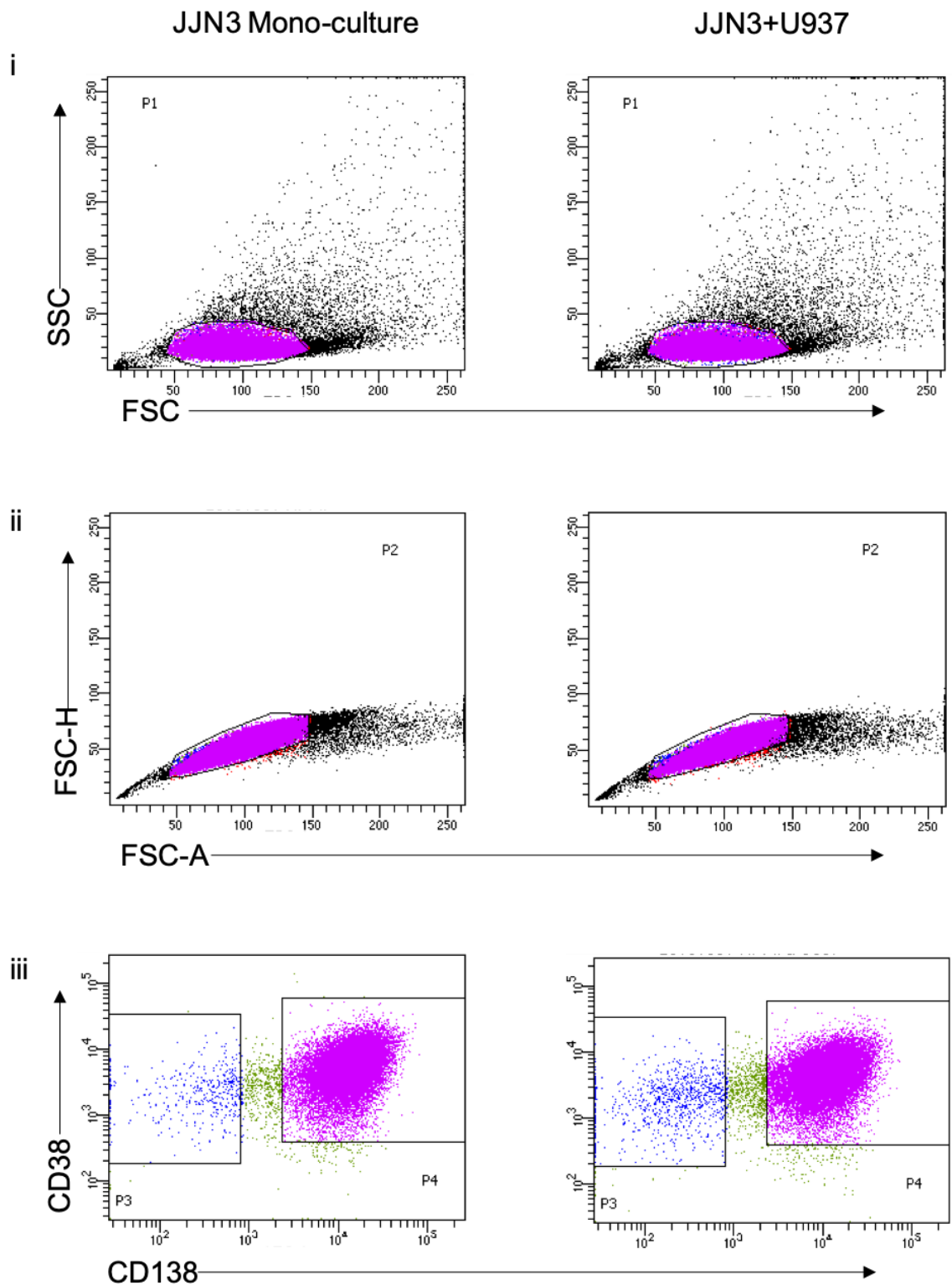
Overall this research has produced a novel co-culture model that is representative of the osteoclastic compartment of the bone marrow niche in multiple myeloma. This has led to the identification of an osteoclast-induced expansion of a proportion of myeloma cells that are CD138<sup>dim</sup> that display significantly altered transcriptomic features in comparison with CD138<sup>bright</sup> cells. The differentially expressed genes identified as a result of RNA-seq analysis has revealed the induction of several pathways that contribute to survival, adhesion, angiogenesis and migration. Further functional assessments of these pathways have led to the conclusion that CD138<sup>dim</sup>

myeloma cells have the potential to be responsible for the chemo-resistant subset of myeloma cells that have greater capacity to migrate, which could highlight these cells as useful therapeutic targets which could prolong or even prevent patient relapse. Additional investigation of these cells could lead to the identification of more novel targets that could further unravel the mechanisms that contribute to myeloma disease pathology.

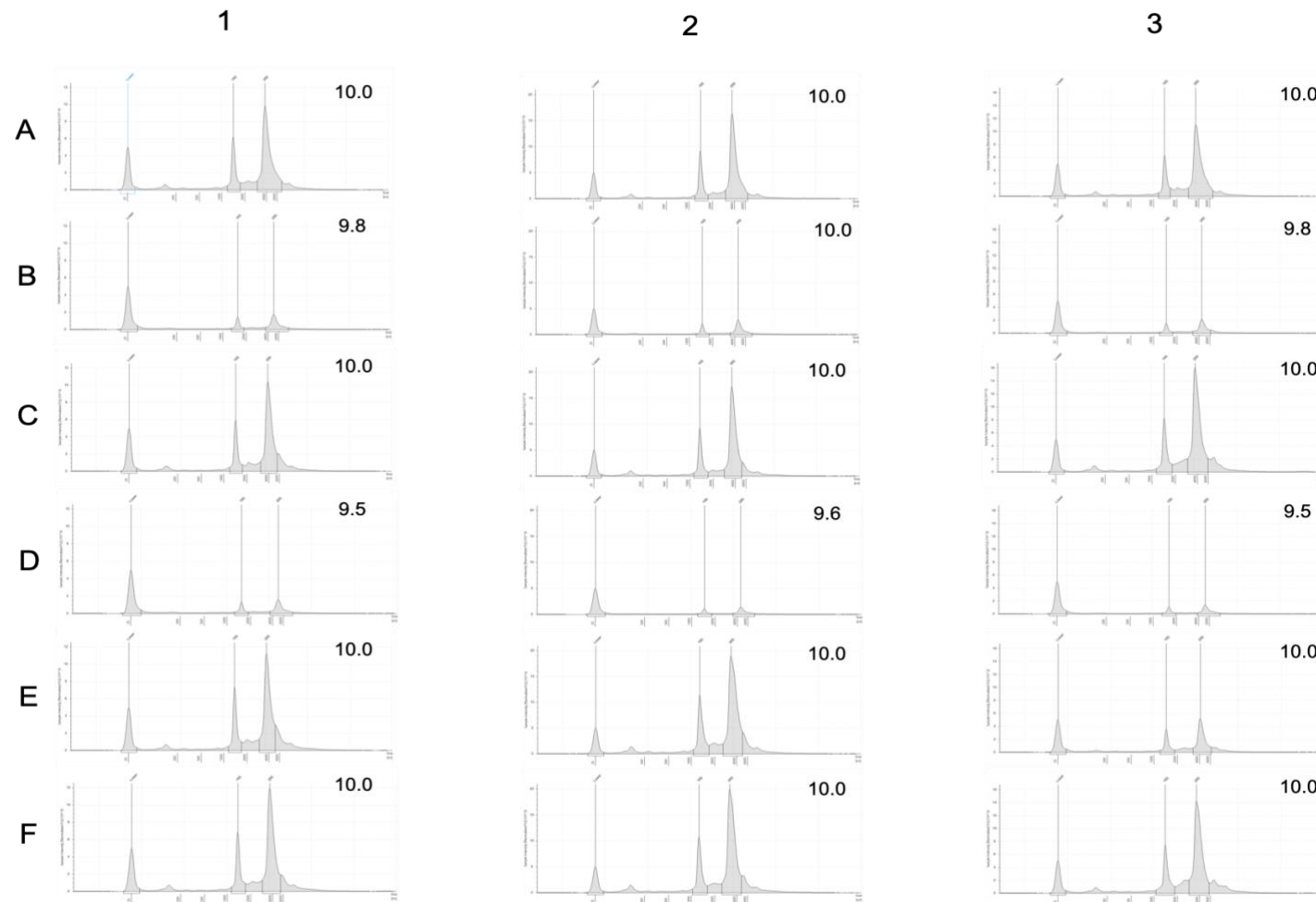
## Supplementary Data



**Supplementary Figure 1a. Gating strategy used to sort CD138<sup>bright</sup> and CD138<sup>dim</sup> H929 cells.** Live cells were identified using forward vs side scatter plots (i), single cells were then identified using forward scatter height vs area plots (ii) and finally CD138 and CD38 expression was determined with CD138<sup>bright</sup> and CD138<sup>dim</sup> myeloma cells being sorted into separate collection tubes for subsequent RNA extraction.



**Supplementary Figure 1b. Gating strategy used to sort CD138<sup>bright</sup> and CD138<sup>dim</sup> JJN3 cells.** Live cells were identified using forward vs side scatter plots (i), single cells were then identified using forward scatter height vs area plots (ii) and finally CD138 and CD38 expression was determined with CD138<sup>bright</sup> and CD138<sup>dim</sup> myeloma cells being sorted into separate collection tubes for subsequent RNA extraction.



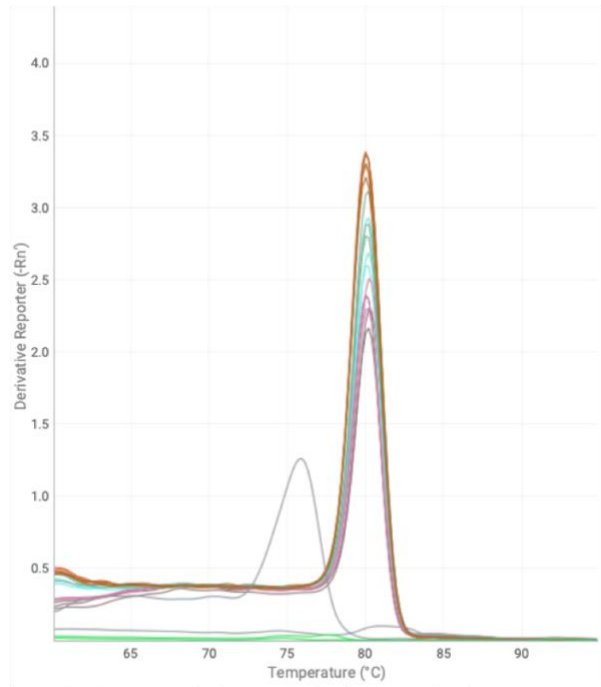
**Supplementary Figure II. RIN plots produced from each RNA sample used in RNA-seq and qPCR experiments.** All three biological replicates were analysed for RNA integrity, the samples are coded as follows: (A) HUCB, (B) HUCD, (C) HMCB, (D) JUCB, (E) JUCD, (F) JMCB. RIN scores are displayed for each sample on the corresponding graph.

IPA Overrepresented Pathway	HMCB vs HUCD			JMCB vs JUCD		
	-log(p-value)	Ratio	z-score	-log(p-value)	Ratio	z-score
<i>14-3-3-mediated Signalling</i>	3.03	0.23	3.53	3.97	0.24	2.92
<i>Actin Cytoskeleton Signalling</i>	5.32	0.24	3.06	3.81	0.21	3.09
<i>Actin Nucleation by ARP-WASP Complex</i>	5.81	0.35	2.84	3.45	0.28	3.74
<i>Acute Phase Response Signalling</i>	2.96	0.21	2.87	3.52	0.22	4.56
<i>Adrenomedullin Signalling Pathway</i>	3.48	0.21	3.28	4.75	0.23	4.03
<i>Agrin Interactions at Neuromuscular Junction</i>	2.80	0.26	2.52	2.20	0.23	3.50
<i>Antioxidant Action of Vitamin C</i>	3.55	0.25	-2.24	2.05	0.21	-2.00
<i>Antiproliferative Role of Somatostatin Receptor 2</i>	1.73	0.21	2.14	4.16	0.28	2.50
<i>Apelin Cardiomyocyte Signalling Pathway</i>	1.72	0.20	3.27	3.50	0.24	2.12
<i>Apelin Endothelial Signalling Pathway</i>	2.73	0.22	3.02	4.40	0.25	2.69
<i>B Cell Receptor Signalling</i>	5.17	0.24	4.52	7.13	0.26	3.59
<i>Cardiac Hypertrophy Signalling</i>	2.91	0.20	3.81	5.92	0.23	5.46
<i>Cardiac Hypertrophy Signalling (Enhanced)</i>	4.62	0.19	5.35	9.73	0.23	6.22
<i>CCR3 Signalling in Eosinophils</i>	2.52	0.21	3.27	3.38	0.23	2.68
<i>CD28 Signalling in T Helper Cells</i>	3.16	0.23	4.08	2.73	0.22	3.13
<i>Chemokine Signalling</i>	2.28	0.24	2.98	3.67	0.28	4.15
<i>Cholecystokinin/Gastrin-mediated Signalling</i>	7.88	0.33	3.33	4.40	0.26	4.43
<i>CNTF Signalling</i>	3.10	0.27	2.52	1.40	0.31	2.24
<i>CREB Signalling in Neurons</i>	2.22	0.19	3.65	2.45	0.24	3.00
<i>CXCR4 Signalling</i>	5.75	0.26	3.36	6.14	0.26	3.67
<i>Dendritic Cell Maturation</i>	2.49	0.20	5.33	8.14	0.39	4.64
<i>EGF Signalling</i>	3.00	0.27	2.83	2.34	0.24	2.50
<i>Endocannabinoid Developing Neuron Pathway</i>	1.58	0.19	2.45	3.22	0.23	2.20
<i>Endothelin-1 Signalling</i>	3.20	0.21	2.47	4.42	0.23	2.41
<i>Ephrin Receptor Signalling</i>	4.14	0.23	3.66	3.47	0.22	4.85
<i>ErbB Signalling</i>	2.28	0.22	3.13	3.53	0.25	3.00
<i>ErbB2-ErbB3 Signalling</i>	2.28	0.24	2.36	2.82	0.25	2.18
<i>ErbB4 Signalling</i>	2.83	0.25	2.52	2.61	0.24	2.18
<i>ERK/MAPK Signalling</i>	3.88	0.22	3.02	4.21	0.22	3.51
<i>Estrogen-Dependent Breast Cancer Signalling</i>	3.11	0.26	2.83	2.91	0.24	2.84
<i>Fc Epsilon RI Signalling</i>	2.73	0.22	3.66	3.64	0.24	2.65
<i>Fcγ Receptor-mediated Phagocytosis in Macrophages and Monocytes</i>	7.59	0.35	4.00	6.78	0.33	4.13
<i>FcγRIIB Signalling in B Lymphocytes</i>	2.73	0.24	2.36	3.30	0.26	2.18
<i>FLT3 Signalling in Hematopoietic Progenitor Cells</i>	3.14	0.25	3.67	2.95	0.24	3.41

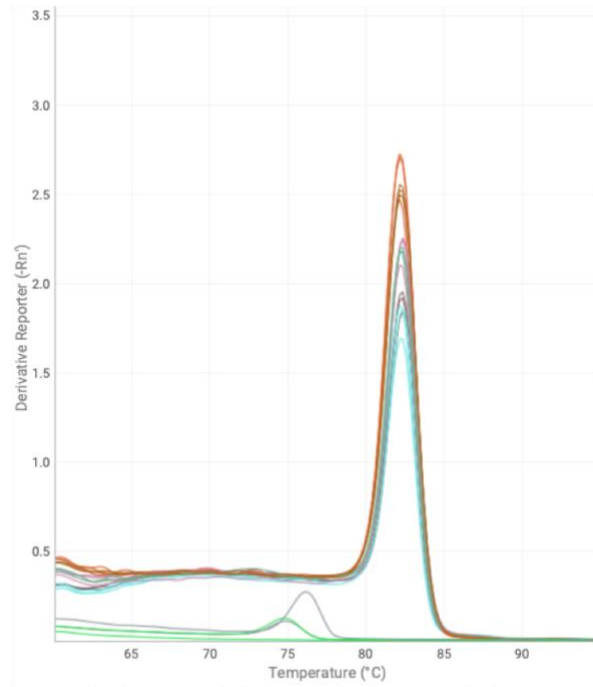
<i>fMLP Signalling in Neutrophils</i>	7.00	0.30	3.67	5.50	0.27	3.53
<i>G Beta Gamma Signalling</i>	2.23	0.21	3.00	3.42	0.24	3.14
<i>GDNF Family Ligand-Receptor Interactions</i>	2.21	0.23	2.50	2.36	0.23	3.00
<i>Glioma Signalling</i>	4.91	0.27	2.40	5.11	0.30	2.99
<i>GM-CSF Signalling</i>	6.58	0.35	2.12	4.71	0.30	2.99
<i>GNRH Signalling</i>	1.92	0.19	3.65	3.23	0.23	2.52
<i>GP6 Signalling Pathway</i>	3.10	0.23	3.65	3.52	0.22	4.80
<i>Growth Hormone Signalling</i>	3.00	0.26	2.84	5.01	0.30	2.20
<i>Gα12/13 Signalling</i>	3.80	0.24	3.05	4.44	0.25	3.31
<i>Gαq Signalling</i>	7.37	0.28	3.48	4.90	0.24	3.21
<i>HGF Signalling</i>	3.42	0.24	3.14	6.69	0.30	3.29
<i>HMGB1 Signalling</i>	4.08	0.23	4.56	4.40	0.23	4.75
<i>Huntington's Disease Signalling</i>	2.99	0.20	2.74	1.37	0.16	2.60
<i>IGF-1 Signalling</i>	3.22	0.24	2.13	2.41	0.22	2.68
<i>IL-1 Signalling</i>	1.68	0.21	3.32	4.07	0.28	3.36
<i>IL-17A Signalling in Airway Cells</i>	2.28	0.24	2.36	1.75	0.21	3.00
<i>IL-17A Signalling in Gastric Cells</i>	1.48	0.28	2.24	4.05	0.44	2.83
<i>IL-2 Signalling</i>	3.91	0.29	2.52	3.20	0.27	3.15
<i>IL-23 Signalling Pathway</i>	2.53	0.27	2.32	2.25	0.25	2.32
<i>IL-3 Signalling</i>	3.69	0.27	3.00	5.31	0.30	2.89
<i>IL-6 Signalling</i>	6.34	0.29	3.68	5.36	0.27	4.12
<i>IL-8 Signalling</i>	10.40	0.30	3.84	11.50	0.30	5.86
<i>Inflammasome Pathway</i>	2.66	0.40	2.83	2.75	0.40	2.83
<i>iNOS Signalling</i>	1.62	0.24	3.32	3.66	0.33	3.87
<i>Integrin Signalling</i>	7.89	0.27	2.67	4.68	0.22	4.82
<i>Leukocyte Extravasation Signalling</i>	7.49	0.27	3.00	10.70	0.30	5.25
<i>LPS-stimulated MAPK Signalling</i>	4.13	0.28	3.53	3.94	0.27	2.86
<i>Macropinocytosis Signalling</i>	3.36	0.26	2.83	4.44	0.28	2.52
<i>Neuroinflammation Signalling Pathway</i>	4.85	0.21	4.82	8.68	0.25	5.18
<i>Neurotrophin/TRK Signalling</i>	1.83	0.22	2.18	1.66	0.21	2.32
<i>NF-κB Activation by Viruses</i>	7.09	0.34	3.18	4.83	0.29	3.14
<i>NF-κB Signalling</i>	3.90	0.23	4.22	4.56	0.23	4.53
<i>NGF Signalling</i>	3.89	0.25	3.65	3.06	0.23	3.53
<i>NRF2-mediated Oxidative Stress Response</i>	6.04	0.25	2.41	2.58	0.19	2.36
<i>Oncostatin M Signalling</i>	4.36	0.37	2.32	3.33	0.33	3.46
<i>Opioid Signalling Pathway</i>	3.07	0.20	3.86	3.93	0.21	3.18

<i>Ovarian Cancer Signalling</i>	1.88	0.19	2.52	3.21	0.22	3.58
<i>P2Y Purigenic Receptor Signalling Pathway</i>	2.98	0.22	3.16	5.90	0.27	3.09
<i>p38 MAPK Signalling</i>	3.82	0.25	3.40	3.31	0.24	3.13
<i>p70S6K Signalling</i>	4.75	0.26	2.33	4.27	0.25	2.61
<i>PAK Signalling</i>	2.77	0.23	2.45	3.33	0.24	3.67
<i>Pancreatic Adenocarcinoma Signalling</i>	4.99	0.27	2.75	3.29	0.23	2.84
<i>Paxillin Signalling</i>	6.34	0.30	3.27	5.74	0.28	3.92
<i>Phospholipase C Signalling</i>	3.82	0.21	2.90	6.09	0.23	3.43
<i>PI3K Signalling in B Lymphocytes</i>	7.38	0.30	5.10	4.62	0.25	3.29
<i>PKC<math>\delta</math> Signalling in T Lymphocytes</i>	1.80	0.19	4.16	3.06	0.21	2.69
<i>Production of Nitric Oxide and Reactive Oxygen Species in Macrophages</i>	8.22	0.28	3.71	9.18	0.28	4.44
<i>PTEN Signalling</i>	4.42	0.26	-2.48	3.17	0.23	-2.12
<i>Rac Signalling</i>	5.61	0.28	2.74	3.83	0.24	4.16
<i>RANK Signalling in Osteoclasts</i>	2.56	0.23	3.58	3.49	0.25	3.40
<i>Regulation of Actin-based Motility by Rho</i>	1.55	0.20	2.18	1.68	0.20	3.15
<i>Renin-Angiotensin Signalling</i>	4.30	0.26	3.65	6.79	0.29	4.24
<i>Role of NFAT in Cardiac Hypertrophy</i>	2.43	0.19	3.16	4.36	0.22	3.70
<i>Role of NFAT in Regulation of the Immune Response</i>	5.24	0.25	4.44	4.36	0.22	3.70
<i>Role of Pattern Recognition Receptors in Recognition of Bacteria and Viruses</i>	3.16	0.22	4.20	7.71	0.28	4.24
<i>SAPK/JNK Signalling</i>	2.93	0.24	2.75	3.89	0.25	2.75
<i>Signalling by Rho Family GTPases</i>	6.20	0.24	2.94	7.04	0.24	4.81
<i>Synaptogenesis Signalling Pathway</i>	2.81	0.19	3.68	3.14	0.19	4.20
<i>Tec Kinase Signalling</i>	5.20	0.25	3.31	12.10	0.33	4.81
<i>TGF-<math>\beta</math> Signalling</i>	2.03	0.22	2.24	3.27	0.25	2.24
<i>Th1 Pathway</i>	2.10	0.20	2.71	3.56	0.23	2.60
<i>Thrombin Signalling</i>	5.65	0.24	2.90	4.68	0.22	2.60
<i>Thrombopoietin Signalling</i>	2.62	0.25	2.52	5.14	0.32	2.71
<i>Toll-like Receptor Signalling</i>	1.53	0.21	2.89	5.03	0.32	3.15
<i>TREM1 Signalling</i>	6.00	0.35	5.10	8.14	0.39	4.64
<i>UVA-Induced MAPK Signalling</i>	3.72	0.25	3.13	6.20	0.30	2.24
<i>UVB-Induced MAPK Signalling</i>	2.34	0.25	2.50	4.32	0.31	2.52
<i>VEGF Family Ligand-Receptor Interactions</i>	2.87	0.24	2.40	1.74	0.20	2.18
<i><math>\alpha</math>-Adrenergic Signalling</i>	1.50	0.20	2.67	3.75	0.26	2.50

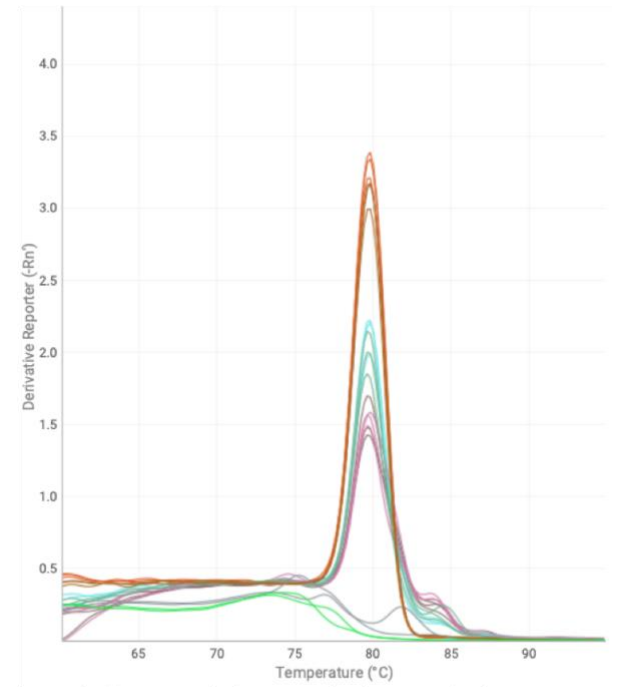
**Supplementary Table I. A table containing a list of the commonly overrepresented pathways in both H929 and JJN3 CD138<sup>dim</sup> cells when compared with respective CD138<sup>bright</sup> monoculture controls.**

**A**

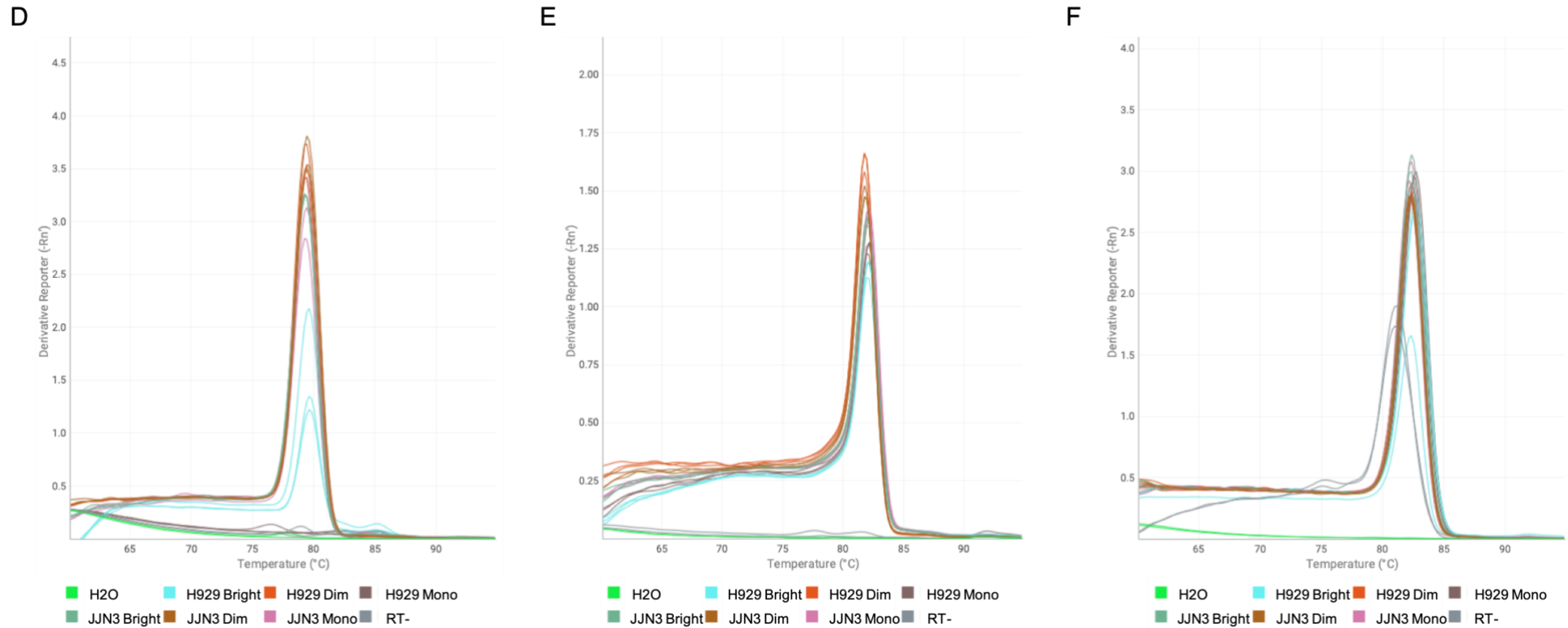
■ H2O    ■ H929 Bright    ■ H929 Dim    ■ H929 Mono  
■ JJN3 Bright    ■ JJN3 Dim    ■ JJN3 Mono    ■ RT-

**B**

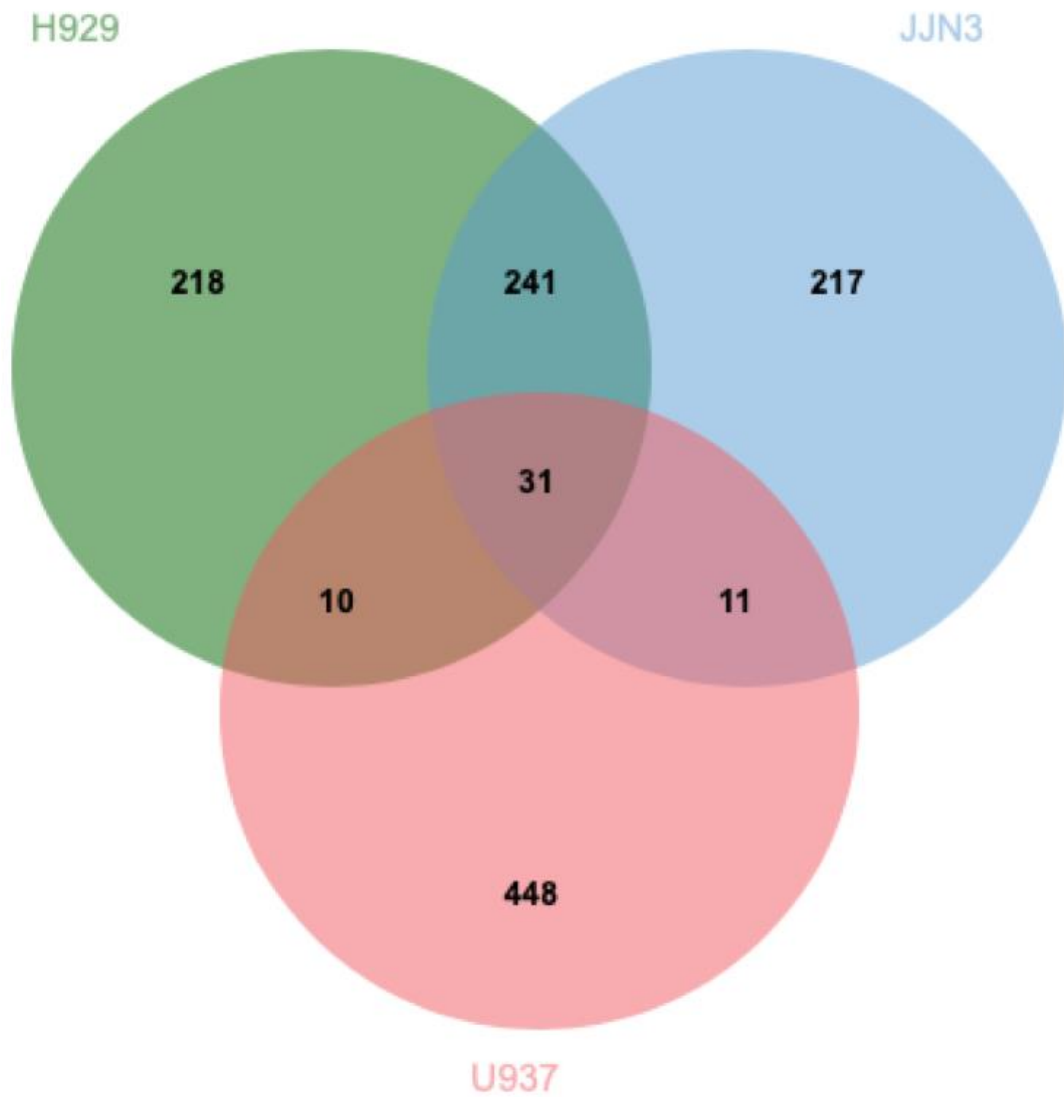
■ H2O    ■ H929 Bright    ■ H929 Dim    ■ H929 Mono  
■ JJN3 Bright    ■ JJN3 Dim    ■ JJN3 Mono    ■ RT-

**C**

■ H2O    ■ H929 Bright    ■ H929 Dim    ■ H929 Mono  
■ JJN3 Bright    ■ JJN3 Dim    ■ JJN3 Mono    ■ RT-



**Supplementary Figure III. Melt curves produced from a qPCR experiment for each gene and sample analysed for validation of gene expression.** Melt curves were produced for each gene targeted for validation, to determine primer target specificity. They are listed as follows: (A) SPP1, (B) SYK, (C) CXCL8, (D) MMP2, (E) CCL2, (F) GAPDH.



**Supplementary Figure IV. A Venn diagram illustrating the commonly expressed genes between CD138<sup>dim</sup> cells from H929 and JJN3 cells and U937 cells treated with PMA.** The top 500 highest differentially expressed genes from CD138<sup>dim</sup> H929 and JJN3 cells co-cultured with differentiated U937 cells were compared with the top 500 highest expressed genes from U937 cells treated with PMA. As RNA-seq was not performed on U937 cells in this research, the U937 dataset was obtained from NCBI GEO datasets which were published by Haney, M.S *et al*, 2018 <sup>367</sup>.





## BIBLIOGRAPHY

1. Solly S. Remarks on the pathology of mollities ossium; with cases. *Med Chir Trans.* 1844;27:435-498.438.
2. Noone AM, Howlader N, Krapcho M, et al. SEER Cancer Statistics Review 1975-2015, National Cancer Institute. Bethesda, MD; 2018.
3. Kyle RA, Rajkumar SV. Multiple myeloma. *N Engl J Med.* 2004;351(18):1860-1873.
4. Palumbo A, Anderson K. Multiple myeloma. *N Engl J Med.* 2011;364(11):1046-1060.
5. Moreau P, Attal M, Facon T. Frontline therapy of multiple myeloma. *Blood.* 2015;125(20):3076-3084.
6. Manier S, Sacco A, Leleu X, Ghobrial IM, Roccaro AM. Bone marrow microenvironment in multiple myeloma progression. *J Biomed Biotechnol.* 2012;2012:157496.
7. Anderson KC, Auclair D, Kelloff GJ, et al. The Role of Minimal Residual Disease Testing in Myeloma Treatment Selection and Drug Development: Current Value and Future Applications. *Clin Cancer Res.* 2017;23(15):3980-3993.
8. Kumar SK, Therneau TM, Gertz MA, et al. Clinical course of patients with relapsed multiple myeloma. *Mayo Clin Proc.* 2004;79(7):867-874.
9. Ferlay J, Shin HR, Bray F, Forman D, Mathers C, Parkin DM. Estimates of worldwide burden of cancer in 2008: GLOBOCAN 2008. *Int J Cancer.* 2010;127(12):2893-2917.
10. Kim K, Lee JH, Kim JS, et al. Clinical profiles of multiple myeloma in Asia-An Asian Myeloma Network study. *Am J Hematol.* 2014;89(7):751-756.
11. Boyd KD, Ross FM, Chiecchio L, et al. Gender disparities in the tumor genetics and clinical outcome of multiple myeloma. *Cancer Epidemiol Biomarkers Prev.* 2011;20(8):1703-1707.
12. Kyle RA, Gertz MA, Witzig TE, et al. Review of 1027 patients with newly diagnosed multiple myeloma. *Mayo Clin Proc.* 2003;78(1):21-33.
13. Kazandjian D. Multiple myeloma epidemiology and survival: A unique malignancy. *Semin Oncol.* 2016;43(6):676-681.
14. Ludwig H, Durie BG, Bolejack V, et al. Myeloma in patients younger than age 50 years presents with more favorable features and shows better survival: an analysis of 10 549 patients from the International Myeloma Working Group. *Blood.* 2008;111(8):4039-4047.
15. Landgren O, Kyle RA, Pfeiffer RM, et al. Monoclonal gammopathy of undetermined significance (MGUS) consistently precedes multiple myeloma: a prospective study. *Blood.* 2009;113(22):5412-5417.
16. Teras LR, Kitahara CM, Birmann BM, et al. Body size and multiple myeloma mortality: a pooled analysis of 20 prospective studies. *Br J Haematol.* 2014;166(5):667-676.
17. Alexander DD, Mink PJ, Adami HO, et al. Multiple myeloma: a review of the epidemiologic literature. *Int J Cancer.* 2007;120 Suppl 12:40-61.
18. Khuder SA, Mutgi AB. Meta-analyses of multiple myeloma and farming. *Am J Ind Med.* 1997;32(5):510-516.

19. Landgren O, Linet MS, McMaster ML, Gridley G, Hemminki K, Goldin LR. Familial characteristics of autoimmune and hematologic disorders in 8,406 multiple myeloma patients: a population-based case-control study. *Int J Cancer*. 2006;118(12):3095-3098.
20. Schinasi LH, Brown EE, Camp NJ, et al. Multiple myeloma and family history of lymphohaematopoietic cancers: Results from the International Multiple Myeloma Consortium. *Br J Haematol*. 2016;175(1):87-101.
21. Chu VT, Berek C. The establishment of the plasma cell survival niche in the bone marrow. *Immunol Rev*. 2013;251(1):177-188.
22. Fairfax KA, Kallies A, Nutt SL, Tarlinton DM. Plasma cell development: from B-cell subsets to long-term survival niches. *Semin Immunol*. 2008;20(1):49-58.
23. Nutt SL, Hodgkin PD, Tarlinton DM, Corcoran LM. The generation of antibody-secreting plasma cells. *Nat Rev Immunol*. 2015;15(3):160-171.
24. Stavnezer J, Guikema JE, Schrader CE. Mechanism and regulation of class switch recombination. *Annu Rev Immunol*. 2008;26:261-292.
25. Schuster SR, Rajkumar SV, Dispenzieri A, et al. IgM multiple myeloma: disease definition, prognosis, and differentiation from Waldenstrom's macroglobulinemia. *Am J Hematol*. 2010;85(11):853-855.
26. Avet-Loiseau H, Garand R, Lodé L, Robillard N, Bataille R. 14q32 Translocations discriminate IgM multiple myeloma from Waldenstrom's macroglobulinemia. *Semin Oncol*. 2003;30(2):153-155.
27. Jancelewicz Z, Takatsuki K, Sugai S, Pruzanski W. IgD multiple myeloma. Review of 133 cases. *Arch Intern Med*. 1975;135(1):87-93.
28. Pisani F, Petrucci MT, Giannarelli D, et al. IgD multiple myeloma a descriptive report of 17 cases: survival and response to therapy. *J Exp Clin Cancer Res*. 2012;31:17.
29. Pandey S, Kyle RA. Unusual myelomas: a review of IgD and IgE variants. *Oncology (Williston Park)*. 2013;27(8):798-803.
30. Rajkumar SV. Multiple myeloma: 2016 update on diagnosis, risk-stratification, and management. *Am J Hematol*. 2016;91(7):719-734.
31. Corso A, Mangiacavalli S. Non-Secretory Myeloma: Ready for a new Definition? *Mediterr J Hematol Infect Dis*. 2017;9(1):e2017053.
32. de Mel S, Lim SH, Tung ML, Chng WJ. Implications of heterogeneity in multiple myeloma. *Biomed Res Int*. 2014;2014:232546.
33. Mali M, Jaakkola P, Arvilommi AM, Jalkanen M. Sequence of human syndecan indicates a novel gene family of integral membrane proteoglycans. *J Biol Chem*. 1990;265(12):6884-6889.
34. O'Connell FP, Pinkus JL, Pinkus GS. CD138 (syndecan-1), a plasma cell marker immunohistochemical profile in hematopoietic and nonhematopoietic neoplasms. *Am J Clin Pathol*. 2004;121(2):254-263.
35. Koda JE, Rapraeger A, Bernfield M. Heparan sulfate proteoglycans from mouse mammary epithelial cells. Cell surface proteoglycan as a receptor for interstitial collagens. *J Biol Chem*. 1985;260(13):8157-8162.
36. Sanderson RD, Lalor P, Bernfield M. B lymphocytes express and lose syndecan at specific stages of differentiation. *Cell Regul*. 1989;1(1):27-35.

37. Wijdenes J, Vooijs WC, Clément C, et al. A plasmocyte selective monoclonal antibody (B-B4) recognizes syndecan-1. *Br J Haematol*. 1996;94(2):318-323.
38. Seidel C, Sundan A, Hjorth M, et al. Serum syndecan-1: a new independent prognostic marker in multiple myeloma. *Blood*. 2000;95(2):388-392.
39. Reid S, Yang S, Brown R, et al. Characterisation and relevance of CD138-negative plasma cells in plasma cell myeloma. *Int J Lab Hematol*. 2010;32(6 Pt 1):e190-196.
40. Witzig TE, Kimlinger T, Stenson M, Therneau T. Syndecan-1 expression on malignant cells from the blood and marrow of patients with plasma cell proliferative disorders and B-cell chronic lymphocytic leukemia. *Leuk Lymphoma*. 1998;31(1-2):167-175.
41. Matsui W, Huff CA, Wang Q, et al. Characterization of clonogenic multiple myeloma cells. *Blood*. 2004;103(6):2332-2336.
42. Matsui W, Wang Q, Barber JP, et al. Clonogenic multiple myeloma progenitors, stem cell properties, and drug resistance. *Cancer Res*. 2008;68(1):190-197.
43. Kawano Y, Fujiwara S, Wada N, et al. Multiple myeloma cells expressing low levels of CD138 have an immature phenotype and reduced sensitivity to lenalidomide. *Int J Oncol*. 2012;41(3):876-884.
44. Franqui-Machin R, Wendlandt EB, Janz S, Zhan F, Tricot G. Cancer stem cells are the cause of drug resistance in multiple myeloma: fact or fiction? *Oncotarget*. 2015;6(38):40496-40506.
45. de Weers M, Tai YT, van der Veer MS, et al. Daratumumab, a novel therapeutic human CD38 monoclonal antibody, induces killing of multiple myeloma and other hematological tumors. *J Immunol*. 2011;186(3):1840-1848.
46. Rawstron AC, Orfao A, Beksac M, et al. Report of the European Myeloma Network on multiparametric flow cytometry in multiple myeloma and related disorders. *Haematologica*. 2008;93(3):431-438.
47. Tembhare PR, Yuan CM, Venzon D, et al. Flow cytometric differentiation of abnormal and normal plasma cells in the bone marrow in patients with multiple myeloma and its precursor diseases. *Leuk Res*. 2014;38(3):371-376.
48. Rawstron A, Barrans S, Blythe D, et al. Distribution of myeloma plasma cells in peripheral blood and bone marrow correlates with CD56 expression. *Br J Haematol*. 1999;104(1):138-143.
49. Rawstron AC, Child JA, de Tute RM, et al. Minimal residual disease assessed by multiparameter flow cytometry in multiple myeloma: impact on outcome in the Medical Research Council Myeloma IX Study. *J Clin Oncol*. 2013;31(20):2540-2547.
50. Short KD, Rajkumar SV, Larson D, et al. Incidence of extramedullary disease in patients with multiple myeloma in the era of novel therapy, and the activity of pomalidomide on extramedullary myeloma. *Leukemia*. 2011;25(6):906-908.
51. Kyle RA, Therneau TM, Rajkumar SV, Larson DR, Plevak MF, Melton LJ. Long-term follow-up of 241 patients with monoclonal gammopathy of undetermined significance: the original Mayo Clinic series 25 years later. *Mayo Clin Proc*. 2004;79(7):859-866.
52. Kyle RA, Therneau TM, Rajkumar SV, et al. Prevalence of monoclonal gammopathy of undetermined significance. *N Engl J Med*. 2006;354(13):1362-1369.
53. Group IMW. Criteria for the classification of monoclonal gammopathies, multiple myeloma and related disorders: a report of the International Myeloma Working Group. *Br J Haematol*. 2003;121(5):749-757.

54. van de Donk NW, Palumbo A, Johnsen HE, et al. The clinical relevance and management of monoclonal gammopathy of undetermined significance and related disorders: recommendations from the European Myeloma Network. *Haematologica*. 2014;99(6):984-996.
55. Katzmann JA, Clark RJ, Abraham RS, et al. Serum reference intervals and diagnostic ranges for free kappa and free lambda immunoglobulin light chains: relative sensitivity for detection of monoclonal light chains. *Clin Chem*. 2002;48(9):1437-1444.
56. Rajkumar SV, Kyle RA, Therneau TM, et al. Serum free light chain ratio is an independent risk factor for progression in monoclonal gammopathy of undetermined significance. *Blood*. 2005;106(3):812-817.
57. Kyle RA, Durie BG, Rajkumar SV, et al. Monoclonal gammopathy of undetermined significance (MGUS) and smoldering (asymptomatic) multiple myeloma: IMWG consensus perspectives risk factors for progression and guidelines for monitoring and management. *Leukemia*. 2010;24(6):1121-1127.
58. Kyle RA, Remstein ED, Therneau TM, et al. Clinical course and prognosis of smoldering (asymptomatic) multiple myeloma. *N Engl J Med*. 2007;356(25):2582-2590.
59. Rajkumar SV, Larson D, Kyle RA. Diagnosis of smoldering multiple myeloma. *N Engl J Med*. 2011;365(5):474-475.
60. Rajkumar SV, Landgren O, Mateos MV. Smoldering multiple myeloma. *Blood*. 2015;125(20):3069-3075.
61. Dispenzieri A, Kyle RA, Katzmann JA, et al. Immunoglobulin free light chain ratio is an independent risk factor for progression of smoldering (asymptomatic) multiple myeloma. *Blood*. 2008;111(2):785-789.
62. Kastritis E, Terpos E, Moulopoulos L, et al. Extensive bone marrow infiltration and abnormal free light chain ratio identifies patients with asymptomatic myeloma at high risk for progression to symptomatic disease. *Leukemia*. 2013;27(4):947-953.
63. Rajkumar SV, Dimopoulos MA, Palumbo A, et al. International Myeloma Working Group updated criteria for the diagnosis of multiple myeloma. *Lancet Oncol*. 2014;15(12):e538-548.
64. Hameed A, Brady JJ, Dowling P, Clynes M, O'Gorman P. Bone disease in multiple myeloma: pathophysiology and management. *Cancer Growth Metastasis*. 2014;7:33-42.
65. Drake MT, Clarke BL, Khosla S. Bisphosphonates: mechanism of action and role in clinical practice. *Mayo Clin Proc*. 2008;83(9):1032-1045.
66. Terpos E, Roodman GD, Dimopoulos MA. Optimal use of bisphosphonates in patients with multiple myeloma. *Blood*. 2013;121(17):3325-3328.
67. Clark AD, Shetty A, Soutar R. Renal failure and multiple myeloma: pathogenesis and treatment of renal failure and management of underlying myeloma. *Blood Rev*. 1999;13(2):79-90.
68. Finkel KW, Cohen EP, Shirali A, Abudayyeh A, Forum AS, NO-N. Paraprotein-Related Kidney Disease: Evaluation and Treatment of Myeloma Cast Nephropathy. *Clin J Am Soc Nephrol*. 2016;11(12):2273-2279.
69. Dimopoulos MA, Kastritis E, Rosinol L, Bladé J, Ludwig H. Pathogenesis and treatment of renal failure in multiple myeloma. *Leukemia*. 2008;22(8):1485-1493.
70. Blimark C, Holmberg E, Mellqvist UH, et al. Multiple myeloma and infections: a population-based study on 9253 multiple myeloma patients. *Haematologica*. 2015;100(1):107-113.

71. Pratt G, Goodyear O, Moss P. Immunodeficiency and immunotherapy in multiple myeloma. *Br J Haematol*. 2007;138(5):563-579.
72. Nucci M, Anaissie E. Infections in patients with multiple myeloma in the era of high-dose therapy and novel agents. *Clin Infect Dis*. 2009;49(8):1211-1225.
73. Varettoni M, Corso A, Pica G, Mangiacavalli S, Pascutto C, Lazzarino M. Incidence, presenting features and outcome of extramedullary disease in multiple myeloma: a longitudinal study on 1003 consecutive patients. *Ann Oncol*. 2010;21(2):325-330.
74. Tiedemann RE, Gonzalez-Paz N, Kyle RA, et al. Genetic aberrations and survival in plasma cell leukemia. *Leukemia*. 2008;22(5):1044-1052.
75. Fernández de Larrea C, Kyle RA, Durie BG, et al. Plasma cell leukemia: consensus statement on diagnostic requirements, response criteria and treatment recommendations by the International Myeloma Working Group. *Leukemia*. 2013;27(4):780-791.
76. van de Donk NW, Lokhorst HM, Anderson KC, Richardson PG. How I treat plasma cell leukemia. *Blood*. 2012;120(12):2376-2389.
77. Bladé J, Fernández de Larrea C, Rosiñol L, Cibeira MT, Jiménez R, Powles R. Soft-tissue plasmacytomas in multiple myeloma: incidence, mechanisms of extramedullary spread, and treatment approach. *J Clin Oncol*. 2011;29(28):3805-3812.
78. Pour L, Sevcikova S, Greslikova H, et al. Soft-tissue extramedullary multiple myeloma prognosis is significantly worse in comparison to bone-related extramedullary relapse. *Haematologica*. 2014;99(2):360-364.
79. Rajan AM, Rajkumar SV. Interpretation of cytogenetic results in multiple myeloma for clinical practice. *Blood Cancer J*. 2015;5:e365.
80. Kumar S, Fonseca R, Ketterling RP, et al. Trisomies in multiple myeloma: impact on survival in patients with high-risk cytogenetics. *Blood*. 2012;119(9):2100-2105.
81. Avet-Loiseau H, Attal M, Moreau P, et al. Genetic abnormalities and survival in multiple myeloma: the experience of the Intergroupe Francophone du Myélome. *Blood*. 2007;109(8):3489-3495.
82. Bergsagel PL, Kuehl WM, Zhan F, Sawyer J, Barlogie B, Shaughnessy J. Cyclin D dysregulation: an early and unifying pathogenic event in multiple myeloma. *Blood*. 2005;106(1):296-303.
83. Hurt EM, Wiestner A, Rosenwald A, et al. Overexpression of c-maf is a frequent oncogenic event in multiple myeloma that promotes proliferation and pathological interactions with bone marrow stroma. *Cancer Cell*. 2004;5(2):191-199.
84. Keats JJ, Reiman T, Maxwell CA, et al. In multiple myeloma, t(4;14)(p16;q32) is an adverse prognostic factor irrespective of FGFR3 expression. *Blood*. 2003;101(4):1520-1529.
85. Fonseca R, Oken MM, Harrington D, et al. Deletions of chromosome 13 in multiple myeloma identified by interphase FISH usually denote large deletions of the q arm or monosomy. *Leukemia*. 2001;15(6):981-986.
86. Fonseca R, Bailey RJ, Ahmann GJ, et al. Genomic abnormalities in monoclonal gammopathy of undetermined significance. *Blood*. 2002;100(4):1417-1424.
87. Avet-Loiseau H, Facon T, Daviet A, et al. 14q32 translocations and monosomy 13 observed in monoclonal gammopathy of undetermined significance delineate a multistep process for the oncogenesis of multiple myeloma. Intergroupe Francophone du Myélome. *Cancer Res*. 1999;59(18):4546-4550.

88. Avet-Louseau H, Daviet A, Sauner S, Bataille R, Myélome IFd. Chromosome 13 abnormalities in multiple myeloma are mostly monosomy 13. *Br J Haematol*. 2000;111(4):1116-1117.
89. Avet-Loiseau H, Li JY, Morineau N, et al. Monosomy 13 is associated with the transition of monoclonal gammopathy of undetermined significance to multiple myeloma. Intergroupe Francophone du Myélome. *Blood*. 1999;94(8):2583-2589.
90. Fonseca R, Bergsagel PL, Drach J, et al. International Myeloma Working Group molecular classification of multiple myeloma: spotlight review. *Leukemia*. 2009;23(12):2210-2221.
91. Chng WJ, Gonzalez-Paz N, Price-Troska T, et al. Clinical and biological significance of RAS mutations in multiple myeloma. *Leukemia*. 2008;22(12):2280-2284.
92. Chng WJ, Huang GF, Chung TH, et al. Clinical and biological implications of MYC activation: a common difference between MGUS and newly diagnosed multiple myeloma. *Leukemia*. 2011;25(6):1026-1035.
93. Avet-Loiseau H, Gerson F, Magrangeas F, et al. Rearrangements of the c-myc oncogene are present in 15% of primary human multiple myeloma tumors. *Blood*. 2001;98(10):3082-3086.
94. Keats JJ, Fonseca R, Chesi M, et al. Promiscuous mutations activate the noncanonical NF-kappaB pathway in multiple myeloma. *Cancer Cell*. 2007;12(2):131-144.
95. Demchenko YN, Glebov OK, Zingone A, Keats JJ, Bergsagel PL, Kuehl WM. Classical and/or alternative NF-kappaB pathway activation in multiple myeloma. *Blood*. 2010;115(17):3541-3552.
96. Agarwal A, Ghobrial IM. Monoclonal gammopathy of undetermined significance and smoldering multiple myeloma: a review of the current understanding of epidemiology, biology, risk stratification, and management of myeloma precursor disease. *Clin Cancer Res*. 2013;19(5):985-994.
97. Durie BG, Salmon SE. A clinical staging system for multiple myeloma. Correlation of measured myeloma cell mass with presenting clinical features, response to treatment, and survival. *Cancer*. 1975;36(3):842-854.
98. Greipp PR, San Miguel J, Durie BG, et al. International staging system for multiple myeloma. *J Clin Oncol*. 2005;23(15):3412-3420.
99. Palumbo A, Avet-Loiseau H, Oliva S, et al. Revised International Staging System for Multiple Myeloma: A Report From International Myeloma Working Group. *J Clin Oncol*. 2015;33(26):2863-2869.
100. Alexanian R, Bergsagel DE, Migliore PJ, Vaughn WK, Howe CD. Melphalan therapy for plasma cell myeloma. *Blood*. 1968;31(1):1-10.
101. Kumar SK, Dispenzieri A, Lacy MQ, et al. Continued improvement in survival in multiple myeloma: changes in early mortality and outcomes in older patients. *Leukemia*. 2014;28(5):1122-1128.
102. Kotla V, Goel S, Nischal S, et al. Mechanism of action of lenalidomide in hematological malignancies. *J Hematol Oncol*. 2009;2:36.
103. Lecker SH, Goldberg AL, Mitch WE. Protein degradation by the ubiquitin-proteasome pathway in normal and disease states. *J Am Soc Nephrol*. 2006;17(7):1807-1819.
104. Hideshima T, Richardson PG, Anderson KC. Mechanism of action of proteasome inhibitors and deacetylase inhibitors and the biological basis of synergy in multiple myeloma. *Mol Cancer Ther*. 2011;10(11):2034-2042.
105. Greenstein S, Ghias K, Krett NL, Rosen ST. Mechanisms of glucocorticoid-mediated apoptosis in hematological malignancies. *Clin Cancer Res*. 2002;8(6):1681-1694.

106. Chng WJ, Dispenzieri A, Chim CS, et al. IMWG consensus on risk stratification in multiple myeloma. *Leukemia*. 2014;28(2):269-277.
107. Brenner H, Gondos A, Pulte D. Recent major improvement in long-term survival of younger patients with multiple myeloma. *Blood*. 2008;111(5):2521-2526.
108. Kumar SK, Dingli D, Lacy MQ, et al. Autologous stem cell transplantation in patients of 70 years and older with multiple myeloma: Results from a matched pair analysis. *Am J Hematol*. 2008;83(8):614-617.
109. Gertz MA, Dingli D. How we manage autologous stem cell transplantation for patients with multiple myeloma. *Blood*. 2014;124(6):882-890.
110. NICE. Myeloma: Diagnosis and Management: NICE Guidelines; 2016.
111. Kaufman JL, Nooka A, Vrana M, Gleason C, Heffner LT, Lonial S. Bortezomib, thalidomide, and dexamethasone as induction therapy for patients with symptomatic multiple myeloma: a retrospective study. *Cancer*. 2010;116(13):3143-3151.
112. Moreau P, Avet-Loiseau H, Facon T, et al. Bortezomib plus dexamethasone versus reduced-dose bortezomib, thalidomide plus dexamethasone as induction treatment before autologous stem cell transplantation in newly diagnosed multiple myeloma. *Blood*. 2011;118(22):5752-5758; quiz 5982.
113. Richardson PG, Weller E, Lonial S, et al. Lenalidomide, bortezomib, and dexamethasone combination therapy in patients with newly diagnosed multiple myeloma. *Blood*. 2010;116(5):679-686.
114. Reeder CB, Reece DE, Kukreti V, et al. Cyclophosphamide, bortezomib and dexamethasone induction for newly diagnosed multiple myeloma: high response rates in a phase II clinical trial. *Leukemia*. 2009;23(7):1337-1341.
115. Sonneveld P, Avet-Loiseau H, Lonial S, et al. Treatment of multiple myeloma with high-risk cytogenetics: a consensus of the International Myeloma Working Group. *Blood*. 2016;127(24):2955-2962.
116. Attal M, Harousseau JL, Stoppa AM, et al. A prospective, randomized trial of autologous bone marrow transplantation and chemotherapy in multiple myeloma. Intergroupe Français du Myélome. *N Engl J Med*. 1996;335(2):91-97.
117. Child JA, Morgan GJ, Davies FE, et al. High-dose chemotherapy with hematopoietic stem-cell rescue for multiple myeloma. *N Engl J Med*. 2003;348(19):1875-1883.
118. Moreau P, Facon T, Attal M, et al. Comparison of 200 mg/m<sup>2</sup> melphalan and 8 Gy total body irradiation plus 140 mg/m<sup>2</sup> melphalan as conditioning regimens for peripheral blood stem cell transplantation in patients with newly diagnosed multiple myeloma: final analysis of the Intergroupe Francophone du Myélome 9502 randomized trial. *Blood*. 2002;99(3):731-735.
119. Gertz MA, Lacy MQ, Inwards DJ, et al. Early harvest and late transplantation as an effective therapeutic strategy in multiple myeloma. *Bone Marrow Transplant*. 1999;23(3):221-226.
120. Rajkumar SV, Kumar S. Multiple Myeloma: Diagnosis and Treatment. *Mayo Clin Proc*. 2016;91(1):101-119.
121. Krishnan A, Pasquini MC, Logan B, et al. Autologous haemopoietic stem-cell transplantation followed by allogeneic or autologous haemopoietic stem-cell transplantation in patients with multiple myeloma (BMT CTN 0102): a phase 3 biological assignment trial. *Lancet Oncol*. 2011;12(13):1195-1203.
122. Bruno B, Rotta M, Patriarca F, et al. A comparison of allografting with autografting for newly diagnosed myeloma. *N Engl J Med*. 2007;356(11):1110-1120.

123. San Miguel JF, Schlag R, Khuageva NK, et al. Bortezomib plus melphalan and prednisone for initial treatment of multiple myeloma. *N Engl J Med*. 2008;359(9):906-917.
124. Benboubker L, Dimopoulos MA, Dispenzieri A, et al. Lenalidomide and dexamethasone in transplant-ineligible patients with myeloma. *N Engl J Med*. 2014;371(10):906-917.
125. Hoering A, Crowley J, Shaughnessy JD, et al. Complete remission in multiple myeloma examined as time-dependent variable in terms of both onset and duration in Total Therapy protocols. *Blood*. 2009;114(7):1299-1305.
126. Magrangeas F, Avet-Loiseau H, Gouraud W, et al. Minor clone provides a reservoir for relapse in multiple myeloma. *Leukemia*. 2013;27(2):473-481.
127. Yang WC, Lin SF. Mechanisms of Drug Resistance in Relapse and Refractory Multiple Myeloma. *Biomed Res Int*. 2015;2015:341430.
128. Attal M, Lauwers-Cances V, Marit G, et al. Lenalidomide maintenance after stem-cell transplantation for multiple myeloma. *N Engl J Med*. 2012;366(19):1782-1791.
129. Palumbo A, Cavallo F, Gay F, et al. Autologous transplantation and maintenance therapy in multiple myeloma. *N Engl J Med*. 2014;371(10):895-905.
130. McCarthy PL, Owzar K, Hofmeister CC, et al. Lenalidomide after stem-cell transplantation for multiple myeloma. *N Engl J Med*. 2012;366(19):1770-1781.
131. Jackson GH, Davies FE, Pawlyn C, et al. Lenalidomide maintenance versus observation for patients with newly diagnosed multiple myeloma (Myeloma XI): a multicentre, open-label, randomised, phase 3 trial. *Lancet Oncol*. 2019;20(1):57-73.
132. Jones JR, Cairns DA, Gregory WM, et al. Second malignancies in the context of lenalidomide treatment: an analysis of 2732 myeloma patients enrolled to the Myeloma XI trial. *Blood Cancer J*. 2016;6(12):e506.
133. Sonneveld P, Schmidt-Wolf IG, van der Holt B, et al. Bortezomib induction and maintenance treatment in patients with newly diagnosed multiple myeloma: results of the randomized phase III HOVON-65/ GMMG-HD4 trial. *J Clin Oncol*. 2012;30(24):2946-2955.
134. Nooka AK, Kaufman JL, Muppidi S, et al. Consolidation and maintenance therapy with lenalidomide, bortezomib and dexamethasone (RVD) in high-risk myeloma patients. *Leukemia*. 2014;28(3):690-693.
135. Palumbo A, Bringhen S, Larocca A, et al. Bortezomib-melphalan-prednisone-thalidomide followed by maintenance with bortezomib-thalidomide compared with bortezomib-melphalan-prednisone for initial treatment of multiple myeloma: updated follow-up and improved survival. *J Clin Oncol*. 2014;32(7):634-640.
136. Laubach J, Garderet L, Mahindra A, et al. Management of relapsed multiple myeloma: recommendations of the International Myeloma Working Group. *Leukemia*. 2016;30(5):1005-1017.
137. McCullough KB, Hobbs MA, Abeykoon JP, Kapoor P. Common Adverse Effects of Novel Therapies for Multiple Myeloma (MM) and Their Management Strategies. *Curr Hematol Malig Rep*. 2018;13(2):114-124.
138. NICE. Carfilzomib for previously treated multiple myeloma.: NICE Guidelines; 2017.
139. NICE. Ixazomib with lenalidomide and dexamethasone for treating relapsed of refractory multiple myeloma.: NICE Guidelines; 2018.

140. NICE. Pomalidomide for multiple myeloma previously treated with lenalidomide and bortezomib.: NICE Guidelines; 2017.
141. Richardson PG, Siegel DS, Vij R, et al. Pomalidomide alone or in combination with low-dose dexamethasone in relapsed and refractory multiple myeloma: a randomized phase 2 study. *Blood*. 2014;123(12):1826-1832.
142. Miguel JS, Weisel K, Moreau P, et al. Pomalidomide plus low-dose dexamethasone versus high-dose dexamethasone alone for patients with relapsed and refractory multiple myeloma (MM-003): a randomised, open-label, phase 3 trial. *Lancet Oncol*. 2013;14(11):1055-1066.
143. Stewart AK, Rajkumar SV, Dimopoulos MA, et al. Carfilzomib, lenalidomide, and dexamethasone for relapsed multiple myeloma. *N Engl J Med*. 2015;372(2):142-152.
144. Moreau P, Masszi T, Grzasko N, et al. Oral ixazomib, Lenalidomide, and Dexamethasone for Multiple Myeloma. *N Engl J Med*. 2016;374(17):1621-1634.
145. Siegel DS, Martin T, Wang M, et al. A phase 2 study of single-agent carfilzomib (PX-171-003-A1) in patients with relapsed and refractory multiple myeloma. *Blood*. 2012;120(14):2817-2825.
146. Lonial S, Dimopoulos M, Palumbo A, et al. Elotuzumab Therapy for Relapsed or Refractory Multiple Myeloma. *N Engl J Med*. 2015;373(7):621-631.
147. Dimopoulos MA, Dytfeld D, Grosicki S, et al. Elotuzumab plus Pomalidomide and Dexamethasone for Multiple Myeloma. *N Engl J Med*. 2018;379(19):1811-1822.
148. Lonial S, Weiss BM, Usmani SZ, et al. Daratumumab monotherapy in patients with treatment-refractory multiple myeloma (SIRIUS): an open-label, randomised, phase 2 trial. *Lancet*. 2016;387(10027):1551-1560.
149. Usmani SZ, Weiss BM, Plesner T, et al. Clinical efficacy of daratumumab monotherapy in patients with heavily pretreated relapsed or refractory multiple myeloma. *Blood*. 2016;128(1):37-44.
150. Dimopoulos MA, Oriol A, Nahi H, et al. Daratumumab, Lenalidomide, and Dexamethasone for Multiple Myeloma. *N Engl J Med*. 2016;375(14):1319-1331.
151. Palumbo A, Chanan-Khan A, Weisel K, et al. Daratumumab, Bortezomib, and Dexamethasone for Multiple Myeloma. *N Engl J Med*. 2016;375(8):754-766.
152. NICE. Daratumumab with bortezomib and dexamethasone for previously treated multiple myeloma.: NICE Guidelines; 2019.
153. Park JH, Rivière I, Gonen M, et al. Long-Term Follow-up of CD19 CAR Therapy in Acute Lymphoblastic Leukemia. *N Engl J Med*. 2018;378(5):449-459.
154. Porter DL, Levine BL, Kalos M, Bagg A, June CH. Chimeric antigen receptor-modified T cells in chronic lymphoid leukemia. *N Engl J Med*. 2011;365(8):725-733.
155. June CH, Sadelain M. Chimeric Antigen Receptor Therapy. *N Engl J Med*. 2018;379(1):64-73.
156. Susanibar Adaniya SP, Cohen AD, Garfall AL. Chimeric antigen receptor T cell immunotherapy for multiple myeloma: A review of current data and potential clinical applications. *Am J Hematol*. 2019;94(S1):S28-S33.
157. Brudno JN, Maric I, Hartman SD, et al. T Cells Genetically Modified to Express an Anti-B-Cell Maturation Antigen Chimeric Antigen Receptor Cause Remissions of Poor-Prognosis Relapsed Multiple Myeloma. *J Clin Oncol*. 2018;36(22):2267-2280.

158. Anthony BA, Link DC. Regulation of hematopoietic stem cells by bone marrow stromal cells. *Trends Immunol.* 2014;35(1):32-37.
159. Lauta VM. A review of the cytokine network in multiple myeloma: diagnostic, prognostic, and therapeutic implications. *Cancer.* 2003;97(10):2440-2452.
160. Hideshima T, Bergsagel PL, Kuehl WM, Anderson KC. Advances in biology of multiple myeloma: clinical applications. *Blood.* 2004;104(3):607-618.
161. Damiano JS, Cress AE, Hazlehurst LA, Shtil AA, Dalton WS. Cell adhesion mediated drug resistance (CAM-DR): role of integrins and resistance to apoptosis in human myeloma cell lines. *Blood.* 1999;93(5):1658-1667.
162. Podar K, Chauhan D, Anderson KC. Bone marrow microenvironment and the identification of new targets for myeloma therapy. *Leukemia.* 2009;23(1):10-24.
163. Urashima M, Chen BP, Chen S, et al. The development of a model for the homing of multiple myeloma cells to human bone marrow. *Blood.* 1997;90(2):754-765.
164. Faid L, Van Riet I, De Waele M, et al. Adhesive interactions between tumour cells and bone marrow stromal elements in human multiple myeloma. *Eur J Haematol.* 1996;57(5):349-358.
165. Hideshima T, Mitsiades C, Tonon G, Richardson PG, Anderson KC. Understanding multiple myeloma pathogenesis in the bone marrow to identify new therapeutic targets. *Nat Rev Cancer.* 2007;7(8):585-598.
166. Alsayed Y, Ngo H, Runnels J, et al. Mechanisms of regulation of CXCR4/SDF-1 (CXCL12)-dependent migration and homing in multiple myeloma. *Blood.* 2007;109(7):2708-2717.
167. Uchiyama H, Barut BA, Mohrbacher AF, Chauhan D, Anderson KC. Adhesion of human myeloma-derived cell lines to bone marrow stromal cells stimulates interleukin-6 secretion. *Blood.* 1993;82(12):3712-3720.
168. Chauhan D, Uchiyama H, Akbarali Y, et al. Multiple myeloma cell adhesion-induced interleukin-6 expression in bone marrow stromal cells involves activation of NF-kappa B. *Blood.* 1996;87(3):1104-1112.
169. Markovina S, Callander NS, O'Connor SL, et al. Bortezomib-resistant nuclear factor-kappaB activity in multiple myeloma cells. *Mol Cancer Res.* 2008;6(8):1356-1364.
170. Lichtenstein A, Tu Y, Fady C, Vescio R, Berenson J. Interleukin-6 inhibits apoptosis of malignant plasma cells. *Cell Immunol.* 1995;162(2):248-255.
171. Dankbar B, Padró T, Leo R, et al. Vascular endothelial growth factor and interleukin-6 in paracrine tumor-stromal cell interactions in multiple myeloma. *Blood.* 2000;95(8):2630-2636.
172. Gupta D, Treon SP, Shima Y, et al. Adherence of multiple myeloma cells to bone marrow stromal cells upregulates vascular endothelial growth factor secretion: therapeutic applications. *Leukemia.* 2001;15(12):1950-1961.
173. Mitsiades CS, Mitsiades N, Poulaki V, et al. Activation of NF-kappaB and upregulation of intracellular anti-apoptotic proteins via the IGF-1/Akt signaling in human multiple myeloma cells: therapeutic implications. *Oncogene.* 2002;21(37):5673-5683.
174. Cines DB, Pollak ES, Buck CA, et al. Endothelial cells in physiology and in the pathophysiology of vascular disorders. *Blood.* 1998;91(10):3527-3561.
175. Ghobrial IM. Myeloma as a model for the process of metastasis: implications for therapy. *Blood.* 2012;120(1):20-30.

176. Rajkumar SV, Mesa RA, Fonseca R, et al. Bone marrow angiogenesis in 400 patients with monoclonal gammopathy of undetermined significance, multiple myeloma, and primary amyloidosis. *Clin Cancer Res*. 2002;8(7):2210-2216.
177. Bisping G, Leo R, Wenning D, et al. Paracrine interactions of basic fibroblast growth factor and interleukin-6 in multiple myeloma. *Blood*. 2003;101(7):2775-2783.
178. Colla S, Morandi F, Lazzaretti M, et al. Do human myeloma cells directly produce basic FGF? *Blood*. 2003;102(8):3071-3072; author reply 3072-3073.
179. Vacca A, Ria R, Semeraro F, et al. Endothelial cells in the bone marrow of patients with multiple myeloma. *Blood*. 2003;102(9):3340-3348.
180. Pellegrino A, Ria R, Di Pietro G, et al. Bone marrow endothelial cells in multiple myeloma secrete CXC-chemokines that mediate interactions with plasma cells. *Br J Haematol*. 2005;129(2):248-256.
181. D'Amato RJ, Loughnan MS, Flynn E, Folkman J. Thalidomide is an inhibitor of angiogenesis. *Proc Natl Acad Sci U S A*. 1994;91(9):4082-4085.
182. Lu L, Payvandi F, Wu L, et al. The anti-cancer drug lenalidomide inhibits angiogenesis and metastasis via multiple inhibitory effects on endothelial cell function in normoxic and hypoxic conditions. *Microvasc Res*. 2009;77(2):78-86.
183. Harada S, Rodan GA. Control of osteoblast function and regulation of bone mass. *Nature*. 2003;423(6937):349-355.
184. Edwards CM, Zhuang J, Mundy GR. The pathogenesis of the bone disease of multiple myeloma. *Bone*. 2008;42(6):1007-1013.
185. Barillé S, Collette M, Bataille R, Amiot M. Myeloma cells upregulate interleukin-6 secretion in osteoblastic cells through cell-to-cell contact but downregulate osteocalcin. *Blood*. 1995;86(8):3151-3159.
186. Karadag A, Oyajobi BO, Apperley JF, Russell RG, Croucher PI. Human myeloma cells promote the production of interleukin 6 by primary human osteoblasts. *Br J Haematol*. 2000;108(2):383-390.
187. Giuliani N, Rizzoli V, Roodman GD. Multiple myeloma bone disease: Pathophysiology of osteoblast inhibition. *Blood*. 2006;108(13):3992-3996.
188. Udagawa N, Takahashi N, Yasuda H, et al. Osteoprotegerin produced by osteoblasts is an important regulator in osteoclast development and function. *Endocrinology*. 2000;141(9):3478-3484.
189. Glass DA, Bialek P, Ahn JD, et al. Canonical Wnt signaling in differentiated osteoblasts controls osteoclast differentiation. *Dev Cell*. 2005;8(5):751-764.
190. Tian E, Zhan F, Walker R, et al. The role of the Wnt-signaling antagonist DKK1 in the development of osteolytic lesions in multiple myeloma. *N Engl J Med*. 2003;349(26):2483-2494.
191. Gunn WG, Conley A, Deininger L, Olson SD, Prockop DJ, Gregory CA. A crosstalk between myeloma cells and marrow stromal cells stimulates production of DKK1 and interleukin-6: a potential role in the development of lytic bone disease and tumor progression in multiple myeloma. *Stem Cells*. 2006;24(4):986-991.
192. Giuliani N, Colla S, Morandi F, et al. Myeloma cells block RUNX2/CBFA1 activity in human bone marrow osteoblast progenitors and inhibit osteoblast formation and differentiation. *Blood*. 2005;106(7):2472-2483.

193. Yaccoby S, Ling W, Zhan F, Walker R, Barlogie B, Shaughnessy JD. Antibody-based inhibition of DKK1 suppresses tumor-induced bone resorption and multiple myeloma growth in vivo. *Blood*. 2007;109(5):2106-2111.
194. Edwards CM, Edwards JR, Lwin ST, et al. Increasing Wnt signaling in the bone marrow microenvironment inhibits the development of myeloma bone disease and reduces tumor burden in bone in vivo. *Blood*. 2008;111(5):2833-2842.
195. Lacey DL, Timms E, Tan HL, et al. Osteoprotegerin ligand is a cytokine that regulates osteoclast differentiation and activation. *Cell*. 1998;93(2):165-176.
196. Boyle WJ, Simonet WS, Lacey DL. Osteoclast differentiation and activation. *Nature*. 2003;423(6937):337-342.
197. Burgess TL, Qian Y, Kaufman S, et al. The ligand for osteoprotegerin (OPGL) directly activates mature osteoclasts. *J Cell Biol*. 1999;145(3):527-538.
198. Jurdic P, Saltel F, Chabadel A, Destaing O. Podosome and sealing zone: specificity of the osteoclast model. *Eur J Cell Biol*. 2006;85(3-4):195-202.
199. Chatterjee D, Chakraborty M, Leit M, et al. The osteoclast proton pump differs in its pharmacology and catalytic subunits from other vacuolar H(+)-ATPases. *J Exp Biol*. 1992;172:193-204.
200. Väänänen K. Mechanism of osteoclast mediated bone resorption--rationale for the design of new therapeutics. *Adv Drug Deliv Rev*. 2005;57(7):959-971.
201. Manolagas SC. Birth and death of bone cells: basic regulatory mechanisms and implications for the pathogenesis and treatment of osteoporosis. *Endocr Rev*. 2000;21(2):115-137.
202. Mundy GR. Myeloma bone disease. *Eur J Cancer*. 1998;34(2):246-251.
203. Terpos E, Dimopoulos MA. Myeloma bone disease: pathophysiology and management. *Ann Oncol*. 2005;16(8):1223-1231.
204. Abe M, Hiura K, Wilde J, et al. Osteoclasts enhance myeloma cell growth and survival via cell-cell contact: a vicious cycle between bone destruction and myeloma expansion. *Blood*. 2004;104(8):2484-2491.
205. Boyce BF, Xing L. The RANKL/RANK/OPG pathway. *Curr Osteoporos Rep*. 2007;5(3):98-104.
206. Atkins GJ, Kostakis P, Vincent C, et al. RANK Expression as a cell surface marker of human osteoclast precursors in peripheral blood, bone marrow, and giant cell tumors of bone. *J Bone Miner Res*. 2006;21(9):1339-1349.
207. Boyce BF, Xing L. Functions of RANKL/RANK/OPG in bone modeling and remodeling. *Arch Biochem Biophys*. 2008;473(2):139-146.
208. Healy CF, Murray JG, Eustace SJ, Madewell J, O'Gorman PJ, O'Sullivan P. Multiple myeloma: a review of imaging features and radiological techniques. *Bone Marrow Res*. 2011;2011:583439.
209. Heider U, Langelotz C, Jakob C, et al. Expression of receptor activator of nuclear factor kappaB ligand on bone marrow plasma cells correlates with osteolytic bone disease in patients with multiple myeloma. *Clin Cancer Res*. 2003;9(4):1436-1440.
210. Giuliani N, Bataille R, Mancini C, Lazzaretti M, Barillé S. Myeloma cells induce imbalance in the osteoprotegerin/osteoprotegerin ligand system in the human bone marrow environment. *Blood*. 2001;98(13):3527-3533.

211. Roux S, Meignin V, Quillard J, et al. RANK (receptor activator of nuclear factor-kappaB) and RANKL expression in multiple myeloma. *Br J Haematol*. 2002;117(1):86-92.
212. Jakob C, Goerke A, Terpos E, et al. Serum levels of total-RANKL in multiple myeloma. *Clin Lymphoma Myeloma*. 2009;9(6):430-435.
213. Sezer O, Heider U, Zavrski I, Kühne CA, Hofbauer LC. RANK ligand and osteoprotegerin in myeloma bone disease. *Blood*. 2003;101(6):2094-2098.
214. Pearse RN, Sordillo EM, Yaccoby S, et al. Multiple myeloma disrupts the TRANCE/osteoprotegerin cytokine axis to trigger bone destruction and promote tumor progression. *Proc Natl Acad Sci U S A*. 2001;98(20):11581-11586.
215. Lacey DL, Tan HL, Lu J, et al. Osteoprotegerin ligand modulates murine osteoclast survival in vitro and in vivo. *Am J Pathol*. 2000;157(2):435-448.
216. Terpos E, Christoulas D, Gavriatopoulou M, Dimopoulos MA. Mechanisms of bone destruction in multiple myeloma. *Eur J Cancer Care (Engl)*. 2017;26(6).
217. Ludwig H, Nachbaur DM, Fritz E, Krainer M, Huber H. Interleukin-6 is a prognostic factor in multiple myeloma. *Blood*. 1991;77(12):2794-2795.
218. Sati HI, Apperley JF, Greaves M, et al. Interleukin-6 is expressed by plasma cells from patients with multiple myeloma and monoclonal gammopathy of undetermined significance. *Br J Haematol*. 1998;101(2):287-295.
219. Tamura T, Udagawa N, Takahashi N, et al. Soluble interleukin-6 receptor triggers osteoclast formation by interleukin 6. *Proc Natl Acad Sci U S A*. 1993;90(24):11924-11928.
220. Kudo O, Sabokbar A, Pocock A, Itonaga I, Fujikawa Y, Athanasou NA. Interleukin-6 and interleukin-11 support human osteoclast formation by a RANKL-independent mechanism. *Bone*. 2003;32(1):1-7.
221. van Zaanen HC, Lokhorst HM, Aarden LA, et al. Chimaeric anti-interleukin 6 monoclonal antibodies in the treatment of advanced multiple myeloma: a phase I dose-escalating study. *Br J Haematol*. 1998;102(3):783-790.
222. Kulie T, Groff A, Redmer J, Hounshell J, Schragger S. Vitamin D: an evidence-based review. *J Am Board Fam Med*. 2009;22(6):698-706.
223. Holick MF. Vitamin D deficiency. *N Engl J Med*. 2007;357(3):266-281.
224. Badros A, Goloubeva O, Terpos E, Milliron T, Baer MR, Streeten E. Prevalence and significance of vitamin D deficiency in multiple myeloma patients. *Br J Haematol*. 2008;142(3):492-494.
225. Ng AC, Kumar SK, Rajkumar SV, Drake MT. Impact of vitamin D deficiency on the clinical presentation and prognosis of patients with newly diagnosed multiple myeloma. *Am J Hematol*. 2009;84(7):397-400.
226. Suda T, Takahashi N, Martin TJ. Modulation of osteoclast differentiation. *Endocr Rev*. 1992;13(1):66-80.
227. Bar-Shavit Z, Teitelbaum SL, Reitsma P, et al. Induction of monocytic differentiation and bone resorption by 1,25-dihydroxyvitamin D3. *Proc Natl Acad Sci U S A*. 1983;80(19):5907-5911.
228. Roodman GD, Ibbotson KJ, MacDonald BR, Kuehl TJ, Mundy GR. 1,25-Dihydroxyvitamin D3 causes formation of multinucleated cells with several osteoclast characteristics in cultures of primate marrow. *Proc Natl Acad Sci U S A*. 1985;82(23):8213-8217.

229. Takahashi N, Udagawa N, Suda T. Vitamin D endocrine system and osteoclasts. *Bonekey Rep.* 2014;3:495.
230. Raisz LG, Trummel CL, Holick MF, DeLuca HF. 1,25-dihydroxycholecalciferol: a potent stimulator of bone resorption in tissue culture. *Science.* 1972;175(4023):768-769.
231. Lwin ST, Edwards CM, Silbermann R. Preclinical animal models of multiple myeloma. *Bonekey Rep.* 2016;5:772.
232. Radl J, De Glopper ED, Schuit HR, Zurcher C. Idiopathic paraproteinemia. II. Transplantation of the paraprotein-producing clone from old to young C57BL/KaLwRij mice. *J Immunol.* 1979;122(2):609-613.
233. Chesi M, Matthews GM, Garbitt VM, et al. Drug response in a genetically engineered mouse model of multiple myeloma is predictive of clinical efficacy. *Blood.* 2012;120(2):376-385.
234. Paton-Hough J, Chantry AD, Lawson MA. A review of current murine models of multiple myeloma used to assess the efficacy of therapeutic agents on tumour growth and bone disease. *Bone.* 2015;77:57-68.
235. Masters JR. HeLa cells 50 years on: the good, the bad and the ugly. *Nat Rev Cancer.* 2002;2(4):315-319.
236. Zlei M, Egert S, Wider D, Ihorst G, Wäsch R, Engelhardt M. Characterization of in vitro growth of multiple myeloma cells. *Exp Hematol.* 2007;35(10):1550-1561.
237. Drexler HG, Matsuo Y. Malignant hematopoietic cell lines: in vitro models for the study of multiple myeloma and plasma cell leukemia. *Leuk Res.* 2000;24(8):681-703.
238. Pellat-Deceunynck C, Amiot M, Bataille R, et al. Human myeloma cell lines as a tool for studying the biology of multiple myeloma: a reappraisal 18 years after. *Blood.* 1995;86(10):4001-4002.
239. Gazdar AF, Oie HK, Kirsch IR, Hollis GF. Establishment and characterization of a human plasma cell myeloma culture having a rearranged cellular myc proto-oncogene. *Blood.* 1986;67(6):1542-1549.
240. Jackson N, Lowe J, Ball J, et al. Two new IgA1-kappa plasma cell leukaemia cell lines (JIN-1 & JIN-2) which proliferate in response to B cell stimulatory factor 2. *Clin Exp Immunol.* 1989;75(1):93-99.
241. Gooding RP, Bybee A, Cooke F, et al. Phenotypic and molecular analysis of six human cell lines derived from patients with plasma cell dyscrasia. *Br J Haematol.* 1999;106(3):669-681.
242. Flanagan AM, Massey HM. Generating human osteoclasts in vitro from bone marrow and peripheral blood. *Methods Mol Med.* 2003;80:113-128.
243. Cody JJ, Rivera AA, Liu J, Liu JM, Douglas JT, Feng X. A simplified method for the generation of human osteoclasts in vitro. *Int J Biochem Mol Biol.* 2011;2(2):183-189.
244. Collin-Osdoby P, Yu X, Zheng H, Osdoby P. RANKL-mediated osteoclast formation from murine RAW 264.7 cells. *Methods Mol Med.* 2003;80:153-166.
245. Bharti AC, Takada Y, Aggarwal BB. Curcumin (diferuloylmethane) inhibits receptor activator of NF-kappa B ligand-induced NF-kappa B activation in osteoclast precursors and suppresses osteoclastogenesis. *J Immunol.* 2004;172(10):5940-5947.
246. Vincent C, Kogawa M, Findlay DM, Atkins GJ. The generation of osteoclasts from RAW 264.7 precursors in defined, serum-free conditions. *J Bone Miner Metab.* 2009;27(1):114-119.

247. Lutter AH, Hempel U, Wolf-Brandstetter C, et al. A novel resorption assay for osteoclast functionality based on an osteoblast-derived native extracellular matrix. *J Cell Biochem.* 2010;109(5):1025-1032.
248. Sundström C, Nilsson K. Establishment and characterization of a human histiocytic lymphoma cell line (U-937). *Int J Cancer.* 1976;17(5):565-577.
249. Aoki H, Akiyama H, Hosoya H, Souda M, Morioku T, Marunouchi T. Transient expression of M-CSF is important for osteoclast-like cell differentiation in a monocytic leukemia cell line. *J Cell Biochem.* 1997;64(1):67-76.
250. Amoui M, Suhr SM, Baylink DJ, Lau KH. An osteoclastic protein-tyrosine phosphatase may play a role in differentiation and activity of human monocytic U-937 cell-derived, osteoclast-like cells. *Am J Physiol Cell Physiol.* 2004;287(4):C874-884.
251. Markovina S, Callander NS, O'Connor SL, et al. Bone marrow stromal cells from multiple myeloma patients uniquely induce bortezomib resistant NF-kappaB activity in myeloma cells. *Mol Cancer.* 2010;9:176.
252. Zhang W, Gu Y, Sun Q, et al. Ex Vivo Maintenance of Primary Human Multiple Myeloma Cells through the Optimization of the Osteoblastic Niche. *PLoS One.* 2015;10(5):e0125995.
253. Giuliani N, Colla S, Lazzaretti M, et al. Proangiogenic properties of human myeloma cells: production of angiopoietin-1 and its potential relationship to myeloma-induced angiogenesis. *Blood.* 2003;102(2):638-645.
254. Yaccoby S, Wezeman MJ, Henderson A, et al. Cancer and the microenvironment: myeloma-osteoclast interactions as a model. *Cancer Res.* 2004;64(6):2016-2023.
255. Strober W. Trypan blue exclusion test of cell viability. *Curr Protoc Immunol.* 2001;Appendix 3:Appendix 3B.
256. Darzynkiewicz Z, Halicka HD, Zhao H. Analysis of cellular DNA content by flow and laser scanning cytometry. *Adv Exp Med Biol.* 2010;676:137-147.
257. GOLDBERG AF, BARKA T. Acid phosphatase activity in human blood cells. *Nature.* 1962;195:297.
258. Ewels P, Magnusson M, Lundin S, Käller M. MultiQC: summarize analysis results for multiple tools and samples in a single report. *Bioinformatics.* 2016;32(19):3047-3048.
259. Wang L, Wang S, Li W. RSeQC: quality control of RNA-seq experiments. *Bioinformatics.* 2012;28(16):2184-2185.
260. Liao Y, Smyth GK, Shi W. featureCounts: an efficient general purpose program for assigning sequence reads to genomic features. *Bioinformatics.* 2014;30(7):923-930.
261. Love MI, Huber W, Anders S. Moderated estimation of fold change and dispersion for RNA-seq data with DESeq2. *Genome Biol.* 2014;15(12):550.
262. Ye J, Coulouris G, Zaretskaya I, Cutcutache I, Rozen S, Madden TL. Primer-BLAST: a tool to design target-specific primers for polymerase chain reaction. *BMC Bioinformatics.* 2012;13:134.
263. Dragan AI, Pavlovic R, McGivney JB, et al. SYBR Green I: fluorescence properties and interaction with DNA. *J Fluoresc.* 2012;22(4):1189-1199.
264. Livak KJ, Schmittgen TD. Analysis of relative gene expression data using real-time quantitative PCR and the 2<sup>-</sup>(Delta Delta C(T)) Method. *Methods.* 2001;25(4):402-408.

265. Kyle RA, Rajkumar SV. Multiple myeloma. *Blood*. 2008;111(6):2962-2972.
266. Susa M, Luong-Nguyen NH, Cappellen D, Zamurovic N, Gamse R. Human primary osteoclasts: in vitro generation and applications as pharmacological and clinical assay. *J Transl Med*. 2004;2(1):6.
267. Riccardi C, Nicoletti I. Analysis of apoptosis by propidium iodide staining and flow cytometry. *Nat Protoc*. 2006;1(3):1458-1461.
268. Bar-Shavit Z. The osteoclast: a multinucleated, hematopoietic-origin, bone-resorbing osteoimmune cell. *J Cell Biochem*. 2007;102(5):1130-1139.
269. Minkin C. Bone acid phosphatase: tartrate-resistant acid phosphatase as a marker of osteoclast function. *Calcif Tissue Int*. 1982;34(3):285-290.
270. Ballanti P, Minisola S, Pacitti MT, et al. Tartrate-resistant acid phosphate activity as osteoclastic marker: sensitivity of cytochemical assessment and serum assay in comparison with standardized osteoclast histomorphometry. *Osteoporos Int*. 1997;7(1):39-43.
271. Ikeda H, Hideshima T, Fulciniti M, et al. The monoclonal antibody nBT062 conjugated to cytotoxic Maytansinoids has selective cytotoxicity against CD138-positive multiple myeloma cells in vitro and in vivo. *Clin Cancer Res*. 2009;15(12):4028-4037.
272. Lin P, Owens R, Tricot G, Wilson CS. Flow cytometric immunophenotypic analysis of 306 cases of multiple myeloma. *Am J Clin Pathol*. 2004;121(4):482-488.
273. Lokhorst HM, Plesner T, Laubach JP, et al. Targeting CD38 with Daratumumab Monotherapy in Multiple Myeloma. *N Engl J Med*. 2015;373(13):1207-1219.
274. Paíno T, Sarasquete ME, Paiva B, et al. Phenotypic, genomic and functional characterization reveals no differences between CD138<sup>++</sup> and CD138<sup>low</sup> subpopulations in multiple myeloma cell lines. *PLoS One*. 2014;9(3):e92378.
275. Jourdan M, Ferlin M, Legouffe E, et al. The myeloma cell antigen syndecan-1 is lost by apoptotic myeloma cells. *Br J Haematol*. 1998;100(4):637-646.
276. Anderson KC, Carrasco RD. Pathogenesis of myeloma. *Annu Rev Pathol*. 2011;6:249-274.
277. Kawano Y, Moschetta M, Manier S, et al. Targeting the bone marrow microenvironment in multiple myeloma. *Immunol Rev*. 2015;263(1):160-172.
278. Oyajobi BO. Multiple myeloma/hypercalcemia. *Arthritis Res Ther*. 2007;9 Suppl 1:S4.
279. Piper K, Boyde A, Jones SJ. The relationship between the number of nuclei of an osteoclast and its resorptive capability in vitro. *Anat Embryol (Berl)*. 1992;186(4):291-299.
280. Boissy P, Saltel F, Bouniol C, Jurdic P, Machuca-Gayet I. Transcriptional activity of nuclei in multinucleated osteoclasts and its modulation by calcitonin. *Endocrinology*. 2002;143(5):1913-1921.
281. Lee SW, Kwak HB, Chung WJ, Cheong H, Kim HH, Lee ZH. Participation of protein kinase C beta in osteoclast differentiation and function. *Bone*. 2003;32(3):217-227.
282. Takashiba S, Van Dyke TE, Amar S, Murayama Y, Soskolne AW, Shapira L. Differentiation of monocytes to macrophages primes cells for lipopolysaccharide stimulation via accumulation of cytoplasmic nuclear factor kappaB. *Infect Immun*. 1999;67(11):5573-5578.
283. Kido S, Inoue D, Hiura K, Javier W, Ito Y, Matsumoto T. Expression of RANK is dependent upon differentiation into the macrophage/osteoclast lineage: induction by 1 $\alpha$ ,25-dihydroxyvitamin D3 and TPA in a human myelomonocytic cell line, HL60. *Bone*. 2003;32(6):621-629.

284. Samura A, Wada S, Suda S, Iitaka M, Katayama S. Calcitonin receptor regulation and responsiveness to calcitonin in human osteoclast-like cells prepared in vitro using receptor activator of nuclear factor-kappaB ligand and macrophage colony-stimulating factor. *Endocrinology*. 2000;141(10):3774-3782.
285. Pondel M. Calcitonin and calcitonin receptors: bone and beyond. *Int J Exp Pathol*. 2000;81(6):405-422.
286. Jordan LA, Erlandsson MC, Fenner BF, et al. Inhibition of CCL3 abrogated precursor cell fusion and bone erosions in human osteoclast cultures and murine collagen-induced arthritis. *Rheumatology (Oxford)*. 2018;57(11):2042-2052.
287. Boyde A, Dillon CE, Jones SJ. Measurement of osteoclastic resorption pits with a tandem scanning microscope. *J Microsc*. 1990;158(Pt 2):261-265.
288. Troen BR. The role of cathepsin K in normal bone resorption. *Drug News Perspect*. 2004;17(1):19-28.
289. Hecht M, von Metzler I, Sack K, Kaiser M, Sezer O. Interactions of myeloma cells with osteoclasts promote tumour expansion and bone degradation through activation of a complex signalling network and upregulation of cathepsin K, matrix metalloproteinases (MMPs) and urokinase plasminogen activator (uPA). *Exp Cell Res*. 2008;314(5):1082-1093.
290. Calame KL. Plasma cells: finding new light at the end of B cell development. *Nat Immunol*. 2001;2(12):1103-1108.
291. Nefedova Y, Landowski TH, Dalton WS. Bone marrow stromal-derived soluble factors and direct cell contact contribute to de novo drug resistance of myeloma cells by distinct mechanisms. *Leukemia*. 2003;17(6):1175-1182.
292. Christensen JH, Jensen PV, Kristensen IB, Abildgaard N, Lodahl M, Rasmussen T. Characterization of potential CD138 negative myeloma "stem cells". *Haematologica*. 2012;97(6):e18-20.
293. Quah BJ, Parish CR. The use of carboxyfluorescein diacetate succinimidyl ester (CFSE) to monitor lymphocyte proliferation. *J Vis Exp*. 2010(44).
294. Kuehl WM, Bergsagel PL. Molecular pathogenesis of multiple myeloma and its premalignant precursor. *J Clin Invest*. 2012;122(10):3456-3463.
295. Liebersbach BF, Sanderson RD. Expression of syndecan-1 inhibits cell invasion into type I collagen. *J Biol Chem*. 1994;269(31):20013-20019.
296. Purushothaman A, Chen L, Yang Y, Sanderson RD. Heparanase stimulation of protease expression implicates it as a master regulator of the aggressive tumor phenotype in myeloma. *J Biol Chem*. 2008;283(47):32628-32636.
297. Barillé S, Akhoundi C, Collette M, et al. Metalloproteinases in multiple myeloma: production of matrix metalloproteinase-9 (MMP-9), activation of proMMP-2, and induction of MMP-1 by myeloma cells. *Blood*. 1997;90(4):1649-1655.
298. Park J, Bae EK, Lee C, et al. Establishment and characterization of bortezomib-resistant U266 cell line: constitutive activation of NF- $\kappa$ B-mediated cell signals and/or alterations of ubiquitylation-related genes reduce bortezomib-induced apoptosis. *BMB Rep*. 2014;47(5):274-279.
299. Kumar SK, Lee JH, Lahuerta JJ, et al. Risk of progression and survival in multiple myeloma relapsing after therapy with IMiDs and bortezomib: a multicenter international myeloma working group study. *Leukemia*. 2012;26(1):149-157.

300. Zhan F, Huang Y, Colla S, et al. The molecular classification of multiple myeloma. *Blood*. 2006;108(6):2020-2028.
301. McCarron MJ, Park PW, Fooksman DR. CD138 mediates selection of mature plasma cells by regulating their survival. *Blood*. 2017;129(20):2749-2759.
302. Mahtouk K, Cremer FW, Rème T, et al. Heparan sulphate proteoglycans are essential for the myeloma cell growth activity of EGF-family ligands in multiple myeloma. *Oncogene*. 2006;25(54):7180-7191.
303. Ridley RC, Xiao H, Hata H, Woodliff J, Epstein J, Sanderson RD. Expression of syndecan regulates human myeloma plasma cell adhesion to type I collagen. *Blood*. 1993;81(3):767-774.
304. Fuhler GM, Baanstra M, Chesik D, et al. Bone marrow stromal cell interaction reduces syndecan-1 expression and induces kinomic changes in myeloma cells. *Exp Cell Res*. 2010;316(11):1816-1828.
305. Yaccoby S. The phenotypic plasticity of myeloma plasma cells as expressed by dedifferentiation into an immature, resilient, and apoptosis-resistant phenotype. *Clin Cancer Res*. 2005;11(21):7599-7606.
306. Yata K, Yaccoby S. The SCID-rab model: a novel in vivo system for primary human myeloma demonstrating growth of CD138-expressing malignant cells. *Leukemia*. 2004;18(11):1891-1897.
307. Fryer RA, Graham TJ, Smith EM, et al. Characterization of a novel mouse model of multiple myeloma and its use in preclinical therapeutic assessment. *PLoS One*. 2013;8(2):e57641.
308. Jang JS, Li Y, Mitra AK, et al. Molecular signatures of multiple myeloma progression through single cell RNA-Seq. *Blood Cancer J*. 2019;9(1):2.
309. López-Corral L, Corchete LA, Sarasquete ME, et al. Transcriptome analysis reveals molecular profiles associated with evolving steps of monoclonal gammopathies. *Haematologica*. 2014;99(8):1365-1372.
310. Broyl A, Hose D, Lokhorst H, et al. Gene expression profiling for molecular classification of multiple myeloma in newly diagnosed patients. *Blood*. 2010;116(14):2543-2553.
311. Mortazavi A, Williams BA, McCue K, Schaeffer L, Wold B. Mapping and quantifying mammalian transcriptomes by RNA-Seq. *Nat Methods*. 2008;5(7):621-628.
312. Trapnell C, Williams BA, Pertea G, et al. Transcript assembly and quantification by RNA-Seq reveals unannotated transcripts and isoform switching during cell differentiation. *Nat Biotechnol*. 2010;28(5):511-515.
313. Marioni JC, Mason CE, Mane SM, Stephens M, Gilad Y. RNA-seq: an assessment of technical reproducibility and comparison with gene expression arrays. *Genome Res*. 2008;18(9):1509-1517.
314. Costa-Silva J, Domingues D, Lopes FM. RNA-Seq differential expression analysis: An extended review and a software tool. *PLoS One*. 2017;12(12):e0190152.
315. Schroeder A, Mueller O, Stocker S, et al. The RIN: an RNA integrity number for assigning integrity values to RNA measurements. *BMC Mol Biol*. 2006;7:3.
316. Sonesson C, Delorenzi M. A comparison of methods for differential expression analysis of RNA-seq data. *BMC Bioinformatics*. 2013;14:91.
317. Zhang ZH, Jhaveri DJ, Marshall VM, et al. A comparative study of techniques for differential expression analysis on RNA-Seq data. *PLoS One*. 2014;9(8):e103207.

318. Rapaport F, Khanin R, Liang Y, et al. Comprehensive evaluation of differential gene expression analysis methods for RNA-seq data. *Genome Biol.* 2013;14(9):R95.
319. Jolliffe IT, Cadima J. Principal component analysis: a review and recent developments. *Philos Trans A Math Phys Eng Sci.* 2016;374(2065):20150202.
320. Bland JM, Altman DG. Statistical methods for assessing agreement between two methods of clinical measurement. *Lancet.* 1986;1(8476):307-310.
321. Storey JD, Tibshirani R. Statistical significance for genomewide studies. *Proc Natl Acad Sci U S A.* 2003;100(16):9440-9445.
322. Bioinformatics Q. Ingenuity Pathway Analysis: Qiagen; 2015.
323. Reinholt FP, Hultenby K, Oldberg A, Heinegård D. Osteopontin--a possible anchor of osteoclasts to bone. *Proc Natl Acad Sci U S A.* 1990;87(12):4473-4475.
324. Saeki Y, Mima T, Ishii T, et al. Enhanced production of osteopontin in multiple myeloma: clinical and pathogenic implications. *Br J Haematol.* 2003;123(2):263-270.
325. Sfiridaki A, Miyakis S, Pappa C, et al. Circulating osteopontin: a dual marker of bone destruction and angiogenesis in patients with multiple myeloma. *J Hematol Oncol.* 2011;4:22.
326. Kobayashi T, Nakamura S, Taniguchi T, Yamamura H. Purification and characterization of a cytosolic protein-tyrosine kinase from porcine spleen. *Eur J Biochem.* 1990;188(3):535-540.
327. Liu D, Mamorska-Dyga A. Syk inhibitors in clinical development for hematological malignancies. *J Hematol Oncol.* 2017;10(1):145.
328. Koerber RM, Held SAE, Heine A, et al. Analysis of the anti-proliferative and the pro-apoptotic efficacy of Syk inhibition in multiple myeloma. *Exp Hematol Oncol.* 2015;4:21.
329. Liu Q, Li A, Tian Y, et al. The CXCL8-CXCR1/2 pathways in cancer. *Cytokine Growth Factor Rev.* 2016;31:61-71.
330. Zingone A, Wang W, Corrigan-Cummins M, et al. Altered cytokine and chemokine profiles in multiple myeloma and its precursor disease. *Cytokine.* 2014;69(2):294-297.
331. Aggarwal R, Ghobrial IM, Roodman GD. Chemokines in multiple myeloma. *Exp Hematol.* 2006;34(10):1289-1295.
332. Page-McCaw A, Ewald AJ, Werb Z. Matrix metalloproteinases and the regulation of tissue remodelling. *Nat Rev Mol Cell Biol.* 2007;8(3):221-233.
333. Arendt BK, Velazquez-Dones A, Tschumper RC, et al. Interleukin 6 induces monocyte chemoattractant protein-1 expression in myeloma cells. *Leukemia.* 2002;16(10):2142-2147.
334. Vande Broek I, Vanderkerken K, Van Camp B, Van Riet I. Extravasation and homing mechanisms in multiple myeloma. *Clin Exp Metastasis.* 2008;25(4):325-334.
335. Demchenko YN, Kuehl WM. A critical role for the NFkB pathway in multiple myeloma. *Oncotarget.* 2010;1(1):59-68.
336. Chesi M, Nardini E, Brents LA, et al. Frequent translocation t(4;14)(p16.3;q32.3) in multiple myeloma is associated with increased expression and activating mutations of fibroblast growth factor receptor 3. *Nat Genet.* 1997;16(3):260-264.
337. Stewart AK, Bergsagel PL, Greipp PR, et al. A practical guide to defining high-risk myeloma for clinical trials, patient counseling and choice of therapy. *Leukemia.* 2007;21(3):529-534.

338. Zheng MM, Zhang Z, Bemis K, et al. The systemic cytokine environment is permanently altered in multiple myeloma. *PLoS One*. 2013;8(3):e58504.
339. Zhang XG, Bataille R, Jourdan M, et al. Granulocyte-macrophage colony-stimulating factor synergizes with interleukin-6 in supporting the proliferation of human myeloma cells. *Blood*. 1990;76(12):2599-2605.
340. Dong M, Globe GC. Role of transforming growth factor-beta in hematologic malignancies. *Blood*. 2006;107(12):4589-4596.
341. Lee JW, Chung HY, Ehrlich LA, et al. IL-3 expression by myeloma cells increases both osteoclast formation and growth of myeloma cells. *Blood*. 2004;103(6):2308-2315.
342. Gadó K, Domján G, Hegyesi H, Falus A. Role of INTERLEUKIN-6 in the pathogenesis of multiple myeloma. *Cell Biol Int*. 2000;24(4):195-209.
343. Ferlin M, Noraz N, Hertogh C, Brochier J, Taylor N, Klein B. Insulin-like growth factor induces the survival and proliferation of myeloma cells through an interleukin-6-independent transduction pathway. *Br J Haematol*. 2000;111(2):626-634.
344. Sprynski AC, Hose D, Caillot L, et al. The role of IGF-1 as a major growth factor for myeloma cell lines and the prognostic relevance of the expression of its receptor. *Blood*. 2009;113(19):4614-4626.
345. Wang YD, De Vos J, Jourdan M, et al. Cooperation between heparin-binding EGF-like growth factor and interleukin-6 in promoting the growth of human myeloma cells. *Oncogene*. 2002;21(16):2584-2592.
346. Börset M, Hjorth-Hansen H, Seidel C, Sundan A, Waage A. Hepatocyte growth factor and its receptor c-met in multiple myeloma. *Blood*. 1996;88(10):3998-4004.
347. Podar K, Tai YT, Davies FE, et al. Vascular endothelial growth factor triggers signaling cascades mediating multiple myeloma cell growth and migration. *Blood*. 2001;98(2):428-435.
348. Lee MS, Kim HS, Yeon JT, et al. GM-CSF regulates fusion of mononuclear osteoclasts into bone-resorbing osteoclasts by activating the Ras/ERK pathway. *J Immunol*. 2009;183(5):3390-3399.
349. Ruef N, Dolder S, Aeberli D, Seitz M, Balani D, Hofstetter W. Granulocyte-macrophage colony-stimulating factor-dependent CD11c-positive cells differentiate into active osteoclasts. *Bone*. 2017;97:267-277.
350. Lust JA, Donovan KA. The role of interleukin-1 beta in the pathogenesis of multiple myeloma. *Hematol Oncol Clin North Am*. 1999;13(6):1117-1125.
351. Dinarello CA. Targeting the pathogenic role of interleukin 1{beta} in the progression of smoldering/indolent myeloma to active disease. *Mayo Clin Proc*. 2009;84(2):105-107.
352. Kim JH, Jin HM, Kim K, et al. The mechanism of osteoclast differentiation induced by IL-1. *J Immunol*. 2009;183(3):1862-1870.
353. Nakamura I, Jimi E. Regulation of osteoclast differentiation and function by interleukin-1. *Vitam Horm*. 2006;74:357-370.
354. Udagawa N, Takahashi N, Katagiri T, et al. Interleukin (IL)-6 induction of osteoclast differentiation depends on IL-6 receptors expressed on osteoblastic cells but not on osteoclast progenitors. *J Exp Med*. 1995;182(5):1461-1468.
355. Harmer D, Falank C, Reagan MR. Interleukin-6 Interweaves the Bone Marrow Microenvironment, Bone Loss, and Multiple Myeloma. *Front Endocrinol (Lausanne)*. 2018;9:788.

356. Herrero AB, García-Gómez A, Garayoa M, et al. Effects of IL-8 Up-Regulation on Cell Survival and Osteoclastogenesis in Multiple Myeloma. *Am J Pathol.* 2016;186(8):2171-2182.
357. Bendre MS, Montague DC, Peery T, Akel NS, Gaddy D, Suva LJ. Interleukin-8 stimulation of osteoclastogenesis and bone resorption is a mechanism for the increased osteolysis of metastatic bone disease. *Bone.* 2003;33(1):28-37.
358. Matsumoto T, Abe M. TGF- $\beta$ -related mechanisms of bone destruction in multiple myeloma. *Bone.* 2011;48(1):129-134.
359. Takeuchi K, Abe M, Hiasa M, et al. Tgf-Beta inhibition restores terminal osteoblast differentiation to suppress myeloma growth. *PLoS One.* 2010;5(3):e9870.
360. Parri M, Chiarugi P. Rac and Rho GTPases in cancer cell motility control. *Cell Commun Signal.* 2010;8:23.
361. Azab AK, Azab F, Blotta S, et al. RhoA and Rac1 GTPases play major and differential roles in stromal cell-derived factor-1-induced cell adhesion and chemotaxis in multiple myeloma. *Blood.* 2009;114(3):619-629.
362. Pollard TD, Borisy GG. Cellular motility driven by assembly and disassembly of actin filaments. *Cell.* 2003;112(4):453-465.
363. Chen R, Zhao H, Wu D, Zhao C, Zhao W, Zhou X. The role of SH3GL3 in myeloma cell migration/invasion, stemness and chemo-resistance. *Oncotarget.* 2016;7(45):73101-73113.
364. Canales RD, Luo Y, Willey JC, et al. Evaluation of DNA microarray results with quantitative gene expression platforms. *Nat Biotechnol.* 2006;24(9):1115-1122.
365. VanGuilder HD, Vrana KE, Freeman WM. Twenty-five years of quantitative PCR for gene expression analysis. *Biotechniques.* 2008;44(5):619-626.
366. Rajkumar AP, Qvist P, Lazarus R, et al. Experimental validation of methods for differential gene expression analysis and sample pooling in RNA-seq. *BMC Genomics.* 2015;16:548.
367. Haney MS, Bohlen CJ, Morgens DW, et al. Identification of phagocytosis regulators using magnetic genome-wide CRISPR screens. *Nat Genet.* 2018;50(12):1716-1727.
368. Brioli A, Melchor L, Cavo M, Morgan GJ. The impact of intra-clonal heterogeneity on the treatment of multiple myeloma. *Br J Haematol.* 2014;165(4):441-454.
369. Kumar S, Kimlinger T, Morice W. Immunophenotyping in multiple myeloma and related plasma cell disorders. *Best Pract Res Clin Haematol.* 2010;23(3):433-451.
370. Flores-Montero J, de Tute R, Paiva B, et al. Immunophenotype of normal vs. myeloma plasma cells: Toward antibody panel specifications for MRD detection in multiple myeloma. *Cytometry B Clin Cytom.* 2016;90(1):61-72.
371. Jourdan M, Caraux A, De Vos J, et al. An in vitro model of differentiation of memory B cells into plasmablasts and plasma cells including detailed phenotypic and molecular characterization. *Blood.* 2009;114(25):5173-5181.
372. Pellat-Deceunynck C, Bataille R. Normal and malignant human plasma cells: proliferation, differentiation, and expansions in relation to CD45 expression. *Blood Cells Mol Dis.* 2004;32(2):293-301.
373. Hajek R, Okubote SA, Svachova H. Myeloma stem cell concepts, heterogeneity and plasticity of multiple myeloma. *Br J Haematol.* 2013;163(5):551-564.

374. Garfall AL, Maus MV, Hwang WT, et al. Chimeric Antigen Receptor T Cells against CD19 for Multiple Myeloma. *N Engl J Med*. 2015;373(11):1040-1047.
375. Moreaux J, Hose D, Reme T, et al. CD200 is a new prognostic factor in multiple myeloma. *Blood*. 2006;108(13):4194-4197.
376. Pellat-Deceunynck C, Bataille R, Robillard N, et al. Expression of CD28 and CD40 in human myeloma cells: a comparative study with normal plasma cells. *Blood*. 1994;84(8):2597-2603.
377. Robillard N, Jegou G, Pellat-Deceunynck C, et al. CD28, a marker associated with tumoral expansion in multiple myeloma. *Clin Cancer Res*. 1998;4(6):1521-1526.
378. Paiva B, Gutiérrez NC, Chen X, et al. Clinical significance of CD81 expression by clonal plasma cells in high-risk smoldering and symptomatic multiple myeloma patients. *Leukemia*. 2012;26(8):1862-1869.
379. Ise T, Nagata S, Kreitman RJ, et al. Elevation of soluble CD307 (IRTA2/FcRH5) protein in the blood and expression on malignant cells of patients with multiple myeloma, chronic lymphocytic leukemia, and mantle cell lymphoma. *Leukemia*. 2007;21(1):169-174.
380. Iqbal MS, Otsuyama K, Shamsasenjan K, et al. Constitutively lower expressions of CD54 on primary myeloma cells and their different localizations in bone marrow. *Eur J Haematol*. 2009;83(4):302-312.
381. Schmidt-Hieber M, Pérez-Andrés M, Paiva B, et al. CD117 expression in gammopathies is associated with an altered maturation of the myeloid and lymphoid hematopoietic cell compartments and favorable disease features. *Haematologica*. 2011;96(2):328-332.
382. Kumar S, Rajkumar SV, Kimlinger T, Greipp PR, Witzig TE. CD45 expression by bone marrow plasma cells in multiple myeloma: clinical and biological correlations. *Leukemia*. 2005;19(8):1466-1470.
383. Alberts B, Johnson A, J L. *Molecular Biology of the Cell* (ed 4th Edition). New York: Garland Science; 2002.
384. Ziegler SF, Ramsdell F, Alderson MR. The activation antigen CD69. *Stem Cells*. 1994;12(5):456-465.
385. Takada Y, Huang C, Hemler ME. Fibronectin receptor structures in the VLA family of heterodimers. *Nature*. 1987;326(6113):607-609.
386. Pellat-Deceunynck C, Barillé S, Puthier D, et al. Adhesion molecules on human myeloma cells: significant changes in expression related to malignancy, tumor spreading, and immortalization. *Cancer Res*. 1995;55(16):3647-3653.
387. Ahsmann EJ, Lokhorst HM, Dekker AW, Bloem AC. Lymphocyte function-associated antigen-1 expression on plasma cells correlates with tumor growth in multiple myeloma. *Blood*. 1992;79(8):2068-2075.
388. Tai YT, Podar K, Mitsiades N, et al. CD40 induces human multiple myeloma cell migration via phosphatidylinositol 3-kinase/AKT/NF-kappa B signaling. *Blood*. 2003;101(7):2762-2769.
389. Urashima M, Chauhan D, Uchiyama H, Freeman GJ, Anderson KC. CD40 ligand triggered interleukin-6 secretion in multiple myeloma. *Blood*. 1995;85(7):1903-1912.
390. Bao L, Lai Y, Liu Y, et al. CXCR4 is a good survival prognostic indicator in multiple myeloma patients. *Leuk Res*. 2013;37(9):1083-1088.
391. Waugh DJ, Wilson C. The interleukin-8 pathway in cancer. *Clin Cancer Res*. 2008;14(21):6735-6741.

392. Li A, Dubey S, Varney ML, Dave BJ, Singh RK. IL-8 directly enhanced endothelial cell survival, proliferation, and matrix metalloproteinases production and regulated angiogenesis. *J Immunol.* 2003;170(6):3369-3376.
393. Kline M, Donovan K, Wellik L, et al. Cytokine and chemokine profiles in multiple myeloma; significance of stromal interaction and correlation of IL-8 production with disease progression. *Leuk Res.* 2007;31(5):591-598.
394. Dinarello CA. Biologic basis for interleukin-1 in disease. *Blood.* 1996;87(6):2095-2147.
395. De Larco JE, Wuertz BR, Furcht LT. The potential role of neutrophils in promoting the metastatic phenotype of tumors releasing interleukin-8. *Clin Cancer Res.* 2004;10(15):4895-4900.
396. Bianchi G, Munshi NC. Pathogenesis beyond the cancer clone(s) in multiple myeloma. *Blood.* 2015;125(20):3049-3058.
397. Robak P, Drozd I, Szemraj J, Robak T. Drug resistance in multiple myeloma. *Cancer Treat Rev.* 2018;70:199-208.
398. Paiva B, Paino T, Sayagues JM, et al. Detailed characterization of multiple myeloma circulating tumor cells shows unique phenotypic, cytogenetic, functional, and circadian distribution profile. *Blood.* 2013;122(22):3591-3598.
399. Muz B, de la Puente P, Azab F, et al. A CD138-independent strategy to detect minimal residual disease and circulating tumour cells in multiple myeloma. *Br J Haematol.* 2016;173(1):70-81.
400. Abdi J, Chen G, Chang H. Drug resistance in multiple myeloma: latest findings and new concepts on molecular mechanisms. *Oncotarget.* 2013;4(12):2186-2207.
401. Meads MB, Gatenby RA, Dalton WS. Environment-mediated drug resistance: a major contributor to minimal residual disease. *Nat Rev Cancer.* 2009;9(9):665-674.
402. Richardson PG, Sonneveld P, Schuster MW, et al. Bortezomib or high-dose dexamethasone for relapsed multiple myeloma. *N Engl J Med.* 2005;352(24):2487-2498.
403. Bertho AL, Santiago MA, Coutinho SG. Flow cytometry in the study of cell death. *Mem Inst Oswaldo Cruz.* 2000;95(3):429-433.
404. McGranahan N, Swanton C. Clonal Heterogeneity and Tumor Evolution: Past, Present, and the Future. *Cell.* 2017;168(4):613-628.
405. Walker BA, Wardell CP, Melchor L, et al. Intraclonal heterogeneity is a critical early event in the development of myeloma and precedes the development of clinical symptoms. *Leukemia.* 2014;28(2):384-390.
406. Mitra AK, Stessman H, Linden MA, Van Ness B. Single-Cell Transcriptomics Identifies Intra-Tumor Heterogeneity in Human Myeloma Cell Lines. *Blood.* 2014;124:3385.
407. Chaidos A, Barnes CP, Cowan G, et al. Clinical drug resistance linked to interconvertible phenotypic and functional states of tumor-propagating cells in multiple myeloma. *Blood.* 2013;121(2):318-328.
408. Caldwell CW, Patterson WP. Relationship between CD45 antigen expression and putative stages of differentiation in B-cell malignancies. *Am J Hematol.* 1991;36(2):111-115.
409. Harada H, Kawano MM, Huang N, et al. Phenotypic difference of normal plasma cells from mature myeloma cells. *Blood.* 1993;81(10):2658-2663.

410. Paiva B, Puig N, Cedena MT, et al. Differentiation stage of myeloma plasma cells: biological and clinical significance. *Leukemia*. 2017;31(2):382-392.
411. Chatterjee S, Behnam Azad B, Nimmagadda S. The intricate role of CXCR4 in cancer. *Adv Cancer Res*. 2014;124:31-82.
412. Busillo JM, Benovic JL. Regulation of CXCR4 signaling. *Biochim Biophys Acta*. 2007;1768(4):952-963.
413. Gales D, Clark C, Manne U, Samuel T. The Chemokine CXCL8 in Carcinogenesis and Drug Response. *ISRN Oncol*. 2013;2013:859154.
414. Zhu YM, Webster SJ, Flower D, Woll PJ. Interleukin-8/CXCL8 is a growth factor for human lung cancer cells. *Br J Cancer*. 2004;91(11):1970-1976.
415. Paiva B, van Dongen JJ, Orfao A. New criteria for response assessment: role of minimal residual disease in multiple myeloma. *Blood*. 2015;125(20):3059-3068.
416. Garfall AL, Stadtmauer EA, Hwang WT, et al. Anti-CD19 CAR T cells with high-dose melphalan and autologous stem cell transplantation for refractory multiple myeloma. *JCI Insight*. 2018;3(8).
417. Nerretter T, Letschert S, Götz R, et al. Super-resolution microscopy reveals ultra-low CD19 expression on myeloma cells that triggers elimination by CD19 CAR-T. *Nat Commun*. 2019;10(1):3137.
418. Sørensen MG, Henriksen K, Schaller S, et al. Characterization of osteoclasts derived from CD14+ monocytes isolated from peripheral blood. *J Bone Miner Metab*. 2007;25(1):36-45.
419. Farrugia AN, Atkins GJ, To LB, et al. Receptor activator of nuclear factor-kappaB ligand expression by human myeloma cells mediates osteoclast formation in vitro and correlates with bone destruction in vivo. *Cancer Res*. 2003;63(17):5438-5445.
420. Lai FP, Cole-Sinclair M, Cheng WJ, et al. Myeloma cells can directly contribute to the pool of RANKL in bone bypassing the classic stromal and osteoblast pathway of osteoclast stimulation. *Br J Haematol*. 2004;126(2):192-201.
421. Moreaux J, Hose D, Kassambara A, et al. Osteoclast-gene expression profiling reveals osteoclast-derived CCR2 chemokines promoting myeloma cell migration. *Blood*. 2011;117(4):1280-1290.
422. Landowski TH, Olashaw NE, Agrawal D, Dalton WS. Cell adhesion-mediated drug resistance (CAM-DR) is associated with activation of NF-kappa B (RelB/p50) in myeloma cells. *Oncogene*. 2003;22(16):2417-2421.
423. Hartmann TN, Burger JA, Glodek A, Fujii N, Burger M. CXCR4 chemokine receptor and integrin signaling co-operate in mediating adhesion and chemoresistance in small cell lung cancer (SCLC) cells. *Oncogene*. 2005;24(27):4462-4471.
424. Pardo-Cabañas M, Molina-Ortiz I, Matías-Román S, et al. Role of metalloproteinases MMP-9 and MT1-MMP in CXCL12-promoted myeloma cell invasion across basement membranes. *J Pathol*. 2006;208(1):108-118.
425. Azab AK, Runnels JM, Pitsillides C, et al. CXCR4 inhibitor AMD3100 disrupts the interaction of multiple myeloma cells with the bone marrow microenvironment and enhances their sensitivity to therapy. *Blood*. 2009;113(18):4341-4351.
426. Bergsagel PL, Kuehl WM. Chromosome translocations in multiple myeloma. *Oncogene*. 2001;20(40):5611-5622.
427. Roodman GD. Osteoblast function in myeloma. *Bone*. 2011;48(1):135-140.

428. Florencio-Silva R, Sasso GR, Sasso-Cerri E, Simões MJ, Cerri PS. Biology of Bone Tissue: Structure, Function, and Factors That Influence Bone Cells. *Biomed Res Int*. 2015;2015:421746.
429. Prideaux M, Wijenayaka AR, Kumarasinghe DD, et al. SaOS2 Osteosarcoma cells as an in vitro model for studying the transition of human osteoblasts to osteocytes. *Calcif Tissue Int*. 2014;95(2):183-193.
430. Kumar S, Witzig TE, Greipp PR, Rajkumar SV. Bone marrow angiogenesis and circulating plasma cells in multiple myeloma. *Br J Haematol*. 2003;122(2):272-274.
431. Tanaka Y, Abe M, Hiasa M, et al. Myeloma cell-osteoclast interaction enhances angiogenesis together with bone resorption: a role for vascular endothelial cell growth factor and osteopontin. *Clin Cancer Res*. 2007;13(3):816-823.
432. Braham MVJ, Minnema MC, Aarts T, et al. Cellular immunotherapy on primary multiple myeloma expanded in a 3D bone marrow niche model. *Oncoimmunology*. 2018;7(6):e1434465.
433. Reagan MR, Mishima Y, Glavey SV, et al. Investigating osteogenic differentiation in multiple myeloma using a novel 3D bone marrow niche model. *Blood*. 2014;124(22):3250-3259.
434. Kirshner J, Thulien KJ, Martin LD, et al. A unique three-dimensional model for evaluating the impact of therapy on multiple myeloma. *Blood*. 2008;112(7):2935-2945.
435. Pessoa de Magalhães RJ, Vidriales MB, Paiva B, et al. Analysis of the immune system of multiple myeloma patients achieving long-term disease control by multidimensional flow cytometry. *Haematologica*. 2013;98(1):79-86.